

# Synthesis of amphiphilic $\beta$ -turn mimetic polymer-conjugates and their organization in model membranes

## Dissertation

zur Erlangung des Doktorgrades der Naturwissenschaften  
(Dr. rer. nat.)

der

Naturwissenschaftlichen Fakultät II  
Chemie, Physik und Mathematik

der Martin-Luther-Universität  
Halle-Wittenberg

vorgelegt von

Frau Marlen Malke  
geb. am 31. Juli 1985 in Luth. Wittenberg

Gutachter

1. Prof. Dr. Wolfgang H. Binder
2. Prof. Dr. rer. nat. habil. Jörg C. Tiller

Verteidigung: 23.06.2016

*„Wie weit Du im Leben kommst,  
wird davon abhängig sein,  
wie weit Du  
zärtlich mit den Kleinen umgegangen bist,  
mitfühlend mit den Alten,  
Anteil nehmend mit denen, die sich anstrengen  
und geduldig mit den Schwachen und den Starken.  
Denn eines Tages wirst Du dies alles gewesen sein.“*

*George Washington Carver (1864-1943)*

---

**Results of this dissertation have been published:**

Parts of this thesis have been published in: Malke, M.; Barqawi, H.; Binder, W. H., Synthesis of an Amphiphilic  $\beta$ -Turn Mimetic Polymer Conjugate. *ACS Macro Lett.* **2014**, 3, (4), 393-397.

Text parts of chapter 4.3 and Figures (4.6, 4.7, A12) were adapted with permission from the American Chemical Society, copyright 2015.

## Danksagung

An dieser Stelle möchte ich mich bei den Mitarbeitern der Makromolekularen Chemie des Institutes für Chemie der Martin-Luther-Universität Halle-Wittenberg für die stets gewährte Unterstützung und Zusammenarbeit bedanken. Mein besonderer Dank gilt Herrn Prof. Dr. W. H. Binder für die Bereitstellung des interessanten Themas und sehr gute Betreuung.

Des Weiteren möchte ich mich an dieser Stelle bei der gesamten Arbeitsgruppe von Prof. Dr. W. H. Binder für das angenehme Arbeitsklima und die stetige Hilfsbereitschaft bedanken, dabei danke ich vor allem meinen Büro- und Laborkollegen Diana, Claudia, Kathi, Flo, Philipp, Steve, Wilton, Paul und Ali mit denen ich in freundschaftlicher Weise sowohl Erfolg als auch Misserfolg teilen durfte. Ebenso danke ich hierbei Dr. Haitham Barqawi für die 2D-Messung (HPLC/MALDI-ToF MS) und Dr. Matthias Schulz für die GUV Messungen.

Auch möchte ich mich bei der Arbeitsgruppe von Prof. Dr. A. Blume bedanken, insbesondere Bob-Dan Lechner für die AFM Messungen und André Hädicke, für die Einweisung und Hilfestellung in der Fluoreszenzmikroskopie und –spektroskopie. Außerdem danke ich der Arbeitsgruppe von Prof. Dr. J. Kressler für die Einweisung und Messerlaubnis am Langmuir Trog. Mein weiterer Dank gilt dem Team um Herrn Dr. D. Ströhl für die Aufnahme sämtlicher NMR-Spektren und der Arbeitsgruppe von Prof. Dr. J. Balbach, insbesondere Herrn Gröger für die Messung der 600 MHz NMR Spektren.

Besonderer Dank gilt unseren „3 Säulen“ der Arbeitsgruppe Frau A. Hassi, Frau S. Tanner und Herrn N. Diedrich, die mir in arbeitstechnischen und administrativen Belangen zur Seite standen. Herausheben möchte ich auch meine „Halle-Familie“: Anke, Susi, Sophie und Norman – danke, dass ihr immer für mich da wart und die Fahrt der Marlen-Achterbahn mitgemacht habt. Ihr habt die Promotionszeit zu etwas ganz Besonderem und Unvergesslichen für mich gemacht.

Besonderer Dank gilt auch meinen Freunden, die mich in all den Jahren meines Studiums seelisch unterstützt haben.

Von ganzem Herzen danke ich meiner Familie und meinem Mann für den Rückhalt auch in schwierigen Zeiten meiner Arbeit.

---

<b>1. Introduction</b>	<b>1</b>
<b>1.1 Folding of biomacromolecules</b>	<b>1</b>
1.1.1 Organization of proteins	1
1.1.1.1 Primary and secondary structure of proteins	2
1.1.1.2 Major protein classes	4
1.1.1.3 Protein folding	5
1.1.2 DNA assembly	7
<b>1.2 Foldamers</b>	<b>8</b>
1.2.1 History and definition of foldamers	8
1.2.2 Driving forces for folding and suitable folded structures	9
1.2.3 Foldamer classification	11
1.2.3.1 Peptidomimetic foldamers – aliphatic foldamers	11
1.2.3.2 Aromatic foldamers	14
1.2.3.3 Foldable Polymers	15
1.2.4 Foldamers and their interactions with membranes	17
1.2.4.1 Folding of oligocholate	18
1.2.4.2 Turn mimetics	19
<b>2. Aim of the work</b>	<b>24</b>
<b>3. Concept</b>	<b>25</b>
<b>4. Results and discussion</b>	<b>27</b>
4.1 Synthesis of $\alpha,\omega$ -functionalized PIBs	27
4.2 Synthesis of the $\beta$ -turn mimetic building blocks	30
4.2.1 Synthesis of the $\beta$ -turn dipeptide (BTD)	30
4.2.2 Synthesis of the sugar azido acid (SAA)	31
4.3 Synthesis of amphiphilic $\beta$ -turn mimetic polymer conjugate	33
4.3.1 Linking methods	33
4.3.1.1 Copper mediated azide/alkyne-“click”-reaction	33
4.3.1.2 Amidation reaction	34
4.3.2 Linkage of the different building blocks	36
4.3.3 Analysis of the intermediates <b>5</b> and <b>8</b> and the $\beta$ -turn mimetic PIB conjugate <b>9</b>	38
4.4 Monolayer experiments of <b>8</b> and <b>9</b> using DPPC as lipid	42
4.4.1 Monolayer compression isotherms of DPPC/ <b>8</b> and DPPC/ <b>9</b> mixtures	43
4.4.2 Epifluorescence microscopy of DPPC/ <b>8</b> and DPPC/ <b>9</b> mixed monolayers	45
4.4.3 AFM measurements	49
4.5 Bilayer experiments of <b>8</b> and <b>9</b> using DPPC as lipid	52
<b>5. Concept to introduce FRET dyes</b>	<b>55</b>
5.1 Results and discussion of introduction of FRET dyes	56
5.1.1 Synthesis of FRET dyes	56
5.1.2 Synthesis of dye labeled amphiphilic polymer conjugate	58
5.2 Fluorescence spectroscopy of mixed DPPC/polymer bilayer membrane	61
<b>6. Concept to elongate the hydrophilic part</b>	<b>64</b>
6.1 Results and discussion of the elongation of the hydrophilic part	65
6.1.1 Synthesis of $\alpha$ -hydroxymethyl- $\omega$ -azido telechelic poly(isobutylene) ( <b>18</b> )	65
6.1.2 Synthesis of the tetraethylene glycol derivatives ( <b>19</b> and <b>21</b> )	67
6.2 Linkage of the different building blocks	68

6.2.1	Synthesis of the first strand using BTD as $\beta$ -turn mimetic	69
6.2.2	Synthesis of the second strand using BTD as $\beta$ -turn mimetic and linkage to the first strand	70
6.2.3	Synthesis of the two strands using SAA as $\beta$ -turn mimetic	72
<b>7.</b>	<b>Experimental Part</b>	<b>74</b>
<b>7.1</b>	<b>Materials and Methods</b>	<b>74</b>
<b>7.2</b>	<b>Synthesis</b>	<b>79</b>
7.2.1	Synthesis of $\alpha$ -hydroxymethyl- $\omega$ -amino telechelic poly(isobutylene) <b>3</b>	79
7.2.2	Synthesis of $\alpha$ -hydroxymethyl- $\omega$ -alkyne telechelic PIB ( <b>5</b> )	80
7.2.3	Synthesis of (3R,6S,7R,8S,9R,9aR)-6-azido-octahydro-7,8,9-trihydroxy-5-oxothiazolo[3,2-a]azepine-3-carboxylic acid (BTD-COOH, <b>6a</b> )	81
7.2.4	Protection of hydroxyl-groups of <b>11</b> with Ac <sub>2</sub> O to achieve <b>6b</b>	81
7.2.5	(2S,3S,4S,5R)-methyl 3,4,5,6-tetraacetoxy-tetrahydro-2H-pyran-2-carboxylate ( <b>7a</b> )	82
7.2.6	(2S,3S,4S,5R,6S)-methyl 3,4,5-triacetoxy-6-bromo-tetrahydro-2H-pyran-2-carboxylate ( <b>7b</b> )	83
7.2.7	(2S,3S,4S,5R,6R)-methyl 3,4,5-triacetoxy-6-azido-tetrahydro-2H-pyran-2-carboxylate ( <b>7c</b> )	83
7.2.8	(2S,3S,4S,5R,6R)-6-azido-tetrahydro-3,4,5-trihydroxy-2H-pyran-2-carboxylic acid ( <b>7</b> )	84
7.2.9	Peptide coupling of <b>3</b> with <b>6</b>	84
7.2.10	Azide/alkyne-“click”-reactions of <b>5</b> with <b>8</b> to achieve <b>9</b>	85
7.2.11	Azide/alkyne-“click”-reactions of <b>5</b> with <b>7c</b> to achieve <b>30</b>	86
7.2.12	Azide/alkyne-“click”-reactions of <b>10</b> with 4-ethynylbenzonitrile to achieve <b>11a</b>	87
7.2.13	Azide/alkyne-“click”-reactions of <b>10</b> with 9-ethynylphenanthrene to achieve <b>12a</b>	87
7.2.14	Hydrolysis of <b>11a</b> to achieve <b>11</b>	88
7.2.15	Hydrolysis of <b>12a</b> to achieve <b>12</b>	89
7.2.16	Boc-protection of <b>3</b> to achieve <b>31</b>	89
7.2.17	Esterification of <b>11b</b> with <b>31</b> to achieve <b>32</b>	90
7.2.18	Deprotection of <b>32</b> to achieve <b>13</b>	91
7.2.19	Peptide coupling of <b>6</b> with <b>13</b> to achieve <b>14</b>	92
7.2.20	Esterification of <b>12b</b> with <b>5</b> to achieve <b>15</b>	93
7.2.21	Azide/alkyne-“click”-reaction of <b>14</b> with <b>15</b> to achieve <b>16</b>	94
7.2.22	Synthesis of $\alpha,\omega$ -dialkynyl tetraethylene glycol ( <b>19</b> )	95
7.2.23	Azide/alkyne-“click”-reactions of <b>19</b> with <b>20</b> to achieve <b>21a</b>	95
7.2.24	Deprotection of <b>21a</b> to achieve <b>21</b>	96
7.2.25	Azide/alkyne-“click”-reactions of <b>19</b> with <b>6a</b> to achieve <b>22</b>	97
7.2.26	Azide/alkyne-“click”-reactions of <b>18</b> with <b>22</b> to achieve <b>24</b>	99
7.2.27	Azide/alkyne-“click”-reactions of <b>3</b> with <b>4</b>	100
7.2.28	Azide/alkyne-“click”-reactions of <b>6a</b> with <b>23</b> to achieve <b>24</b>	102
7.2.29	Hydrolysis of <b>22</b> to <b>33</b>	102
7.2.30	Azide/alkyne-“click”-reactions of <b>6b</b> with <b>23</b> to achieve <b>34</b>	103
7.2.31	Azide/alkyne-“click”-reactions of <b>18</b> with <b>21a</b> to achieve <b>35</b>	104
7.2.32	Deprotection of <b>35</b> to achieve <b>36</b>	105
7.2.33	Peptide coupling of <b>6a</b> with <b>20a</b> to achieve <b>37</b>	106
7.2.34	Peptide coupling of <b>6</b> with <b>21</b> to achieve <b>38</b>	106
7.2.35	Peptide coupling of <b>6</b> with <b>36</b> to achieve <b>39</b>	107
7.2.36	Protection of hydroxyl-groups of <b>39</b> with Ac <sub>2</sub> O to achieve <b>40</b>	108
7.2.37	Azide/alkyne-“click”-reactions of <b>19</b> with <b>40</b> to achieve <b>41</b>	108
7.2.38	Azide/alkyne-“click”-reactions of <b>18</b> with <b>41</b> following by deprotection/hydrolysis to achieve <b>42</b>	109
7.2.39	Azide/alkyne-“click”-reactions of <b>23</b> with <b>40</b>	110
7.2.40	Azide/alkyne-“click”-reaction of <b>23</b> with <b>7c</b> to achieve <b>43</b>	112
<b>8.</b>	<b>Summary</b>	<b>113</b>
<b>9.</b>	<b>Literature</b>	<b>121</b>
<b>10.</b>	<b>Appendix</b>	<b>132</b>

**Abbreviations**

abs	absolute
Ac <sub>2</sub> O	acetic anhydride
AcOH	acetic acid
AFM	atomic force microscopy
BOP	benzotriazol-1-yloxytris(dimethylamino)phosphonium hexafluorophosphate
BPB	3-bromopropoxybenzene
BroP	bromotris(dimethylamino)phosphonium hexafluorophosphate
BTD	β-turn dipeptide
<i>t</i> -BuOH	<i>tert</i> -butanol
“click”	copper mediated azide/alkyne-“click”-reaction
CuBr(PPh <sub>3</sub> ) <sub>3</sub>	bromotris(triphenylphosphine)copper(I)
CuI·P(OEt) <sub>3</sub>	iodo(triethylphosphite)copper(I)
Cu(MeCN) <sub>4</sub> PF <sub>6</sub>	tetrakis(acetonitrile)copper(I) hexafluorophosphate
DCC	dicyclohexylcarbodiimide
DCM	dichloromethane
DCTB	trans-2-[3-(4- <i>tert</i> -butylphenyl)-2-methyl-2-propenylidene]malononitrile
DIPEA	<i>N,N</i> -diisopropylethylamine
DMAP	4-dimethylaminopyridine
DMF	<i>N,N</i> -dimethylformamide
DMSO	dimethylsulfoxide
DOPC	1,2-dioleoyl- <i>sn</i> -glycero-3-phosphocholine
DPPC	1,2-dipalmitoyl- <i>sn</i> -glycero-3-phosphocholine
DSC	differential scanning calorimetry
L-DPPC	1,2-dipalmitoyl- <i>sn</i> -glycero-3-phosphocholine
<i>Dt</i> BP	2,6-di- <i>tert</i> -butylpyridine
EA	ethyl acetate
EDC	1-(3-dimethylaminopropyl)-3-ethylcarbodiimide
ESI-ToF MS	electrospray ionization time-of-flight mass spectrometry
Et <sub>2</sub> O	diethyl ether
HATU	<i>O</i> -(7-azabenzotriazole-1-yl)-1,1,3,3-tetramethyluronium hexafluorophosphate
HBTU	<i>O</i> -(benzotriazol-1-yl)-1,1,3,3-tetramethyluronium hexafluorophosphate
<i>n</i> -Hex	<i>n</i> -hexane
HOBt	1-hydroxybenzotriazole
HOSu	<i>N</i> -hydroxysuccinimide
HPLC	high performance liquid chromatography
LA	lewis acid
LB	Langmuir-Blodgett
LCCP	living carbocationic polymerization
LiTFA	lithiumtrifluoroacetate
MALDI-ToF MS	matrix-assisted laser desorption/ionization time-of-flight mass spectrometry
<i>m</i> -CPBA	meta-chloroperbenzoic acid
MeOH	methanol
α-MSE	α-methylstyrene epoxide
MTBE	methyl- <i>tert</i> -butyl ether
Na-asc	sodium ascorbate
NMM	<i>N</i> -methymorpholine

## Content

---

NMR	nuclear magnetic resonance
PDI	polydispersity index
PEG	poly(ethylene glycol)
PfPOH	pentafluorophenyl
PIB	poly(isobutylene)
PMDETA	<i>N,N,N',N',N''</i> -pentamethyldiethylenetetramine
i-Prop	iso-propanol
py	pyridine
PyBOP	(benzotriazol-1-yloxy)tripyrrolidinophosphonium hexafluorophosphate
Rh-DHPE	1,2-dihexadecanoyl-sn-glycero-3-phosphoethanolamine- <i>N</i> -(lissamine rhodamine B sulfonyl)
RI	refractive index
Rt	room temperature
SEC	size exclusion chromatography
TBAHS	tetrabutylammoniumbisulfate
TBDMSCl	<i>tert</i> -butyldimethylsilyl chloride
TBTA	tris-(benzyltriazolylmethyl)amine
Tf	triflate
TFA	trifluoroacetic acid
THF	tetrahydrofuran
TLC	thin layer chromatography
TMS	trimethyl(3-phenoxy-1-propynyl)silane
tol	toluene



## 1. Introduction

*“In Nature, everything is connected to everything else, everything crossed, everything exchanges with everything, everything changes, one into the other”* — Gotthold Ephraim Lessing

Complexity in Nature originates from hierarchical organization of biomolecular components and interactions between them. Most of the biological and chemical functions like molecular recognition, information storage and catalysis, carried out by biomacromolecules (e.g. proteins and DNA) are determined by folding into well-defined three-dimensional structures in solution. To understand the meaning of this folding for the functions of biomacromolecules, artificial systems such as synthetic nonbiological oligomers, which can adopt those functions by achieving ordered solution conformation, has become part of the interest. This subject is known as the field of “*foldamers*”<sup>1, 2</sup>. The folding of biomacromolecules and also artificial foldamers will be discussed in the following chapters.

### 1.1 Folding of biomacromolecules

#### 1.1.1 Organization of proteins

Proteins are the building blocks of life, therefore they have to fulfill several tasks. They specify shape and structure of cells and are involved in the whole living functions despite the fact that they are composed of only 20 amino acids. In order to complete the tasks a certain spatial form of the protein is necessary thus it is forced to fold in a defined manner (Figure 1.1).

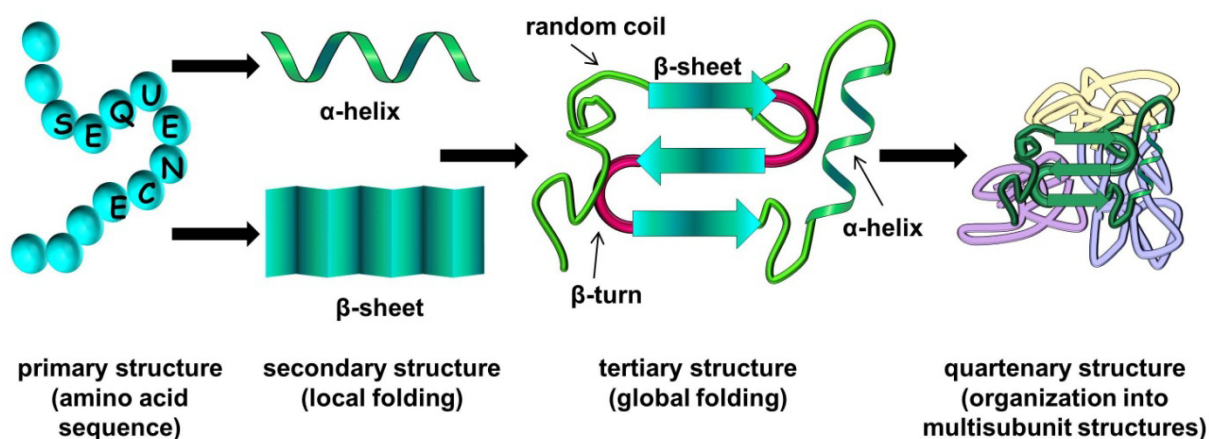


**Figure 1.1.** Hierarchical structure organization of proteins. (Figure was redrawn according to National Human Genome Research Institute)<sup>3</sup>

The building plan is initially given by the sequence of the amino acids, building the amino acid chain (primary structure) which then folds into a local regular structure (secondary structure). These include the  $\alpha$ -helix, the pleated  $\beta$ -sheet and the  $\beta$ -turn, which all result mainly by the sum of intramolecular

## 1. Introduction

hydrogen bonds (attractive forces). Further electrostatic attractions (e.g. dipole-dipole interaction) between the side chains, van der Waals interactions (dispersion forces) or even cross linkages of covalent disulfide bridges between two cysteine units subsequently lead to the tertiary structure. The last level of protein organization which can be reached is the quaternary structure, which is the result of aggregation of two or more polypeptide chains. If the folding was correct, active sites are generated, thus the proteins can perform their tasks.<sup>4</sup>

### 1.1.1.1 Primary and secondary structure of proteins

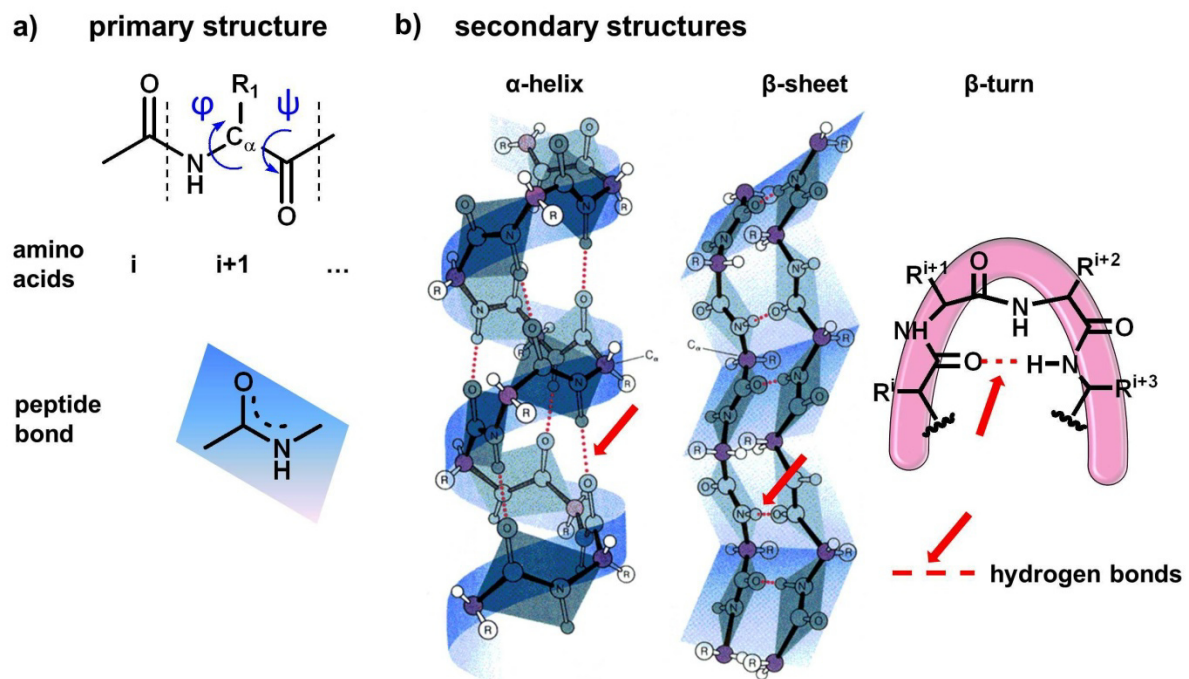


**Figure 1.2.** Structure building in proteins. a) primary structure. b) secondary structures. (The drawings of the secondary structures  $\alpha$ -helix and  $\beta$ -sheet are from Irving Geis and are taken from <https://scimedia.files.wordpress.com/2011/02/fi6p3.gif>.)<sup>5</sup>

The folding into  $\alpha$ -helices,  $\beta$ -sheets and  $\beta$ -turns is important, but why are these secondary structures formed and how they are stabilized? As mentioned previously proteins are assembled out of the repertoire of 20 natural amino acids. Their basic structure is equal, as they have at the one end the active amino residue and at the other end the active carboxylate, which are spaced by a methylene group. This methylene group can be functionalized in different ways. Due to this sidechains the amino acids differ in their structure and therefore in their size, flexibility and polarity. The single amino acids are then linked under formation of a peptide bond building the amino acid chains (primary structure) with the protein backbone and the outstanding sidechains. Figure 1.2a shows a schematic section of an amino acid chain. In biochemistry the indication is fixed, the chains were drawn from the N-terminus to the C-terminus and counted in the way of the first amino acid as equal to “ $i$ ”, the second to “ $i+1$ ” etc.

## 1. Introduction

Also the torsion angles are defined, “ $\psi$ ” as the torsion angle between “ $C_\alpha - C$ ” and “ $\phi$ ” as torsion angle between “ $N - C_\alpha$ ”. The direction of positive rotation about  $\phi$  and  $\psi$  is given by the arrows (clockwise when looking in either direction from the  $C_\alpha$ ). In a fully stretched-out polypeptide chain (like Figure 1.2a) they correspond to  $\phi = \psi = 180^\circ$ . In contrast, the peptide bond cannot rotate freely as the  $\pi$ -electrons are delocalized between “ $O - C - N$ ” thus this bond has a partial double bond character and is planar. As the natural environment of proteins is water the surface of a compact protein is often determined by hydrophilic residues, whereas the hydrophobic residues are located in the core region. Therefore, the amino acid chains have to arrange and fold in such a manner that the hydrophobic residues can assemble in the core. This drives the polar backbone into the interior, where it is forced to form secondary structures with internal hydrogen bonds.<sup>6, 7</sup> The most frequently encountered regular secondary structures are thereby the  $\alpha$ -helix and the  $\beta$ -sheet. However, the formed secondary structure elements,  $\alpha$ -helix,  $\beta$ -sheet and  $\beta$ -turn have to be stabilized (Figure 1.2b). This is mainly carried out by hydrogen bonds (in Figure 1.2b red dotted lines) between the  $C=O$  (hydrogen bond acceptor) and  $N-H$  (hydrogen bond donor) of a peptide bond: for an  $\alpha$ -helix this noncovalent interaction is along the backbone whereas for a  $\beta$ -sheet these stabilizing forces are between adjacent amino acid chains. The  $\beta$ -turn holds a niche existence beside the main secondary structure elements, nevertheless it fulfills important tasks, as it changes the direction of the amino acid chains and combines  $\beta$ -sheets mostly. Again this secondary structure is stabilized by hydrogen bonds.

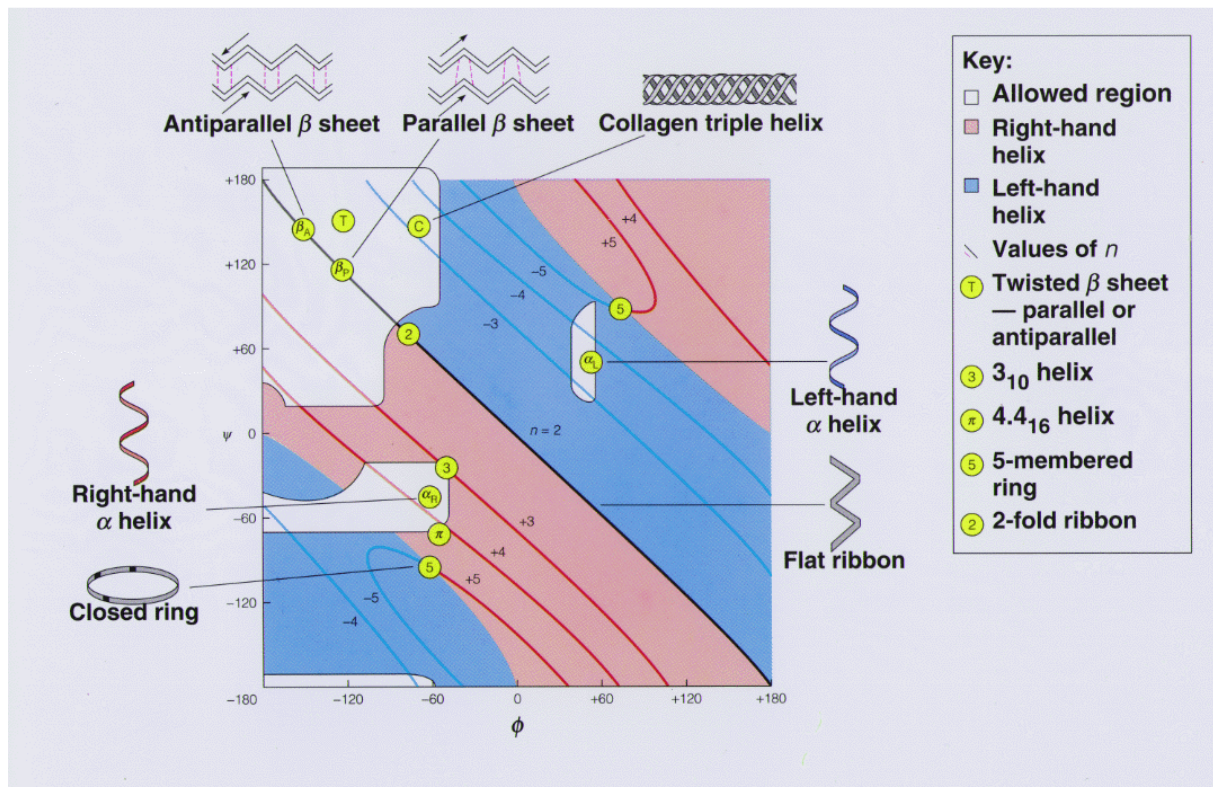


**Figure 1.3.** Ramachandran plot – a map estimating the abundance of secondary structure elements. (The Figure was taken from Biochemistry 3<sup>rd</sup> Edition)<sup>8</sup>

Which secondary structures are formed depends on the sequence of the amino acid chain and on the combination of the two torsion angles  $\phi$  and  $\psi$ . The peptide bond of the backbone is fixed and therefore not determining the secondary structure. To estimate the abundance of secondary structure elements like  $\alpha$ -helix and  $\beta$ -sheet the so called “Ramachandran-plot” can be used.<sup>9</sup> This diagram represents the potential energy distribution for the combination of the torsion angles  $\phi$  and  $\psi$  for given proteins with  $\phi$  and  $\psi$  as coordinates. It describes which structures are sterically possible and which are not. As basis for the calculation of this map serves the Pauling-Corey dimensions of a peptide bond.<sup>10,11</sup> Figure 1.3 shows a schematic representation of a Ramachandran plot using Poly-L-alanine as example. The bright areas show the regions of allowed conformations, which generally vary according to the bulkiness of the side chains. One region gives the combination of  $\phi$  and  $\psi$  for antiparallel and parallel  $\beta$ -sheets, and the collagen helix; another one shows the values for right-handed  $\alpha$ -helix and the third one marks the region for the left-handed  $\alpha$ -helix. Although the left-handed  $\alpha$ -helix is sterically allowed it does not occur as it is energetically less favored than the right-handed. The colored lines across the map correspond to helices with  $n$  residues per turn. Remarkable are the line corresponding to the flat ribbon ( $n = 2$ ) bisecting the graph and the values marking closed rings ( $n = 5$ ). In general the helix is right-handed when  $n$  is positive (rose regions) and left-handed when  $n$  is negative (blue region). Important secondary structures are highlighted by the yellow circles, their exact assignment can be taken from the legend in Figure 1.3.<sup>8</sup>

### 1.1.1.2 Major protein classes

Depending on their overall shape, i.e. secondary and tertiary structure and the resulting functional properties, proteins can be subdivided into two major classes: *fibrous* proteins and *globular* proteins. Fibrous proteins (structural proteins) are filamentous or elongated molecules with well-defined secondary structures. Most of them provide structural stiffness and rigidity together with a certain amount of elasticity thus playing structural roles in animal cells and tissues, e.g. keratins in hair and fingernails and collagen in the skin. In contrast to the extended, filamentous forms of the fibrous proteins the numerous water-soluble globular proteins (spheroproteins) not only fold into secondary structure but also into compact tertiary structures. The globular proteins play an important role in chemical processes of a cell such as synthesis, transport and metabolism. A typical example is myoglobin, it enables the efficient transport of oxygen from lungs to the respective cells. About 70 % of the secondary structure of myoglobin is found to be an  $\alpha$ -helix, this helix is bent and folded into a compact tertiary structure. A pocket within the compact structure holds the heme group, this noncovalently bounded group carries the oxygen binding site of myoglobin. The membrane proteins are a special group of globular proteins, as they are often composed of high content of hydrophobic amino acids, mainly in the embedded membrane regions. Most of the membrane proteins that span the membrane have a bundle of  $\alpha$ -helical segments. Other, like two molecules of gramicidin A, form a

pore through the membrane using a helical conformation, thus enabling the transport of  $K^+$  and  $Na^+$ . In general membrane proteins have the functions to transport substances or chemical signals through the membrane, or serve as receptors.<sup>8</sup>

### 1.1.1.3 Protein folding

Structural analysis of numerous proteins show that the polypeptide backbone folds in order to adopt a particular conformation. This process is known as protein folding. Decades ago C. Anfinsen postulated that the native structure of a protein is the thermodynamically stable structure. The protein folding pattern into three-dimensional structures (secondary and tertiary structure) is determined by the amino acid sequence (primary structure) as well as by the solution conditions and not by the kinetic folding route.<sup>12</sup> In a classical experiment Anfinsen showed that ribonuclease lost its secondary and tertiary structure in denaturing solution and after removal of the denaturant it spontaneously refold into its original structure. Remarkable thereby is that all disulfide bridges are formed in the correct places taking into account that the eight Cysteine units, building the four intrachain bonds, have 105 possible combinations. Therefore, weak interactions directing the protein folding and the correct positions of the disulfide bridges can be assumed.<sup>7</sup>

As Nature always strives for minimal energy the protein folding as thermodynamically favored process follows as well the energy minimum. This means that the overall energy change on folding must be negative ( $\Delta G < 0$ , free energy equation:  $\Delta G = \Delta H - T\Delta S$ ). On the one hand the folding leads to a loss in conformational entropy ( $\Delta S < 0$ ), as the protein collapses into its compact native state from its open denatured configurations, which works against the folding. On the other hand it gains enthalpy from the favorable noncovalent interactions ( $\Delta H \ll 0$ ). The factors for protein folding and stabilization will be discussed in the following<sup>8, 13-15</sup>:

#### - Hydrogen bonds

Protein structures are composed of secondary structures such as  $\alpha$ -helix,  $\beta$ -sheet and  $\beta$ -turn which are mainly stabilized by hydrogen bonds. Furthermore, amide protons (hydrogen bond donor) and carbonyls (hydrogen bond acceptor) which are not involved in the formation of secondary structures can interact with side chain groups forming a network of internal hydrogen bonds. As single hydrogen bonds are relatively weak in aqueous solution, the sum of all hydrogen bonds is decisive for the stability.

#### - van der Waals interactions

As the interior of a folded protein is tightly packed, a maximum contact between the side chains will take place. These weak interactions between uncharged molecular groups in a close-range are another example, that the sum of such weak forces is important for stabilization.

### - Electrostatic interactions

Some amino acids are positively or negatively charged at neutral pH and can therefore attract or repel. In the case of an electrostatic attractive force between two opposite charged groups so called salt bridges within a protein are formed.

### - Hydrophobic interactions

As mentioned previously (formation of secondary structures) the hydrophobic residues endeavor to reduce the contact to water while minimizing the surface. Therefore, amino acid chains arrange and fold in the way that the hydrophobic residues predominantly assemble in the core region of a protein whereas the hydrophilic ones are more commonly on the proteins surface. This driving force is also known as hydrophobic effect.

### - Disulfide bonds

Once the protein folding has occurred, the compact structure can be further stabilized by the formation of disulfide bonds between cysteine residues.

One major question in understanding the spontaneous folding of proteins is whether this process is a randomly folding over all possible conformations into the energetically most favored conformation. In 1968, Levinthal refuted this concept in an apparent contradiction – “Levinthal’s paradox”<sup>16, 17</sup>:

How long would such a random search of folding take? A small protein with an amino sequence containing only 100 units in a random conformation is considered. If each residue can have 10 different conformations such a protein would be able to adopt  $10^{100}$  different conformations. If the protein folds randomly, by converting one structure into another within  $10^{-13}$  seconds, it would still take  $10^{77}$  years to randomly search through all conformations. As this time scale is far away of the span of life, this randomly folding obviously cannot be the case.<sup>7</sup> This together with the observations of Anfinsen, that the refolding of a denatured protein into its native folded structure is within seconds or less<sup>18</sup>, lead to another understanding of protein folding.

Studies showed that the protein folding goes through a series of possible intermediate conformations following an ordered path, whereby different pathway models resulted. The *hierarchical model*, which has been demonstrated for a few small proteins, assumes that secondary structures are locally formed first. Then longer-range interactions, for example between two  $\alpha$ -helices, will take place followed by further nucleation until the complete folding is reached.<sup>7, 18</sup> The second model – *the molten globule model* – supposed that hydrophobic residues group together and the chain collapsed into a compact structure in which secondary and tertiary folding took place whereby the number of possible conformations is reduced. As most of the hydrophobic residues are caged in the core, the polar backbone atoms have to form hydrogen-bonded secondary structures. Due to the remaining hydrophobic residues at the surface, the proteins folds further through multiple conformations over subdomains with tertiary structures until the compact, native structure is reached.<sup>7, 8</sup>

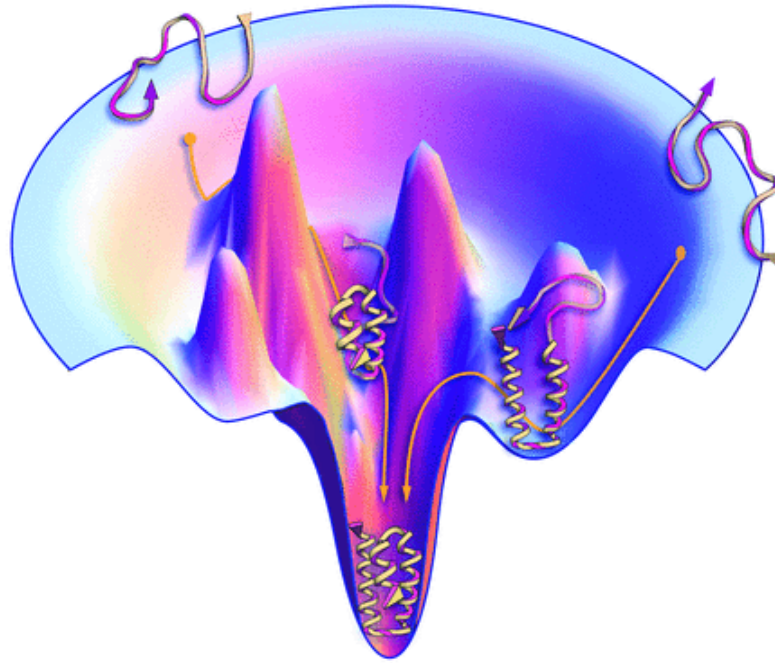


**Figure 1.4.** Protein folding following a funnel-shaped, rugged energy landscape with kinetic traps. (The Figure was taken from K. A. Dill and J. L. MacCallum)<sup>14</sup>

The reality probably lies in a combination of both models, instead of the one and only pathway, several routes can be considered. Therefore, the protein folding process can be thermodynamically viewed as funnel-shaped, rugged energy landscape with kinetic traps (Figure 1.4). The folding process starts from the top of the funnel where many high-energetic, unfolded structures rapidly collapse to more compact structures, thus the number of possible conformations decreases. Kinetic traps (moats or wells) along the sides of the funnel represent semistable intermediates which slow down the folding. At the bottom of the funnel only a few low-energy, folded structures left until the final, native structure is reached.<sup>7, 8, 12, 14</sup>

### 1.1.2 DNA assembly

Another prominent example of biomacromolecular organization is the deoxyribonucleic acid (DNA) as it stores our whole genetic information. In 1953 Watson and Crick published the structure of DNA for the first time. Thereby, they found a double helical structure consisting of two biopolymer strands.<sup>19</sup> Figure 1.5 shows the schematic representation of DNA. The DNA is composed of the phosphate-deoxyribose backbone and the four paired nucleobases thymine (T), adenine (A), guanine (G) and cytosine (C) (Figure 1.5a). These bases are defined string together along the phosphate-deoxyribose backbone and are covalently bonded to it. Between two of those complementary strands hydrogen bonds are formed. This base pairing follows defined rules given by the hydrogen bonding pattern, T – A and G – C always give a base pair respectively. Due to the base pairing between the two strands a double strand is formed. As mentioned previously the hydrophobic bases of the DNA avoid the contact with surrounding water and therefore they self-assemble into stacks whereas the backbone

## 1. Introduction

is exposed to the outside. To enlarge this effect two chains unite via hydrogen bonding between the complementary bases – building the double helix (Figure 1.5b).

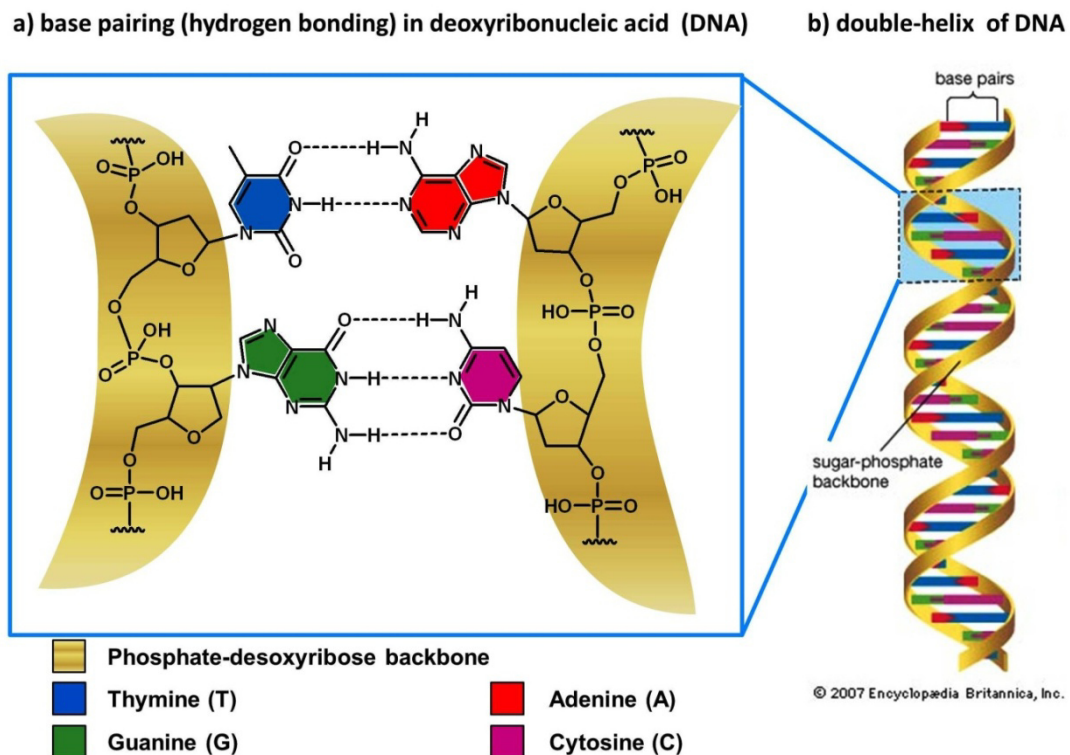


**Figure 1.5.** Schematic representation of deoxyribonucleic acid (DNA). a) base pairing (hydrogen bonding) in DNA and b) double-helix of DNA. (The drawing of the DNA double helix structure is taken from Encyclopedia Britannica)<sup>20</sup>

After the structure of the DNA was clarified scientists wanted to find the dimension of the molecule<sup>21-25</sup>, in 1981 Mandelkern *et al.* combined measurements of rotational and translational friction coefficients of rod-like DNA molecules in dilute aqueous solution given the hydrodynamic diameter of 22 to 26 Å and the length per base pair of 3.3 Å.<sup>26</sup> Indeed the individual repeating units are very small, nevertheless DNA polymers can be very large. For instance the DNA of chromosome 1 the largest human chromosome is build up from more than 220 million base pairs thus having a length of 74 mm along the chain.<sup>27</sup>

## 1.2 Foldamers

### 1.2.1 History and definition of foldamers

On the one hand scientists want to understand how Nature works, therefore complex systems are broken down into simplified models. On the other hand it is a challenge to mimic Nature and its properties whereby the field of *biomimetics* was founded. According to Webster's dictionary the concept is defined as “*The study of the formation, structure, or function of biologically produced*



*substances and materials (as enzymes or silk) and biological mechanisms and processes (as protein synthesis or photosynthesis) especially for the purpose of synthesizing similar products by artificial mechanisms which mimic natural ones.*"<sup>28</sup>

To limit the large field of biomimetics we focus on the mimicking of biomacromolecules. Going back to the example of proteins it should be possible to replace amino acid chains by synthetic chains. The design of such a peptide sequence is thereby relatively simple, but the crucial role plays the information for further assembly in such blocks.<sup>29</sup> The most interesting functions of biomacromolecules like molecular recognition, information storage and catalysis are determined by the folding into well-defined three-dimensional structures. To understand the meaning of this folding for the functions of biomacromolecules, synthetic polymer chains, which can adopt those functions by achieving ordered solution conformation, has become part of the interest. This subject is known as the field of foldamers.<sup>1, 2</sup> Gellman firstly used the term of *foldamers* for "any polymer with a strong tendency to adopt a specific compact conformation".<sup>1</sup> For proteins the term *compact* is thereby referred to the tertiary structure, which is as mentioned previously the assembly of regular repeated motifs (secondary structure) like  $\alpha$ -helices,  $\beta$ -sheets and  $\beta$ -turns. It was proposed that the first step in foldamer design must be the synthesis of new backbones with a conformational preference in solution. However, this first, simple definition opens the research field for a lot of different classes of flexible macromolecules. In 2001 Hill *et al.*<sup>2</sup> gave a more restrictive definition for foldamers. They defined foldamers as "any oligomer that folds into a conformationally ordered state in solution, the structures of which are stabilized by a collection of noncovalent interactions between nonadjacent monomer units." A uniform definition of the term *foldamers* is still an open issue. It is mainly used to describe artificial oligomers and polymers, which spontaneously and reversibly adopt defined secondary structures due to a sum of folding forces.

### 1.2.2 Driving forces for folding and suitable folded structures

In general the folding and self-assembly is unusual for synthetic oligomers and polymers, as they prefer in melt or in solution a random coil conformation, thus a lot of unfolded states exist. For building up compact conformations, e.g. folded structures, driving forces providing the folding are necessary. Firstly, steric factors like bulky groups or rigid elements can direct the foldamer into preferred conformations. In addition, similar driving forces as known for proteins (see 1.1.1.3) contribute the folding. These are as mentioned previously the hydrophobic effect, the tendency of hydrophobic residues to assemble in polar/aqueous solution, and the noncovalent interactions, which are known in chemistry as supramolecular interactions<sup>30, 31</sup> Such supramolecular interactions are hydrogen bonding, van der Waals interactions,  $\pi$ - $\pi$  stacking,  $\pi$ -cation and  $\pi$ -anion interactions, electrostatic interactions (attractive or repulsive interactions like ion-ion, ion-dipole, dipole-dipole) and metal-donor atom coordination. Again hydrogen bonding is the *key interaction* for most

## 1. Introduction

assemblies, which is in good agreement with the stabilization of natural assemblies (e.g. proteins, DNA).<sup>32</sup> As single supramolecular interactions are mostly relatively weak in comparison to covalent bonds (8 kJ/mol vs. 400 kJ/mol) the combination of a bundle of different forces is suitable, thus allowing the link of diverse strengths and dynamics.<sup>33</sup>

For the design of the foldamers Hill *et al.* made clear, that such oligomeric structures are only able to build up simple secondary structures as helices or sheets due to their size. Thus, for the folding into higher assemblies the tertiary structure larger molecules like polymers will be necessary. As the understanding and evidence of tertiary structures of synthesized foldamers is very complex, they focused on the understanding of the properties of known foldamers with various different secondary structures.<sup>2</sup>

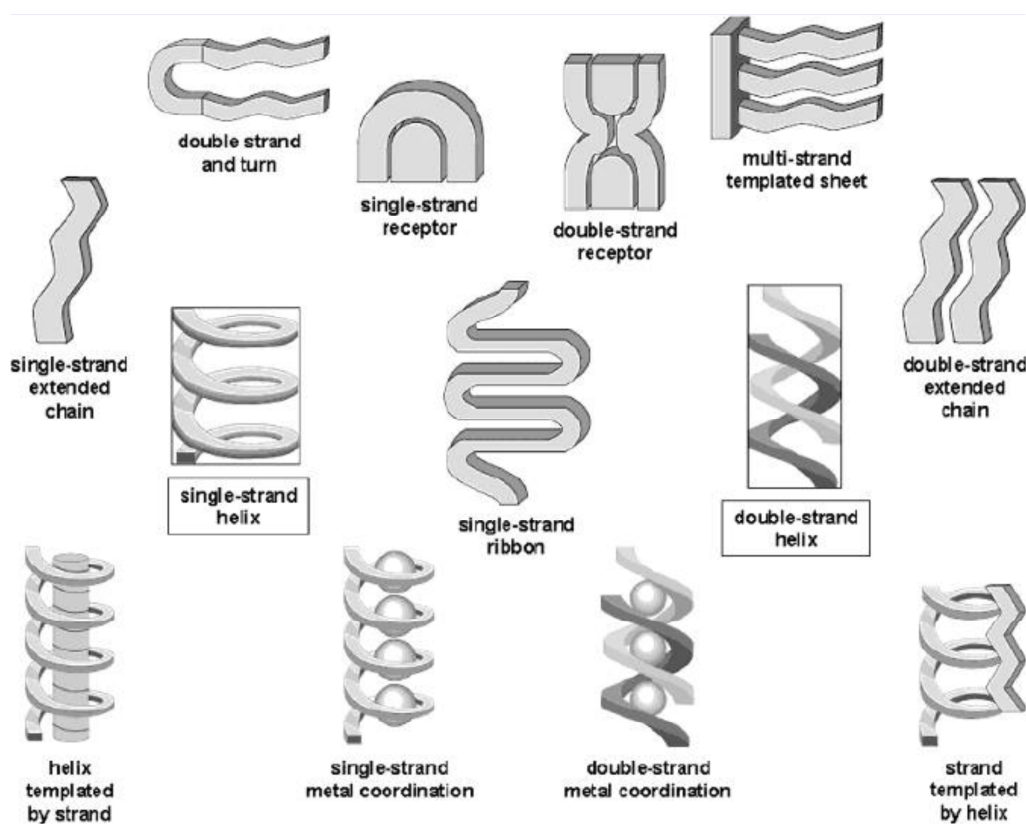


**Figure 1.6.** Schematic representation of different types of foldamer secondary structures (taken from literature<sup>2</sup>).

Beside the already shown native, folded structures like  $\alpha$ -helix (here framed: single-strand helix) and double-strand helix (also framed, e.g. DNA) other folding topologies can be adopted, depending on the design of the foldamers (e.g. choice of structure of the repeating unit) and the interplay of the different folding forces (Figure 1.6). As it can be seen single-strands and single-strand helical conformations build the basic folding motives. They can further assemble into higher and more stable structures like double-strand helices or double-strands. Also the combination of the two basic types like a helix-templated strand is possible. Moreover, complexations of metal ions such as single-strand metal

coordination lead to folded structures using the host-guest system, which is known from supramolecular chemistry. Those systems (e.g. helix-templated strand, single-strand metal coordination), which only fold due to the assembly of two or more molecules can be defined as *foldamer hybrids*.<sup>34</sup>

### 1.2.3 Foldamer classification

As the field of foldamers is wide Hill *et al.*<sup>2</sup> classified foldamers into two main groups: a) single-stranded foldamers (peptidomimetics and their abiotic analogues) that only fold and b) multiple-stranded foldamers (nucleotidomimetic foldamers and multistranded abiotic foldamers), which associate and fold. In 2007 Goodman *et al.* sorted foldamers in two general molecular classes, the “aliphatic” foldamers and the “aromatic” foldamers determined by the presence or absence of aromatic units.<sup>35</sup> The latter typology I will use in the following in addition with a third class – the foldable polymers.

#### 1.2.3.1 Peptidomimetic foldamers – aliphatic foldamers

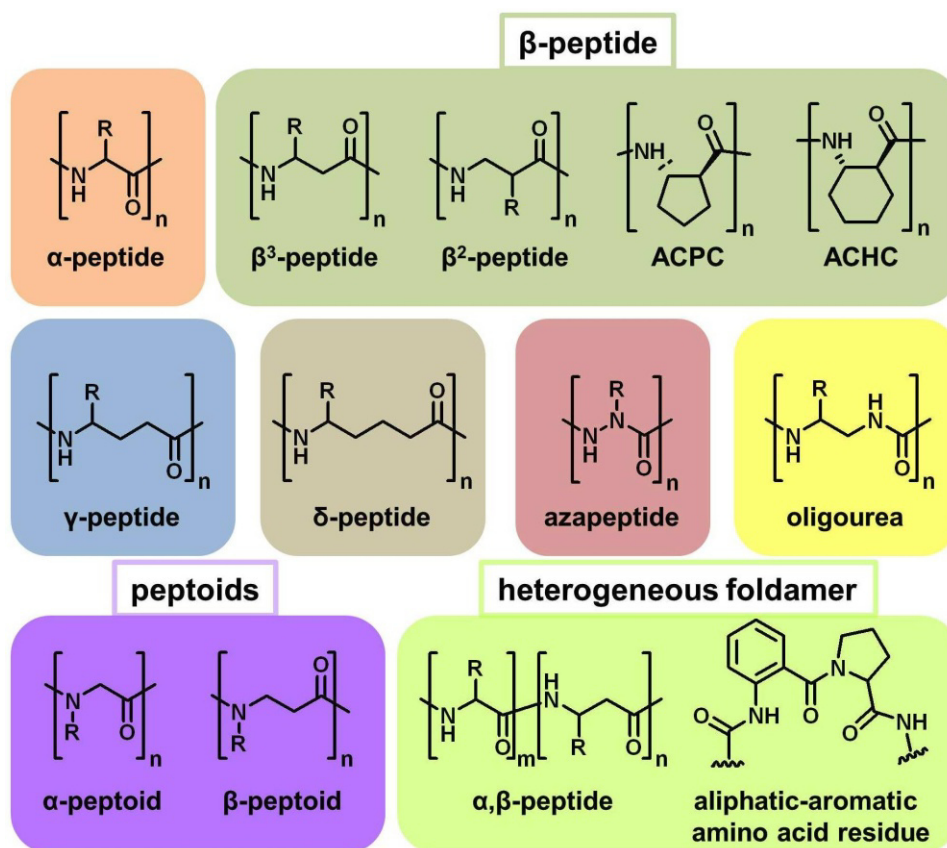
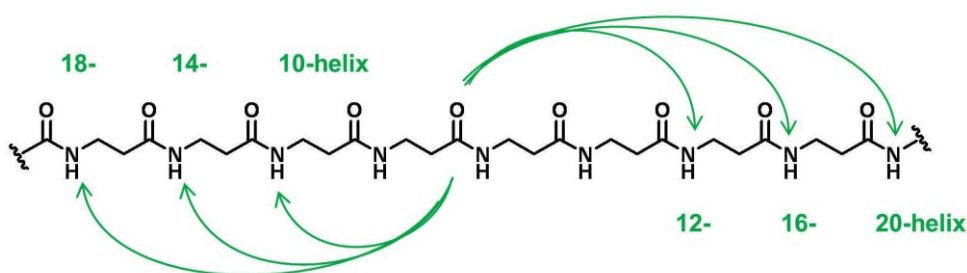


Figure 1.7. Examples of peptidomimetic foldamers.

## 1. Introduction

As one would suggest the class of peptidomimetic foldamers is highly oriented towards their parent structures – the polypeptides. Peptidomimetic foldamers are synthesized in order to replace peptide substrates of enzymes or peptide ligands of protein receptors. Therefore, “*peptidomimetic strategies include the modification of amino acid side chains, the introduction of constraints to fix the location of different parts of the molecule, the development of templates that induce or stabilize secondary structures of short chains, the creation of scaffolds that direct side-chain elements to specific locations, and the modification of the peptide backbone.*”<sup>2</sup> Figure 1.7 shows examples of peptidomimetic foldamers. They are aliphatic nature and their saturated carbon chains are separating amide or urea groups. Moreover, these classes are kinetically and thermodynamically stable, and are able to mimic some functions of bioactive peptides.<sup>36</sup> The  $\alpha$ -peptides occur naturally, however the  $\beta$ -peptides are more prominent and more thoroughly characterized.<sup>1, 37-39</sup> In comparison to  $\alpha$ -peptides they have an extra methylene group between the amide groups, the side chain can be thereby in vicinity to the amine ( $\beta^3$ ) or in vicinity to the carbonyl group ( $\beta^2$ ). Rigidified  $\beta$ -peptides where the saturated carbon atoms are fixed in a cyclopentyl ring (*trans*-2-aminocyclopentanecarboxylic acid residue, *trans*-ACPC) or in a cyclohexyl ring (*trans*-2-aminocyclohexanecarboxylic acid residue, *trans*-ACHC) are also known.<sup>1</sup>  $\beta$ -peptides are able to adopt a variety of structures, including helices, turns and sheet-like structures.<sup>35, 36</sup>



**Figure 1.8.** Possible intramolecular H-bonding in  $\beta$ -peptides resulting in helical folding.

Gellman and Hill proposed 6 possible helices available to  $\beta$ -peptides based on intramolecular H-bond arrangements; 10-, 12-, 14-, 16-, 18- and 20-helix, whereby the numeral defines the H-bonded ring size (Figure 1.8).<sup>1, 2</sup> However, five distinct helices using  $\beta$ -peptides were found: a 14-, a 12-, a 10-, the 12/10 and an 8-helix.<sup>40</sup> Thereby, the 14-helix is favored from constrained residues like ACHC or  $\gamma$ -branched  $\beta^3$ -amino acids (e.g.  $\beta^3$ hVal). The  $\beta$ -peptidic 12-helix is mostly formed from constrained cyclic residues e.g. ACPC and pyrrolidine as well as from heptamers with up to two  $\beta^3$  or  $\beta^2$  residues. Using alternating  $\beta^2$ - and  $\beta^3$ -monosubstituted residues a 10/12-helix conformation consisting of an intertwined network of 10- and 12-membered hydrogen-bonded rings were formed ( $\beta^3/\beta^2$ -sequence giving 12/10 helix respectively). Contrary to the previous conformations the 10-helix and the 8-helix have not been observed for oligomers with homologated proteinogenic amino acids, forming an 8-helix is for example known from (2R,3S)-2-hydroxy-3-aminocarboxylic acid moieties with Val, Ala

## 1. Introduction

and Leu side chains.<sup>40, 41</sup>  $\gamma$ -peptides prefer helix and turn-conformations, for example  $\gamma^4$ -peptides form a 14-helix.<sup>2, 40-42</sup>

Whereas in peptides the side chain is connected to the  $\alpha$ -carbon, the side chain in peptoids is linked to the nitrogen of the backbone, thus they are known as poly-N-substituted glycine.<sup>41</sup> As chiral centers in the backbone are missing and the amide protons are substituted by mostly aliphatic side chains backbone-mediated hydrogen bonding is impossible, thus backbone handedness is not given.<sup>36</sup> Nevertheless, these foldamers prefer helical conformations, moreover their helical handedness originates from the  $\alpha$ -chiral, aliphatic and aromatic side chains. For example *N*-(1-cyclohexylethyl)glycine pentamer shows a helix with cis-amide bonds,  $\sim 3$  residues per turn and a pitch of  $\sim 6.7$  Å.<sup>43</sup> Beside the helical conformation peptoid nanosheets have been synthesized by parallel all-*trans* peptoids oligomers bearing 2-aminoethyl and 2-carboxyethyl side chains. These structures mimic very well  $\beta$ -sheet secondary structures, thus enabling the application in functional engineering and as robust lipid-membrane analogs.<sup>44, 45</sup> Furthermore, cyclic peptoids are synthesized to develop long-range constraints to direct oligomer conformation, thus controlling the overall topological characteristics. Such cyclic foldamers promise binding interactions with targeted biomolecules, molecular recognition, catalytic activities and the capacity for complex self-assembly.<sup>46</sup>

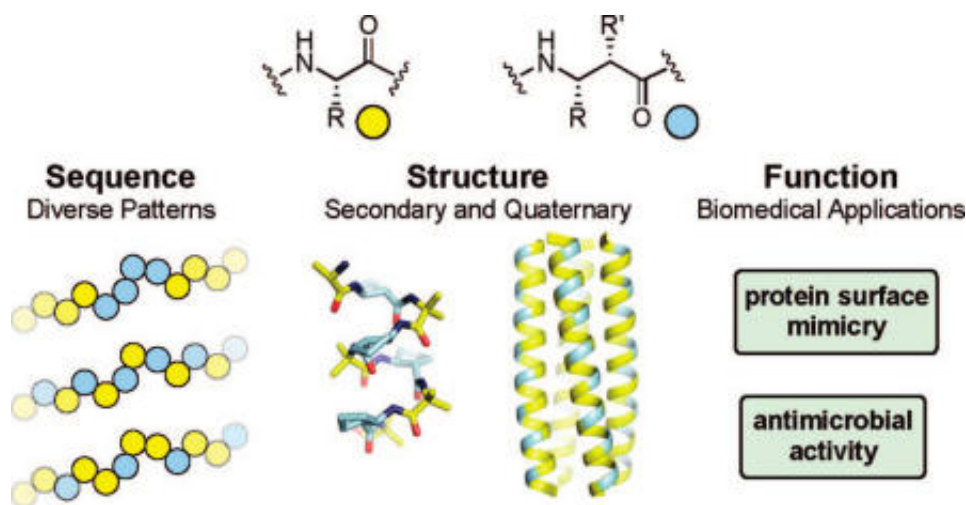


**Figure 1.9.** Foldamers with heterogeneous backbones. a) different combinations of  $\alpha$ - and  $\beta$ -peptides forming  $\alpha,\beta$ -peptides resulting in b) secondary and quaternary structure formation and c) therefore different biomedical applications. (Figure was taken from Horne and Gellman<sup>47</sup>)

Although the previous classes already showed a great structural diversity, mimicking higher ordered structures and functions of biomolecules is rare. A general folding code based on the chemical and physical rules that control the formation of protein structures is not found. Moreover, the design or even the prediction of a folded protein is still challenging.<sup>48</sup> Unlike to this previous classes based on homogenous backbones the single classes can be mixed and combined resulting in heterogeneous foldamers (Figure 1.7), thus expanding the structural and functional repertoire of foldamers. One of the first combinations was for example  $\alpha/\beta$ -peptide foldamers, whereby the single classes can be used

## 1. Introduction

in blocks forming hybrid oligomers or more or less statistically (Figure 1.9). Thereby, in addition to the previously found secondary structures, tertiary as well as helix bundle quaternary structure formations were found.<sup>47, 49</sup> Likewise,  $\alpha/\gamma$ - and  $\beta/\gamma$ -hybrids have been synthesized showing different conformations like helices;  $\beta$ -sheet like folding; twisted, double reverse turn or  $C_{13}$ -turn.<sup>42, 50</sup> The use of heterogeneous foldamers with higher ordered structure promise the mimicking of larger surface structures of proteins and could be efficient inhibitors of protein-protein interactions involved in many diseases.<sup>49</sup> Further biological applications can be their interaction with biological systems for recognition and inhibition of difficult targets like bacterial cell membrane,<sup>51, 52</sup> protein-RNA interactions,<sup>53</sup> enzymes<sup>54</sup> or even receptors.<sup>50</sup> Beside the combination of  $\alpha$ ,  $\beta$  and  $\gamma$ -peptides heterogeneous foldamers can be formed from aliphatic-aromatic acid building blocks thus enlarging the structural pool.<sup>55, 56</sup> These included reverse turn structures<sup>57-60</sup> e.g. based on anthranilic acid-proline conjugate (Ant-Pro, structure see Figure 1.7)<sup>61</sup>, helices<sup>62, 63</sup>, sheet structures<sup>64-66</sup> and strand mimics<sup>67-69</sup>. As before due to the number of different folding structures several applications are possible like the use as molecular receptors, chemical sensors and actuators and as catalysts.<sup>56</sup> Due to the use of aromatic foldamer units this class takes up an intermediate position between the aliphatic peptidomimetic foldamers and aromatic foldamers.

### 1.2.3.2 Aromatic foldamers

The previously described peptidomimetic foldamers are based on a variation of parent chain molecules, which are aliphatic nature. Moreover, the resulting higher structures, mainly secondary structures, are formed and stabilized by hydrogen-bonding. Thereby the introduction of rigidified, cyclic units promotes and enhanced the helical conformation. Due to the use of more rigid, aromatic units, folding into helices and sheets is introduced and stabilized by specific geometric constraints as well as  $\pi$ - $\pi$  stacking additionally to hydrogen bonding and hydrophobic interactions.<sup>2, 35</sup> Figure 1.10 shows a small selection of aromatic foldamers.

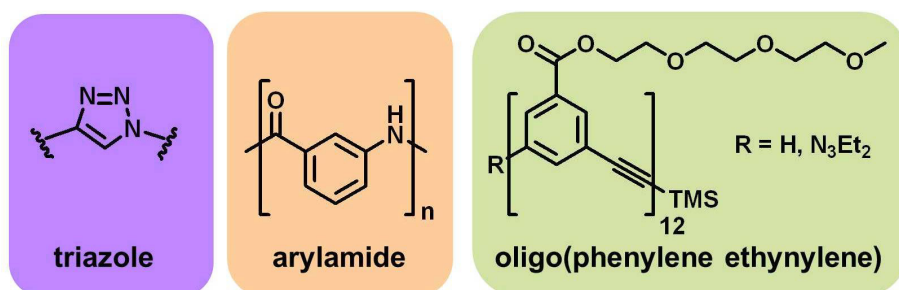


**Figure 1.10.** Examples of single chain foldamers.

The first class, the 1,4-disubstituted-1,2,3-triazoles are heteroaromatic compounds and can be formed by copper mediated azide/alkyne-“click”-reaction (CuAAC, see chapter 4.3.1.1). A direct comparison

## 1. Introduction

between amide bond and 1,4-disubstituted-1,2,3-triazole shows their structural (relative planarity) and electronic similarity, therefore amide to triazole substitution is possible. For this reason it could be count to the peptidomimetic foldamers, too. As this unit is resistant to enzymatic degradation, hydrolysis and oxidation it is attractive for replacing more labile moieties in biological compounds.<sup>70</sup> Furthermore, the via CuAAC formed 1,4-disubstituted-1,2,3-triazoles were used to generate double-stranded DNA by covalently crosslinking of complementary strands<sup>71, 72</sup> as well as they generated and stabilized helix bundles<sup>73</sup> and  $\beta$ -turn mimetics<sup>74, 75</sup>. Another group, the arylamides and in 3-substituted arylamides, form local hydrogen bonds e.g. hydrogen bonds with neighboring amides and therefore self assemble into helices<sup>76, 77</sup> or linear foldamer conformations<sup>78-80</sup>. The formation of  $\beta$ -sheet foldamers due to  $\pi$ - $\pi$  aromatic stacking when using aromatic oligoamides was reported, too.<sup>81</sup> Foldamers based on arylamides show antimicrobial activity<sup>80, 82</sup> when inserted into bilayer membranes as well as they can be applied as preorganized receptors<sup>83</sup>. The third group, the arylene ethynyls e.g. phenylene ethynylene oligomers<sup>84</sup> (Figure 1.10) are composed of hydrophobic ring systems with polar side chains, thus the folding is driven by solvophobic and  $\pi$ -stacking interactions. Due to the design of this foldamer the rotational freedom is reduced and is only given for each triple bond, thus in apolar solvents unfolded, flexible random coils exist. An increase in the solvent polarity leads to a helical conformation in order to reduce the unfavorable contact to the solvent.<sup>15, 85, 86</sup>

### 1.2.3.3 Foldable Polymers

Beside all the previously reported foldamers (peptidomimetic, aliphatic foldamers and (hetero)aromatic foldamers) based on oligomeric structures, single chain folding of synthetic polymers arised in the last years. The single chain folding can be introduced via covalent and noncovalent interactions resulting in polymeric nanoparticles and biomacromolecules mimicry.<sup>87</sup> In the following I will focus on the single chain folding of synthetic polymers similar to biomacromolecules due to noncovalent interactions.

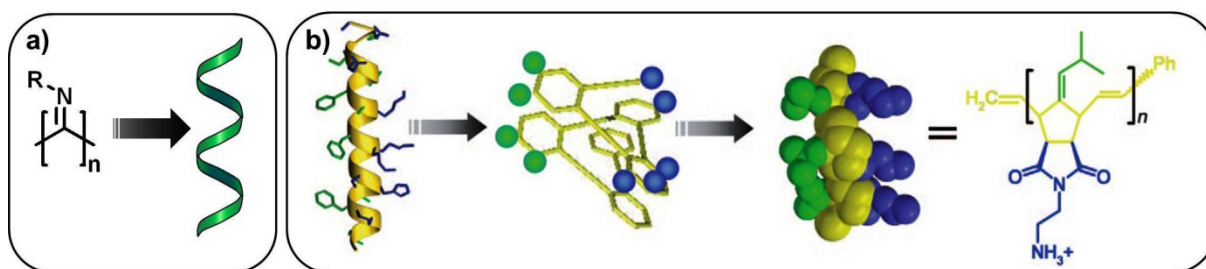


**Figure 1.11.** Folding of synthetic polymers into helical conformation. (Figure 1.11b was taken from Tew and Lienkamp<sup>88</sup>)

Figure 1.11 shows synthetic polymers, which fold into helical conformations. One of the first helical polymers was polyisocyanide bearing bulky substituents (Figure 1.11a). The folding into the helical

## 1. Introduction

conformation is thereby the sum of repulsive electronic interactions of the nitrogen lone pair electrons and the steric repulsion of the bulky substituents.<sup>89, 90</sup> Other prominent examples of helical polymers are polyacetylenes, polyisocyanates, polycarbodiimides and polymethacrylates.<sup>91</sup> Additional interesting helical polymers are polynorbornene-imides, Figure 1.11b shows one example. Based on the knowledge of natural antimicrobial peptides (AMPs) synthetic mimics of antimicrobial peptides (SMAMPs) are synthesized (Figure 1.11b from left to right). Studies showed that the AMPs are facially amphiphilic molecules with hydrophilic, positively charged groups at one side (blue) and hydrophobic groups at the opposite side (green), which direct the conformation of the backbone (yellow) and therefore the helical conformation of the molecule.<sup>88</sup>

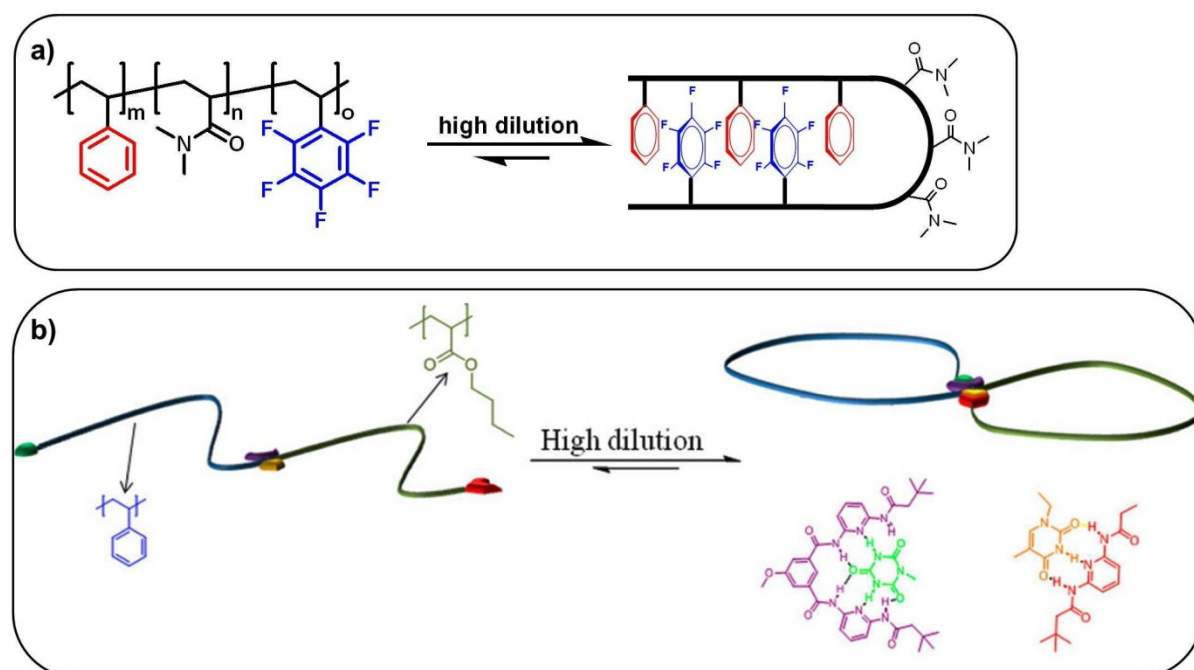


**Figure 1.12.** Schematic representation of single-chain folding induced by high dilution. (Figure 1.12a was reproduced according to Weck *et al.*<sup>92</sup>, Figure 1.12b was taken from Barner-Kowollik *et al.*<sup>93</sup>)

Beside the folding into helical conformations other folding structures are known. Figure 1.12 presents polymers, which assemble from their open, unfolded structure to the regular, folded conformation after high dilution. Weck *et al.*<sup>92</sup> synthesized triblock copolymers containing styrene (electron-rich), *N,N*-dimethylacrylamide and 2,3,4,5,6-pentafluorostyrene (electron-deficient) as blocks (Figure 1.12a). As a result of high dilution, this single-chain system folded into  $\beta$ -hairpin mimic, due to quadrupole interactions between electron-rich and electron-deficient blocks. Another interesting example, mimicking simple natural protein structures by single-chain folding, was the work of Barner-Kowollik *et al.*<sup>93</sup>. The synthesized diblock copolymer, containing styrene and *n*-butyl acrylate blocks with orthogonal hydrogen bonding elements, folds under high dilution into a closed ring. This process is reversible, as the driving force for the self-association is the noncovalent interaction between the orthogonal recognition motifs (thymine-diaminopyridine and cyanuric acid-Hamilton wedge).



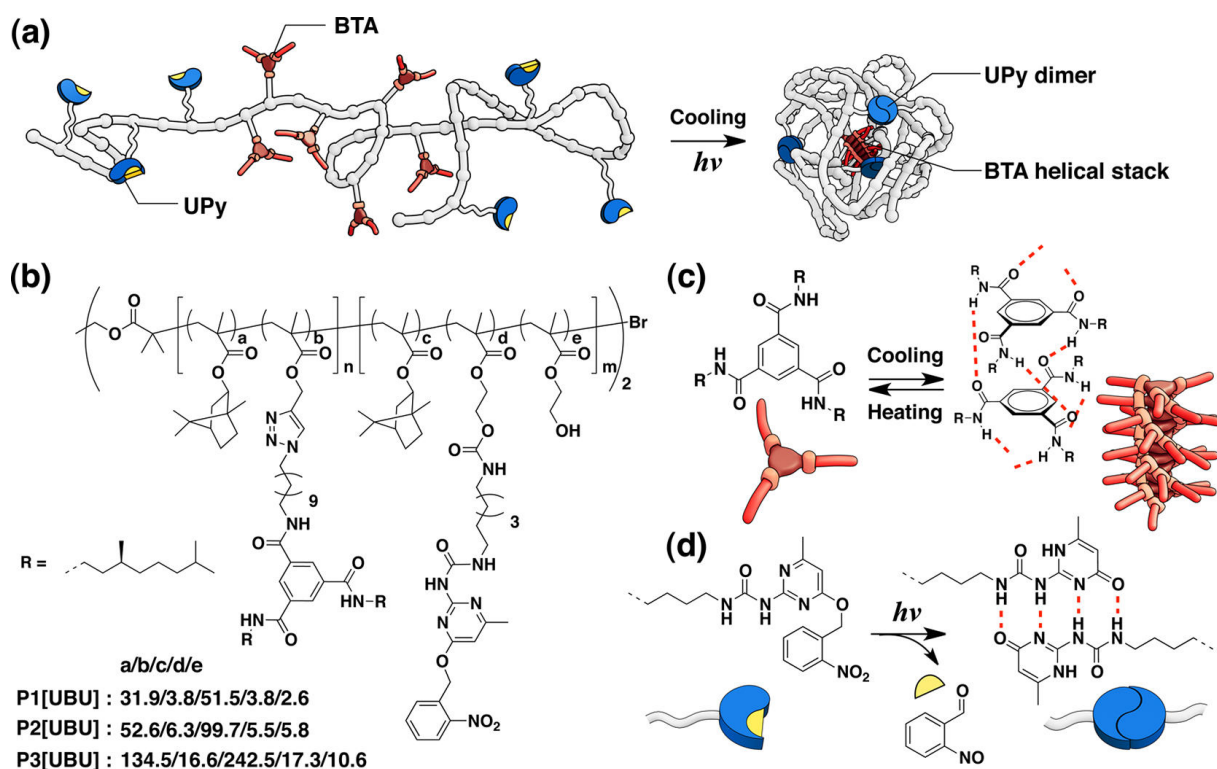


**Figure 1.13.** a) Single-chain folding of a triblock copolymer with BTA and UPy moieties. b) chemical structure of the triblock copolymers. c) helical self-assembly of chiral BTAs. d) photoinduced dimerization of *o*-nitrobenzyl-protected UPys. (Figure was taken from Meijer *et al.*<sup>94</sup>)

Up to here the previously examples described the mimicry of simple natural protein structures, which fold due to different driving forces like noncovalent interactions, steric repulsion and in some cases high dilution. The last example in this section mimics a more complex, compact conformation similar to natural proteins (Figure 1.13). Therefore, Meijer *et al.*<sup>94</sup> synthesized ABA triblock copolymers that fold into a compact conformation cross-linked via orthogonal self-assembly (Figure 1.13a). The ABA triblock copolymer consist of postfunctionalized polymethacrylate as backbone with block A having *o*-nitrobenzyl-protected 2-ureidopyrimidone (UPy) moieties and block B bearing benzene-1,3,5-tricaroxamide (BTA) moieties. Under cooling the BTA units self-assemble into helical stacks through intramolecular threefold-symmetric hydrogen-bonding. Further, the UV introduced UPy deprotection leads to a collapse of the open, partially folded polymer into the compact protein-like conformation, which is stabilized by the intramolecular UPy association. Therefore orthogonally self-assembled domains were obtained mimicking  $\alpha$ -helix and  $\beta$ -sheet.

#### 1.2.4 Foldamers and their interactions with membranes

As it could be seen a big effort towards foldamers was undertaken in the last years to understand, but even more to mimic biomolecules and their functions. In the following I will focus on foldamers and their interactions with membranes as this will be part of my own work.

### 1.2.4.1 Folding of oligocholate

As important features membrane proteins have to transport nutrients in and wastes out. Therefore, such biofoldamers have to work in different polar environments like water or in/on lipid membranes. However, most of the foldamers in literature fold in homogeneous solution and in the solid state.<sup>1, 2, 35</sup> Thus the groups Zhang and Zhao reported on the synthesis of oligocholate foldamers and their use as transporters across lipid membranes.<sup>95-100</sup> Initially Cho and Zhang<sup>95</sup> investigated the conformations of different functionalized oligocholate foldamers in homogeneous solution (Figure 1.14a), ionic and nonionic micelles and lipid bilayers. They found out that the folding in homogeneous solutions is dominated by the preferential solvation, which is a variation of solvophobic interactions. Instead of aggregation to minimize the exposition to the surrounding solvent, direct aggregation of cholates is not possible. Due to their rigid backbone it folds into a helix. Thereby the polar solvent (MeOH) is microphase separated from the bulk inside the cavity of the helix, where it acts as a bridge to hydrogen-bond with the hydroxyl and amide groups favoring the helical folding.<sup>95</sup>

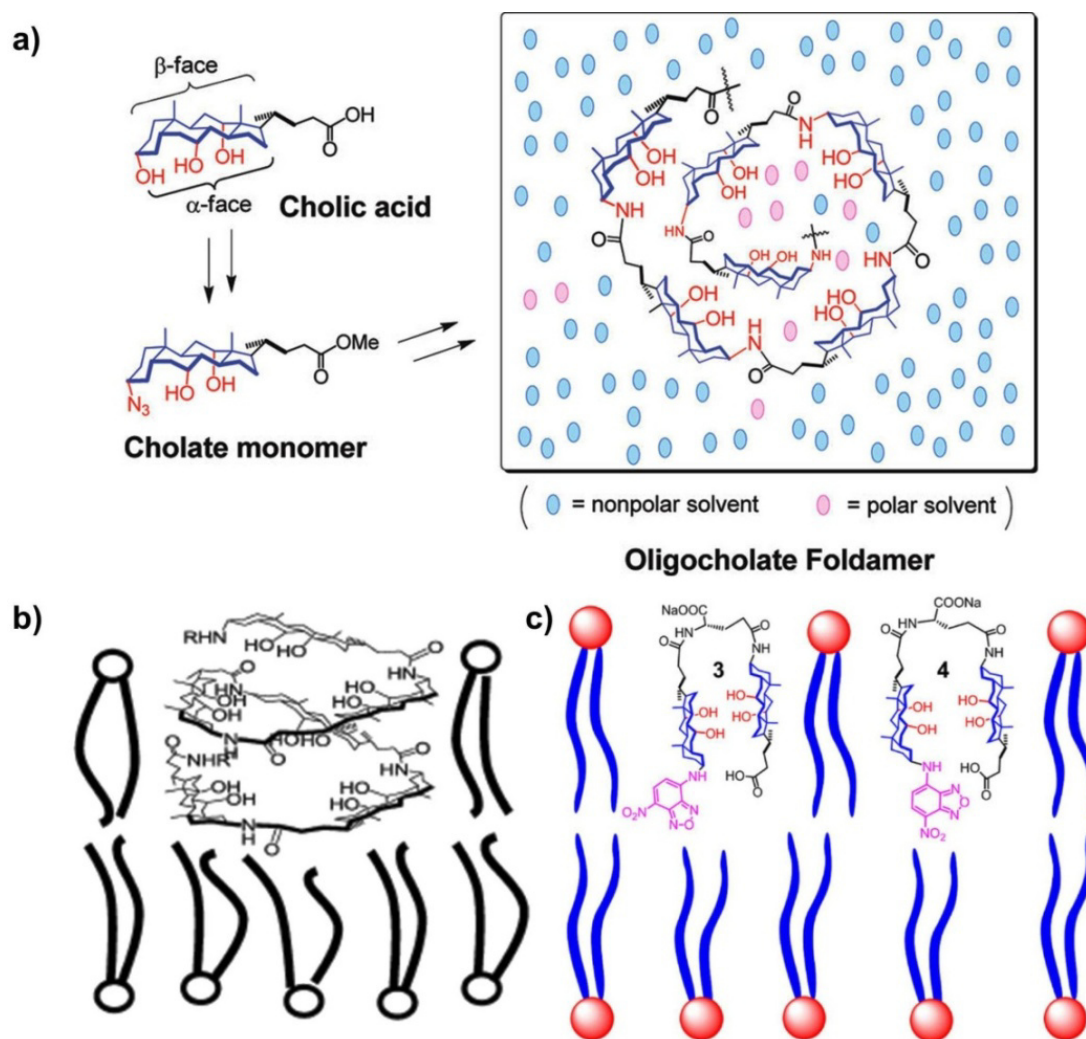


**Figure 1.14.** Folding of oligocholates. a) Solvophobic folding in a mixture of polar and nonpolar solvents, b) folding in a lipid bilayer and c) possible conformations of the folded 3 and 4 in the lipid bilayer. (Pictures were taken from literature<sup>95, 96, 100</sup>)

Based on this knowledge Zhang and Zhao<sup>96</sup> designed pyrene-labeled oligocholate foldamers via azide/alkyne-“click”-reaction and investigated their ability to transport hydrophilic molecules across lipid bilayers using fluorescence and UV/vis spectroscopy. It turns out that a poor folding in solution results in faster transport in the membranes, thus making oligocholates attractive as membrane protein mimics. The unexpected correlation for the oligocholate carriers they tried to explain by the more readily unfolding of less capable folders making the release of the guest easier.<sup>96</sup> Driven by the promising applications of oligocholates in delivery and controlled release they investigated the influence of the rigidity of their foldamers onto the folding and the conformational stability. The results showed that the conformation of an intermediate rigidity is highly sensitive to its microenvironment, thus making it a good candidate as transporter.<sup>97</sup> The synthesis of flexible oligocholates enables the transport of different sized hydrophilic molecules across lipid bilayers, whereby their transport mechanism is strongly influenced by the guest.<sup>99</sup> Beside the use of oligocholates where multiple cholates build one chain and fold in lipid membranes into helical conformation (Figure 1.14b) the use of bischolate foldamers leads to a turn like folding when incorporated into bilayer membranes (Figure 1.14c). Furthermore, these conformationally switchable water-soluble fluorescent bischolate foldamers act as membrane-curvature sensors, what is normally known for proteins and protein-derived peptides only. Thereby, each component of the bischolate perform a certain task: the amphiphilic  $\beta$ -cholate (blue-red) interacts with water and the membrane, the glutamic acid part (black) enables the necessary flexibility for the intramolecular interaction of the two cholates and the fluorophore (magenta) reports the switch from the water-soluble state to the membrane-bound state in dependence on the curvature.<sup>100</sup>

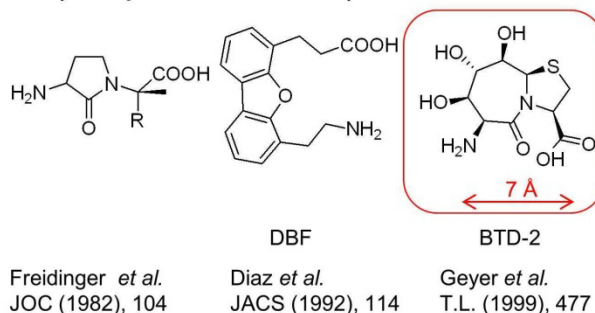
### 1.2.4.2 Turn mimetics

As mentioned previously turns are one of the secondary structure elements in proteins. There they fulfill important tasks, as they mostly combine  $\beta$ -sheets and change the direction of the amino acid chains, this refolding leads to antiparallel  $\beta$ -sheet formation. The “ $\beta$ -turn” is the most common turn beside “ $\alpha$ -turn” and “ $\gamma$ -turn”. They differ according to the number of amino acid chains which are forming the loop. In Figure 1.15 a natural  $\beta$ -turn is schematically represented, analogously to the amino acid sequence (primary structure, Figure 1.2a) the involved amino acid chains are counted as  $i$ ,  $i+1$  etc. The  $\beta$ -turn consist of four amino acids, whereby between the carboxyl group of the first amino acid and the amine function of the fourth amino acid ( $i$  and  $i+3$ ) a hydrogen bond is formed, thus this bridging is known as  $4 \rightarrow 1$  linkage with an end-to-end distance up to  $5.2 \text{ \AA}$ .<sup>102</sup> Corresponding to this for  $\alpha$ -turns  $5 \rightarrow 1$  linkages are characteristic and for  $\gamma$ -turns  $3 \rightarrow 1$ , whereby latter is due the small size found in very tight regions.<sup>6, 101</sup> As natural turns are stabilized by hydrogen bonding their size and thus the spatial end-to-end distance is limited to this value as their strength and range depends on this noncovalent force. Beside hydrogen bonding other noncovalent interactions can be used for

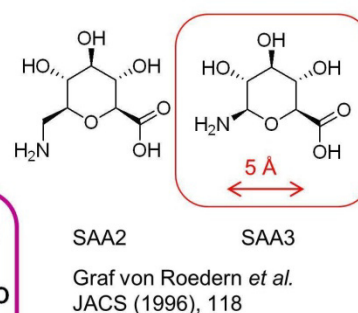
## 1. Introduction

stabilization in order to mimic turns. Furthermore, the basic structure of  $\beta$ -turn mimetics is mostly formed from medium ring heterocycles (e.g. cyclopeptides<sup>103</sup>), medium ring bicyclic scaffolds, macrocyclic turns,<sup>101</sup> and aromatic compounds<sup>104</sup>.

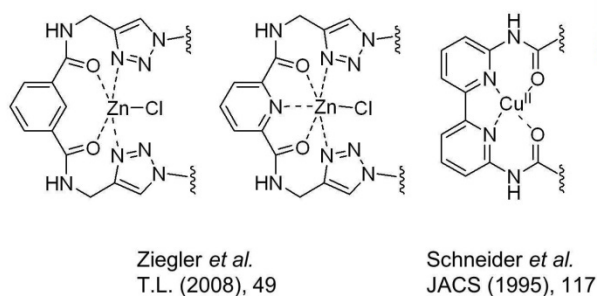
### 1) Purely geometrically constrained $\beta$ -turns (fixed $\beta$ -turn conformation)



### 2) Carbohydrate based $\beta$ -turns



### 3) Supramolecular induced $\beta$ -turns via addition of salts



### 4) Photoswitchable $\beta$ -turn

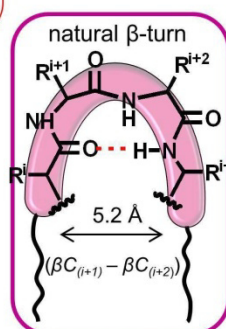
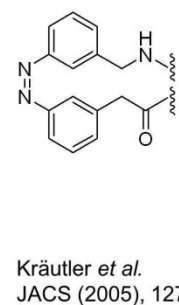


**Figure 1.15.** Selection of  $\beta$ -turn mimetics and in the center the dimensions of a natural  $\beta$ -turn. 1) Purely geometrically constrained  $\beta$ -turns with a fixed  $\beta$ -turn conformation; 2) Carbohydrate based  $\beta$ -turns, 3) Supramolecular induced  $\beta$ -turns via “click”-reaction and/or addition of salts for stabilization and 4) Photoswitchable  $\beta$ -turn.<sup>105-111</sup>

Figure 1.15 shows a small selection of  $\beta$ -turn mimetics and their classification according to their structural features. The first group builds the purely geometrically constrained  $\beta$ -turns, which have a fixed  $\beta$ -turn conformation and therefore do not need extra stabilization via supramolecular interactions. The so called Freidinger Lactam was the first  $\beta$ -turn mimetics with a restricted  $\beta$ -turn conformation synthesized by Freidinger *et al.*<sup>105, 112</sup> according to a lactam derivative of leucine. They successfully demonstrated the incorporation of a conformational constraint dipeptide unit into linear bioactive peptides and suggested future applications due to the inference of biological conformation and increased biological potency. Another example out of this group is the  $\beta$ -turn dipeptide BTD-2 from Geyer *et al.*<sup>107, 113, 114</sup> This purely geometrically constrained  $\beta$ -turn has a fixed conformation. The distance between the amine functionality on the one side and the carboxylic moiety on the other side is according to the X-ray structure only 7 Å.<sup>115</sup> Moreover, its polyol structure is known for membrane affinity as well as interaction with membranes.<sup>116</sup> Therefore, this highlighted  $\beta$ -turn mimetics will be analogously used in my work.

## 1. Introduction

---

The second group corresponds to the carbohydrate based  $\beta$ -turn mimetics. The sugar amino acids (SAA) 2 and 3 were synthesized and designed by Graf von Roedern *et al.* as new non-peptide peptidomimetics utilizing carbohydrates as peptide building blocks.<sup>108</sup> The only structural difference between these both mimetics is the inserted methylene group next to the amine functionality in SAA-2, making this a flexible turn. Whereas, SAA-3 is due to its structural constraint conformation known to be a stable  $\beta$ -turn.<sup>108</sup> Furthermore, its calculated distance between the amine functionality on the one side and the carboxylic moiety on the other side is only 5 Å,<sup>117</sup> which is similar to a natural  $\beta$ -turn. Similar to BTD-2 it is a polyol and therefore it should have membrane activities as well, this together with other structural features makes this highlighted mimetics another promising candidate for the future application in my work.

In contrast to the previous already fixed  $\beta$ -turns, the third group represents supramolecular induced  $\beta$ -turns via addition of salts for stabilization. Ziegler *et al.*<sup>109</sup> synthesized isophthalamide and pyridine-2,6-dicarboxamide ligands triazole-linked to two sugar units via Cu<sup>I</sup> mediated azide/alkyne-“click”-reaction. After addition of ZnCl<sub>2</sub> stable tetra and penta-coordinated complexes were formed fixing the turn formation.<sup>118</sup> Schneider and Kelly investigated the nucleation of  $\beta$ -sheet structures.<sup>110</sup> As  $\beta$ -turn unit they used a bipyridine-based amino acid due to the addition of Cu<sup>II</sup> they induced a conformational change from transoid to cisoid, thus the formed  $\beta$ -turn nucleates a  $\beta$ -sheet structure.

Last but not least the fourth group - the photoswitchable  $\beta$ -turns - with azobenzene as representative. Kräutler *et al.*<sup>111</sup> investigated the replacement of natural  $\beta$ -turns by a diazobenzene unit. Diazobenzene exist in two conformations, the thermodynamically more stable *trans*-isomer and the *cis*-isomer. Latter, is generated by UV-irradiation at 365 nm giving the turn structure. If this  $\beta$ -turn is not further stabilized it spontaneously reverts back via thermal isomerization within seconds to days depending on the functionalization at the phenyl rings.<sup>111</sup> Based on this work other working groups were inspired for further applications of this photoswitchable turn. According to previous work the turn unit can be used as nucleating agent for strand sequences, which stabilizes the turn formation due to multiple hydrogen bonds between the amino acid chains.<sup>111, 119</sup> Furthermore, it should help in understanding Alzheimer's disease. A causative role thereby plays the Amyloid- $\beta$  (A $\beta$ ) self-assembly into cross- $\beta$  amyloid fibrils. Doran *et al.* incorporated the photoswitchable turn mimetic into the turn region of A $\beta$ 42 to control the turn nucleation and therefore understanding the role of the turn nucleation in A $\beta$  self-assembly. They found out that the *trans*-type formed fibrils similar to the wild-type, whereas the *cis*-type formed nonfibril aggregates that were nontoxic. Therefore, they proved that  $\beta$ -turn intermediates are not strictly required for A $\beta$  fibril or cytotoxic oligomer formation.<sup>120</sup> The photoswitchable azobenzene derivatives were further used for binding and releasing anions.<sup>121</sup> It was also used for the controlled reversible recognition of *E.coli* bacteria using azobenzene mannosides derivatives. While the *trans* form binds *E.coli* the photoswitch to the *cis* form leads to a release of these bacteria.

Instead of using only one turn in secondary structures, multiple turn elements can be incorporated. Gobbo *et al.*<sup>122, 123</sup> designed two-dimensional turn elements for oligo(alkyl amides) for surface-

## 1. Introduction

confined foldamers (Figure 1.16). Therefore, they introduced alkoxyated *ortho*-catechol units as turn mimic into oligo(alkyl amides). They varied the length of the carboxylate alkyl spacer length as well as the numbers of included turn elements. Thereby, this primary flexible system undergoes 2D folding upon adsorption at an organic liquid-solid interface.

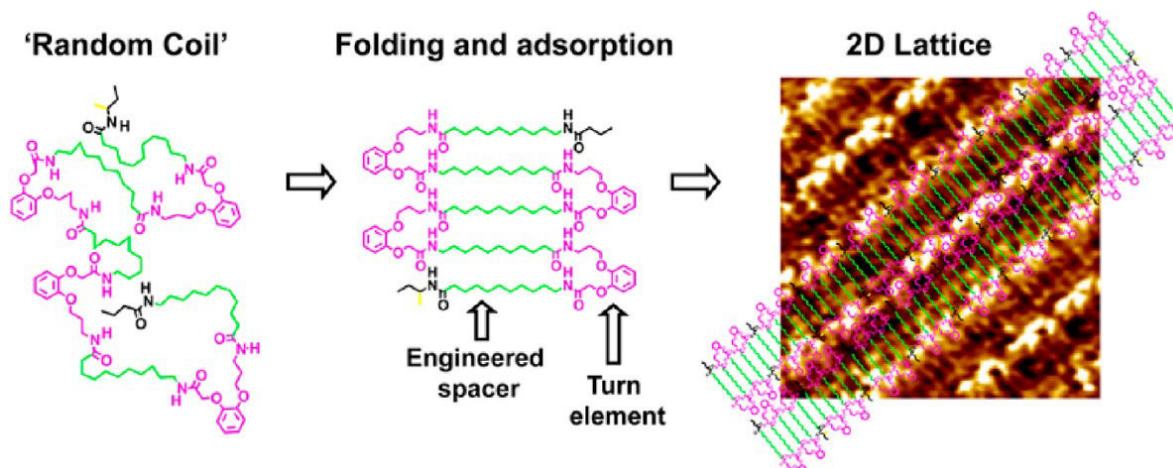


**Figure 1.16.** Preprogrammed 2D folding of conformationally flexible oligo(alkyl amides). (picture taken from Gobbo *et al.*<sup>122</sup>)

This in-plane folding and self-assembly behavior was proven via submolecularly resolved scanning tunnel microscopy (STM). The 2D folding could be explained by the nucleation of the turn mimic and additional stabilization by mainly hydrogen bonding of the oligo(alkyl amides) as well as by favorable molecule-substrate interactions (van der Waals interactions). They claimed that “*the high spatial control over positioning of functional groups coupled with the modular nature of the building blocks provides a simple, efficient, and versatile route to surface patterning with nanometer-scale precision.*”<sup>122</sup>

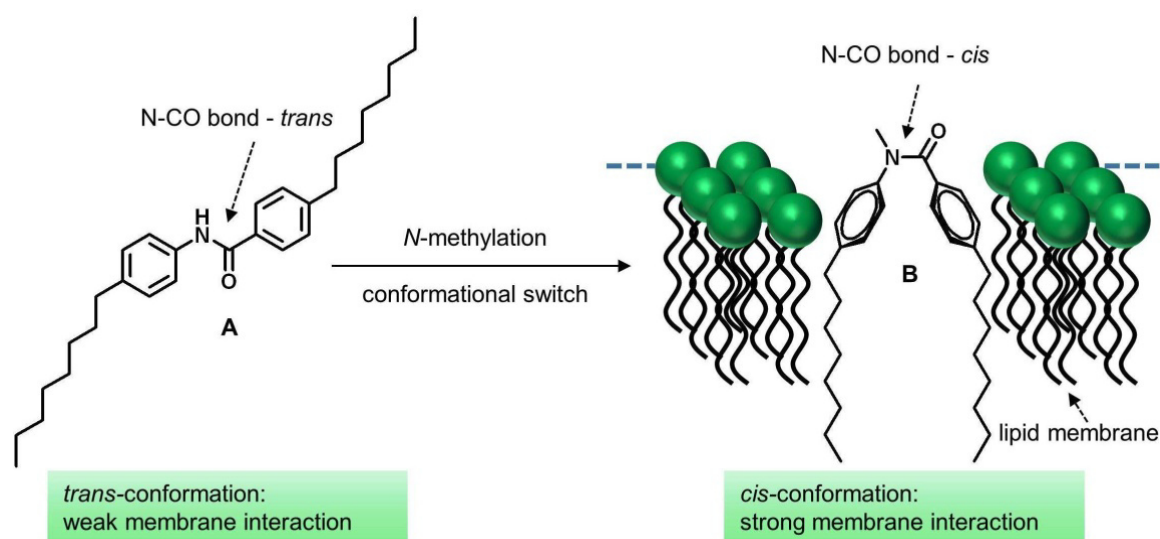
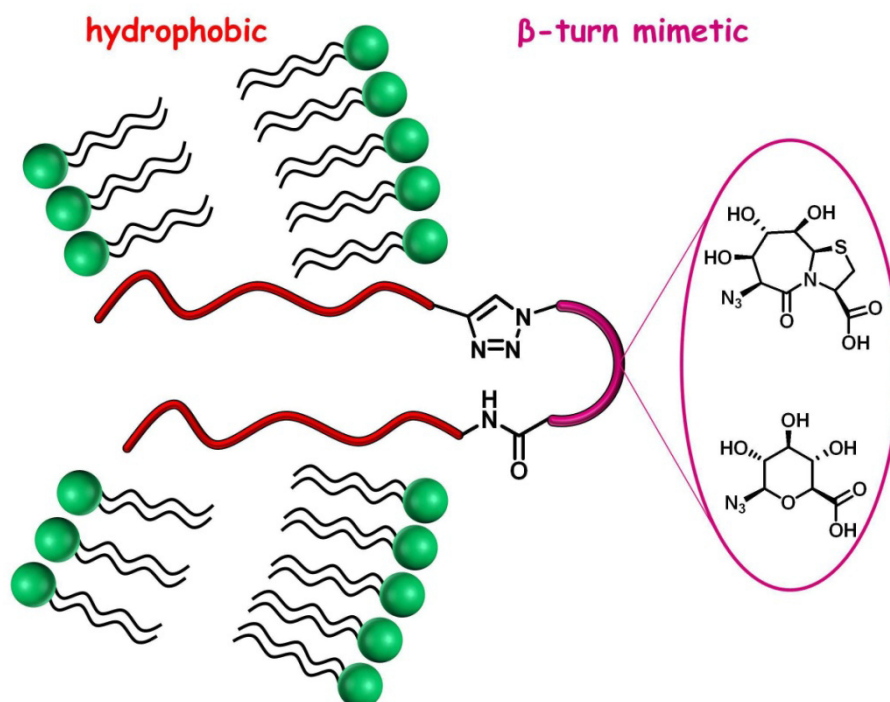


**Figure 1.17.** Structure of *trans*-benzanilide **A** and *cis*-benzanilide **B**. Schematic depicting insertion of *cis*-benzanilide **B** with a lipid membrane. (Figure was redrawn according to Dennison *et al.*<sup>124, 125</sup>)

Another highly interesting work which aroused our interest towards the incorporation of  $\beta$ -turn mimics into polymer strands and the investigation of the interaction of such folded system with lipid membranes is the following.<sup>124-126</sup> Since years the antibiotic resistance in medical science is a huge problem, therefore it is necessary to understand how membrane-active substances target or disrupt membranes, thus causing cell death.<sup>126</sup> Dennison *et al.*<sup>124, 125</sup> investigated the interaction between phospholipid monolayers and the *cis*- (**A**) and the *trans*-benzanilide (**B**) suggesting a strong dependence between conformation and membrane binding driven by amphiphilicity (Figure 1.17). Thus, they used isotherm measurements where they incorporated both substances separately into a composite lipid mix monolayer of DOPE (91 %), DOPG (3 %) and *E. coli* cardiolipin (6 %) that mimic *E. coli* membrane. They found out, that the *N*-unsubstituted benzanilidine **A** with its thermodynamically stable *trans*-conformation has a weak interaction with the membrane. However, *N*-methylation of this compound leads to a conformational switch to the *cis*-form (**B**, analogously to turn mimic) resulting in strong membrane interaction. Although both compounds (**A** and **B**) have comparable physicochemical properties and similar binding values, the *cis*-form penetrates stronger into the lipid system, which they explained by the enhanced dipole of **B**. Resulting they suggest that this stronger membrane activity makes **B** to a suitable candidate of novel antibiotics.

## 2. Aim of the work



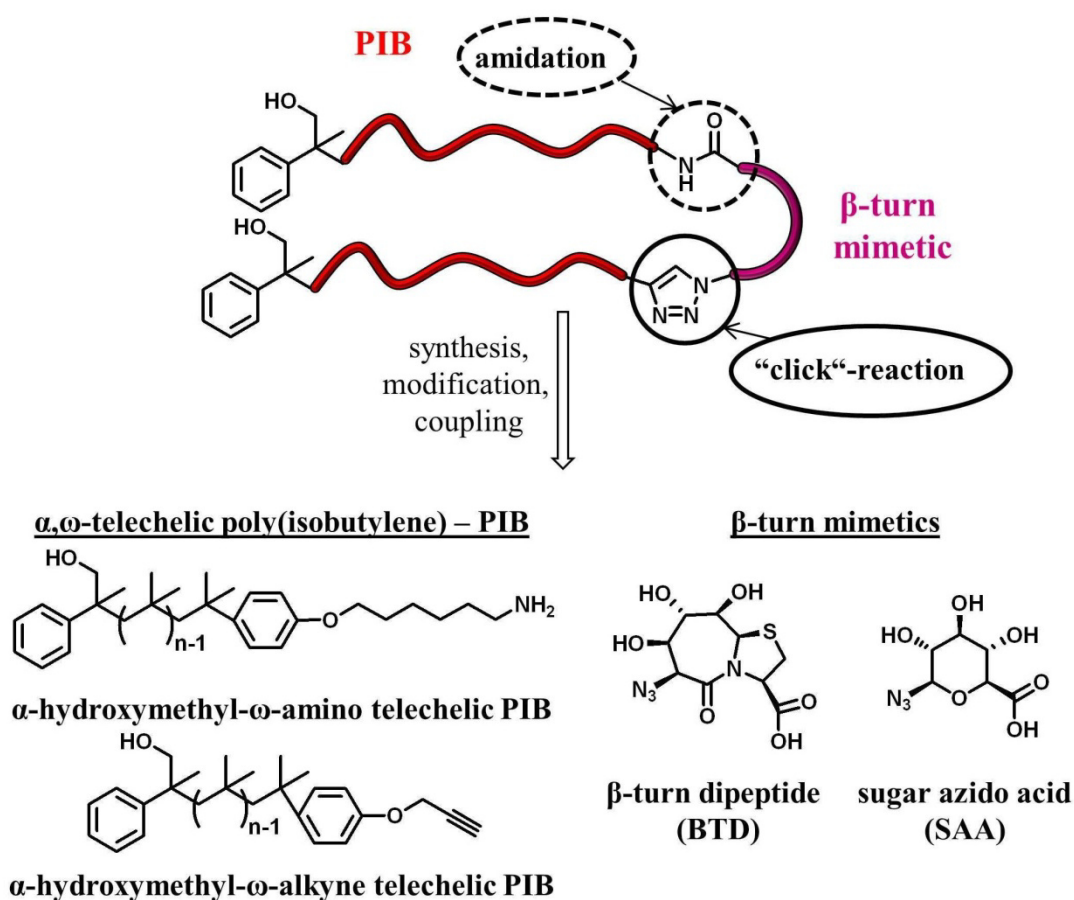
**Scheme 2.1.** Schematic representation of amphiphilic  $\beta$ -turn mimetic polymer conjugates incorporated into a lipid bilayer membrane.

The aim of the work is the synthesis of amphiphilic polymer conjugates containing a  $\beta$ -turn mimetic element and the investigation of their organization in lipid bilayer membrane. These conjugates should be based on two hydrophobic polymer strands, which are connected onto the same hydrophilic folding element. The hydrophilic  $\beta$ -turn mimetic should serve as anchor in the water phase whereas the hydrophobic polymer strands should orientate into the hydrophobic region of the bilayer membrane. To directly relate differences of membrane behavior to content of incorporated polymer conjugate highly defined polymers with defined molecular weights, narrow molecular weight distribution and complete end group functionalization are required. Therefore, biocompatible poly(isobutylene) will be chosen and synthesized via living carbocationic polymerization. For the hydrophilic folding elements the  $\beta$ -turn dipeptide (BTD) and the sugar azido acid (SAA) will be used. Both are purely geometrically constrained  $\beta$ -turns with a fixed conformation.

These amphiphilic polymer conjugates will be inserted into a lipid membrane forming a lipid/hybrid mixture, where the interaction between the folding element and the lipids will be investigated. For monolayer experiments Langmuir measurements will be coupled with epifluorescence microscopy and AFM, and bilayer hybrid membranes will be investigated via fluorescence microscopy and fluorescence spectroscopy.



## 3. Concept



**Scheme 3.1.** Retrosynthetic concept towards amphiphilic polymer conjugates containing a  $\beta$ -turn mimetic element (BTD or SAA) by the linkage of the different building blocks.

To investigate the organization of amphiphilic polymer conjugates, containing a  $\beta$ -turn mimetic element, when incorporated into lipid membranes the synthesized polymer conjugates have to fulfill various criteria. The amphiphilic polymer conjugate has to be synthesized on the model of natural membranes mainly consisting of phospholipids bearing a small polar head group and two longer nonpolar tails – therefore hydrophilic  $\beta$ -turn mimetic elements and hydrophobic polymer chains are needed as tailor-made building blocks. For defined linkages of the hydrophobic polymer chains onto the  $\beta$ -turn mimetic elements two chemically different reactions are required (Scheme 3.1). These linkages can be accomplished by the use of the  $\text{Cu}^{\text{I}}$  mediated azide/alkyne-“click”-reaction (further used in short form: “click”-reaction) which is known for high conversion, while tolerating several functional groups. Thus, azide and alkyne moieties at the (chain) - ends of the building blocks are necessary. For the second linkage the amidation reaction known from peptide synthesis can be used where amine and carboxylic acid moieties are needed. Both methods are known for their high yield, high selectivity and the formation of stable products under mild conditions, thus making them essential for the functionalization of polymers and biomolecules.

### 3. Concept

---

As hydrophilic  $\beta$ -turn mimetic elements the  $\beta$ -turn dipeptide (BTD) and the sugar azido acid (SAA) were chosen. BTD is a purely geometrically constrained  $\beta$ -turn with a fixed conformation and SAA is a carbohydrate based  $\beta$ -turn also with a fixed conformation. These building blocks can be synthesized following the procedures from literature.<sup>113, 114, 127-130</sup> Since both  $\beta$ -turn mimetics are functionalized on the one end with an azide group and at the other end with a carboxylic acid group hydrophobic polymer chains containing an alkyne functionality respectively an amine group are necessary as counter parts, therefore the hydrophobic, biocompatible poly(isobutylene) (PIB) was chosen. PIB can be synthesized via living carbocationic polymerization using  $\alpha$ -methylstyrene epoxide (MSE) as initiator and a) 6-phenoxyhexylamine as quencher to achieve  $\alpha$ -hydroxymethyl- $\omega$ -amino telechelic PIB or b) trimethyl(3-phenoxy-1-propynyl)silane as quencher to obtain  $\alpha$ -hydroxymethyl- $\omega$ -alkyne telechelic PIB. The received PIBs are well defined corresponding to narrow molecular weight distribution, targeted molecular weights (3000 – 5000 g/mol) and complete end group functionalization. Due to the bifunctionality of the synthesized PIBs post modification is feasible.

After successful syntheses of the building blocks, amphiphilic polymer conjugates having one hydrophobic poly(isobutylene) strand linked to a  $\beta$ -turn mimetic as well as those bearing two poly(isobutylene) chains on one  $\beta$ -turn mimetic should be synthesized. Thus, the influence of the number of connected polymer strands onto the same folding element could be investigated. The purities of the building blocks and of the final amphiphilic polymer conjugates should be proven by NMR spectroscopy, MALDI-ToF-MS measurements and HPLC. Moreover, investigations of the interaction of the amphiphilic  $\beta$ -turn mimetic polymer conjugates with lipid mono- and bilayers are required. Therefore, mixed lipid/polymer membranes will be constructed from DPPC and the amphiphilic polymer conjugates. The formation of mixed/demixed domains as well the folding of the amphiphilic polymer conjugates of the monolayers can be investigated using Langmuir-film techniques coupled with epifluorescence microscopy and AFM. For the investigation of the effects onto bilayers confocal laser microscopy using giant unilamellar vesicles (GUVs) and fluorescence spectroscopy using small unilamellar vesicles (SUVs) can be used.

### 4. Results and discussion

#### 4.1 Synthesis of $\alpha,\omega$ -functionalized PIBs

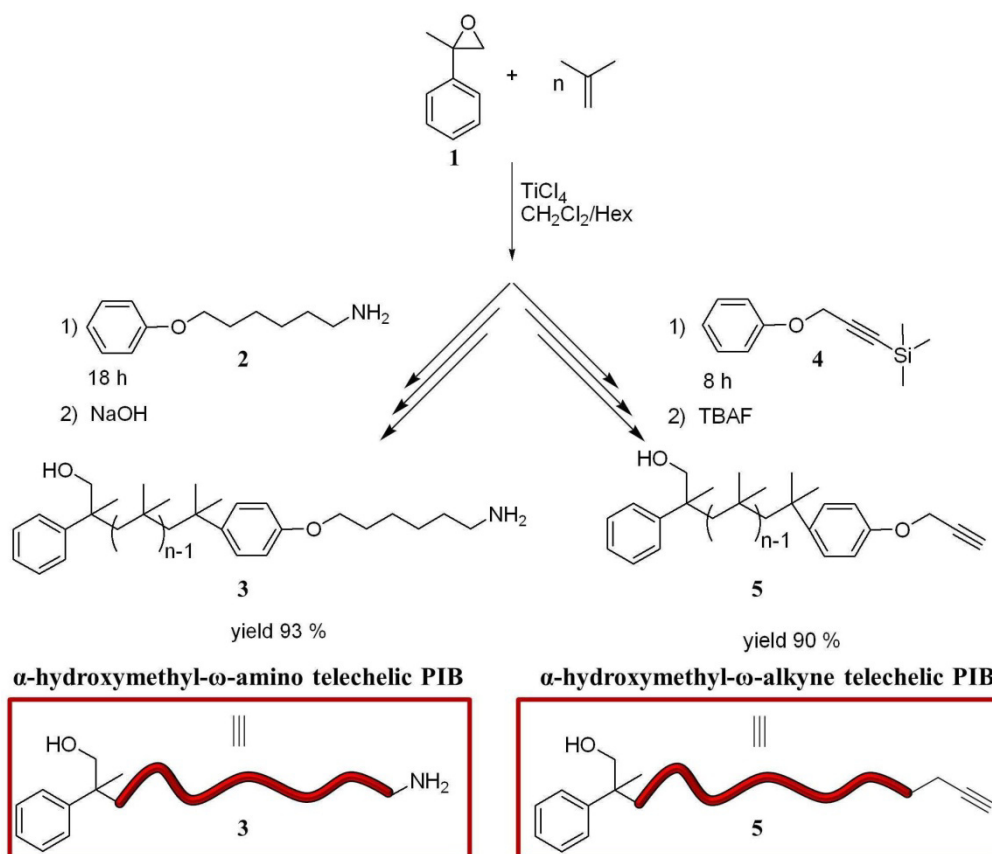
The common polymerization of isobutylene is the living carbocationic polymerization (LCCP) which was developed by J. P. Kennedy *et al.*<sup>131, 132</sup> in the 1980s. To obtain poly(isobutylenes) (PIB) with defined molecular weights ( $M_n$ ), narrow distributed molecular weights (small polydispersity indices (PDI)) and defined end groups<sup>133</sup> several criteria have to be met. Therefore, the choice of initiators, co-initiators (Lewis acids like  $\text{BCl}_3$  and  $\text{TiCl}_4$ )<sup>132, 134</sup>, temperature, solvents ( $\text{CHCl}_3$ ,  $\text{CH}_2\text{Cl}_2$ , n-hexane/ $\text{CH}_2\text{Cl}_2$  v/v 60/40)<sup>132, 134</sup> and additives (e.g. 2,6-di-*tert*-butylpyridine (DtBP))<sup>135, 136</sup> is important to avoid side reactions like  $\beta$ -proton elimination from the living chain ends.

To achieve  $\alpha,\omega$ -telechelic PIBs a combination of two different approaches **a)** using an initiator bearing a functional group<sup>137</sup> and **b)** quantitative end-quenching of living chain ends with transformation of the end groups are necessary. **a)** The first approach, the use of functional initiators, is strongly limited, due to the high sensitivity of LCCP against polar groups. One useful initiator is the  $\alpha$ -methylstyrene epoxide as reported by Puskas *et al.*<sup>137, 138</sup> which introduces a hydroxymethyl moiety onto the  $\alpha$ -end. Although the  $\alpha$ -methylstyrene epoxide is difficult to purify and the efficiency is only 20-30 % due to the reported side reactions, a livingness of the polymerization was proven.<sup>137, 138</sup> **b)** The second approach is the most common, whereas the number of quenching reagents for direct end group functionalization is limited, for example using diphenylethylene<sup>139</sup>, furane<sup>140</sup> or allyltrimethylsilane (ATMS)<sup>141</sup>, lead to only a limited structural variability of the PIBs. One crucial contribution for end group functionalization was the work of Morgan and Storey with the use of alkoxybenzene compounds which react in an electrophilic aromatic substitution reaction (Friedel-Crafts alkylation) with the active chain end.<sup>142, 143</sup>

Due to the combination of  $\alpha$ -methylstyrene epoxide (**1**) as initiator<sup>137, 138</sup> and alkoxybenzene compounds<sup>142, 143</sup> as quencher,  $\alpha,\omega$ -functionalized PIBs could be obtained.<sup>144</sup> This method enables fast and easy building up of PIBs bearing different end groups. Scheme 4.1 shows the synthetic route towards  $\alpha$ -hydroxymethyl- $\omega$ -amino telechelic PIB (**3**) and  $\alpha$ -hydroxymethyl- $\omega$ -alkyne telechelic PIB (**5**). The polymerization conditions are the same for both, only the time for the quenching process varies.

A) For the synthesis of  $\alpha$ -hydroxymethyl- $\omega$ -amino telechelic PIB (**3**) 6-phenoxyhexylamine (**2**) was used as quencher. However, the direct quenching with such a nucleophile is per se impossible, due to the reaction of the amine with the  $\text{TiCl}_4$  and the PIB carbenium ion. Latter would lead to a proton abstraction from the carbenium ion resulting in *endo/exo* olefinic PIBs. Therefore, the amine group is complexed with an excess of  $\text{TiCl}_4$  to reduce its nucleophilicity. During the quenching the alkylation rate drastically slowed down, as HCl was generated from the alkylation reaction. On the one hand the amine was protonated and on the other hand the complex  $[\text{Ti}_2\text{Cl}_9]^-$  was formed, which decreased the amount of  $\text{TiCl}_4$ .<sup>143</sup>

## 4. Results and discussion



**Scheme 4.1.** Synthetic route towards  $\alpha$ -hydroxymethyl- $\omega$ -amino telechelic PIB (3) and  $\alpha$ -hydroxymethyl- $\omega$ -alkyne telechelic PIB (5).

As the quenching was incomplete after 9 h (quenching time given by literature<sup>143</sup>) the quenching time was extended to 18 h. The achieved PIB was functionalized with a protonated amine group which was transformed to the amine functionalized PIB 3 by washing with NaOH. The deprotonation via  $\text{NaHCO}_3$  and  $\text{Na}_2\text{CO}_3$  was not successfully as protonated amine was still visible in  $^1\text{H-NMR}$  [resonances at 2.99 ppm ( $\text{H-13}^+$ ) and 8.37 ppm ( $\text{NH}_3^+$ )]. The molecular weight was determined by SEC and NMR spectroscopy, the results are listed in table 4.1. As it can be seen the calculated and experimental determined molecular weights match very well and the PDIs are acceptable.

**Table 4.1.** Results for the polymerization of  $\alpha$ -hydroxymethyl- $\omega$ -amino telechelic poly(isobutylene) (3).

PIB	$m_{\text{th}}$ [g]	$M_{\text{n(th)}}$ [g/mol]	$M_{\text{n(SEC)}}^{\text{a}}$ [g/mol]	PDI	$M_{\text{n(NMR)}}$ [g/mol]	yield
3a	3	3000	3400	1.50	4350	2.5 g 83 %
3b	3	4000	3800	1.42	4500	2.8 g 93 %
3c	5	5000	5000	1.30	6050	4.4 g 88 %

a) Polyisobutylene standards were used for conventional external calibration.

## 4. Results and discussion

B) For the synthesis of  $\alpha$ -hydroxymethyl- $\omega$ -alkyne telechelic PIB (**5**) trimethyl(3-phenoxy-1-propynyl)silane (TMS, **4**) was used as quencher. A direct quenching with an alkyne is impossible due to the activity of the triple bond for polymerization, resulting in carbocationic addition across the triple bond. Therefore, the active group was protected with trimethyl silane.<sup>143</sup> This group then could be cleaved off easily from the polymer by the use of TBAF to achieve  $\alpha$ -hydroxymethyl- $\omega$ -alkyne telechelic PIB (**5**, SEC:  $M_n = 4700$  g/mol, PDI = 1.39).

The complete end group functionalization of the final PIBs (**3** and **5**) were proven via NMR spectroscopy (Figure 4.1) and MALDI-ToF MS (Appendix Figure A4). Figure 4.1a shows the <sup>1</sup>H-NMR spectrum of  $\alpha$ -hydroxymethyl- $\omega$ -amino telechelic PIB (**3**). Due to the steric hindrance of the phenyl group of the initiator part the rotation of the hydroxyl methyl is hindered, therefore the two protons (H-2 and H-2') of the methylene group in vicinity to the hydroxyl group have different chemical environments which is visible in the <sup>1</sup>H-NMR spectra by splitting of the signals. By comparing the integral values referring to the protons H-2/2' of the initiator unit and H-6 and H-13 of the quencher unit which are in the ratio 1:1:2:2 the complete end group functionalization could be confirmed. Also all other signals could be assigned, thus evidencing the structure containing a  $\beta$ -turn mimetic element.

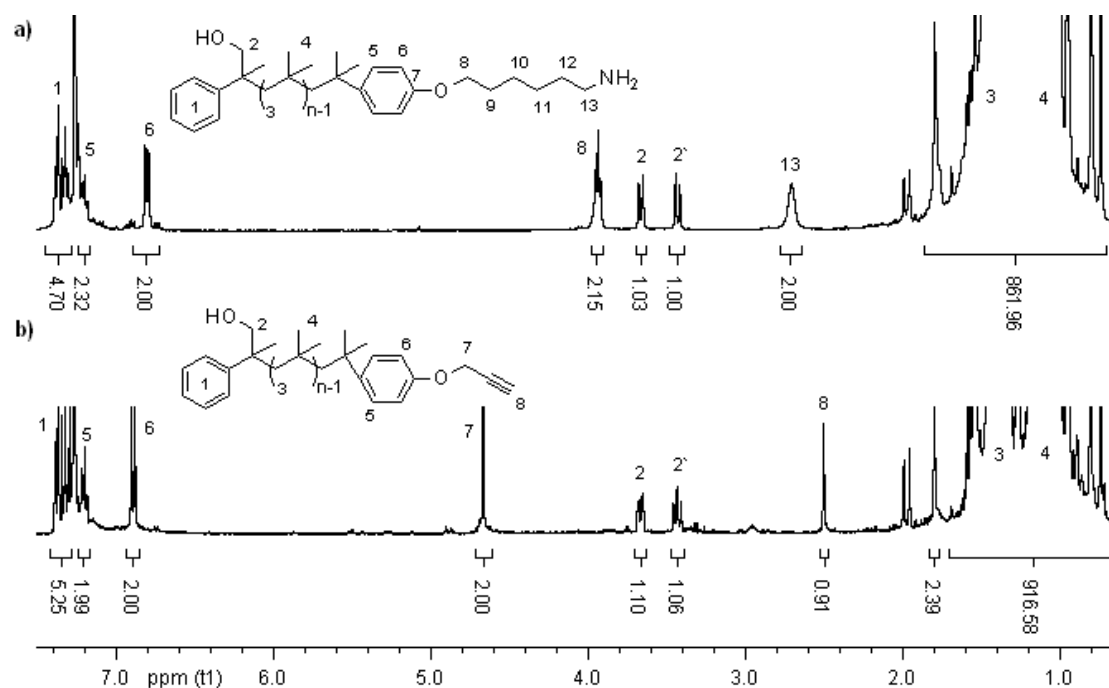


**Figure 4.1.** Overlay of the <sup>1</sup>H-NMR spectra (CDCl<sub>3</sub>, 400 MHz) of a)  $\alpha$ -hydroxymethyl- $\omega$ -amino telechelic PIB (**3**) and b)  $\alpha$ -hydroxymethyl- $\omega$ -alkyne telechelic PIB (**5**).

Figure 4.1b shows the <sup>1</sup>H-NMR spectrum of  $\alpha$ -hydroxymethyl- $\omega$ -alkyne telechelic PIB (**5**). Comparing the integral values of the methylene protons (H-2/2') related to the initiator part with the methylene protons H-7 in vicinity to the alkyne moiety proves the complete end group

## 4. Results and discussion

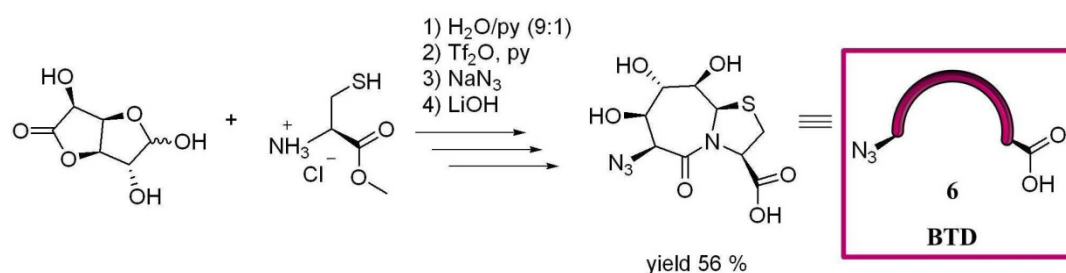
functionalization (integral ratio 1:1:2). The signal H-8 of the alkyne group cannot be used for proofing complete end group functionalization as this group causes an anisotropic effect, therefore the integral values can differ up to 30 %. As the  $\alpha$ -hydroxymethyl- $\omega$ -amino telechelic PIB (**3**) and the  $\alpha$ -hydroxymethyl- $\omega$ -alkyne telechelic PIB (**5**) were synthesized successfully and their purities, especially the complete end group functionalization, were evidenced these building blocks could be used for the synthesis of an amphiphilic polymer conjugate

### 4.2 Synthesis of the $\beta$ -turn mimetic building blocks

As these  $\beta$ -turn mimetic building blocks are later part of the amphiphilic polymer conjugates whose folding should be investigated when incorporated into a lipid membrane, the  $\beta$ -turn should be anchored in the polar head group region of the lipids. Decisive factors for choosing these  $\beta$ -turn mimetic building blocks were beside their hydrophilicity and their fixed  $\beta$ -turn conformation, their functionalities on both ends. An azide functionality on the one side and a carboxylic moiety on the other side then facilitate the defined linkage of the  $\beta$ -turn mimetics via “click”-reaction respectively amidation onto the PIB chains **3** and **5**.

#### 4.2.1 Synthesis of the $\beta$ -turn dipeptide (BTD)

Scheme 4.2 shows the synthetic route towards the  $\beta$ -turn dipeptide (BTD, **6**). This purely geometrically constrained  $\beta$ -turn has a fixed conformation, the distance between the azide functionality on the one side and the carboxylic moiety on the other side is according to the X-ray structure only 7 Å.<sup>115</sup> Moreover, its polyol structure is known for membrane affinity as well as interaction with membranes.<sup>116</sup>



**Scheme 4.2.** Synthetic route towards BTD (**6**).

The precursor the BTD methyl ester (**6a**) was synthesized according to literature<sup>113, 114</sup> starting with the condensation of D-glucurono-3,6- lactone and L-cysteine methyl ester hydrochloride in a solvent mixture of water/pyridine (9:1) forming the  $\beta$ -turn dipeptide bearing a hydroxyl functional group on the one side and the carboxylic acid methyl ester on the other side. Transformations of the hydroxyl

## 4. Results and discussion

group into the triflate group and then into the azide group followed by the hydrolysis of the methyl ester via LiOH yielded the BTD-COOH (**6**).

The successful synthesis of the BTD methyl ester (**6a**) was proven via NMR spectroscopy and ESI-ToF MS. Figure 4.2a shows the  $^1\text{H-NMR}$  spectrum of **6a**, where all signals could be assigned to the structure and the integral values match. Another evidence for the purity is given by the ESI-ToF MS, the experimental molecular weight of 341.0571 g/mol agrees with the calculated one of 341.0532 g/mol according to the sodium adduct. The nearly quantitative hydrolysis of BTD methyl ester (**6**) to BTD-COOH (**6**) was as well proven via NMR spectroscopy and ESI-ToF MS. Figure 4.2b shows the  $^1\text{H-NMR}$  spectrum of **6**, where again all signals could be assigned to the structure and the integral values match.

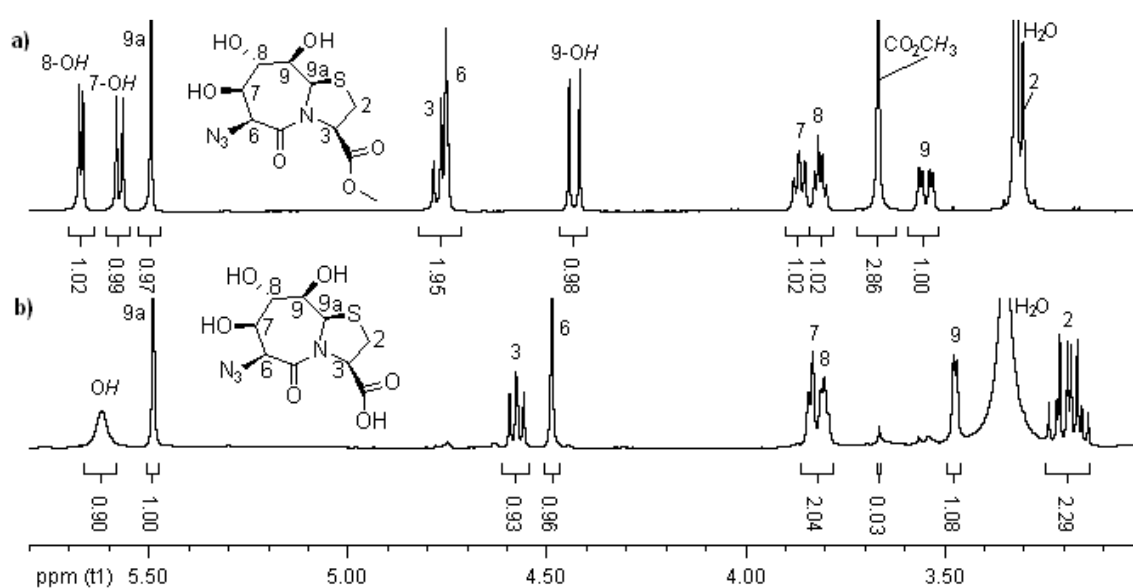


**Figure 4.2.** Overlay of the  $^1\text{H-NMR}$  spectra (DMSO- $d_6$ , 400 MHz) of a) BTD methyl ester (**6a**) and b) BTD-COOH (**6**).

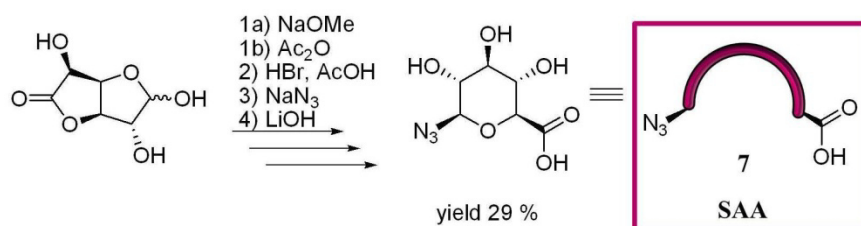
The shift of the methylene group (H-2) from 3.30 ppm to 3.19 ppm as well from the methine (H-3) from 4.77 ppm to 4.58 ppm proves the hydrolysis. Moreover, the vanishing (just 1 % remaining) of the signal for the methyl group from the ester (CO<sub>2</sub>CH<sub>3</sub>) at 3.67 ppm shows the successful ester cleavage. ESI-ToF MS of **6** shows no peak for the former BTD methyl ester (**6a**), the molecular weights 311.0865 g/mol and 317.0944 g/mol agree with the calculated molecular weights 311.0638 g/mol [M+Li]<sup>+</sup> and 317.0720 g/mol [M-H+2Li]<sup>+</sup> respectively.

### 4.2.2 Synthesis of the sugar azido acid (SAA)

Scheme 4.3 shows the synthetic route towards the sugar azido acid (SAA, **7**). This SAA and its analogues were clearly typified as  $\beta$ -turn in literature.<sup>108</sup> The conformation of this  $\beta$ -turn mimetic is

## 4. Results and discussion

fixed and the calculated distance between the azide functionality on the one side and the carboxylic moiety on the other side is only 5 Å.<sup>117</sup>



**Scheme 4.3.** Synthetic route towards SAA-COOH (**7**).

The sugar azido acid (SAA, **7**) was synthesized according to literature<sup>114, 127-130</sup>. In a first step D-glucurono-3,6- lactone was converted to the methyl ester and then acetylated yielding an  $\alpha$ - $\beta$  anomeric mixture of **7a** bearing an acetyl moiety on the one side and a carboxylic acid methyl ester on the other side.<sup>127</sup> The separation of the  $\alpha$ - and  $\beta$ -anomers was not necessary as after treatment with hydrobromic acid the acetyl group was transformed into a bromide group resulting the  $\alpha$ -anomer (**7b**) only due to the anomeric effect.<sup>127, 128</sup> Then the bromide group could be easily converted via phase transfer catalyzed S<sub>N</sub>2-reaction into the azido group and so yielding the  $\beta$ -anomer (**7c**).<sup>129, 130</sup> After hydrolysis with LiOH<sup>114</sup> the SAA **7** having azido and carboxylic acid moieties could be obtained.

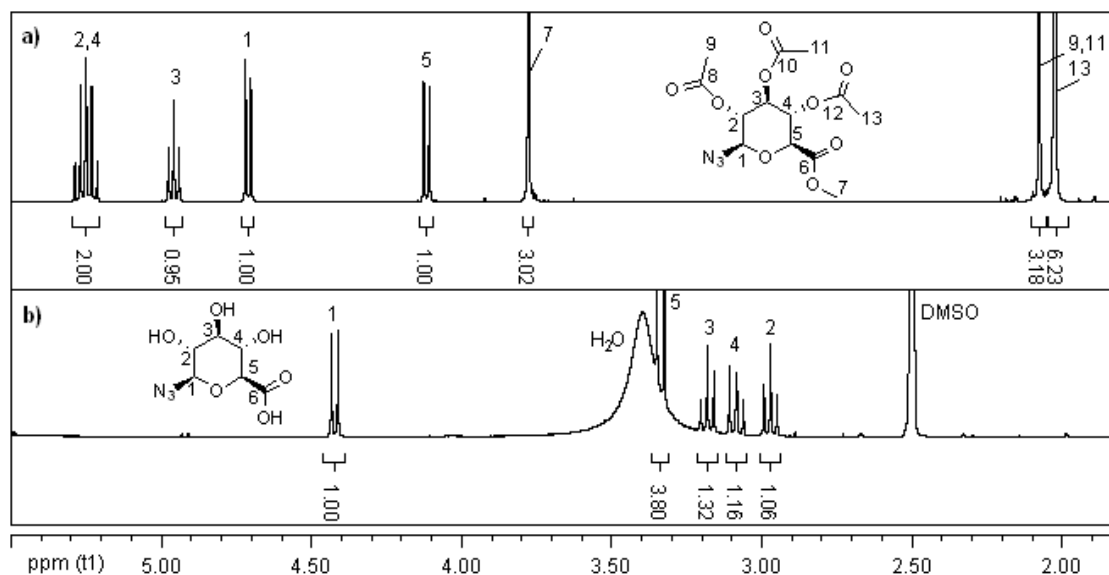


**Figure 4.3.** Overlay of the <sup>1</sup>H-NMR spectra of a) SAA methyl ester (**7c**; CDCl<sub>3</sub>, 400 MHz) and b) SAA (**7**; DMSO<sub>d6</sub>, 400 MHz).

The purities of the SAA methyl ester (**7c**) and the hydrolyzed SAA (**7**) were proven via NMR spectroscopy, ESI-ToF MS and specific rotation. Figure 4.3a shows the <sup>1</sup>H-NMR spectrum of the SAA methyl ester (**7c**), where all signals could be assigned to the structure and the integral values match. This could be underpinned by the ESI-ToF MS measurement, the experimental determined signal at



382.1175 g/mol agrees with the calculated one of 382.0857 g/mol according to the sodium adduct. The value of the specific rotation ( $[\alpha]_D^{20}$  ( $c = 1$ , MeOH) =  $-28.6^\circ$ ) comparing with the literature value ( $[\alpha]_D^{23} = -29.4^\circ$ )<sup>145</sup> proves the  $\beta$ -anomer formation. The successful hydrolysis yielding SAA **7** was confirmed via <sup>1</sup>H-NMR spectroscopy (Figure 4.3b), showing the disappearance of the methyl group corresponding to the former ester (H-7) as well as of the acetyl groups (H-9,11,13). Another evidence for the complete hydrolysis is given by ESI-ToF MS, the signal at 218.0535 g/mol matches with the calculated molecular weight of 218.0408 g/mol according to the carboxylate of **7**. Here again the value of the specific rotation ( $[\alpha]_D^{20}$  ( $c = 1$ , MeOH) =  $-25.0^\circ$ , Lit.<sup>146</sup>  $[\alpha]_D$  ( $c = 0.7$ , acetone) =  $-23.0^\circ$ ), proves the  $\beta$ -anomer formation.

### 4.3 Synthesis of amphiphilic $\beta$ -turn mimetic polymer conjugate

Parts of this chapter were published in: Malke, M.; Barqawi, H.; Binder, W. H., Synthesis of an Amphiphilic  $\beta$ -Turn Mimetic Polymer Conjugate. *ACS Macro Lett.* **2014**, 3, (4), 393-397. Copyright 2015 American Chemical Society.

#### 4.3.1 Linking methods

As the syntheses of the different tailor-made building blocks (**3**, **5**, **6** and **7**) were successful and their purities were proven, they could be linked to achieve the  $\beta$ -turn mimetic amphiphilic polymers. Therefore, a) the copper mediated azide/alkyne-“click”-reaction and b) the amidation reaction should be used. Both methods are known for their high yield, high selectivity and the formation of stable products under mild conditions, thus making them essential for the functionalization of polymers and biomolecules.

##### 4.3.1.1 Copper mediated azide/alkyne-“click”-reaction

The breakthrough of the azide/alkyne-“click”-reaction acquired Meldal<sup>147</sup> and Sharpless<sup>148, 149</sup> in 2002. Due to the use of copper(I) catalytic system only 1,4-substituted-1,2,3-triazoles were formed regioselectively and the reaction was accelerated in such a way allowing the 1,3 dipolar cycloaddition at room temperature.<sup>150</sup> The azide/alkyne-“click”-reaction between terminal alkynes and azides is known to be highly efficient, while tolerating functional groups and different solvents, therefore offering a wide scope of linking functional groups onto polymers.<sup>151-156</sup> Beside the numerous applications in macromolecular science<sup>151, 152, 157, 158</sup> it is adopted in various other fields like biology<sup>159</sup>, medicinal science<sup>160</sup> and technological areas<sup>161</sup>. Moreover, this coupling technique could be used for the synthesis of peptide conjugates.<sup>162-165</sup> Thereby, the formation of the 1,2,3-triazole linkage plays an important role, as this unit is resistant to enzymatic degradation, hydrolysis and oxidation, thus making this linking unit attractive for replacing more labile moieties in biological compounds. A direct

## 4. Results and discussion

comparison between amide bond and 1,4-disubstituted-1,2,3-triazole proofs their structural (relative planarity) and electronic similarity, therefore amide to triazole substitution is possible.<sup>70</sup>

In practice, the copper(I)-catalyst can be generated *in situ*, or a copper(I)-halide is used together with a stabilizing ligand. The ligands are necessary to enhance the rate of reaction and to protect the copper(I) from oxidation.<sup>166</sup> Additionally, Fokin, Jin and co-workers<sup>167</sup> claimed the formation of 1,5-substituted-1,2,3-triazoles by a reaction of organic azides and alkynes, which is catalyzed by ruthenium(II). This Ru-catalyzed process, RuAAC, is highly tolerant towards functional groups and shows a high acceptance to both azides and terminal or internal alkynes. However, the reaction needs high temperatures (80 °C).<sup>167</sup>

**Table 4.2.** Excerpt of possible catalyst systems, solvents and bases for CuAAC/RuAAC.<sup>168, 169</sup>

<b>catalyst</b>	<b>solvent</b>	<b>base (ligand)</b>
Cu(II)SO <sub>4</sub> ·5 H <sub>2</sub> O/sodium ascorbate	hexane	DIPEA
Cu(II)SO <sub>4</sub> ·5 H <sub>2</sub> O/copper	toluene	TBTA ( <b>29</b> )
Cu(I)X X = Br, I	THF	2,2'-bipyridine
Cu(I)(PPh <sub>3</sub> ) <sub>3</sub> Br	CH <sub>2</sub> Cl <sub>2</sub> /CHCl <sub>3</sub>	PMDETA
Cu(I)(MeCN) <sub>4</sub> PF <sub>6</sub>	DMF	
copper cluster	acetonitrile	
Ru(PPh <sub>3</sub> ) <sub>3</sub> Cl <sub>2</sub>	water	

Table 4.2 gives an excerpt of possible catalyst-systems, solvents and bases for CuAAC.<sup>151, 168</sup> The first group of the Cu(I) catalysts can be generated *in situ* by reduction of Cu(II) salts using sodium ascorbate or metallic copper.<sup>170</sup> The second group, representing the biggest and most used group in practice, are the Cu(I) catalysts which can be Cu(I) halides (e.g. CuBr, CuI) or organosoluble Cu(I) species like [CuBr(PPh<sub>3</sub>)<sub>3</sub>] and [Cu(MeCN)<sub>4</sub>PF<sub>6</sub>]. Whereby the latter are known to be more effective in organic solvents than the Cu(I) halides.<sup>171</sup> The use of copper clusters of Cu/Cu oxide nanoparticles, sized 7-10 nm<sup>172</sup> as well as copper cluster around 2 nm<sup>173</sup> have been described in literature also. To stabilize the Cu(I) oxidation state ligands (often amino bases) are used making the “click”-reaction less susceptible against oxygen due to the reducing character.<sup>151, 166, 169, 174, 175</sup> Furthermore, the ligand has an important influence on the rate, thus the correct choice can accelerate the azide/alkyne-“click”-reaction. For example the effects of amine ligands on the copper(I)-catalyzed azide/alkyne-“click”-reaction were extensively studied, resulting in TBTA (**29**) as best ligand.<sup>150, 169</sup>

### 4.3.1.2 Amidation reaction

The amidation is another possibility for easy linkage of building blocks. Therefore, these building blocks have to be functionalized with a carboxylic acid group and as counterpart the amine group.

## 4. Results and discussion

Inspired from Nature this reaction is mainly used in the chemical synthesis of peptides. To achieve synthetic peptides and proteins with molar masses up to 10,000 Da coupling agents with high coupling yields > 99.5 % and without racemisation are necessary. As we are not interested in building-up peptides, but in the use of this coupling method for the linkage of a  $\beta$ -turn onto a polymer strand the coupling should be fast and quantitative without/easily removable side products. Common to all of the different coupling methods is the activation of the carboxylic acid via a coupling agent, forming an intermediate which can be a mixed anhydride, an activated ester or an acid halide, which then reacts with the amine moiety forming the desired peptide bond. An excerpt of possible coupling agents will be discussed in the following.

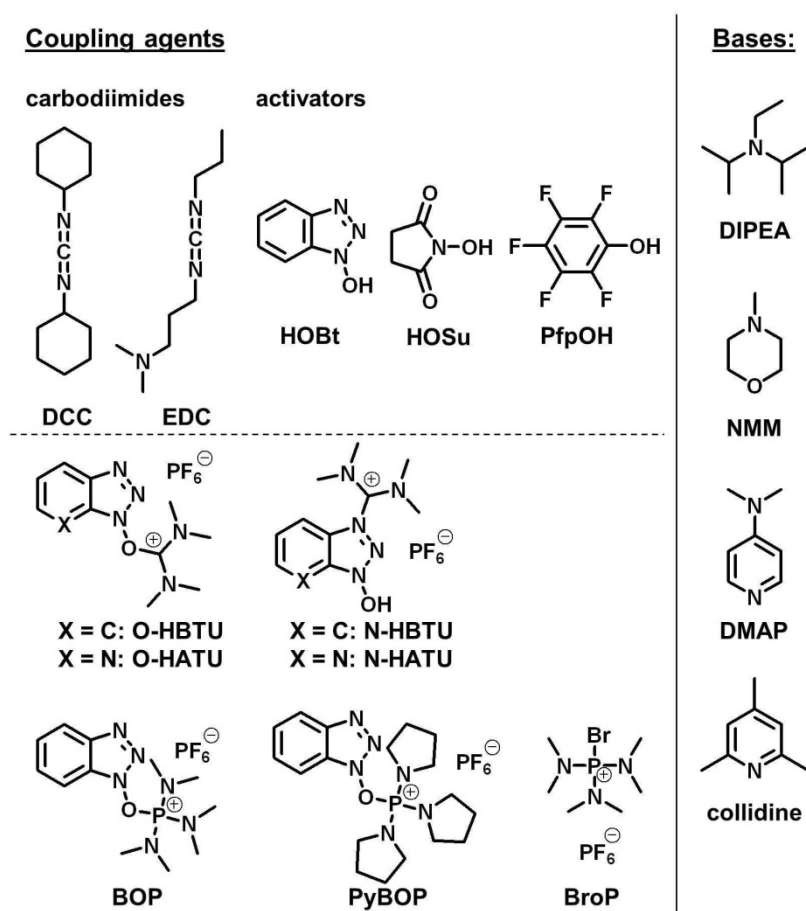


**Figure 4.4.** An overview of common coupling agents and bases in peptide chemistry.<sup>176-180</sup>

Figure 4.4 shows an overview of common coupling agents and bases in peptide chemistry.<sup>176-180</sup> As classical coupling agents count the carbodiimides reagents like DCC<sup>181-183</sup> and EDC<sup>184</sup> together with the activators HOBt, HOSu and PfpOH. The first reported carbodiimide was DCC<sup>185</sup>, using this coupling agent peptide coupling is fast and with a high yield. Moreover, it is non-sensitive against moisture and it even worked under aqueous conditions as well as the product could be easily separated from the by-product as the by-product is insoluble in most solvents. The breakthrough using carbodiimides was the combination with activators like DCC/HOBt, as the additives could enhance the

reaction rate and reduce the racemisation.<sup>176, 186</sup> Thereby, HOBt avoids a hyperactivation of the carboxylic acid, thus side reactions like cyclisation, urea formation and racemisation could be suppressed.<sup>180</sup> As activators HOSu<sup>187</sup> and PfpOH also could be applied for the *in situ* formation of the active esters, which are so stable that they could be isolated and purified via column chromatography.<sup>179</sup> Based on the promising features of the activated esters other ones were synthesized, isolated and used as activating reagent, common to most is the salt structure with the very weakly nucleophile PF<sub>6</sub><sup>-</sup> as counter ion. For example *O*-/*N*-HBTU and *O*-/*N*-HATU are known as excellent coupling reagents, which can be used solely or together with HOBt. Thereby, free aliphatic hydroxyl functions are not affected and the harmless by-products can be easily removed.<sup>178</sup> Both *O*- and *N*-HBTU are existent, but *O*-HBTU is known to be more reactive.<sup>180</sup> Moreover, further increase in reactivity was achieved by the introduction of nitrogen into the phenyl part to achieve HATU (N-guanidium salt).<sup>188</sup> Due to this pyridine nitrogen in vicinity to the amine the nucleophilicity is increased and thus the reactivity.<sup>189</sup>

Furthermore, phosphonium reagents could be used as peptide coupling reagents. One of the first was BroP however racemisation was observed in Young's test.<sup>190</sup> Based on the knowledge of the application of HOBt, suppressing the racemization, the synthesis of the phosphonium reagents was adapted and BOP<sup>191</sup> and PyBOP<sup>192, 193</sup> were introduced. BOP is stable, non-hygroscopic and good soluble in organic solvents, moreover it is more efficient than the combination of DCC/HOBt. But, poisonous hexamethylphosphoramide (HMPA) is generated as by-product, due to this reason PyBOP (pyrrolidine instead of dimethyl amine moieties) can be used.<sup>176, 179</sup>

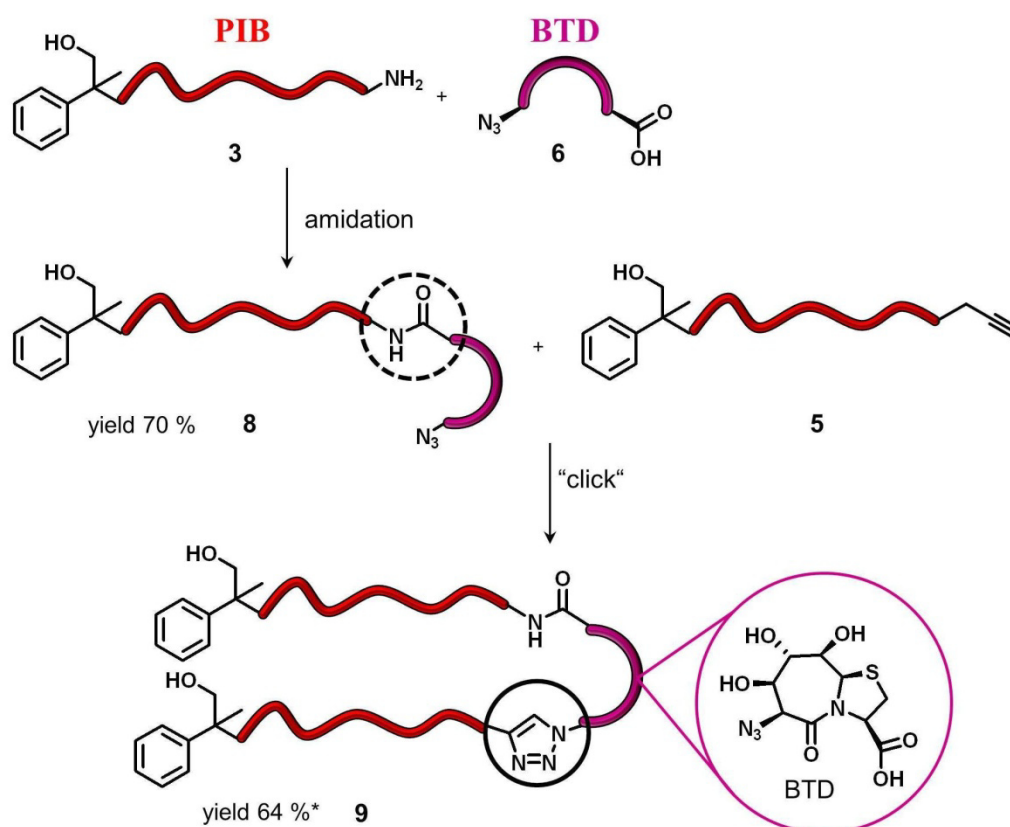
Beside the coupling reagents the choice of base is also important in peptide coupling reactions. Especially non-nucleophilic bases like DIPEA, NMM, DMAP and collidine (tertiary amines) are considered as useful bases.<sup>176, 194</sup>

### 4.3.2 Linkage of the different building blocks

Scheme 4.4 shows the synthetic route towards the amphiphilic polymer conjugate containing BTD as  $\beta$ -turn mimetic **9** (syntheses and characterization see experimental part). In a first step the synthesized building blocks, the  $\alpha$ -hydroxymethyl- $\omega$ -amino telechelic PIB (**3**) and the BTD **6** (bearing the azide functionality on the one side and the active carboxylic acid group on the other side), were linked via an amidation reaction using PyBOP/NMM as coupling reagents resulting the PIB-BTD **8**. To this first strand the second strand, the  $\alpha$ -hydroxymethyl- $\omega$ -alkyne telechelic PIB (**5**), was then coupled via the Cu(I)-mediated azide/alkyne-“click”-reaction<sup>168</sup> to achieve the final PIB conjugate **9** where two PIB strands are connected to the one  $\beta$ -turn mimetic BTD. However, the linkage of the second strand onto the same  $\beta$ -turn mimetic is quite challenging. The  $\beta$ -turn mimetic has a constrained conformation and the space between the two reactive linking groups (azide and carboxylic acid group distance: 7 Å)<sup>115</sup> is reduced, therefore the linking reactions are kinetically hindered and the reactivity especially for the

## 4. Results and discussion

linkage of a second PIB strand onto the  $\beta$ -turn mimetic is drastically reduced for both groups. This influence of the steric factors became obviously when PMDETA (bulky base) was used as base, resulting in no formation of the PIB conjugate **9**. Whereas the use of the less bulky base DIPEA lead to the formation of the product **9** with a yield of 64 % determined after column chromatography, but with traces of **8**. For ultrapure PIB conjugate **9** this crude product was further purified via preparative HPLC using HPLC graded, freshly distilled THF.



**Scheme 4.4.** Synthetic route towards amphiphilic polymer conjugate containing BTM as  $\beta$ -turn mimetic.

The synthetic route should be repeated for the use of the SAA (**7**) as  $\beta$ -turn mimetic, but the first step the amidation already failed. Therefore, we tried to start the linkage from the other side. Although the "click"-reaction of PIB **5** with the SAA (**7c**) (OAc protected hydroxyl groups, azide and carboxylic acid methyl ester end groups) worked ( $^1\text{H-NMR}$  see Appendix FigureA7), the crucial next step, the deprotection/hydrolysis, failed. Even though different bases (LiOH, NaOMe, hydrazine-hydrate) and different solvents/-mixtures (THF, MeOH, dioxane and water) were tried and the reaction conditions varied from 12 h at room temperature up to 7 d at 50 °C - no hydrolyzed product could be achieved. To overcome this problem the already deprotected/hydrolyzed SAA (**7**) was directly used for the "click"-reaction with the PIB strand **5**, but no "click" product was formed.

### 4.3.3 Analysis of the intermediates **5** and **8** and the $\beta$ -turn mimetic PIB conjugate **9**

In the following section the purities of the intermediates **5** and **8** as well as of the final product **9** will be discussed in detail, especially as **8** and **9** will be then used for the membrane experiments. Therefore, extensive spectroscopic, spectrometric and chromatographic characterizations were conducted (additional spectra see Appendix Figure A8-A12).

Figure 4.5 shows an overlay of the  $^1\text{H}$ -NMR spectra of a) PIB-BTD **8** and b) PIB-BTD-PIB **9** enabling the direct comparison between both structures. With the aid of 2D-NMR spectroscopy (HH-COSY and HSQC) together with the  $^1\text{H}/^{13}\text{C}$  spectra of the starting compounds **3**, **5** and **6** all peaks could be assigned to the structures. The synthesis of the first strand PIB-BTD **8** and therefore the formation of the amide bond is given by the shift of the signal of the methylene group in vicinity to the former amine (H-9) from 2.70 ppm to 3.27 ppm (Figure 4.4a). Also the appearance of the broad singlet at 6.69 ppm according to the NH-proton indicates the formation of the amide bond and thus the linkage of PIB **3** onto BTD **6**. Moreover, the integral values of the PIB initiator (H-2/2') and the PIB quencher (H-6, 7) match with the integral values of the  $\beta$ -turn mimetic BTD. The integration of the region 0.5-2 ppm of the polymer backbone gives the calculated  $M_{n(\text{NMR})}$  of 5600 g/mol.

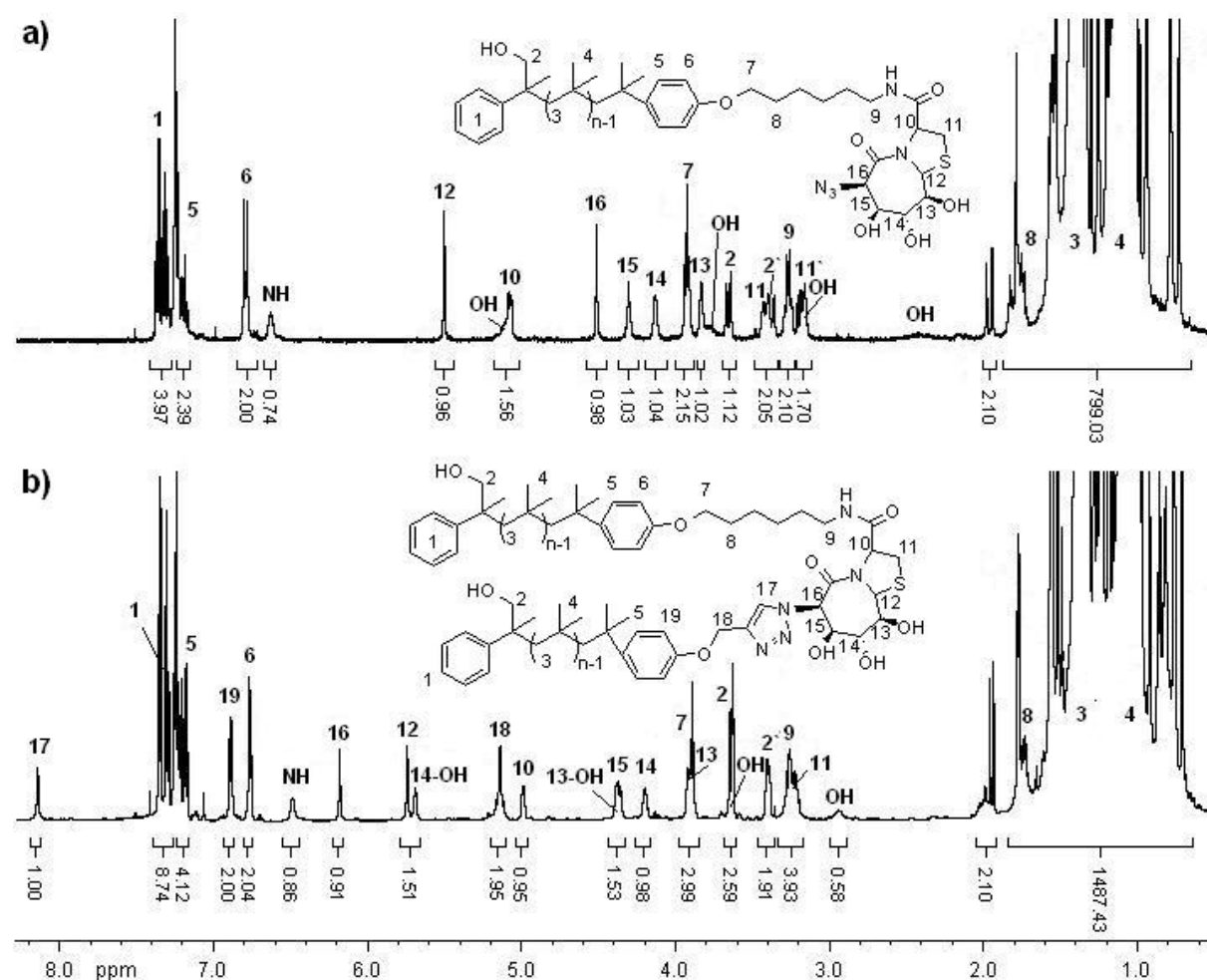


**Figure 4.5.**  $^1\text{H}$ -NMR overlay of a) PIB-BTD **8** and b) PIB-BTD-PIB **9**.

## 4. Results and discussion

The appearance of the singlet of the newly formed triazole moiety at 8.16 ppm (H-17) together with the shift of the methine group in vicinity to the former azide to 6.20 ppm (H-16) clearly indicate the linkage of the second PIB strand **5** onto the first PIB-BTD strand **8** resulting in the fully linked PIB conjugate **9** via Cu(I) mediated azide/alkyne-“click”-reaction (Figure 4.4b). Moreover, the shift of the resonance of the methylene group in vicinity to the former alkyne to 5.16 ppm (H-18) as well as the vanishing of the methine resonance of the former alkyne group proof the formation of **9**. Here again the integral values of the PIB initiators (H-2/2') and the PIB quenchers (H-6,7 and H-18,19) agree with the integral values of the  $\beta$ -turn mimetic BTD. The integration of the region 0.5-2 ppm of the polymer backbone gives the calculated  $M_{n(\text{NMR})}$  of 10,400 g/mol evidencing the linkage of both PIB chains to the BTD.

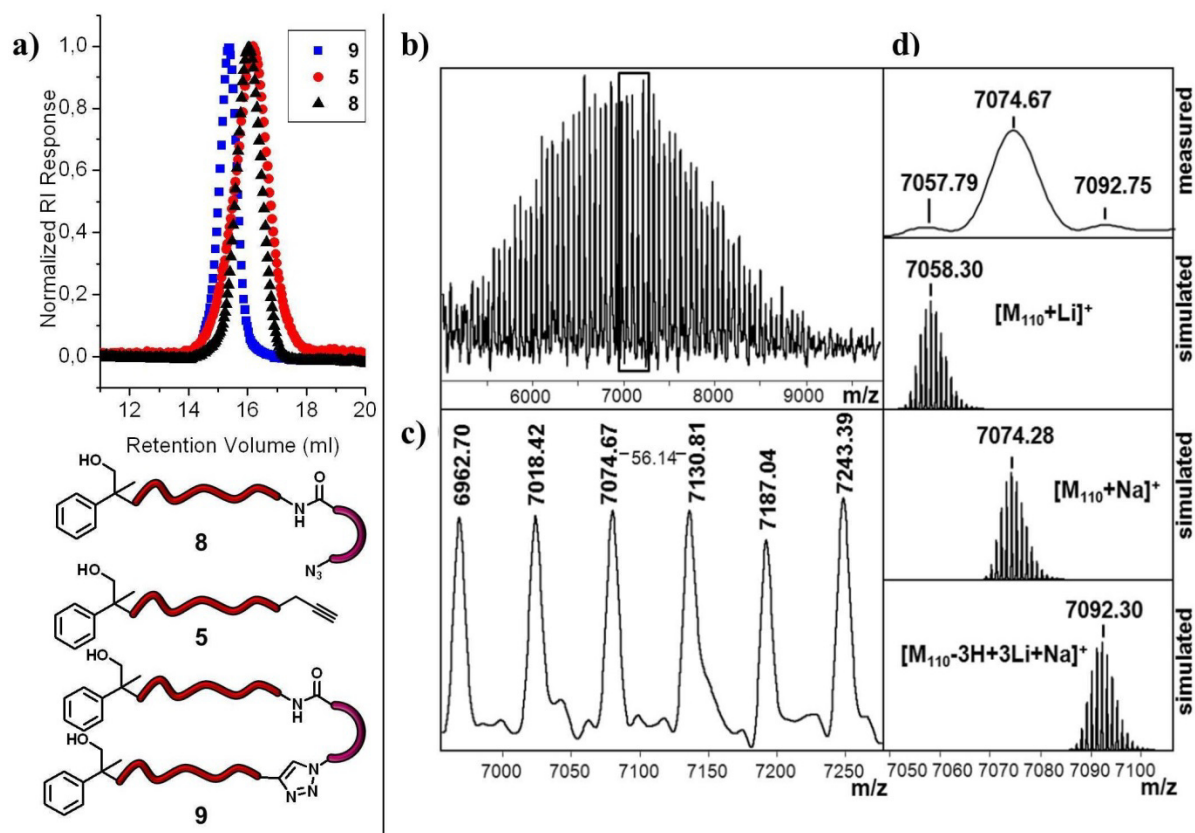


**Figure 4.6.** a) Normalized SEC RI traces (1 mL/min, THF) of the single PIB strands **5** ( $M_n = 4700$  g/mol, PDI = 1.39) and **8** ( $M_n = 5300$  g/mol, PDI = 1.20) and the fully linked product **9** ( $M_n = 10,100$  g/mol, PDI = 1.16). MALDI-ToF MS of **9** b) the region from 5000-10,000 Da, c) expanded spectrum according to highlighted region in (a) and c) expanded spectrum with a listed view of the simulated peaks. Reproduced with permission from [Malke, M.; Barqawi, H.; Binder, W. H., Synthesis of an Amphiphilic  \$\beta\$ -Turn Mimetic Polymer Conjugate. \*ACS Macro Lett.\* \*\*2014\*\*, 3, \(4\), 393-397. Copyright 2015 American Chemical Society.](#)

The comparison of the molecular weights of the single PIB strands **5** and **8** with the resulting  $\beta$ -turn mimetic PIB conjugate **9** determined via SEC is a further possibility to proof the successful full linkage. Figure 4.6a shows the normalized RI response over the retention volume, providing molecular weights ( $M_n$ ) and the molecular weight distribution/polydispersity index ( $M_w/M_n = \text{PDI}$ ) using PIB

standards for calibration. The analyses of the traces of the single PIB strands **5** and **8** show nearly similar monomodal distribution  $M_n = 4700$  g/mol respectively  $M_n = 5300$  g/mol and relatively narrow PDIs of 1.39 respectively 1.20. As a result of the fully linkage of both PIB strands to the  $\beta$ -turn mimetic BTD the SEC trace of the PIB conjugate **9** is shifted to shorter retention time. Thus, the molecular weight is increased to  $M_n = 10,100$  g/mol, which corresponds to the sum of the single PIB strands **5** and **8** and is in good agreement with  $M_n$  calculated from  $^1\text{H-NMR}$ . This together with the narrow PDI of 1.16 and no formation of a shoulder evidences the formation and the purity of the final product **9**. Furthermore, additional information to the molecular weights and much more important to clarify the structure, MALDI-ToF MS was carried out. Figure 4.6b shows the MALDI-ToF MS of the fully linked  $\beta$ -turn mimetic PIB conjugate **9** with a mass distribution of 5500 to 9000 g/mol and a maximum at 7000 g/mol. The chemical identity of **9** could be proven by the distance between two peaks indicating the repetitive unit of 56.1 g/mol corresponding to PIB (Figure 4.5c) for all of the peaks of the three different series. That these three different series could be assigned to the same product **9** with 110 repetitive units of isobutylene and different salts is shown in Figure 4.5d giving an expanded spectrum with a listed view of the simulated peaks. The signals at 7057.79 g/mol and 7074.67 g/mol corresponded with the simulated values of 7058.30 g/mol and 7074.28 g/mol for the Li-adduct respectively the Na-adduct. Whereas, the signal at 7092.75 g/mol of the third series showed different ionization behavior, as three protons of the hydroxyl groups of the  $\beta$ -turn mimetic PIB conjugate **9** were exchanged with three Li-ions and one Na-ion (for ionization) giving the calculated value of 7092.30 g/mol. Even though the molecular weight determined via MALDI-ToF MS is significantly lower than calculated via  $^1\text{H-NMR}$  spectroscopy and SEC an overlay with the single PIB strand **8** ( $M_{n,\text{max}} = 3500$  g/mol, see Appendix Figure A9) demonstrate the shift of the molecular weight and the disappearance of **8**. Moreover, the maximum at 7000 g/mol is in good accordance with the double molecular weight of the single PIB **5** and **8** strands (having similar molecular weights), evidencing the linkage of both single PIB strands and thus the formation of **9**. The lower molecular weights in MALDI-ToF MS could be explained by the challenging polarizability of the nonpolar PIB resulting in difficult ionization. The nature of the functional end groups is decisive for the “flying” of PIB in MALDI-ToF MS as well as shorter chains with a more favorable ratio of end group to PIB backbone can absorb better.

Concluding the proof of the complete linkage of both PIB strands (**3** and **5**) onto the central unit BTD (**6**) and the ultimate purity of the final PIB conjugate **9** 2D-LC/SEC-(MALDI-ToF)-MS<sup>195, 196</sup> should be conducted based on the successful application of this method in our group. Barqawi *et al.*<sup>195</sup> worked out the separation of telechelic- and block copolymers by a combination of LCCC (liquid chromatography under critical conditions, first dimension) and SEC (second dimension) using the differences in polarity and hydrodynamic volume. Therefore, this method should be able to distinguish between the single strands PIB **5** and **8** and the fully linked PIB **9**. At first the LCCC conditions of  $\alpha$ -hydroxymethyl- $\omega$ -bromo telechelic poly(isobutylene) **17c-e** with molecular weights of 4000 g/mol



## 4. Results and discussion

(PDI = 1.4), 8000 g/mol (PDI = 1.3) and 15,000 Da (PDI = 1.2) using a reversed phase column (RP C-18, Waters Atlantis<sup>®</sup>-T3) were found at MTBE/MeOH = 85.2:14.8 (v/v) at a flow rate of 0.1 mL and a temperature of 30 °C. Under these conditions all three model PIBs **17c-e** show the same retention time in the LC trace, because under critical conditions the separation of polymers based on their functionality solely, as the effect of their molecular weight is eliminated.<sup>195</sup> Then the LC traces of **5**, **8** and **9** were measured at the critical conditions of PIB (Figure 4.7a).

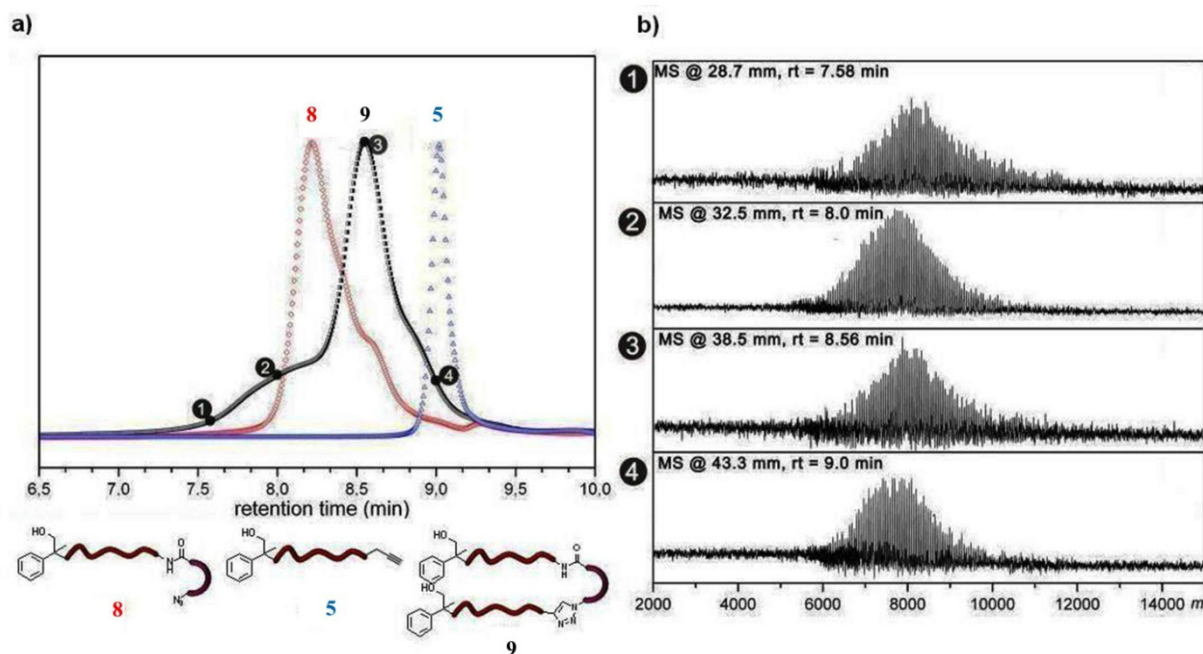


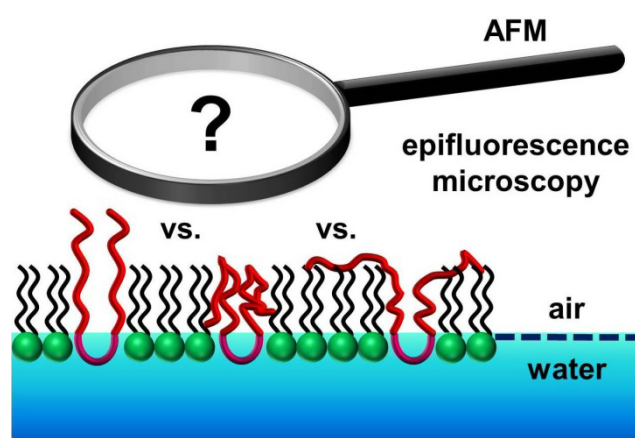
**Figure 4.7.** LC/MALDI-ToF MS of **9**. a) LC trace of **5**, **8** and **9** measured at critical conditions of PIB (MTBE/MeOH = 85.2:14.8 (v/v)) at a flow rate of 0.1 mL/min, T = 30 °C, b) MALDI-ToF MS spectra of the correlated fractions of **9** proving the purity of the final amphiphilic  $\beta$ -turn mimetic PIB conjugate. Reproduced with permission from Malke, M.; Barqawi, H.; Binder, W. H., Synthesis of an Amphiphilic  $\beta$ -Turn Mimetic Polymer Conjugate. *ACS Macro Lett.* **2014**, 3, (4), 393-397. Copyright 2015 American Chemical Society.

As a reversed phase column was used the retention time increased with decreasing polarity, therefore the single strand PIB-BTD **8** bearing the hydrophilic  $\beta$ -turn mimetic BTD elutes before the less polar PIB **5** bearing the alkyne moiety, in between the final product **9** was eluted. Having a deeper look into the LC trace of **9** shoulder formation is visible, which might be concluded that the final product consists of unremoved **5** and **8**. To dissolve this problem the first dimension (LCCC) should be directly coupled to a second dimension, the SEC, by collecting the eluents coming out of the first dimension in two switching loops and pumping them through the SEC column. But preliminary experiments using  $\alpha$ -hydroxymethyl- $\omega$ -bromo telechelic poly(isobutylene) **17** with molecular weights of 4000 g/mol (**17c**) and 15,000 g/mol (**17e**) and a SEC column with a range of 1-30 kDa (PSS SDV HighSpeed 5  $\mu$ m 500 Å) showed that this coupling is not useful, as a 50:50 mixture gives in the first dimension one trace and in the second dimension one curve with an average molecular weight of 10,400 g/mol (see Appendix Figure A10). Therefore, experiments using the SEC dimension solely

were conducted (see Appendix Figure A11). Mixtures of PIB **17c** and **17e** were measured in different ratios (90:10-10:90) showing a shift of an average molecular weight to higher molecular weights when increasing the amount of **17e**. Shouldering of the peaks or even two separated peaks could not be achieved. This means, that an insufficient separation in the first dimension will not lead to a separation in the second dimension when using molecular weights around 4000 g/mol and 15,000 g/mol. As each loop for collecting the first dimension fractions has a volume of 200  $\mu\text{L}$  and the flow rate is 0.1 mL/min the loops switch every 2 min, this means that the LC-information gets lost for peaks within these 2 min when their molecular weights are too equal.

That's why we modified this method by coupling LC with MALDI-ToF MS to prove the purity of **9** and clarifying the shoulder formation of the LC trace of **9** in Figure 4.7a. Figure 4.7b shows the MALDI-ToF MS spectra of directly correlated fractions of the fully linked PIB **9** showing clearly just one series from 6000 Da to 10,000 Da. If there would be traces of unremoved single PIB strands **5** and **8** additional series smaller than 5000 Da would be observed. To substantiate this hypothesis a control experiment using a mixture of **9** and **8** (20:80 = w/w) was conducted, clearly demonstrating the separation efficiency of the used LC-technique by showing two separated series for **8** (4000-6000 Da) and **9** (6000-9000 Da) (see Appendix Figure A12). Moreover, the correlated MALDI-ToF MS spectra Figure 4.6b show a slight shift from higher molecular weights to lower molecular weights according to increasing retention time of the first dimension, which indicates SEC behavior.<sup>195</sup> Therefore, the shoulder formation of the LC trace of the  $\beta$ -turn mimetic PIB conjugate **9** is explainable as SEC effect. Due to the linkage of both single strands **5** and **8** to achieve **9** the polarity and the molecular weight was changed, therefore the LCCC conditions for the model PIBs **17** doesn't match for the investigated PIB conjugate **9**. The LC/MALDI-ToF MS also proofed the high purity of the final  $\beta$ -turn mimetic PIB conjugate **9**.

#### 4.4 Monolayer experiments of **8** and **9** using DPPC as lipid



**Scheme 4.5.** Schematic diagram for studying the folding of  $\beta$ -turn mimetic PIB conjugate **9** when incorporated into a monolayer membrane (DPPC) using different polymer to lipid ratios and coupling to imaging methods like epifluorescence microscopy and AFM.

To investigate the folding of  $\beta$ -turn mimetic PIB conjugate **9** when incorporated into a membrane Langmuir monolayer measurements were conducted, which serve as model for half a bilayer membrane (Scheme 4.5). Therefore, mixed hybrid membranes composed of DPPC and PIB with different ratios of DPPC/PIB were extensively investigated. As comparison for folding effects the single strand **8** where one PIB strand is connected to the  $\beta$ -turn mimetic BTD was used. Due to the amphiphilic structure of **8** and **9** the hydrophilic  $\beta$ -turn mimetic BTD should serve as anchor in the water phase whereas the hydrophobic PIB chains should orientate along the water/air interface. To get a deeper look into the behavior of the mixed hybrid membranes during the compression of the Langmuir measurements imaging methods as epifluorescence microscopy and atomic force microscopy (AFM) were used. In the following the compression isotherms of DPPC/**8** and DPPC/**9**, the directly correlated epifluorescence microscopy images and AFM images at defined pressures will be discussed.

### 4.4.1 Monolayer compression isotherms of DPPC/**8** and DPPC/**9** mixtures

Monolayer compression isotherms were conducted for the pure compounds DPPC, **8** and **9**, and for the DPPC/polymer mixtures with different molar ratios (Figure 4.8a-c). Figure 4.8a shows the compression isotherms for the pure PIB-BTD **8** (black curve) and PIB-BTD-PIB **9** (red curve). The first increase of the pressure of the isotherm (lift-off) of **8** was observed at  $161 \text{ \AA}^2$ , whereas the lift-off of the isotherm of **9** was shifted to  $322 \text{ \AA}^2$ . This doubling of the mean molecular area (mma) value is in exact agreement with the double molecular weight of **9** in comparison to **8**. Then the surface pressures increase for both until the films collapse which is indicated by the formation of the plateaus. The small tip at the beginning of the plateaus marks a metastable state. For the isotherm of **8** the plateau ( $\pi = 37 \text{ mN m}^{-1}$ ) starts at a mma value of  $73 \text{ \AA}^2$  and ends at  $18 \text{ \AA}^2$  (measurement stopped at this value as the limit for compression of the Langmuir trough was reached). If this plateau would be the from literature known *roll-over* collapse where triple layers are formed then the pressure should increase after 1/3 of the starting mma value of the plateau, this means the pressure should increase at approximately  $24 \text{ \AA}^2$ .<sup>197, 198</sup> That becomes clearer for the isotherm of **9**, the plateau ( $\pi = 35 \text{ mN m}^{-1}$ ) starts at a mma value of  $145.04 \text{ \AA}^2$  and ends at  $30.05 \text{ \AA}^2$  (measurement stopped at this value as the limit for compression of the Langmuir trough was reached), which is nearly 1/5  $\rightarrow$  indicating a “five-fold” layer. Therefore we assume, that we do not have the defined *roll-over*, but that we are “losing” material. As PIB is insoluble in water the lost material is not going into the water phase. Hysteresis experiments substantiate this and show that the amphiphilic PIB conjugates are well spread at the air-water interface. Thus, we conclude that “overlayers” are formed at the air-water interface.<sup>199</sup> In Figure 4.7b and c the compression isotherm for pure DPPC (black curve) is shown. The lift-off starts at a mma value of  $\sim 90 \text{ \AA}^2$  followed, due to further compression, by the characteristic plateau at  $\sim 4 \text{ mN m}^{-1}$  which is known as the phase transition from the liquid-expanded to the liquid-condensed state (LE/LC

## 4. Results and discussion

coexistence region).<sup>200, 201</sup> After this plateau the surface pressure increases strongly confirming the liquid-condensed state (LC).

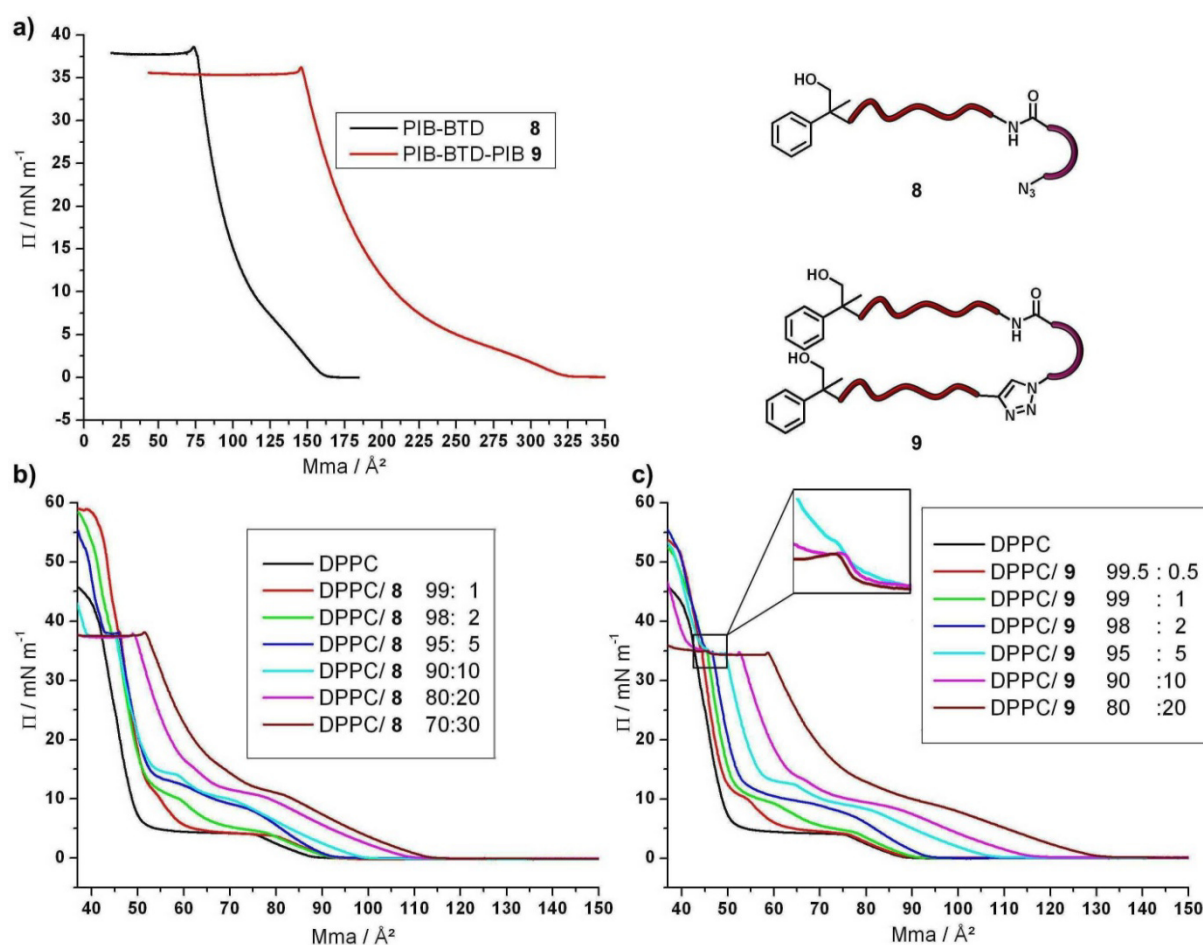


**Figure 4.8.**  $\Pi$ -A isotherms of (a) the pure PIBs **8** and **9**, (b) DPPC/**8** mixtures and (c) DPPC/**9** mixtures at 20 °C. The black curve represents the isotherm of the pure DPPC and the different colored curves represent the different molar ratios of the DPPC/polymer mixtures.

Figure 4.8b shows the monolayer isotherms of the DPPC/**8** mixtures with 1-30 % content of **8**. The lift-off areas of the mixtures are shifted to higher mean molecular areas with higher content of **8** however they differ from the calculated values. As the experimental values of the lift-off area are smaller than the expected ones attractive lipid/polymer interactions are concluded. This behavior was already observed in our group for PIB-PEO copolymers.<sup>202</sup> In contrast to this previous work and to the isotherms of the pure compounds, two plateaus could be observed during compression, whereby with increasing content of **8** the surface pressures for these plateaus increase as well. As the transition state of the lipid monolayer (LE/LC, first plateau) is at higher pressure (up to 10  $\text{mN m}^{-1}$ ) in comparison to pure DPPC, the PIB-BTD (**8**) strengthens the expanded phase. This means that the amphiphilic polymer molecules disturb the rearrangement of the lipid molecules at the air-water interface due to their partial miscibility with the LE phase of the DPPC, thus hindering the lipid packing. The second plateau (up to 15  $\text{mN m}^{-1}$ ) gives a hint for a second transition, what we believe is the new arrangement/ordering of the polymer molecules, meaning that the apolar PIB chains straighten up, but

are still tilted. This could be confirmed by further compression due to the existence of the previously titled “collapse” plateau ( $\pi = 37 \text{ mN m}^{-1}$ ) where the polymer molecules lift up from the subphase to build upper layers or squeeze out, whereby the length of this plateau is directly correlated to the mol fraction of **8**. After this plateau the behavior of the isotherms is depending on the DPPC molecules. The pressure of the isotherms increases drastically up to  $58 \text{ mN m}^{-1}$  at which point then the whole monolayer collapse. This region is known as the transition of the lipid molecules from the liquid condensed state to the solid phase state.<sup>201</sup>

Similar isotherm behavior could be observed for the DPPC/**9** mixtures with 0.5-20 % content of **9** (Figure 4.8c). Here again the shift of the lift-off areas to higher values correlates with the used mol fraction of **9**, but it is smaller than the calculated values, which was explained previously, as well as the two plateaus in the low pressure region ( $0\text{-}15 \text{ mN m}^{-1}$ ) are present as before. As mentioned previously the lift-off of the pure **9** was at the double  $\text{mma}$  value as for **8** due to the doubling of the molecular weight, this phenomenon is similar to the shape of the isotherms. For example the shape of the curve of DPPC/**8** 90:10 (pale blue) is similar to the curve of DPPC/**9** 95:5 (pale blue). At these ratios the used PIB is not mol equivalent but mass equivalent. Up to this point it seems that there are no perceptible differences whether one PIB chain is linked to the  $\beta$ -turn mimetic BTD or two PIB chains are linked to the same BTD molecule. But having a deeper look into the “collapse” plateau ( $\pi = 35 \text{ mN m}^{-1}$ ) a step at an area of  $45.5 \text{ \AA}^2$  per molecule within the plateau is visible (see zoom-in region Figure 4.7c), this area is in exact agreement with the calculated area ( $45 \text{ \AA}^2$ ) which is occupied by one molecule of BTD in a liquid condensed monolayer. Therefore, the third transition can be clearly attributed to the presence of the two PIB chains on the same  $\beta$ -turn mimetic BTD and marks a transition within the  $\beta$ -turn mimetic PIB conjugate **9** which is the ordering of the chains along one  $\beta$ -turn mimetic BTD molecule.

### 4.4.2 Epifluorescence microscopy of DPPC/**8** and DPPC/**9** mixed monolayers

To underpin the hypotheses from the compression isotherms and to get more information about the behavior of **8** and **9** in mixed monolayers during the compression, the Langmuir measurements were directly coupled to epifluorescence microscopy (all epifluorescence images not shown here can be found in the Appendix). For visualization the dye Rh-DHPE was used in a very small amount (0.01 mol %) in order not to influence the properties of the lipid/polymer mixtures at the air/water interface. This dye is known to be soluble preferentially in the less ordered LE domains of the monolayer, therefore these domains are bright and the ordered LC domains, which are excluded from the dye, are dark.<sup>203</sup>

Figure 4.9 shows the epifluorescence images of the monolayers of DPPC/**8** with different molar ratios (a-c) 99:1, (d-f) 98:2, and (g-i) 90:10 in the region of the second transition state (second plateau) at the air/water interface at  $20^\circ\text{C}$ . For the compression isotherm of DPPC/**8** 99:1 the image taken at a

## 4. Results and discussion

pressure of  $5.6 \text{ mN m}^{-1}$  (Figure 4.8a) is similar to pure L-DPPC (see Appendix Figure A14) with the propeller domains (LC domains) having the chirality-dependent curling direction to the left. The DPPC is the phase dominating factor, due to the high line tension between the LE and LC phase the propeller are compact. With increasing pressure ( $7.3 \text{ mN m}^{-1}$ , Figure 4.9b) a thinning of the propeller tips and spiral formation can be observed. This phenomenon was already observed for DPPC cospread with cholesterol or perfluorinated PGMA and could be explained by the reduced line tension, due to the formation of a new LC DPPC/polymer/LE DPPC boundary. Therefore, a partial miscibility of the amphiphilic PIB **8** with the LE phase of DPPC could be concluded.<sup>204</sup> Due to further compression (Figure 4.9c) the phase boundaries, which were clear before, are vanishing and the dye is forced into the LC phase.

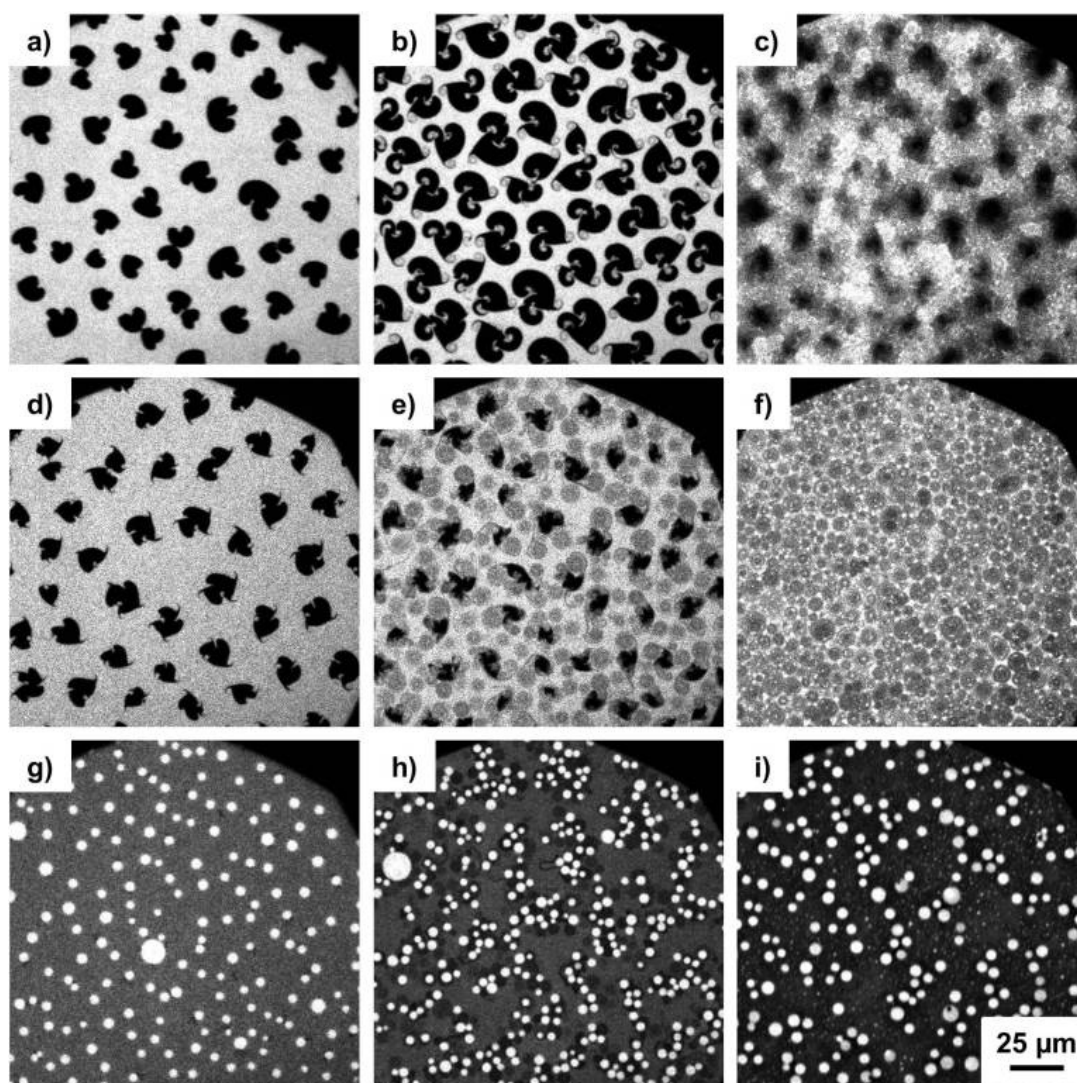


**Figure 4.9.** Epifluorescence microscopy images of monolayers of DPPC/**8** with different molar ratios (a-c) 99:1, (d-f) 98:2, and (g-i) 90:10 at the air/water interface at  $20^\circ\text{C}$ . The images were recorded at constant compression of the spread monolayer in the region of the second transition state (second plateau) at the following surface pressures: (a)  $5.6$ , (b)  $7.3$ , (c)  $11.3$ , (d)  $7.6$ , (e)  $9.1$ , (f)  $11.2$ , (g)  $9.7$ , (h)  $11.7$  and (i)  $14.5 \text{ mN m}^{-1}$ .

With increasing content of the amphiphilic PIB **8** (2 mol %) and progressing compression the thinning of the propeller tips and the spiral formation is increasing. Furthermore, bridging between the different domains could be observed (Figure 4.9d-e). The LC DPPC phase is decreasing, while the newly formed LC DPPC/polymer/LE DPPC boundary is increasing. Moreover, the forcing of the dye into the LC phase becomes clearer because only grey spirals with small bright dots on a bright background instead of black domains are visible (Figure 4.9f). Figure 4.9g-h shows the images of the compression isotherm with 10 mol % **8**. In contrast to the previous measurements, where just a small content of **8** was used, no propeller domains are visible (Figure 4.9g,  $9.7 \text{ mN m}^{-1}$ ). The first black domains (LC DPPC) appear at the boundaries to the bright round LE domains, which are the polymer rich phase as they are increasing with increasing content of **8** (see Appendix). Therefore, the grey background is the lipid rich LE phase. With further compression (Figure 4.9h,  $11.7 \text{ mN m}^{-1}$ ) this bright domains are clustering like pearls on a string, and the dark LC domains are growing, elongating and are hardly visible as spirals or as bridges between different clusters. Within the second plateau (Figure 4.9i,  $14.5 \text{ mN m}^{-1}$ ) again small bright domains appear from the dark background indicating the constraint of the dye into the ordered LC domains.

In conclusion from the images discussed here, the images in the Appendix and image analyses the increase of the content of the amphiphilic polymer **8** is accompanied by the decrease of the contrast bright-dark. Therefore, the Rh-dye is soluble in both LE phases, of the DPPC and of the polymer. The first plateau shows the transition of the LE phase to the LC phase of the lipid rich domains and the second plateau shows the transition of the LE phase to the LC phase of the lipids in the polymer-mixed phase as the transitions are located at the newly formed LC DPPC/polymer/LE DPPC boundary. After this second plateau an increase of the pressure up to the third plateau could be observed which we believe is the diffusion of residual lipids of the polymer rich bright domains (LE phase) into the ordered LC phases, which is visible in the shrinkage of these bright domains.

Figure 4.10 shows the epifluorescence images of the monolayers of DPPC/**9** with different molar ratios (a-c) 99.5:0.5, (d-f) 99:1, and (g-i) 90:10 in the region of the second transition state (second plateau) at the air/water interface at  $20^\circ\text{C}$ . The first ratio 99.5:0.5 (DPPC/**9**) is the mass equivalent ratio to DPPC/**8** 99:1, as it could be seen for the compression isotherms the shape of the curves (Figure 4.8b and c, red curves) is similar, therefore identical behavior of the molecules during the compression will be expected. The image taken at a pressure of  $5.8 \text{ mN m}^{-1}$  (Figure 4.10a) is relatively similar to the equivalent image (Figure 4.9a, using 1 mol % of **8**), the black propeller domains (LC domains) are as well chirality dependent showing the curling to the left. But in contrast to the propeller domains of the pure L-DPPC (see Appendix Figure A50) they are irregular and not so compact. The non-uniform size and shape indicates the non-equilibrium behavior in the monolayer<sup>201</sup> and substantiate the coexistence of different phases within the second plateau. They are thinned out at the

propeller tips, which would indicate that the previously mentioned newly formed LC DPPC/polymer/LE DPPC boundary already exists with just a very small amount of **9** and at low pressures.

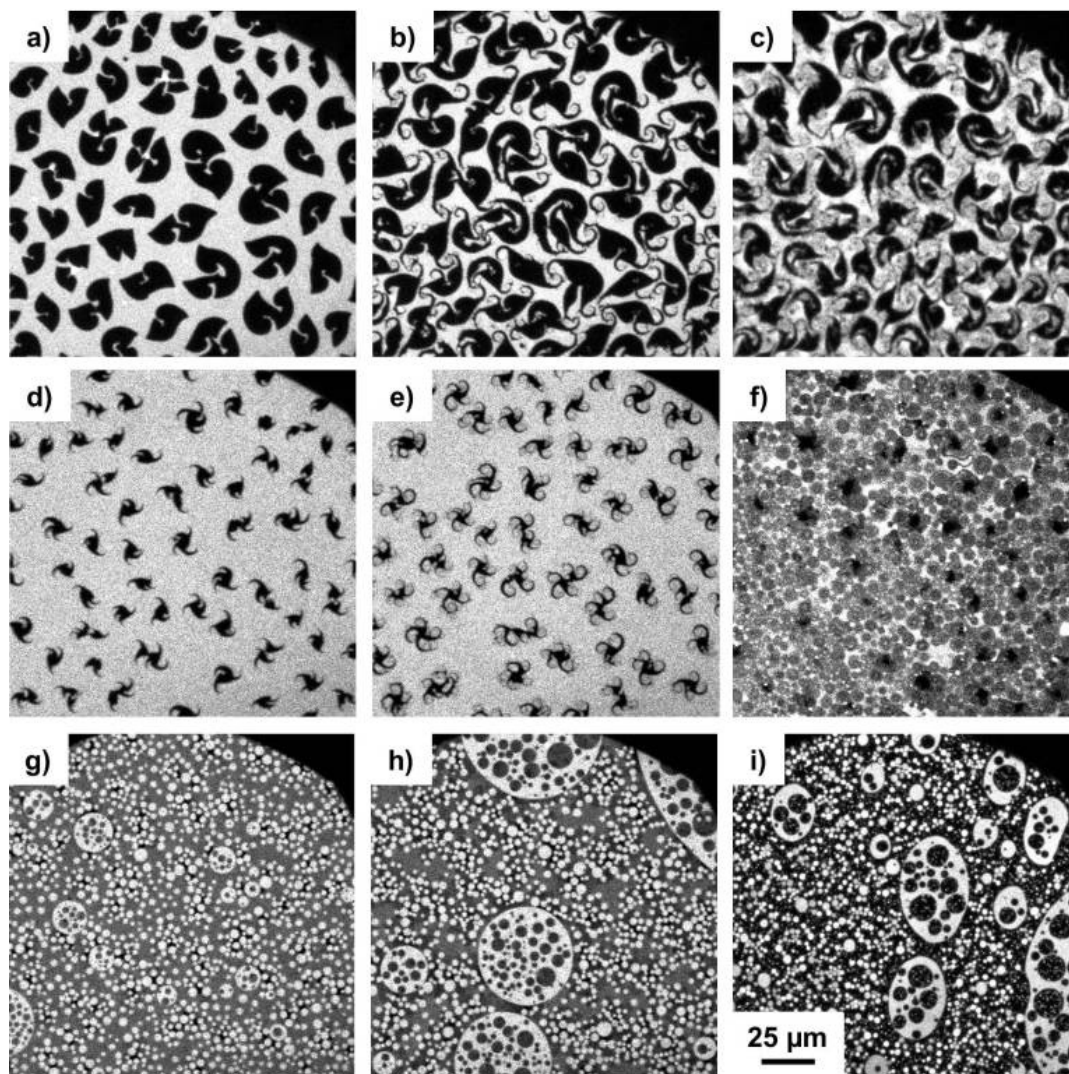


**Figure 4.10.** Epifluorescence microscopy images of monolayers of DPPC/**9** with different molar ratios (a-c) 99.5:0.5, (d-f) 99:1, and (g-i) 90:10 at the air/water interface at 20°C. The images were recorded at constant compression of the spread monolayer in the region of the second transition state (second plateau) at the following surface pressures: (a) 5.8, (b) 7.2, (c) 7.6, (d) 6.6, (e) 6.9, (f) 9.7, (g) 9.4, (h) 10.3 and (i) 29.2  $\text{mN m}^{-1}$ .

Due to further compression the thinning of the propeller tips increases and spiral formation together with branching at the edges could be observed (Figure 4.10b, 7.2  $\text{mN m}^{-1}$ ). This indicates a strong reduction in the line tension and a stronger dominating LC DPPC/polymer/LE DPPC boundary and therefore increased miscibility of the amphiphilic PIB **9** with the LE phase of DPPC in comparison with its “one arm” equivalent **8**. Then the former clear boundaries are vanishing and the dye is again forced into the LC phase (Figure 4.10c). With increasing content of **9** to 1 mol % (mass equivalent to DPPC/**8** 98:2) the black LC domains are getting smaller, more irregular and instead of three arm propeller almost all have four propeller blades which are strongly thinned (Figure 4.10d). Again proceeding thinning of the propeller tips and spiraling could be observed with increasing pressure



(Figure 4.10e). Moreover, the forcing of the dye into the LC phase becomes clearer because only grey spirals with small bright dots on a bright background instead of black domains are visible (Figure 4.10f). Figure 4.10 g-h shows the images of the compression isotherm with 10 mol % of **9**. In contrast to the previous measurements using just a small content of **9** no propeller domains are visible (Figure 4.10g, 9.4 mN m<sup>-1</sup>). The first black domains (LC DPPC) appear at the boundaries to the bright round LE domains, which differ in their size and can include smaller round grey domains. Moreover, the black LC domains seem to bridge the bright domains. As it was observed for the previous work using **8** as amphiphilic PIB, with increasing content of **9** (see Appendix) the bright domains increase as well. Therefore, they could be assigned to the polymer rich LE phase, and the grey background constitutes the lipid rich LE phase. Due to further compression the dark LC domains grow and stronger clustering between the bright LE domains and the dark LC domains could be observed (Figure 4.10g, 10.3 mN m<sup>-1</sup>). While continuing compression the previously round shaped domains become oval and the contrast between dark and bright increases together with a shrinkage of the single domain size. Even here the dye is forced into the ordered LC domain as bright small dots appear out of the dark background Figure 4.10h, 29.2 mN m<sup>-1</sup>).

It could be shown, that both amphiphilic PIB conjugates **8** and **9** are behaving nearly similar when incorporated into a monolayer membrane using DPPC as lipid and varying the mixing ratios, but the use of epifluorescence microscopy is only helpful for the phase transitions in the low pressure region. As it can be seen from images in the Appendix, with pressures higher than 30 mN m<sup>-1</sup> no differences according to contrast, shape and size of the single domains could be observed as they are just visible as small bright dots on a dark background. But the transitions within the third plateau are at pressures around 35 mN m<sup>-1</sup> and especially the step within the third plateau using **9** instead of **8** is the only difference between their compression isotherms. However, it may also mean that indeed the previously mentioned ordering of the two PIB chains linked to one  $\beta$ -turn mimetic BTM takes place at this step within the third plateau.

### 4.4.3 AFM measurements

Atomic force microscopy is a technique which can directly image the surface structure of samples at atomic height scale (here 10 nm AFM tip). Therefore, it can be used as imaging method in regions where the epifluorescence microscopy has already reached the resolution limit. To understand the molecular organization of mixed DPPC/**8** and DPPC/**9** monolayers in a ratio of 90:10, we conducted AFM measurements using the Langmuir Blodgett (LB) technique. As the region within the third plateau is the coexistence of two phases/states, one sample before the plateau (30 mN m<sup>-1</sup>) and one sample after the plateau (40 mN m<sup>-1</sup>) were measured. Thereby, the pressure at 30 mN m<sup>-1</sup> is comparable to the internal pressure of biological membranes.<sup>205</sup> Figure 4.11 shows the AFM topography (a, b, d and e) and topology images (c and f) of mixed monolayer of DPPC/**8** 90:10 mol% transferred at surface pressures of (a-c) 30 mN m<sup>-1</sup> and (d-f) 40 mN m<sup>-1</sup>. As the topography images

## 4. Results and discussion

show no defects a complete transfer from the monolayer onto the Si-wafer can be concluded. At a transfer pressure of  $30 \text{ mN m}^{-1}$  (Figure 4.11a-b) the image shows randomly distributed cylindrical PIB domains mostly dominated with a height of  $\sim 17 \text{ nm}$  out of the plane lipid monolayer (LC domain) or out of round shaped plateaus (height  $\sim 7 \text{ nm}$ , due to partial squeeze out of the PIB), thus having three different domains.

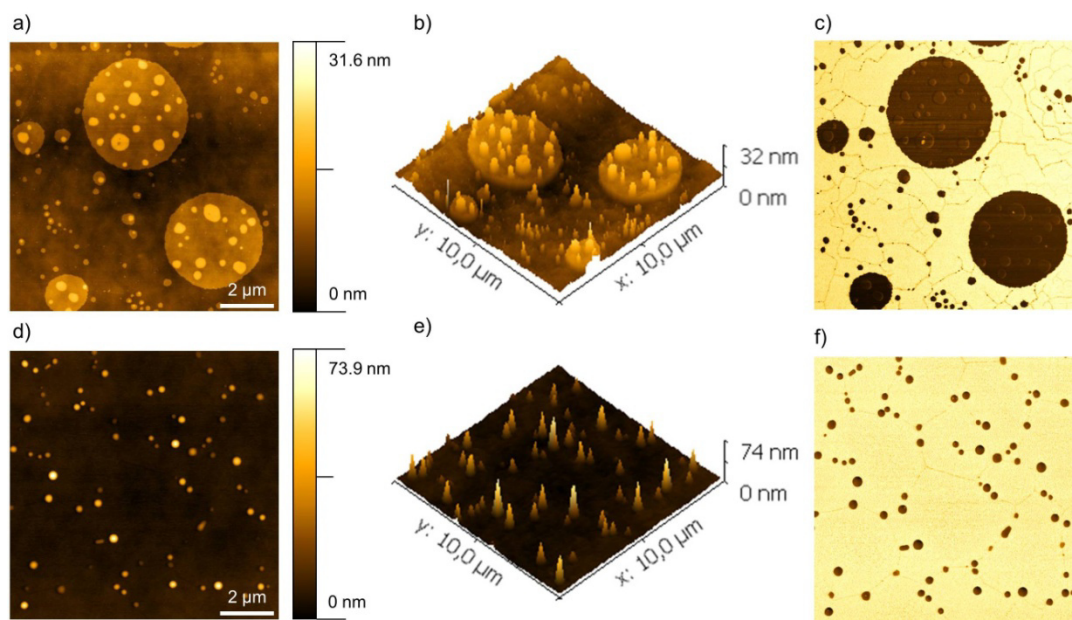
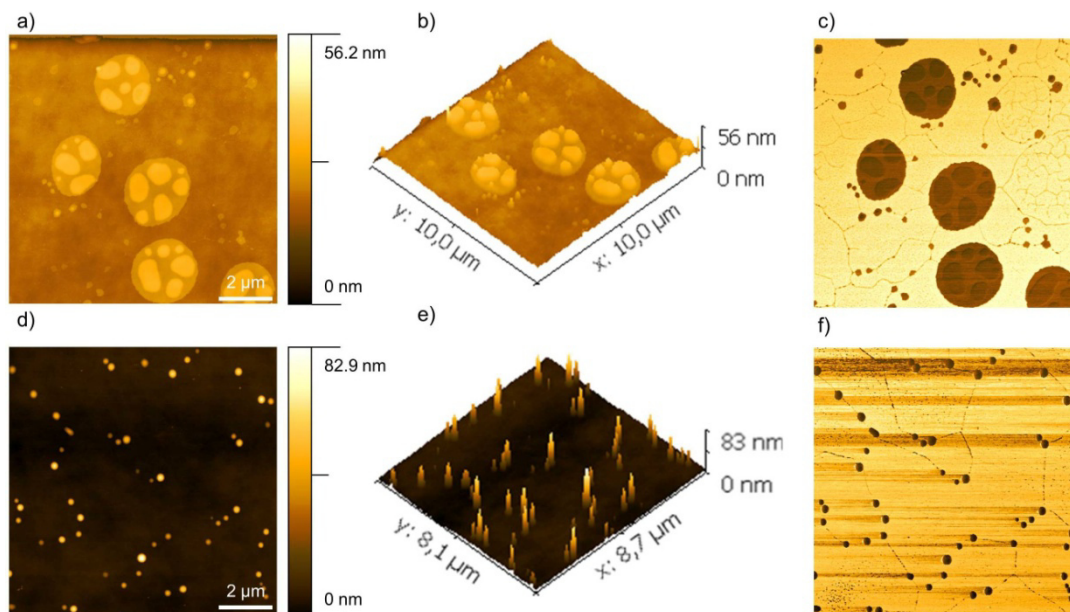


**Figure 4.11.** AFM topography (a, b, d and e) and topology images (c and f) of mixed monolayer of DPPC/**8** 90:10 mol% transferred at a surface pressures of (a-c)  $30 \text{ mN m}^{-1}$  and (d-f)  $40 \text{ mN m}^{-1}$ .

These cylindrical structures are in fact disc like domains considering their dimensions, whereby their height correlates with a single-folded PIB chain.<sup>197, 206</sup> Taking into account the topology image (phase image, Figure 4.11c, brown: soft, bright: hard) two different phases/domains are visible; the brown, round shaped domains and therefore soft domains (the polymer rich phase) and the surrounding harder lipid monolayer (LC phase). Moreover, this plane lipid monolayer is cross cut by a network of small paths, together with small dark dots lined up as a string of pearls, which are only visible in the phase image. As these network and dots appear dark, they are softer than the surrounding LC phase of the lipid and show the previously mentioned newly formed LC DPPC/polymer/LE DPPC boundary, which substantiate the previously hypothesis of the partially mixing of the polymer with the lipid at this interface. In the image of the sample taken after the third plateau at  $40 \text{ mN m}^{-1}$  (Figure 4.11d-f) the round PIB plateaus are vanished and just two phases – cone like PIB domains out of the plane lipid phase – are visible in the topography image (Figure 4.11d,e). These structures appearing here as cylinders, which are in fact disc like domains as mentioned before, have a mostly dominated height of  $40 \text{ nm}$  (maximum height of  $60 \text{ nm}$ ), indicating the further squeeze out of the polymer **8**. With increasing pressure these domains are decreasing concerning their area, but increasing regarding their height. As visible in the phase image (Figure 4.11f) they appear at the dark lines, at the phase

## 4. Results and discussion

boundary, of the above mentioned network. Thus, the amphiphilic PIB **8** is forced stronger into the lipid domains and subsequently squeezed out.



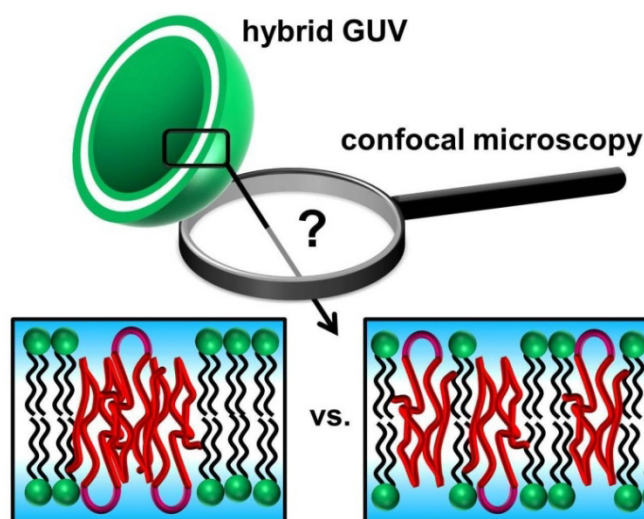
**Figure 4.12.** AFM topography (a, b, d and e) and topology images (c and f) of mixed monolayer of DPPC/9 90:10 mol% transferred at a surface pressures of (a-c) 30 mN m<sup>-1</sup> and (d-f) 40 mN m<sup>-1</sup>.

Figure 4.12 shows the AFM topography (a, b, d and e) and topology images (c and f) of mixed monolayer of DPPC/9 90:10 mol% transferred at surface pressures of (a-c) 30 mN m<sup>-1</sup> and (d-f) 40 mN m<sup>-1</sup>. Again the topography images show no defects, thus complete transfers of the monolayers onto the Si-wafers could be concluded. Nearly similar to Figure 4.12a,b the height images of DPPC/9 90:10 mol% transferred at a surface pressures of 30 mN m<sup>-1</sup> (Figure 4.12a,b) show three different phases, disc like PIB domains (height ~ 15 nm) mostly out of a PIB plateau (height ~ 5 nm) surrounded by the plane LC domain of the lipid. Thereby, the height of the PIB discs using amphiphilic PIB **9** is in good agreement with the assimilable sample using **8** and correlates with a single-folded PIB chain. Also the phase image (Figure 4.12c) shows the three different phases, proofing the PIB discs squeezed out (dark: soft) of the PIB rich plateau domains which are surrounded by the LC phase of the lipid (bright: hard) whereby the plane lipid domain is again cross cut by a softer network – the LC DPPC/polymer/LE DPPC boundary. With increasing transfer pressure to 40 mN m<sup>-1</sup> (Figure 4.12d-f) the PIB plateaus vanished again and cone like PIB domains out of the plane lipid LC domains are formed. Thereby their height increased up to 80 nm (mainly dominated height ~ 40 nm) together with a clearly decrease of their domain size. For the phase image (Figure 4.12f) two different phases exist, the softer cone-like PIB domains, which are surrounded by the second one, the already condensed and therefore hard LC domain of the lipids. The network lines where the cone-like PIB domains are squeezed out are better visible, proofing the deeper penetration of the PIB into the LC domains of the lipid followed by the stronger squeeze out of the polymer.

Both amphiphilic PIBs, PIB **8** having one PIB chain linked to the  $\beta$ -turn mimetic BTD and PIB **9** where both PIB chains are linked on one  $\beta$ -turn mimetic BTD, show three phases at a transfer pressure of  $30 \text{ mN m}^{-1}$ , 1) disc like PIB domains out of 2) a PIB plateau which is surrounded by 3) the condensed lipid phase. With increasing pressure the PIB plateaus are vanishing and cone-like PIB domains out of the plane lipid phase are visible, whereby the maximum height (80 nm) using **9** is higher as the maximum height using **8** (60 nm). This can be explained by the better stabilizing effect of higher aggregates with elongated chains due to the linkage of two chains onto one  $\beta$ -turn mimetic BTD.

### 4.5 Bilayer experiments of **8** and **9** using DPPC as lipid

Preliminary Langmuir monolayer measurements, which serve as model for half a bilayer membrane, already showed slightly different behavior using  $\beta$ -turn mimetic PIB conjugate **8** (one PIB chain linked to  $\beta$ -turn mimetic BTD) or **9** (both PIB chains linked to one  $\beta$ -turn mimetic BTD). To investigate the behavior of the conjugates when incorporated into a more natural like membrane, mixed giant unilamellar vesicles (GUVs) were prepared as model for bilayer membranes and analyzed via confocal microscopy.



**Scheme 4.6.** Schematic diagram for studying the polymer distribution (PIB rich domains vs. homogeneous distributed PIB) of  $\beta$ -turn mimetic PIB conjugate **8** or **9** when incorporated into a bilayer membrane (DPPC) using different polymer to lipid ratios and coupling to confocal microscopy.

However, this method only enables the investigation of the polymer distribution, whether PIB rich domains are built or the PIB is homogeneously distributed in the lipid bilayer (Scheme 4.6). The GUVs were prepared by electroformation which emerged as method of choice in our group and Rh-DHPE was used as fluorescence dye, which is known to be preferentially soluble in the less ordered phase as it is squeezed out of the more ordered liquid condensed phase.<sup>202</sup> At first hybrid GUVs using the amphiphilic PIB conjugate **8** and DPPC in different molar ratios were investigated. Figure 4.13 shows

## 4. Results and discussion

the confocal microscopy images of mixed DPPC/**8** GUVs with different molar ratios and taken after a certain time (a-c) 92:8 direct, after 24 h and after 120 h, and (d-e) 84:16 direct and after 48 h.

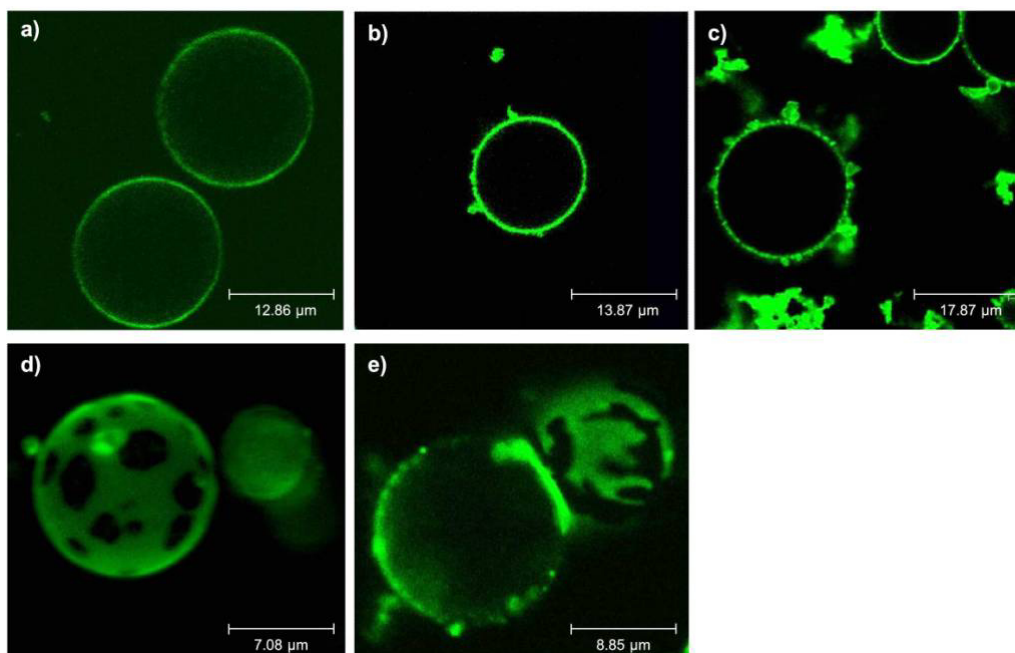


**Figure 4.13.** Confocal microscopy images of mixed DPPC/**8** GUVs with different molar ratios and taken after certain time. (a-c) 92:8 direct, after 24 h and after 120 h, and (d-e) 84:16 direct and after 48 h.

When using 8 mol% of PIB **8** numerous, homogenous, smooth and spherical GUVs were obtained directly after preparation (Figure 4.13a) indicating that the PIB molecules and lipid molecules are well mixed. After 24 h the amount of the GUVs decreased and budding at the surface could be observed (Figure 4.13b). With proceeding aging time (after 120 h, Figure 4.13c) most of the GUVs are destroyed and the remaining ones show budding and worm like protrusion over the whole surface. This means that over time the initially intact GUVs decomposed as they break up. Using the double amount of PIB **8** (16 mol%) the GUVs are again smooth and spherical, but they show phase separation directly after the preparation (Figure 4.13d). However, these dark compact domains cannot be clearly assigned to the lipid-rich or polymer-rich phase as already discussed in literature.<sup>202</sup> They just mark the region of higher ordered liquid-condensed phase of the mixed DPPC/**8** bilayer from which the dye is excluded. Interestingly after 48 h (Figure 4.13e) the shape of the dark domains changed into dendritic structure, which indicates a stronger penetration of the two phases and can be a hint for partial mixing over time. Moreover, the previously budding at the surface of the former smooth GUVs could be observed again. Measurements using 35 mol% PIB **8** were accomplished and repeated, but always no GUVs were formed. This shows that the amphiphilic PIB **8** itself cannot build up GUVs and if its amount in the hybrid GUVs is too high, they are not stable anymore.

A comparison with the monolayer measurements is just roughly possible. In monolayer experiments using 10 mol% of **8** well dispersed small round shaped domains (polymer rich LE phase) on a black background (lipid LC phase) were visible and with 20 mol% of **8** bigger irregular domains have been

## 4. Results and discussion

observed, which increased with increasing PIB up to 30 mol% (for epifluorescence images see Appendix).

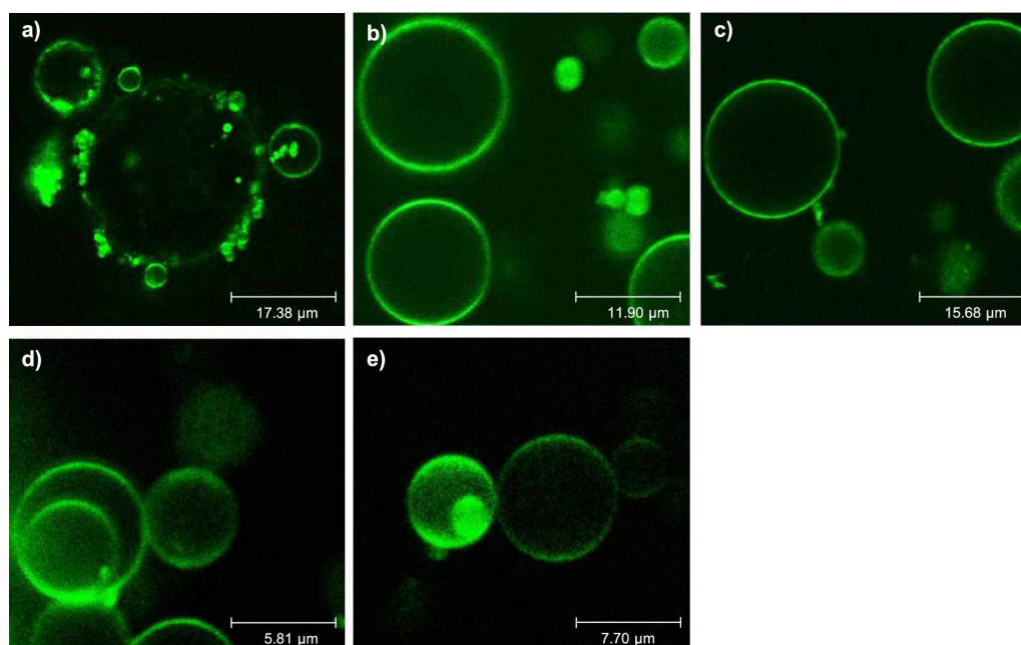
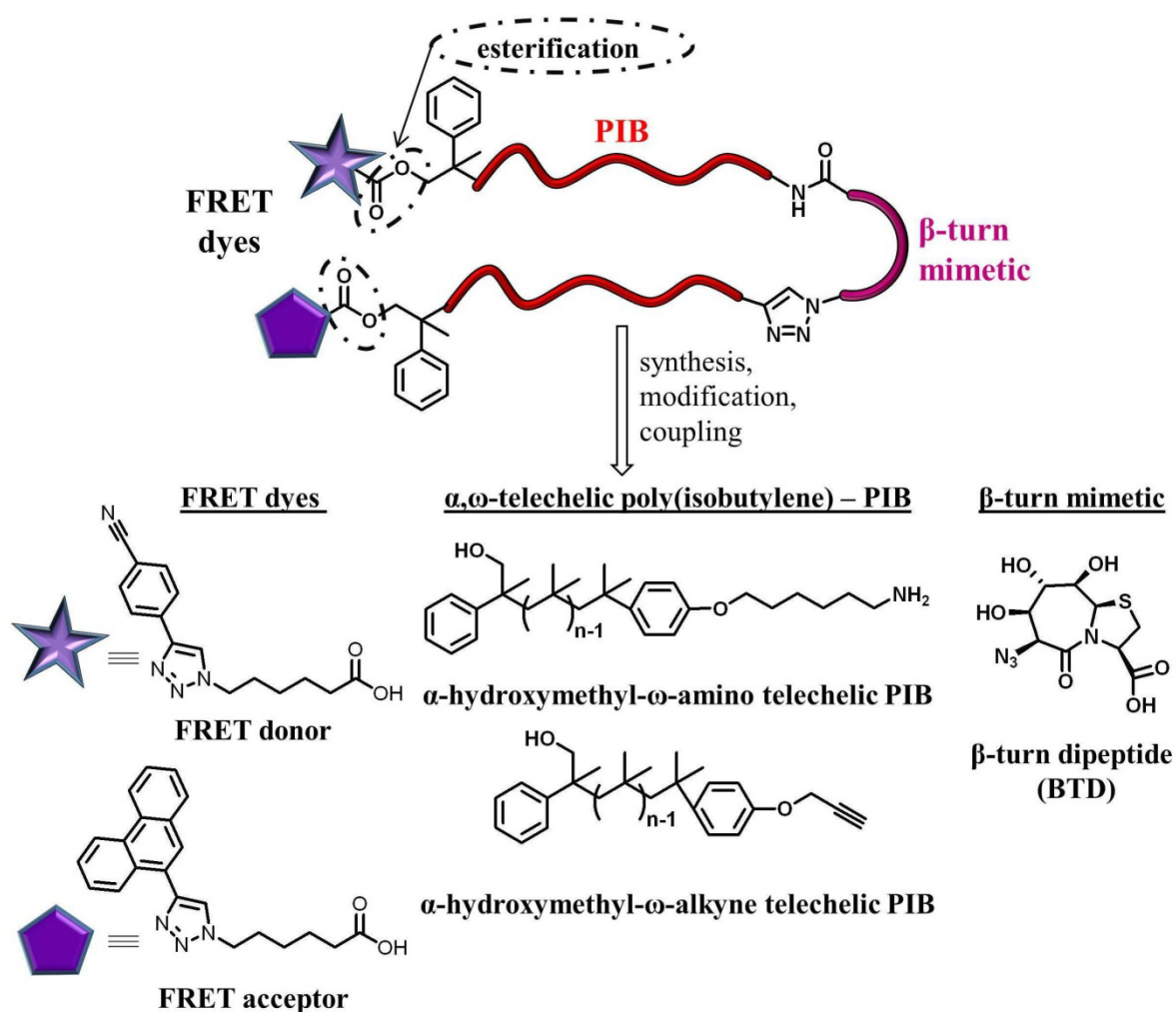


**Figure 4.14.** Confocal microscopy images of mixed DPPC/**9** GUVs with different molar ratios and taken after certain time. (a) 96:4, (b-c) 92:8 direct and after 24 h, (d) 90:10 and (e) 84:16.

As mentioned previously, the amphiphilic  $\beta$ -turn mimetic PIB conjugate **9**, bearing two PIB chains on the same BTM molecule, is with regard to the mass the double of **8**. If only the mass is the determining factor of the behavior inside the membrane, then mass equivalent incorporated PIB conjugates **8** and **9** should behave similar. The monolayer investigations already showed that the behavior is similar, but that there are differences, thus we can conclude that indeed the connection of two PIB chains onto the same  $\beta$ -turn mimetic leads two better mixing with the lipid molecules. Figure 4.14a shows the confocal microscopy image of mixed GUVs using DPPC/**9** 96:4 which is the mass equivalent ratio to DPPC/**8** 92:8. Again round shaped homogenous GUVs were obtained. However, they varied in size and moreover numerous small GUVs adsorb at the surface of bigger ones. Using the double amount of **9** numerous, smooth, homogenous and spherical GUVs were formed, also after 24 h they did not changed, only a few budding could be observed (Figure 4.14b-c). This means that the doubling of the molar amount of **9** led to more regular and stable GUVs. Even an increase to 10 mol% (Figure 4.14d) and up to 16 mol% (Figure 4.14e) resulted in the same shape of smooth, homogenous and spherical GUVs, in contrast to previous experiments using **8** no phase separation could be observed. Therefore, the amphiphilic  $\beta$ -turn mimetic PIB conjugate **9** was over the whole investigated range of different molar ratios miscible with the DPPC molecules. This clearly proves that indeed the linkage of two PIB chains on one  $\beta$ -turn unit lead to different membrane interactions than the equivalent structure just having one PIB chain.

## 5. Concept to introduce FRET dyes

FRET stands for Fluorescence (Förster)-Resonance-Energy-Transfer and is a common method to determine the distance between biomolecules which are labeled e.g. with dyes (donor-acceptor pair). Thereby, the distant-dependent interaction between the excited states of the donor and acceptor molecules is measured as the excitation energy from the FRET donor is transferred non-radiative to the FRET acceptor. This FRET event can take place only if the donor and acceptor molecules are in close proximity (10-100 Å), the fluorescence emission spectrum of the donor overlap with the absorption or excitation spectrum of the acceptor and both dipoles are oriented parallel.<sup>207, 208</sup> In practice fluorescence spectroscopy is conducted whereby the donor is excited. At the same time the fluorescence of the donor decrease while the fluorescence of the acceptor increase.



**Scheme 5.1.** Retrosynthetic concept towards amphiphilic polymer conjugate containing a  $\beta$ -turn mimetic element,  $\alpha,\omega$  telechelic PIBs and FRET suitable dyes by the linkage of the different building blocks.

In chapter 4 the syntheses of the amphiphilic  $\beta$ -turn mimetic PIB conjugates using  $\alpha$ -hydroxymethyl- $\omega$ -amino telechelic PIB (**3**) and  $\alpha$ -hydroxymethyl- $\omega$ -alkyne telechelic PIB (**5**) as hydrophobic part and the  $\beta$ -turn mimetics BTD **6** and SAA **7** as hydrophilic parts were discussed. It became clear that the linkage of the single building blocks is quiet challenging due to the close proximity of the two reactive groups forming the  $\beta$ -turn structure (BTD: 7 Å<sup>115</sup>, SAA: 5 Å<sup>117</sup>). Using BTD **6** as  $\beta$ -turn mimetic the complete  $\beta$ -turn mimetic PIB conjugate **9** could be obtained and its purity was extensive discussed, as well as mono- and bilayer experiments were conducted. Whereas, the synthesis of a complete  $\beta$ -turn mimetic polymer conjugate using SAA as  $\beta$ -turn mimetic failed.

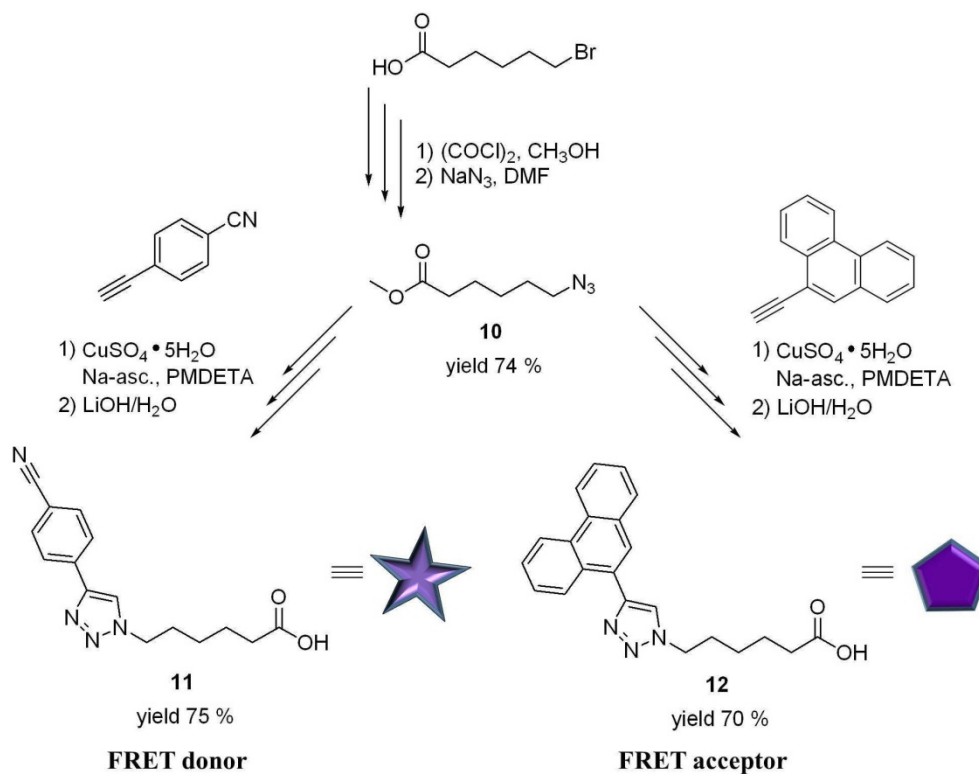
Therefore, we decided to modify the PIB conjugate **9** with FRET suitable dyes at the  $\alpha$ -termini (Scheme 5.1). As both termini bear hydroxyl groups, dyes with carboxylic acid groups are needed, which should be then connected via esterification onto the single strands. The dye functionalized amphiphilic  $\beta$ -turn mimetic PIB conjugate should be then incorporated into a bilayer membrane to get a deeper look into the folding of the modified PIB conjugate **9**. When both FRET dyes are in close proximity the FRET event should take place, proofing the folding of the PIB strands due to the  $\beta$ -turn mimetic element. As the selected FRET pair (4-ethynylbenzotrile and 9-ethynylphenanthrene) together with the “click”-reaction for the linkage of these dyes onto proteins is known in literature<sup>209</sup>, we decided to use these dyes in a modified way. Moreover, we have chosen these dyes as they should be embedded in the less polar bilayer-water interface (between the polar head group region and the hydrophobic core).<sup>210</sup> If we would choose more hydrophilic dyes they will be embedded in the polar head group region and contrary more hydrophobic dyes will be incorporated in the hydrophobic core region, but these pushing/pulling effects of the dyes we wanted to avoid as their sole function should be the imaging of the folding process.

### 5.1 Results and discussion of introduction of FRET dyes

#### 5.1.1 Synthesis of FRET dyes

Scheme 5.2 shows the synthetic route towards the FRET dyes **11** and **12** bearing carboxylic acid groups for the linkage onto the hydroxyl groups at the  $\alpha$ -termini of the PIB conjugate **9** via esterification. Therefore, at first the linker **10** bearing the azide group on the one end and the carboxylic methyl ester group on the other end was synthesized having five methylene groups between these moieties as spacer to avoid the explosive character of this azide compound. The linker **10** was then “clicked” onto the FRET dyes followed by the hydrolysis of the final “click”-products to achieve the FRET dyes **11** and **12** bearing carboxylic acid groups in a good yield. The “click”-reaction with an already hydrolyzed linker bearing the carboxylic acid moiety instead of the carboxylic methyl ester was carried out analogously but no “click”-product could be obtained.





**Scheme 5.2.** Synthetic route towards FRET dyes **11** (FRET donor) and **12** (FRET acceptor).

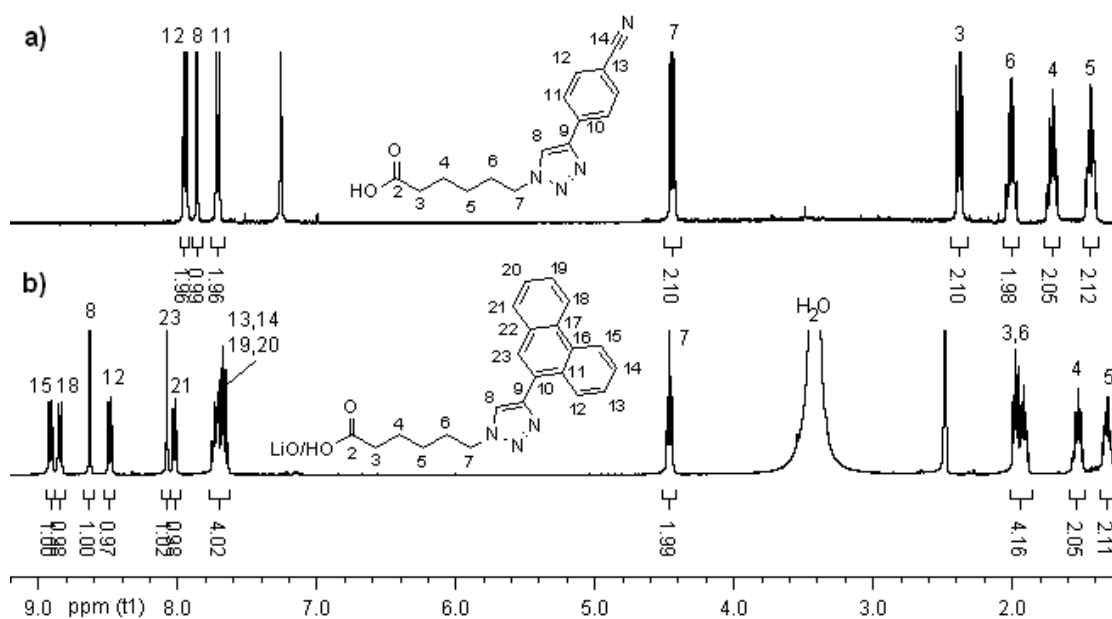
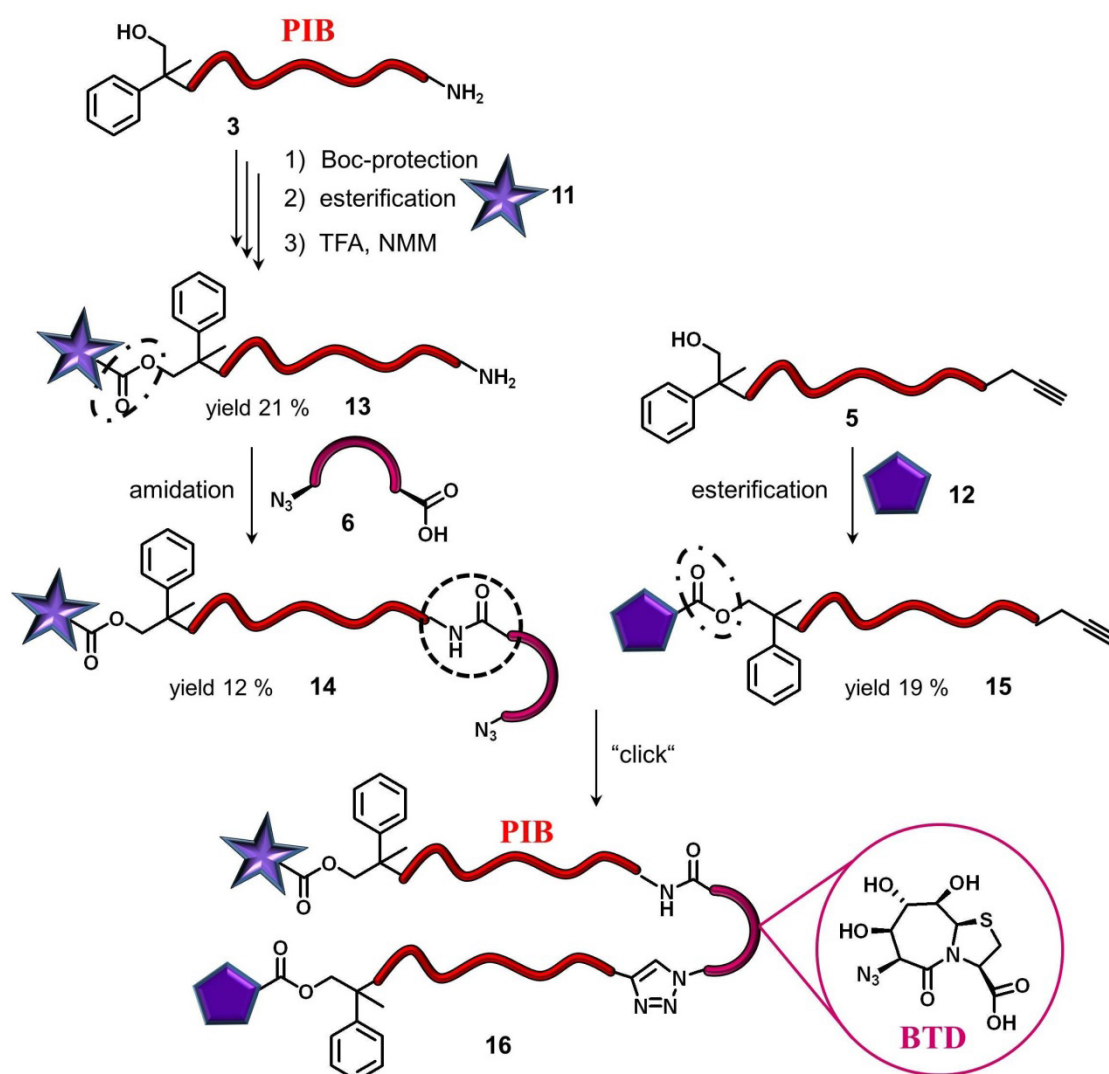


**Figure 5.1.**  $^1\text{H}$ -NMR overlay of a) FRET donor **11** ( $\text{CDCl}_3$ ) and b) FRET acceptor **12** ( $\text{DMSO-d}_6$ ).

The purity of the FRET dyes **11** and **12** was proven via ESI-ToF MS (see Experimental Part) and NMR spectroscopy. Figure 5.1a shows the  $^1\text{H}$ -NMR spectrum of the FRET donor **11** where all signals could be assigned to the structure. Moreover, the appearance of the triazole proton H-8 at 7.86 ppm together with the matching of the integral values (ratio 2:2) of the methylene group in vicinity to the

former azide (H-7) and the methine group of the “dye-part” (H-11) prove the formation of the “click”-product. Figure 5.1b shows the  $^1\text{H-NMR}$  spectrum of the FRET acceptor **12** here again the integral values of the methylene group in vicinity to the former azide (H-7) and the methine group of the “dye-part” (H-12) match. Furthermore, the appearance of the singlet of the newly formed triazole (H-8) at 8.63 ppm indicates the linkage of the FRET dye onto the linker. Last but not least all the other signals could be assigned to the structure and their integral values match very well.

### 5.1.2 Synthesis of dye labeled amphiphilic polymer conjugate



**Scheme 5.3.** Synthetic route towards dye labeled amphiphilic polymer conjugate containing BTM as  $\beta$ -turn mimetic.

For the synthesis of the dye labeled amphiphilic polymer conjugate the dyes have to be connected to the single PIB strands before they were linked to build up the complete  $\beta$ -turn mimetic PIB conjugate.

Otherwise a controlled labeling of the two strands is impossible as both  $\alpha$ -termini are functionalized with hydroxyl groups. Scheme 5.3 shows the synthetic route towards the dye labeled amphiphilic polymer conjugate containing BTD as  $\beta$ -turn mimetic.

In a first step of the synthesis of the first strand the amine group of the  $\alpha$ -hydroxymethyl- $\omega$ -amino telechelic PIB **3** has to be protected with a Boc-protecting group. As the reactivity of the amine group is higher than of the hydroxyl group it would react with the FRET donor **11** preferred forming a peptide bond and therefore blocking this end for the next step the coupling to the  $\beta$ -turn mimetic BTD **6**. Then the FRET donor **11** was activated by generating *in situ* an acyl chloride via the treatment with oxalyl chloride in  $\text{CH}_2\text{Cl}_2$  followed by the direct esterification with the Boc-protected  $\alpha$ -hydroxymethyl- $\omega$ -amino telechelic PIB **31**.<sup>211, 212</sup> After deprotection of the amine the PIB **13**, containing the FRET donor one the one end and the active amine functionality on the other end, could be obtained in a yield of 21 %. To complete the synthesis of the first strand the  $\beta$ -turn mimetic BTD **6** was coupled via amidation in accordance to previous work (see chapter 4.3.1) yielding the first strand **14** labelled with the FRET donor (yielding 30 % polymer containing 40 % of **14**).

For the synthesis of the second strand **15** the coupling of the FRET acceptor was carried out similar to the first strand, the activated FRET acceptor **12** was generated *in situ* and then directly linked via esterification to the  $\alpha$ -hydroxymethyl- $\omega$ -alkyne telechelic PIB **5**. With the knowledge from the previous work (chapter 4.3.1) the dye labelled single strands should be then coupled via the Cu(I)-mediated azide/alkyne-“click”-reaction<sup>168</sup> to achieve the final dye labelled PIB conjugate **16** were two PIB strands are connected to the one  $\beta$ -turn mimetic BTD. As described previously, the linkage of the second strand onto the same  $\beta$ -turn mimetic is quiet challenging and failed at this moment. Due to the drastic loss of substance during the single synthesis steps especially for getting rid of unreacted dye the last step could be conducted just once.

To proof the purities of the intermediates and the final product SEC, MALDI-ToF MS and NMR spectroscopy were conducted. All data and spectra can be found in the Appendix. To clarify the structure Figure 5.2 shows the MALDI-ToF MS of **13** and **15**. Figure 5.2a shows the MALDI-ToF MS of the PIB **13** containing the FRET donor with a mass distribution of 1500 to 5000 g/mol and a maximum at 2500 g/mol. The chemical identity of **13** could be proven by the distance between two peaks indicating the repetitive unit of 56.1 g/mol corresponding to PIB. Moreover, Figure 5.2b shows the expanded spectrum of **13** with a listed view of the simulated peaks. As it can be seen the signal at 2445.376 g/mol agreed with the calculated value of 2445.413 g/mol as H-adduct and the signal at 2451.381 g/mol corresponded with the simulated value of 2445.421 g/mol for Li-adduct.

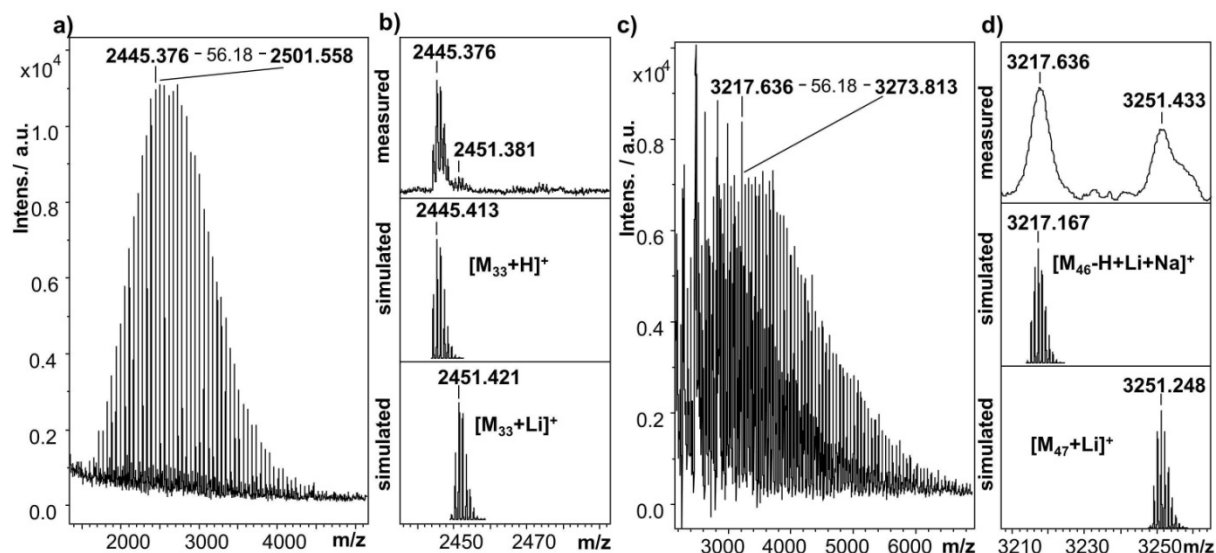


**Figure 5.2.** MALDI-ToF MS of a) **13** with the region from 1500-5000 Da and b) expanded spectrum of **50** with a listed view of the simulated peaks; and c) of **15** with the region from 2000-7000 Da and d) expanded spectrum of **15** with a listed view of the simulated peaks.

This together with the <sup>1</sup>H-NMR spectrum (see Appendix Figure A35) clearly proves the structure of the intermediate **13**. Figure 5.2c shows the MALDI-ToF MS of the PIB **15** containing the FRET acceptor with a mass distribution of 2000 to 7000 g/mol and a maximum at 3300 g/mol. Again the distance between two peaks indicating the repetitive unit of 56.1 g/mol corresponds to PIB for all of the peaks of the two different series. That these two different series could be assigned to the same product **15** with 46/47 units of isobutylene and different salts is shown in Figure 5.2d giving an expanded spectrum with a listed view of the simulated peaks. The signal at 3251.433 g/mol corresponded with the simulated value of 3251.248 g/mol and 3251.248 g/mol for the Li-adduct. Whereas, the signal at 3217.636 g/mol of the first series showed different ionization behavior, as one proton of the PIB **15** was exchanged with one Li-ions and one Na-ion (for ionization) giving the calculated value of 3217.167 g/mol. Even though the molecular weight determined via MALDI-ToF MS is lower than calculated via <sup>1</sup>H-NMR spectroscopy [**13** (5200 g/mol) and **15** (5400 g/mol)] and SEC [**13** (5600 g/mol) and **15** (5200 g/mol)] the MALDI-ToF MS spectra show clearly the successful linkage of the FRET dyes to the single strands. The lower molecular weights in MALDI-ToF MS could be explained by the challenging polarizability of the nonpolar PIB resulting in difficult ionization. The nature of the functional end groups is decisive for the “flying” of PIB in MALDI-ToF MS as well as shorter chains with a more favorable ratio of end group to PIB backbone can absorb better.

The PIB-BTD containing the FRET donor (**14**) could be synthesized successfully as it was proven by <sup>1</sup>H-NMR spectroscopy (see Appendix Figure A36) and MALDI-ToF MS (see Appendix Figure A37), but couldn't be isolated via column chromatography. Therefore, this crude product was used for the

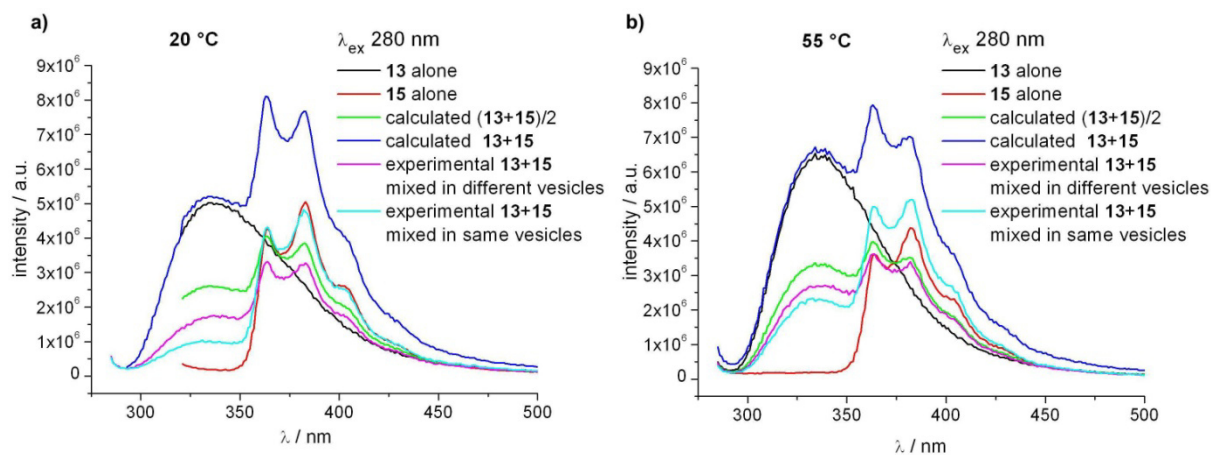
last step, the linkage of the two single strands **14** and **15** to build up the complete dye labelled PIB conjugate **16**. The MALDI-ToF MS of the isolated product (see Appendix Figure A39) shows three different series (A 1500-3000, B 3000-5000 and C 5500-8500) especially the last series could lead to the assumption of the successful synthesis of **16** as the shift of the MALDI-ToF MS is similar to this of the PIB conjugate **9**. Therefore, this region was analyzed giving two different structure possibilities for the same peak ( $M_{n,exp} = 6880.140$  g/mol). On the one hand it could be the assumed product **16** corresponding to the calculated value of 6880.699 g/mol as Li-adduct and on the other hand it could be **14** with the azide moiety reduced to an amine giving a calculated value of 6880.087 g/mol where one proton is exchanged by one Na-ion and one Na-ion is used for ionization. For better clarification of the structure  $^1\text{H-NMR}$  spectroscopy was conducted (see Appendix Figure A40 and A41). The  $^1\text{H-NMR}$  spectrum shows clearly that it cannot be our wanted product **16** as signals which we expect and know from **9**, particularly the signal of the triazole proton, cannot be found in this spectrum as well as the integral values of the single strands do not match. Therefore, we assume that we have a mixture of the single strands after column chromatography and the increase of the molecular weight could be explained due to the separation of the molecular weights by fractionated column chromatography (increasing molecular weight with increasing elution time).

### 5.2 Fluorescence spectroscopy of mixed DPPC/polymer bilayer membrane

Originally it was planned to investigate the assumed folding of a dye labelled PIB conjugate (**16**) when incorporated into a bilayer membrane using FRET studies. Even though the product couldn't be achieved preliminary experiments concerning fluorescence spectroscopy should be conducted using the dye labelled single strands **13** and **15** to get an idea of the behaviour of these compounds when incorporated into a bilayer membrane. As the purity of the single strands **13** and **15** was proven, the single strands with the FRET donor respectively FRET acceptor could be investigated via fluorescence spectroscopy when incorporated into lipid bilayer membranes using DPPC as lipid. Therefore, sonicated, extruded LUVs (2mM in  $\text{H}_2\text{O}$ ) composed of DPPC/polymer (99:1) were generated. In this context, 1 mol % of PIB **13** or **15** are equal to 6 mass %, where FRET between two single chains bearing the FRET donor respectively the FRET acceptor could be excluded in mixed vesicles. For planned FRET studies fluorescence absorption and emission spectra of the FRET donor **13** and FRET acceptor **15** were conducted at 20 °C and at 55 °C [above transition of DPPC ( $T_m = 41$  °C)<sup>213</sup>] (see Appendix Figure A42). As it can be seen the emission spectrum of **13** (red curve,  $\lambda_{max} = 336$  nm) overlapped significantly with the absorption spectrum of **15** (blue curve,  $\lambda_{max} = 383$  nm), whereas contrary to literature<sup>209</sup> a selective excitation of the FRET donor **15** at ~ 280 nm is not possible, because both FRET dyes absorb concurrently under these conditions. Therefore, "classical" FRET studies (selective excitation of the FRET donor, transfer of the energy to the FRET acceptor visible in a decrease of the intensity of the emission spectrum of the FRET donor while an increase of the

## 5. Introduction of FRET dyes

intensity of the emission spectrum of the acceptor will be observed) will not be possible. When exciting at this wavelength the FRET donor and the FRET acceptor will be excited at the same time but in comparison to single spectra/original spectra a decrease of the intensity of the emission spectra of the FRET donor should be observed while the intensity of the emission spectra of the FRET acceptor should increase.<sup>209</sup>



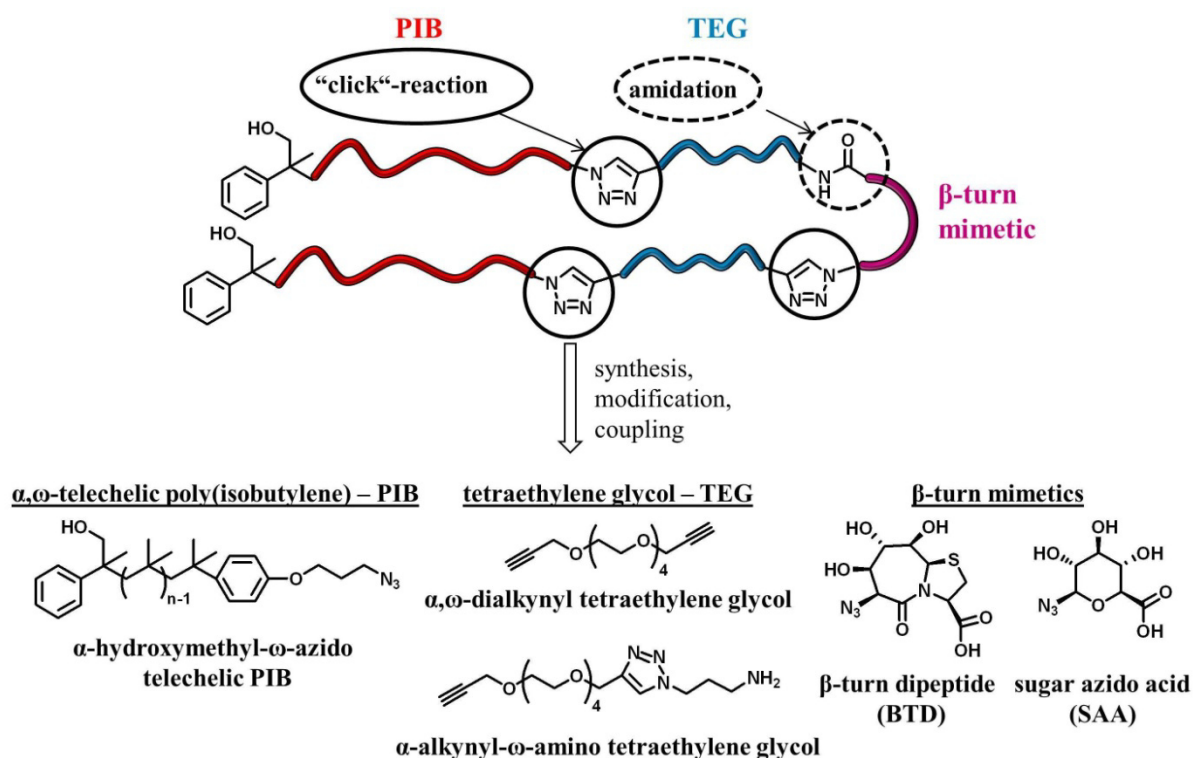
**Figure 5.3.** Fluorescence emission spectra of mixed DPPC/polymer (99:1) bilayer using **13** or **15** single, **13** and **15** mixed in same membrane and mixture of **13** and **15** in different membranes, as well as the calculated curves of the mixtures at a) 20 °C and b) at 55 °C.

Figure 5.3 shows the fluorescence emission spectra of mixed DPPC/polymer (99:1) vesicles using **13** or **15** single (black curve respectively red curve), **13** and **15** mixed in same vesicle (pale blue curve) and mixture of **13** and **15** (magenta curve) in different vesicles, as well as the calculated curves (green and blue curve) of the mixtures at a) 20 °C and b) at 55 °C excited at 280 nm. At 20 °C (Figure 5.3a) the intensities of the maximum of the emission spectra of **13** and **15** single (black curve respectively red curve) are equal, whereas at 55 °C (Figure 5.3b) the intensity of the emission maximum of **13** increase and of **15** decrease. Based on the single curves of **13** and **15** curves of the mixed vesicles could be calculated, which should help for interpretation. There are two different types of mixtures, in *type I* **13** and **15** are incorporated separately in different vesicles and then a 1:1 mixture of the vesicles was conducted. Thereby, the initial concentration of the vesicle solutions was 2 mM each and after mixing again 2 mM, but the concentration of each dye in the same volume (given by the quartz cuvette) is after mixing just half due to the dilution effect. Therefore, the calculated curve for the first mixture (green curve) is given by the sum of the intensities of the two single curves divided by 2. The second possibility of a 1:1 mixture (*type II*) is the incorporation of **13** and **15** in the same bilayer membrane (DPPC) with the ratio **13/15**/DPPC = 1:1:98 (2 mM). Thus the calculation of this mixed curve (blue curve) was done by the addition of the single curves. Both calculations were done assuming that no FRET takes place under these conditions.

As it can be seen in Figure 5.3a at 20 °C the curve of the mixed membrane *type I* (magenta curve) is nearly similar to the calculation of *type I* (green curve) with an overall decrease of the intensity in comparison to calculation. The curve of the mixed membrane *type II* (pale blue curve) shows similar behavior to the calculation *type I*, but the intensity of the donor part (**13**) is less than calculated and of the acceptor part (**15**) is higher than calculated, but it is not FRET behavior as the acceptor intensity is similar and not higher than the intensity of the single curve of **15**. Thus at 20 °C the system is relatively stiff and the position of the molecules is nearly fixed.

At 55 °C (Figure 5.3b) the experimental curve of the mixed membrane *type I* (magenta curve) is again nearly similar to the calculation of *type I* (green curve) and the intensity over the whole curve decreased just slightly. Thus, the mixed vesicles, where the dye labeled polymers are separately incorporated into the DPPC bilayer, show similar behavior independently from temperature under (20 °C) or above (55 °C) the transition temperature of DPPC ( $T_m = 41 \text{ °C}$ )<sup>213</sup>. Whereas, the curve of the mixed membrane *type II* (pale blue curve) indicates FRET behavior, which is visible by the decrease of the intensity of the donor part (**13**) in comparison to the fluorescence of **13** (black curve). Simultaneously the fluorescence intensity of the acceptor part (**15**) increased comparing to the emission of **15** (red curve). As this behavior was not observed at 20 °C it cannot be a problem of the sample preparation. We assume that above the transition the system is so fluid that DPPC and PIB are demixing and the PIBs bearing the FRET dyes aggregate when mixed in the same membrane. This clearly shows that the FRET preliminary experiments are dependent on the type of mixing and the measuring temperature. It can be concluded that the 1 mol % of the PIBs **13** and **15** are too high as the FRET already takes place by physically mixing of the single strands. Although <sup>1</sup>H-NMR spectroscopy already shows that the complete dye labelled PIB conjugate **16** couldn't be obtained, fluorescence spectroscopy according to previously conditions was conducted though. Figure A43 (see Appendix) shows an overlay of the emission spectra of **13**, **15** and “**16**” at 20 °C and 55 °C excited at 280 nm. If “**16**” will be the complete dye labelled PIB conjugate a similar curve to the mixed membrane *type II* (pale blue curve in Figure 5.3) should be observed but this is not the case. This unfortunately proves again that the synthesis of the complete dye labelled PIB conjugate **16** failed. Thus the final FRET studies for investigating the folding of such structure when incorporated into a bilayer couldn't be conducted.

## 6. Concept to elongate the hydrophilic part



**Scheme 6.1.** Retrosynthetic concept towards amphiphilic block “copolymers” containing a  $\beta$ -turn mimetic element (BTD or SAA) by the linkage of the different building blocks.

To investigate the influence of a hydrophilic elongation a hydrophilic part should be placed between the hydrophobic PIB and the hydrophilic beta-turn. Therefore, biocompatible tetraethylene glycol (TEG) derivatives should be used. For the synthesis of the amphiphilic block “copolymers” containing a  $\beta$ -turn mimetic element (BTD or SAA) the different building blocks should be synthesized, eventually modified and coupled as it was done previously (Scheme 6.1). These linkages can be accomplished again by the use of “click”-reaction and amidation as the reactive groups are alkyne and azide moieties as well as amine respectively carboxylic acid functionalities.

Via living carbocationic polymerization using  $\alpha$ -methylstyrene epoxide (MSE) as initiator and 3-bromopropoxybenzene (BPB) as quencher, following by conversion from the bromine to the azide group well defined hydrophobic  $\alpha$ -hydroxy- $\omega$ -azido telechelic polyisobutylene (PIB,  $M_n \sim 4000$  g/mol, PDI = 1.3) can be synthesized.<sup>144</sup> For the hydrophilic building blocks tetraethylene glycol (TEG) derivatives can be synthesized by the transformation of tetraethylene glycol into the needed structures ( $\alpha,\omega$ -dialkynyl tetraethylene glycol and  $\alpha$ -alkynyl- $\omega$ -amino tetraethylene glycol). For the last building blocks - the  $\beta$ -turn mimetic building blocks - the already synthesized BTD and SAA could be used. The purity of the final amphiphilic polymer conjugates should be proven by NMR spectroscopy, MALDI-ToF-MS measurements and HPLC. Moreover, investigations of the interaction of the  $\beta$ -turn mimetic amphiphilic block “copolymers” with lipid mono- and bilayers are required. The lipid/polymer membrane will be constructed from DPPC and the amphiphilic polymer conjugate. The



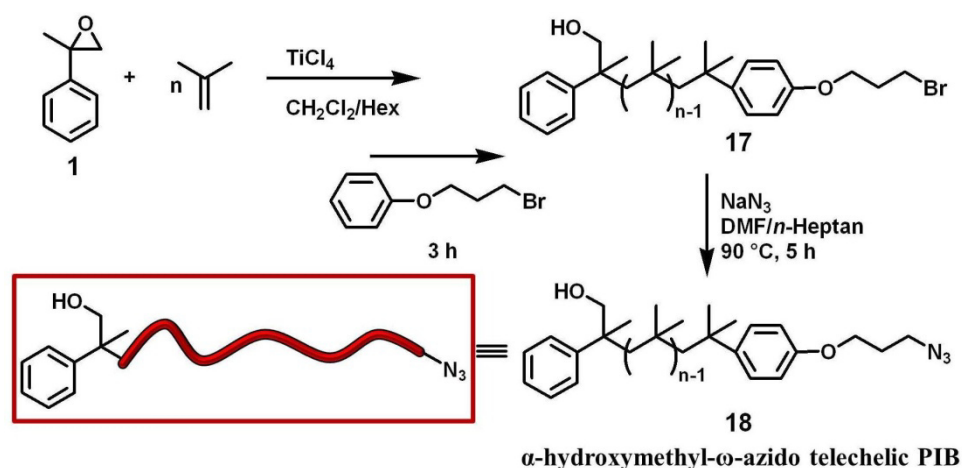
## 6. Elongation of the hydrophilic part

formation of mixed/demixed domains as well the folding of the amphiphilic polymer conjugates of the monolayers can be investigated using Langmuir-film techniques coupled with epifluorescence microscopy and AFM. For the investigation of the effects onto bilayers a) confocal laser microscopy using giant unilamellar vesicles (GUVs) and b) fluorescence spectroscopy using small unilamellar vesicles (SUVs) can be applied.

### 6.1 Results and discussion of the elongation of the hydrophilic part

#### 6.1.1 Synthesis of $\alpha$ -hydroxymethyl- $\omega$ -azido telechelic poly(isobutylene) (**18**)

To achieve  $\alpha,\omega$ -functionalized PIBs a combination of  $\alpha$ -methylstyrene epoxide (**1**) as initiator and alkoxybenzene compounds as quenchers can be used.<sup>144</sup> Especially the use of 3-bromopropoxybenzene (BPB) as quencher yielding a bromide terminated PIB is part of our interest. This can be easily converted into the azido-telechelic PIB which we want to use for the azide/alkyne-“click”-reactions.



**Scheme 6.2.** Synthetic route towards  $\alpha$ -hydroxymethyl- $\omega$ -azido telechelic PIB (**18**).

Scheme 6.2 shows the synthetic route towards  $\alpha$ -hydroxymethyl- $\omega$ -azido telechelic PIB (**18**). The polymerization and transformation of  $\alpha$ -hydroxymethyl- $\omega$ -bromo telechelic poly(isobutylene) (**17**,  $M_n \sim 4000$  g/mol) was carried out according to Olubummo *et al.*<sup>144</sup> by using  $\alpha$ -methylstyrene epoxide (**1**) as initiator and subsequently quenching with 3-bromopropoxybenzene (BPB).

The molecular weight was determined by size exclusion chromatography (SEC) and NMR spectroscopy, the results are listed in Table 6.1 showing that the calculated and experimental determined molecular weights match very well and the PDIs are narrow. The complete end group functionalization was proven via NMR spectroscopy (Figure 6.1a) by comparing the integral values referring to the protons H-2/2' of the initiator unit and H-9 of the quencher unit which are in the ratio 1:1:2. Due to the steric hindrance of the phenyl group of the initiator part the rotation of the hydroxyl methyl is hindered, therefore the two protons (H-2 and H-2') of the methylene group in vicinity to the

## 6. Elongation of the hydrophilic part

hydroxyl group have different chemical environments which is visible in the  $^1\text{H-NMR}$  spectra by splitting of the signals.

**Table 6.1.** Results for the polymerization of  $\alpha$ -hydroxymethyl- $\omega$  bromo telechelic PIB (**17**).

PIB	$m_{\text{th}}$ [g]	$M_{n(\text{th})}$ [g/mol]	$M_{n(\text{SEC})}^{\text{a}}$ [g/mol]	PDI	$M_{n(\text{NMR})}$ [g/mol]	yield
<b>17a</b>	3	3000	3400	1.28	3600	2.9 g 97 %
<b>17b</b>	3	3000	3300	1.50	3500	2.8 g 93 %
<b>17c<sup>b</sup></b>	3	4000	4200	1.44	4500	2.9 g 97 %

a) Polyisobutylene standards were used for conventional external calibration.

b) Synthesized by Wilton Osim, Martin-Luther-University Halle-Wittenberg.

Afterwards, the  $\alpha$ -hydroxymethyl- $\omega$ -bromo telechelic PIB (**17b**) was transformed to the  $\alpha$ -hydroxymethyl- $\omega$ -azido telechelic PIB (**18**) by nucleophilic substitution reaction with sodium azide ( $\text{NaN}_3$ ) using *n*-heptane and DMF as solvents in a mixture of 50/50 = v/v, whereby the nonpolar *n*-heptane dissolves the PIB and the polar DMF the  $\text{NaN}_3$ . For optimal mixing of the reagents and therefore optimal reaction conditions the mixture was heated to 90 °C at which the biphasic solvent mixture gets monophasic. The final  $\alpha$ -hydroxymethyl- $\omega$ -azido telechelic PIB (**18**) was analyzed via SEC giving  $M_n$  of 3600 g/mol and a PDI of 1.26.

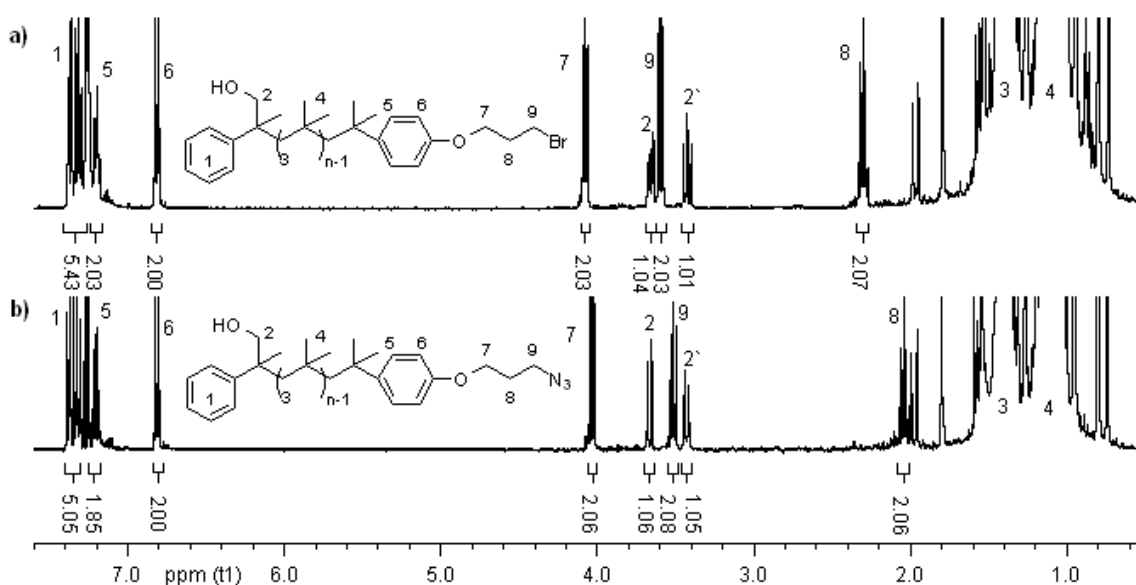


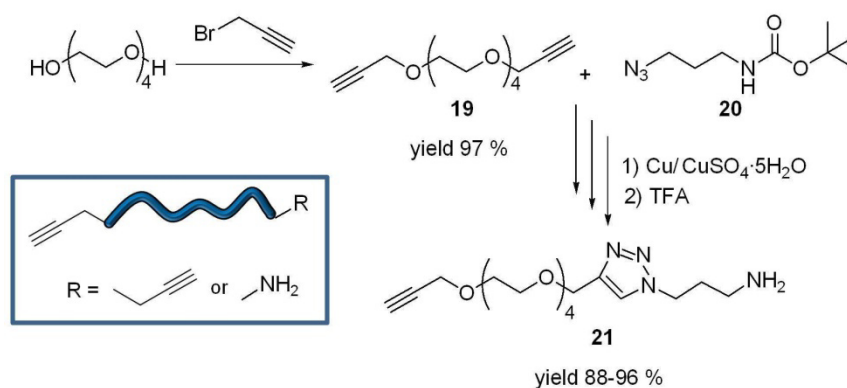
**Figure 6.1.** Overlay of the  $^1\text{H-NMR}$  spectra ( $\text{CDCl}_3$ , 400 MHz) of a)  $\alpha$ -hydroxymethyl- $\omega$  bromo telechelic PIB (**17b**) and b)  $\alpha$ -hydroxymethyl- $\omega$ -azido telechelic PIB (**18**).

## 6. Elongation of the hydrophilic part

Figure 6.1b shows the  $^1\text{H-NMR}$  spectra of  $\alpha$ -hydroxymethyl- $\omega$ -azido telechelic PIB (**18**). Comparing the integral values referring to the protons H-2/2' of the initiator unit and H-9 of the quencher unit which are in the ratio 1:1:2 indicates a complete end group functionalization. The shift of the methylene group in vicinity to the azide from 3.60 ppm to 3.51 ppm as well as the shift of H-8 from 2.31 ppm to 2.04 ppm proves the complete conversion into the azido-telechelic PIB **18**.

### 6.1.2 Synthesis of the tetraethylene glycol derivatives (**19** and **21**)

For the synthesis of the tetraethylene glycol derivatives (**19** and **21**, Scheme 6.3) tetraethylene glycol was used as starting material and could be easily transformed into the  $\alpha,\omega$ -dialkynyl tetraethylene glycol (**19**) by a combined synthesis of Dimonie et al.<sup>214</sup> and Mahouche et al.<sup>215</sup>. The direct synthesis of the  $\alpha$ -alkynyl- $\omega$ -amino-tetraethylene glycol would be possible starting from tetraethylene glycol in a four step synthesis but just with an overall yield of 12%.<sup>216</sup>



**Scheme 6.3.** Synthetic route towards  $\alpha,\omega$ -dialkynyl tetraethylene glycol (**19**) and tetraethylene glycol derivative **21**.

In this work we decided to use the azide/alkyne-“click”-reaction<sup>217</sup> for the synthesis of the  $\alpha$ -alkynyl- $\omega$ -amino-tetraethylene glycol (**21**) using  $\alpha,\omega$ -dialkynyl tetraethylene glycol (**19**) and tert-butyl 3-azidopropylcarbamate (**20**, Boc-protected 3-azido-propylamine (**20a**)) as reactants followed by the quantitative deprotection of the amine group. Both reactants of the azide/alkyne-“click”-reaction could be easily synthesized in a nearly quantitative yield. By using 0.2 equivalents of copper powder and  $\text{CuSO}_4\cdot 5\text{H}_2\text{O}$  the yield was with 96% nearly quantitative, but just 40% of the  $\alpha$ -alkynyl groups remained after “click”-reaction. Therefore, we decided to decrease the amount of the copper species to 0.1 equivalents resulting in a slightly decrease of the yield (88%) but increasing the proportion of  $\alpha$ -alkynyl groups after the “click”-reaction. The azide/alkyne-“click”-reaction without Boc-protection of the amine group of 3-azido-propylamine (**20a**) was carried out analogously but without formation of the click product **21** (see Experimental Part). Figure 6.2 shows the overlaid  $^1\text{H-NMR}$  spectra of a)  $\alpha,\omega$ -dialkynyl tetraethylene glycol (**19**) and b)  $\alpha$ -alkynyl- $\omega$ -amino-tetraethylene glycol (**21**). a)

## 6. Elongation of the hydrophilic part

Comparing the integral values from the tetraethylene glycol backbone of signal H-4 with the methylene protons H-3 in vicinity to the alkyne moiety proves the complete end group functionalization. The signal H-1 of the alkyne group cannot be used for proofing complete end group functionalization as this group causes an anisotropic effect, therefore the integral values can differ up to 30 %. b) A clear proof of the successful linking of  $\alpha,\omega$ -dialkynyl tetraethylene glycol (**19**) and tert-butyl 3-azidopropylcarbamate (**20**) is given by the appearance of the resonance of the newly formed triazole moiety at 8.10 ppm.

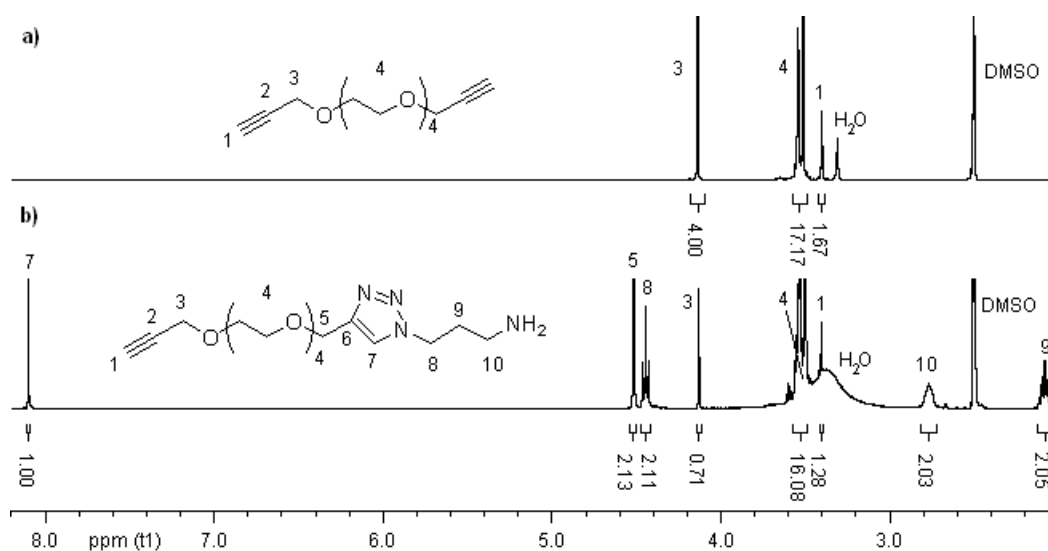


**Figure 6.2.** Overlay of the <sup>1</sup>H-NMR spectra (DMSO-d<sub>6</sub>, 400 MHz) of a)  $\alpha,\omega$ -dialkynyl tetraethylene glycol (**19**) and b)  $\alpha$ -alkynyl- $\omega$ -amino-tetraethylene glycol (**21**).

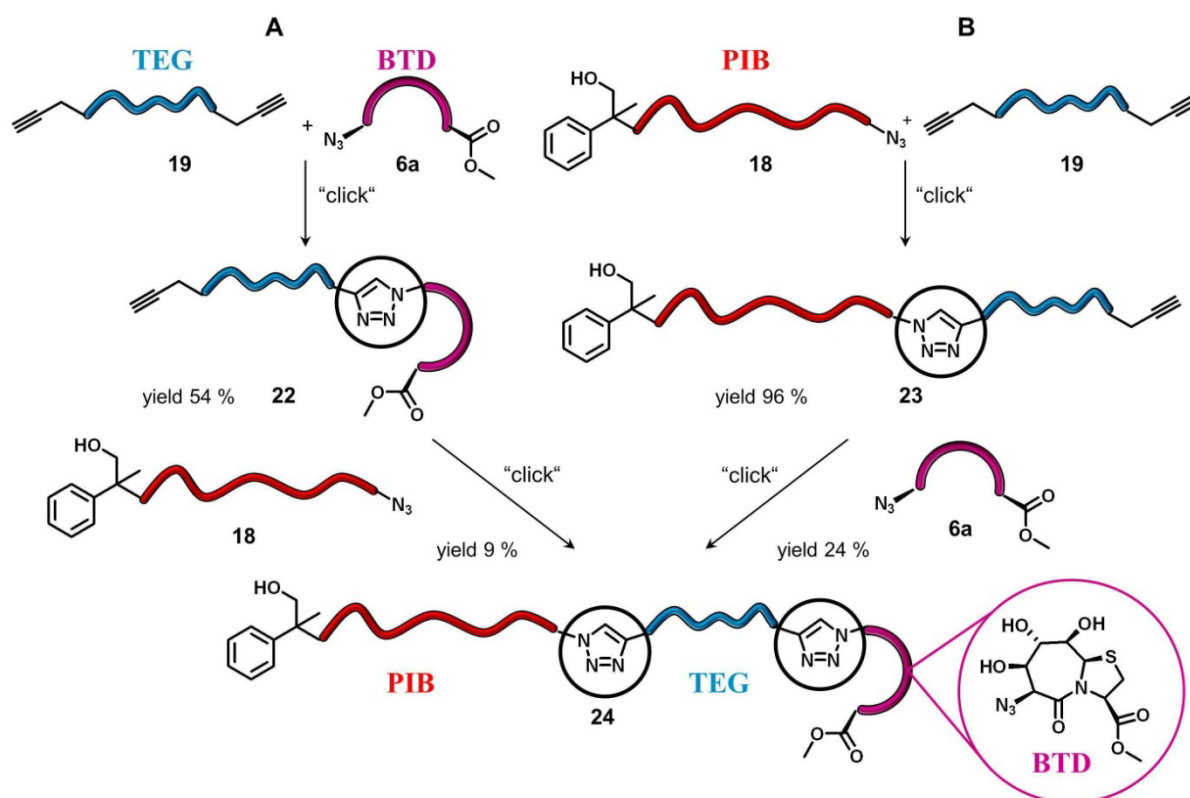
Moreover, the shift of the methylene group in vicinity to the former alkyne (H-5) to 4.52 ppm together with the assignment of all signals evidenced the formation of **21**. But comparing the integral values of the methylene group in vicinity to the former azide (H-8) with the methylene group in vicinity to the alkyne group at the  $\alpha$ -terminus (H-3) which are in a ratio of 2:0.7 shows that just 70 % of the “click”-product **21** are functionalized with the alkyne moiety and the remaining 30 % only bear hydroxyl groups at the  $\alpha$ -terminus. This could be confirmed via ESI-ToF MS, the main signal at 393.2018 g/mol agrees with calculated value of 393.2108 g/mol as sodium adduct [**21**+Na]<sup>+</sup> and the minor signal at 355.1858 g/mol corresponded with the simulated value of 355.1957 g/mol for the hydroxyl functionalized “click”-product as sodium adduct.

### 6.2 Linkage of the different building blocks

As the synthesis of the different building blocks (**6**, **7**, **18**, **19** and **21**) was successful and their purities were proven, they could be linked to achieve the  $\beta$ -turn mimetic amphiphilic polymers. Therefore, the copper mediated azide/alkyne-“click”-reaction and the amidation reaction should be used.

### 6.2.1 Synthesis of the first strand using BTD as $\beta$ -turn mimetic

A lot of possibilities for linking the different building blocks are existent; it can be done either sequentially or by the synthesis of two single strands which were coupled together in a last step. Scheme 6.4 shows the first attempt for linking the different building blocks, using BTD as  $\beta$ -turn mimetic, towards the first strand (experimental details and analysis see Experimental Part). As it can be seen two approaches were possible. In approach A) at first the TEG **19** was linked to the BTD **6a** via “click”-reaction<sup>218-220</sup> achieving TEG-BTD **22**. This part was then connected via “click”-reaction to the azido-telechelic PIB (**18**) yielding PIB-TEG-BTD **24** in an overall yield of 5 %. Approach B) started with the linkage of the azido-telechelic PIB (**18**) and TEG **19** yielding PIB-TEG **23**, followed by further “click”-reaction with the BTD **6a** resulting in the same end structure PIB-TEG-BTD **24** but with an overall yield of 24 %. To increase the yield of the first strand PIB-TEG-BTD the hydroxyl groups of **6a** were protected by acetylation reaction achieving the BTD **6b**, then it was analogously linked to PIB-TEG **23** resulting in the acetylated equivalent (**34**) of **24** with a yield of 90 %. To complete the synthesis of the first strand, the PIB-TEG-BTD **24** (or **34**) has to be hydrolyzed yielding the free carboxylic acid which is necessary for further linking of the second strand bearing the amine functionality to achieve the amphiphilic block “copolymer” containing BTD as  $\beta$ -turn mimetic element.



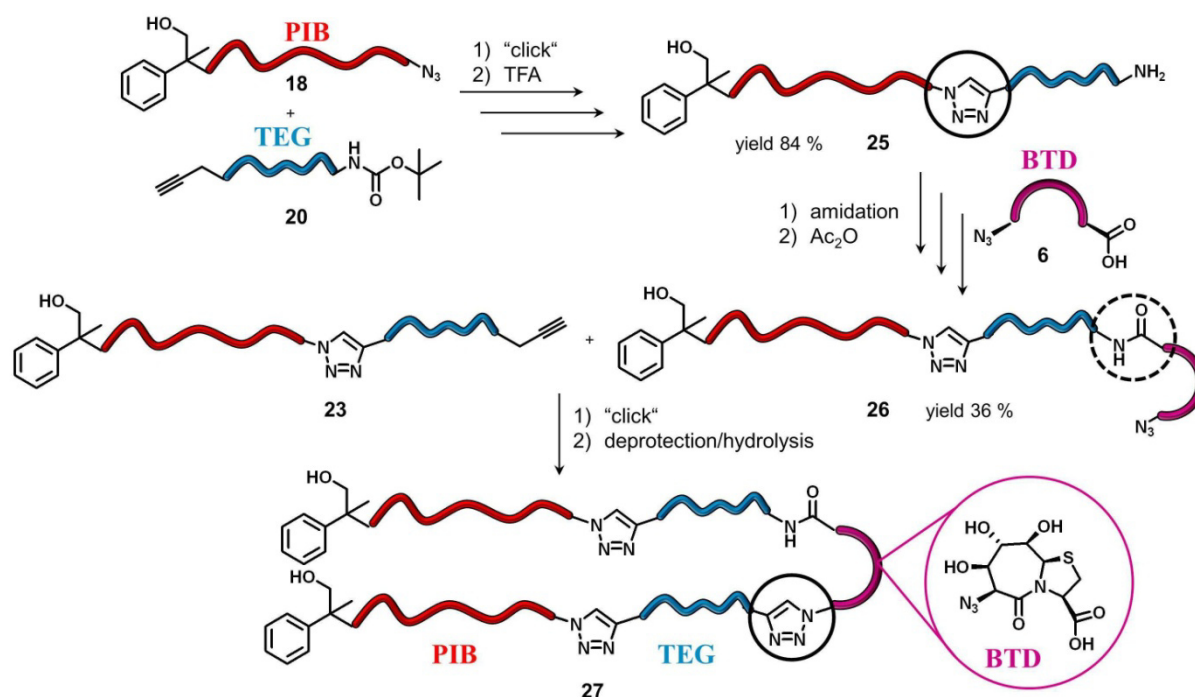
**Scheme 6.4.** First attempt for linking the different building blocks, using BTD as  $\beta$ -turn mimetic, towards the first strand.

## 6. Elongation of the hydrophilic part

Therefore, hydrolysis/deprotection was tried according to previous work (Chapter 4.3.1) with different bases (LiOH, NaOMe, hydrazine-hydrate) using different solvents/-mixtures (THF, MeOH, dioxane, H<sub>2</sub>O) and varying reaction conditions from 12 h at room temperature up to 7 d at 50 °C. Unfortunately no complete hydrolyzed/deprotected PIB-TEG-BTD bearing the carboxylic acid moiety could be obtained, only partial hydrolysis/deprotection could be observed. One big problem was the precipitation of the polymer after the partial hydrolysis/deprotection. After redissolving and extension of the reaction time and/or further addition of a base, decomposition of the PIB-TEG-BTD was observed. Thus BTD was hydrolyzed at the beginning yielding the  $\beta$ -turn with the azide moiety on the one side and a carboxylic acid on the other side (**6**) and the “click”-reactions were analogously conducted to the previous ones, but no “click” product was obtained.

As this first attempt was not successful a new strategy was necessary. Therefore, the PIB-TEG **23** could serve as first strand and the BTD **6** should be linked to the second strand.

### 6.2.2 Synthesis of the second strand using BTD as $\beta$ -turn mimetic and linkage to the first strand



**Scheme 6.5.** Synthesis of the second strand using BTD as  $\beta$ -turn mimetic and linkage to the first strand **23**.

The synthesis of the second strand using BTD as  $\beta$ -turn mimetic and linkage to the first strand **23** is presented in Scheme 6.5 (experimental details and analysis see Experimental Part). As the two reactive moieties of the  $\beta$ -turn mimetic BTD (azide group and carboxylic acid group) are in close proximity (X-ray structure distance between active moieties 7 Å)<sup>115</sup> the linkage of both polymer strands onto the

## 6. Elongation of the hydrophilic part

BTD is quite challenging. Starting with the synthesis of the second strand, at first azido-telechelic PIB (**18**) was “clicked” to TEG **20** followed by the deprotection of the amine group to achieve amino functionalized PIB-TEG **25** in a yield of 84 %. Without protection of the amine group and using  $\alpha$ -alkynyl- $\omega$ -amino-tetraethylene glycol (**20a**) for the “click”-reaction, no “click” product **25** was obtained. Then BTD **6** was coupled via amidation using PyBOP/NMM as coupling agent resulting in PIB-TEG-BTD **26**. For further “click”-reaction with the first strand PIB-TEG **23** it was necessary to protect the hydroxyl groups of the BTD via Steglich acetylation which were directly deprotected after “click”-reaction to achieve the complete  $\beta$ -turn mimetic amphiphilic block “copolymer” **27** in a yield of 30 % but with impurity of small molecular weight PIB (for details see MALDI-ToF MS discussion below). This “click”-reaction was also carried out analogously to the previous one without protection of the hydroxyl groups but no “click” product was obtained. Furthermore, a stepwise building up of the complete amphiphilic  $\beta$ -turn mimetic block “copolymer” **27** was carried out. Starting from PIB-TEG-BTD **26** and the “click”-reaction with  $\alpha,\omega$ -dialkynyl TEG (**19**) and further “click”-reaction with  $\alpha$ -hydroxymethyl- $\omega$ -azido telechelic PIB (**18**) followed by deprotection of the hydroxyl groups the complete amphiphilic  $\beta$ -turn mimetic block “copolymer” **27** could be as well achieved but with an overall yield of just 4 % for the linking steps. Moreover, the obtained product could not be purified, thus unreacted starting material was left.

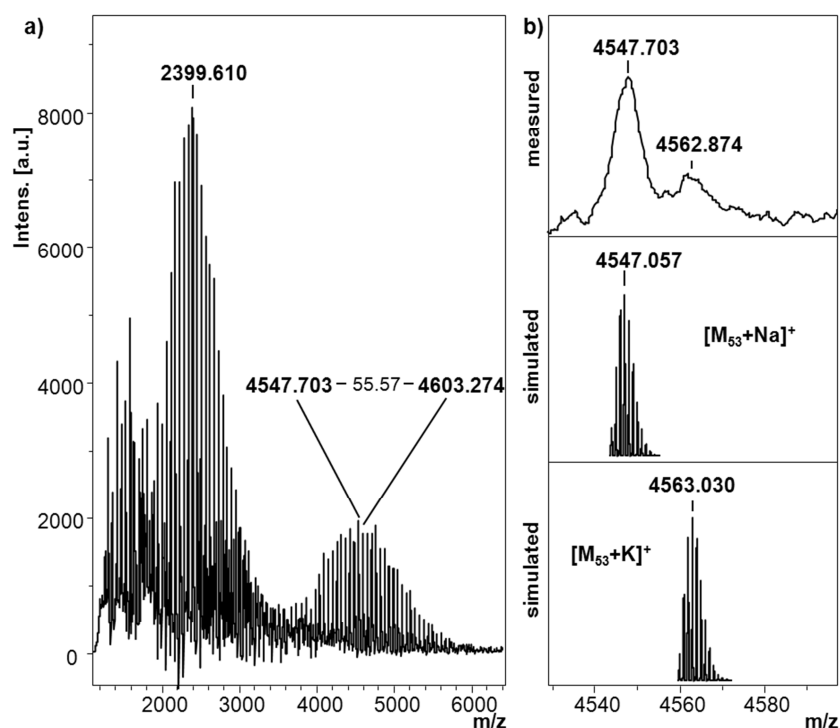


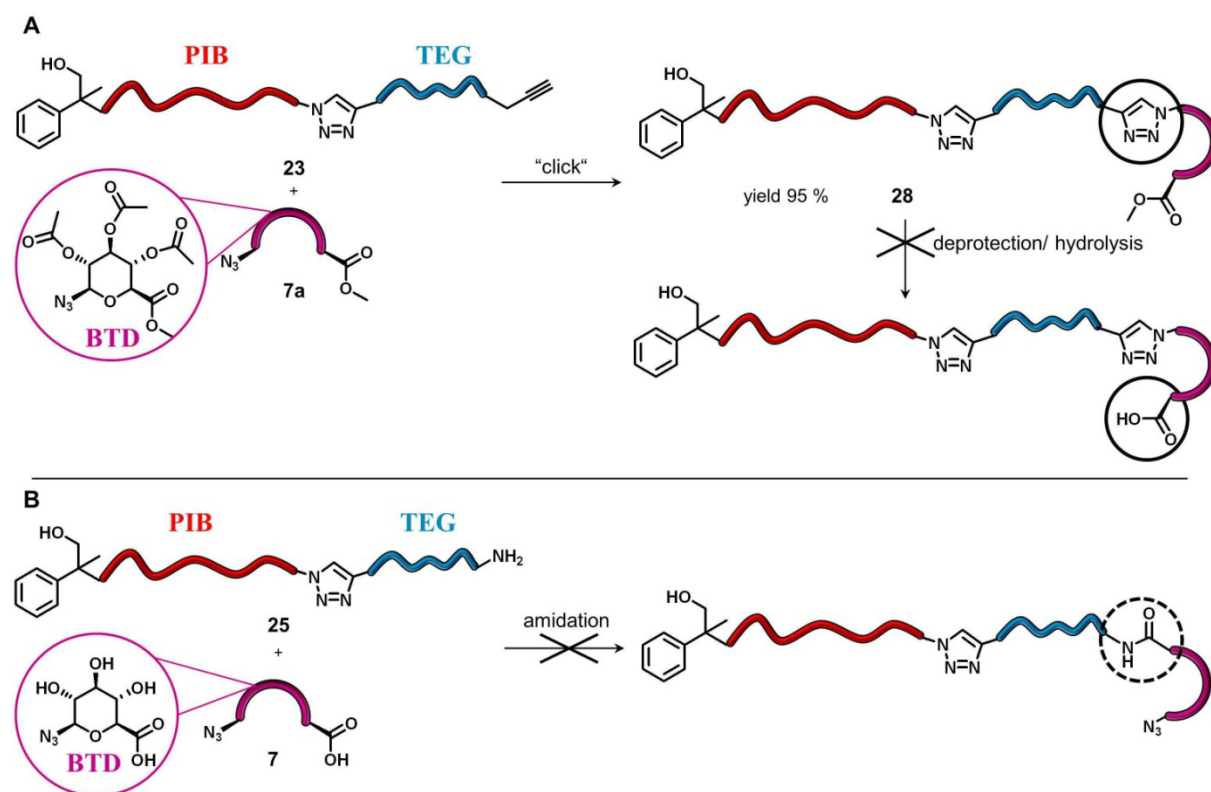
**Figure 6.3.** MALDI-ToF-MS of **27** of a) the region 1000-6000 Da and b) expanded spectrum with a listed view of the simulated peaks.

Matrix-Assisted Laser Desorption/Ionization Time-of-Flight Mass Spectrometry (MALDI-ToF MS) was carried out to prove the structure of the complete amphiphilic  $\beta$ -turn mimetic block “copolymer”

## 6. Elongation of the hydrophilic part

**27** after purification with preparative HPLC. Figure 6.3a shows the region 1000-6000 Da as it can be seen two different series the small molecular weight series 1000-3500 Da and higher molecular weight series 3500-6000 Da are present. Figure 6.3b shows the expanded spectrum of the region with higher molecular weight with a listed view of the simulated peaks. As it can be seen the signal at 4547.703 g/mol agreed with the calculated value of 4547.057 g/mol as Na-adduct and the signal at 4562.874 g/mol corresponded with the simulated value of 4563.030 g/mol for K-adduct. Therefore, the structure of the complete amphiphilic  $\beta$ -turn mimetic block “copolymer” **27** could be proven. Nevertheless, the first series  $M_n = 2399.610$  g/mol can be assigned to the PIB-TEG-OH (equivalent of **23**, but hydroxyl groups instead of alkyne groups) which matches with the simulated value of 2400.372 Da as lithium adduct. The loss of the alkyne groups of the TEG part during the azide/alkyne-“click”-reaction was already observed in chapter 6.2 for the synthesis of  $\alpha$ -alkynyl- $\omega$ -amino-tetraethylene glycol (**21**). All in all **27** could be synthesized successfully, but not purified. As the  $R_f$  value of the product **27** and the side product PIB-TEG-OH are the same (eluent  $\text{CHCl}_3 \rightarrow \text{CHCl}_3/\text{MeOH} = 70:1$ ,  $R_f = 0.2$ ) purification by column chromatography was not successful. Moreover, the further purification via preparative SEC and HPLC using THF as eluent lead only to less content of the PIB side product, but no complete purification of the product **27**.

### 6.2.3 Synthesis of the two strands using SAA as $\beta$ -turn mimetic



**Scheme 6.6.** Two different approaches of the synthesis of two strands using SAA as  $\beta$ -turn mimetic.



## 6. Elongation of the hydrophilic part

---

Due to the similarity of the  $\beta$ -turn mimetics BTD and SAA the linkage of the building blocks PIB-TEG onto the SAA were conducted analogously to the previous work (chapter 6.3.1. and 6.3.2).

Scheme 6.6 shows the two different approaches of the synthesis of the two strands using SAA as  $\beta$ -turn mimetic. A) The first approach shows analogue to chapter 6.3.1 B the linkage of the SAA **7a** onto the PIB-TEG **23** building block via azide/alkyne-“click”-reaction to achieve the click product PIB-TEG-SAA **28** in a yield of 95 % (NMR and MALDI-ToF MS see Appendix Figure A63 and A64). The further step, the deprotection/hydrolysis, was again not successful. As described before (chapter 6.3.1) the deprotection/hydrolysis was tried under different conditions; varying the amount of LiOH (4-120 eq), the temperature (room temperature-50 °C) and the reaction time (14 h – 2 weeks). However, no complete hydrolyzed/deprotected PIB-TEG-SAA bearing the carboxylic acid moiety could be obtained, only partial hydrolysis/deprotection could be observed. One big problem again was the precipitation of the polymer after the partial hydrolysis/deprotection. After redissolving and extension of the reaction time and/or further addition of base, decomposition of the PIB-TEG-SAA was observed. Likewise the azide/alkyne-“click”-reaction was carried out with SAA **7** with already deprotected hydroxyl groups and bearing the carboxylic acid moiety, but equally to the “click”-reaction with BTD **6** no “click” product could be obtained.

B) Therefore, in accordance with chapter 6.3.2 the  $\beta$ -turn mimetic SAA should be linked via amidation to the second strand (PIB-TEG **25**) bearing the amine functionality at the  $\omega$ -terminus. However, no peptide coupling could be obtained. At first according to the previous work PyBOP/NMM<sup>114</sup> was used as coupling agent, as this was not successful EDC·HCl/HOBt<sup>108, 221</sup> was applied. The latter is already known in literature where a PIB-amine was coupled with picolinic acid *N*-oxide to form the amidation product the PIB-supported pyridyl *N*-oxide.<sup>221</sup> Also EDC·HCl/HOBt was used for peptide coupling of SAA and peptides.<sup>108</sup>

As amphiphilic block “copolymers” containing a  $\beta$ -turn mimetic element (BTD or SAA) could not be purified or even the synthesis of the complete structure failed, further experiments investigating the influence of the elongation of the hydrophilic part could not be conducted.

### 7. Experimental Part

#### 7.1 Materials and Methods

D-Glucurono-3,6-lactone and Trifluoromethanesulfonic anhydride were obtained from TCI Europe. (Benzotriazol-1-yloxy)tripyrrolidinophosphonium hexafluorophosphate (PyBOP) was purchased from Merck. *N*-methyldimorpholine (NMM) was obtained from VWR. 1,2-Dipalmitoyl-sn-glycero-3-phosphocholine (L-DPPC) was purchased from Avanti Polar Lipids (Alabaster, AL, USA) and 1,2-dihexadecanoyl-sn-glycero-3-phosphoethanolamine-*N*-(lissamine rhodamine B sulfonyl) (Rh-DHPE) was purchased from Invitrogen (Karlsruhe, Germany) and used without further purifications. All other chemicals were obtained from Sigma-Aldrich and used without further purification if not mentioned otherwise. Dichloromethane (DCM), DMF (*N,N*-dimethylformamide) and pyridine were predried over CaCl<sub>2</sub> and freshly distilled over CaH<sub>2</sub> under nitrogen atmosphere. *N*-hexane was refluxed over concentrated H<sub>2</sub>SO<sub>4</sub> and oleum for 48 h to remove olefins. The organic layer was washed with a NaHCO<sub>3</sub> solution and distilled water, dried over Na<sub>2</sub>SO<sub>4</sub> and stored over KOH. Subsequently it was freshly distilled over KOH and sodium under dry nitrogen atmosphere before use. Tetrahydrofuran (THF) was predried over KOH, toluene over CaCl<sub>2</sub> and freshly distilled over sodium and benzophenone under dry atmosphere of nitrogen before used. Methanol was freshly distilled over CaH<sub>2</sub> before use. Isobutylene (Fluka) was dried by passing the gas through a column packed with potassium hydroxide and condensed at -80 °C in a two-neck round bottom flask equipped with a septum.

The initiator for LCCP ( $\alpha$ -methylstyrene epoxide (MSE, **1**)) was synthesized by the epoxidation of methyl styrene with 3-chloroperoxybenzoic acid following to literature.<sup>222, 223</sup> The synthesis of the quencher 6-phenoxyhexylamine (**2**) was adopted from Morgan et al.<sup>143</sup> and was synthesized by B.Sc. Enerelt Sanchin.<sup>224</sup> The synthesis of the quenching agent trimethyl(3-phenoxy-1-propynyl)silane (TMS, **4**) was done according to Morgan et al.<sup>143</sup> The synthesis of the 7,5-bicyclic thiazolidine lactam methyl ester (**6**) was carried out according to literature.<sup>113, 114</sup> Methyl 6-azidohexanoate (**10**) was synthesized according to Srinivasan<sup>225</sup>. The  $\alpha$ -hydroxymethyl- $\omega$ -bromo telechelic poly(isobutylenes) (PIBs, **17a-e**) with  $M_n = 3000, 4000, 8000$  and  $15,000$  g/mol were synthesized and transformed to  $\alpha$ -hydroxymethyl- $\omega$ -azido telechelic poly(isobutylenes) (**18**) according to Olubummo et al.<sup>144</sup> The synthesis of 3-azido-propylamine (**20a**) was carried out according to Liu et al.<sup>226</sup> and the protection of the amine group to achieve *tert*-butyl 3-azidopropylcarbamate (**20**) was done according to Xiao<sup>227</sup>. Tris-(benzyltriazolylmethyl)amine (TBTA, **29**) was synthesized according to Lee et al.<sup>228</sup> The starting material benzyl azide was synthesized by M.Sc. Philipp Michael (MLU) according to Mourer et al.<sup>229</sup> and tripropargyl amine was synthesized during my diploma thesis<sup>230</sup>. The iodo(triethylphosphite)copper(I) was synthesized during my diploma thesis, too.<sup>230</sup>

## 7. Experimental Part

---

*Column chromatography* was performed on Kieselgel 60 silica gel. *Preparative thin layer chromatography (TLC)* was carried out on TLC aluminium sheets (silica gel 60 F<sub>254</sub>) from Merck KGaA. Ce(SO<sub>4</sub>)<sub>2</sub>·4 H<sub>2</sub>O (1g), dissolved in concentrated H<sub>2</sub>SO<sub>4</sub> (2.75 ml) and distilled water (47 ml), and “blue stain”, consisting of Ce(SO<sub>4</sub>)<sub>2</sub>·4 H<sub>2</sub>O (1 g), (NH<sub>4</sub>)<sub>6</sub>Mo<sub>7</sub>O<sub>24</sub>·4 H<sub>2</sub>O, concentrated H<sub>2</sub>SO<sub>4</sub> (6 ml) and distilled water (90 ml) were used as oxidation agents. *Dialysis* was performed using *ZelluTrans* (ROTH) regenerated cellulose dialysis tubings with a molecular weight cut-off (MWCO) of 1000 Da (nominal), 45 mm width and 27 µl thickness. The polymer was dialyzed (minimum) for 2, 4 and 12 h in CHCl<sub>3</sub>.

### Spectroscopic Methods

*Nuclear Magnetic Resonance (NMR) Spectroscopy.* <sup>1</sup>H-NMR and <sup>13</sup>C-NMR spectra were recorded at 27 °C on a VARIAN GEMINI 400/600 (400/600 MHz) spectrometer in CDCl<sub>3</sub> (Armar AG, 99.8 Atom %D). The chemical shifts were recorded in ppm and referred to the solvent residue peak (CDCl<sub>3</sub> 7.26 ppm (<sup>1</sup>H) and 77.0 ppm (<sup>13</sup>C)). MestReC (v4.9.9.6)/MestreNova (6.0.2) was used for data interpretation. The measurements were conducted by the team of Dr. D. Ströhl and S. Gröger (working group Prof. Dr. J. Balbach).

### Chromatographic Methods

*Size Exclusion Chromatography (SEC).* SEC spectra were recorded on a Viscotek GPCmax VE 2002 Solvent/Sample Module or on a Viscotek GPCmax VE2002 system combined with a Viscotek TDA30L (triple detector array) using a H<sub>HR</sub>H Guard-17369 and GMH<sub>HR</sub>-N-18055 column in THF. The measurement was performed at constant column and detector (refractive index) temperature at 35 °C with a flow rate of 1 mL/min. Polyisobutylene standards were obtained from PSS (Polymer Standards Service) and used for conventional external calibration. Standards with a molecular weight of 320, 1500, 7450, 21500, 40400, 72100, 117000, 247000 367000 and 578000 g/mol were used. The investigated samples were dissolved in THF (>99.9%); analyses of the results of the SEC experiments were achieved using OmniSec (4.5.6) software. The measurements were conducted by S. Tanner.

*High Performance Liquid Chromatography (HPLC).* HPLC spectra were performed on a LaChrom Elite by Hitachi VWR equipped with a pump (L2100), an auto sampler (L-2200), a degasser, a diode array detector (DAD L-2455) and a column oven (L-2300) with temperature control (temperature set limit = 0–70 °C). The measurements were carried out on a reversed phase column (RP C-18) Waters Atlantis<sup>®</sup>-T3, 5 µm, 100 Å, dimension 4.6 × 250 mm. Methyl-*tert*-butyl ether (MTBE) HPLC grade purchased from ROTH and Methanol (MeOH) HPLC grade purchased from Merck were applied as the mobile phase system. The critical condition of α-hydroxymethyl-ω-bromo telechelic PIB (M<sub>n</sub> = 4000, 8000 and 15,000 g/mol) was found at MTBE/MeOH = 85.2:14.8 (v/v) at a temperature of

## 7. Experimental Part

---

30 °C.<sup>195</sup> Temperatures were maintained constant ( $\pm 0.2$  K) throughout all experiments, and the injected sample volume was 10  $\mu\text{L}$ . The DAD signals were recorded on EZchrom elite software version 3.3.2 SP2 with an operating wavelength from 190 to 900 nm at a sampling width of 800 ms to obtain sufficient data points across peaks.

*Preparative High Performance Liquid Chromatography (HPLC).* Preparative HPLC for final purification were conducted on a modified Medium Pressure Liquid Chromatography together with HPLC column system. Therefore, the HPLC column system (precolumn XBridge™ Prep C18, 5  $\mu\text{m}$ , 19x10 mm, Guard Holder Assy 19x10 mm and column XBridge™ Prep C18, 10  $\mu\text{m}$ , 19x100 mm) was combined with the BÜCHI pump manager C-615, the BÜCHI pump module C-605, the BÜCHI fraction collector C-660, the Agilent Technologies 1260 Infinity RI detector and the Agilent Instant Pilot. Tetrahydrofuran (THF) HPLC grade purchased from VWR and Methanol (MeOH) HPLC grade purchased from Merck were applied as the mobile phase system. The purification of the final poly(isobutylene)-product (**9**) was performed at constant temperature (35 °C) with a flow rate of 2.5 mL/min and analyses of the results of the experiments were achieved using BÜCHI Sepacore Record 1.0 software.

### Spectrometric Methods

*Matrix-Assisted Laser Desorption/Ionization Time-of-Flight Mass Spectrometry (MALDI-ToF MS).* MALDI-ToF MS measurements were performed on a Bruker Autoflex III system (Bruker Daltonics) operating in reflection and linear modes. Data evaluation was carried out on flexAnalysis software (3.4). Ions were formed by laser desorption (smart beam laser at 355, 532, 808, and  $1064 \pm 5$  nm; 3 ns pulse width; up to 2500 Hz repetition rate), accelerated by a voltage of 19-20 kV and detected as positive ions. The matrix solution was prepared by dissolving trans-2-[3-(4-*tert*-butylphenyl)-2-methyl-2-propenylidene]malononitrile (DCTB, purchased from Sigma Aldrich) in THF with a concentration of 20 mg/mL. Polymer samples were dissolved in THF with a concentration of 20 mg/mL. The salt Lithiumtrifluoroacetate, (LiTFA, purchased from Sigma Aldrich) was dissolved with a concentration of 20 mg/mL in THF. The solutions of the matrix, the polymer, and the salt were mixed in a volume ratio of 25:5:1, and 1  $\mu\text{L}$  of each mixture was spotted on the MALDI target. The instrument was externally calibrated with a poly(ethylene glycol) monomethyl ether (PEG) standard ( $M_n = 4200$  g/mol,  $M_w/M_n = 1.05$ ) applying a quadratic calibration method.

*Electrospray Ionization Time-of-Flight Mass Spectrometry (ESI-ToF MS).* ESI-ToF MS measurements were conducted on a Bruker Daltonics micrOTOF II. The samples were dissolved in Methanol with a concentration of 1 mg/mL (if necessary NaCl (10 v%, 20 mg/mL in H<sub>2</sub>O) were added) and measured via direct injection, with a flow rate of 180  $\mu\text{L}/\text{h}$ . Measurements were done in positive mode with a capillary voltage of 4.5 kV. Spectra were analyzed with Bruker DataAnalysis 4.0 software; isotopic patterns are simulated with Bruker Compass IsotopePattern. The measurements were conducted by S. Tanner.

### Coupling Technique

*Liquid Chromatography coupled to MALDI-TOF MS (LC/MALDI-TOF MS).* The HPLC outlet (first dimension) is connected to a liquid chromatography transfer module (LCT, Leap Technologies, Carrboro, NC), where sample fractions were mixed with DCTB (20 mg/mL) and lithium trifluoroacetate (5 mg/mL) and conveyed to the TM-sprayer. DCTB and LiTFA were premixed in a 50:1 v/v ratio (matrix:salt) and transferred using an isocratic pump with a flow rate of 2 mL/min. To achieve a uniform and consistent coating, the nozzle height was set to 8 cm, nitrogen was used as a carrier gas with a pressure of 5 bar, and the fractions were deposited on home-built LCT-MALDI-target with a spray speed of 9 mm/min at 125 °C in a spray linear mode. This target was then transferred to a MALDI-TOF and the fractions were measured as usual. The spraying process was monitored using LEAP Technologies control software enabling a direct correlation of the retention time with the measured mass spectra.<sup>195</sup>

### Monolayer experiments

*Surface pressure ( $\pi$ ) measurements* of the pure compounds and of different binary mixed systems of the PIBs and DPPC at the air/water interface *via* Langmuir film technique were performed using a Langmuir trough system (KSV, Helsinki, Finland) with a maximum available surface of 76.800 mm<sup>2</sup>. The used ultrapure water (as subphase and for cleaning of the trough) was purified by a Purelab Option system (ELGA Ltd., Celle, Germany; total organic carbon < 5 ppm; conductivity < 0.055  $\mu\text{S}\cdot\text{cm}^{-1}$ ). All compression measurements were performed at constant temperature (20 °C). The investigated mixture of PIB and DPPC was dissolved in chloroform (HPLC grade, Sigma Aldrich) at a concentration of 1 mM. Defined amounts of the prepared solutions (different molar ratios of DPPC to PIB) were spread on the subphase using a digital microsyringe (Hamilton). Each surface pressure measurement using a compression rate of 5 mm $\cdot$ min<sup>-1</sup> was started 15 minutes after spreading to ensure the full evaporation of the solvent and a uniform monolayer formation.

*Epifluorescence microscopy.* Imaging of monolayers at the air/water interface was performed using an “Axio Scope A1 Vario” epifluorescence microscope (Carl Zeiss MicroImaging, Jena, Germany) with a Langmuir Teflon trough (maximum area 264 cm<sup>2</sup>, two movable barriers; Riegler & Kirstein GmbH, Berlin, Germany). The trough was mounted on an x-y stage (Märzhäuser, Wetzlar, Germany) with x-y-z motion control (Mac5000 system, Ludl Electronic Products, Hawthorne, NY, USA). The air/water surface was imaged by a 100 W mercury arc lamp, a long-distance objective (LD EC Epiplan-NEOFLUAR 50x) was used and the respective wavelengths were selected with a filter/beam splitter combination. An excitation wavelength of 557 nm and an emission wavelength of 571 nm were used with the appropriate Zeiss filter set (filter set 20, green light). The fluorescence images were taken during compression with a speed of 4 cm<sup>2</sup>/min and recorded using an EM-CCD camera (ImageEM C9100-13, Hamamatsu, Herrsching, Germany). The analysis and data acquisition were done using

AxioVision software (Carl Zeiss MicroImaging, Jena, Germany). All presented images show areas of individually contrast-adjusted raw data.

Monolayer films of pure or mixed compounds in different molar ratios were prepared with a total spreading concentration of 1 mM in chloroform (HPLC-grade, Carl Roth, Karlsruhe, Germany) and fluorescently labeled rhodamine-DHPE (0.01 mol%) was added to the stock solution. A defined volume of the solution was then spread on the water surface and after 15 minutes the compression was started.

*Langmuir–Blodgett (LB) films.* The deposition of polymer films formed at air/water interface was carried out on silicon wafer. For this purpose, the surface of silicon wafer was cleaned directly before using. They were placed in a Helmanex solution (1 % in H<sub>2</sub>O) at 50 °C for 10 min using ultrasound, rinsed with Helmanex solution and then rinsed with double deionized water. This washing procedure was repeated, for using CHCl<sub>3</sub> and H<sub>2</sub>O. In the last step they were cleaned using a plasma-cleaner. After treatment, the silicon wafers were immersed into the water subphase of the Langmuir trough. The polymer solution was then spread onto the water surface and after 15 min of waiting; the surface was compressed using a compression rate of 84 mm/min until the desired transfer surface pressure was achieved. After waiting for 5 min at this surface pressure, the film was then transferred onto the silicon substrate by vertical uptake through the films using a constant rate of 2 cm/min. Finally, the LB films were dried in desiccator at room temperature for 24 h.

*Atomic force microscopy (AFM).* The surface morphology of LB films was investigated using AFM Multimode V with Nanoscope VII Controller (Bruker, Santa Barbara, USA) coupled with reflected-light microscopy (Olympus MM10, Olympus Europa Holding GmbH, Hamburg, Germany). The AFM was operated in tapping mode using TESPA cantilever (Nano and More, Wetzlar, Germany) with nominal spring constant of 42 N/m, resonance frequencies of about 320 kHz and tip radii smaller than 10 nm. Pictures were taken at an acquisition speed of 1 Hz with lateral resolution of 512 × 512 pixels. The measurements were conducted by B.-D. Lechner.

### **Bilayer experiments**

*Electroformation-preparation of GUVs.* The giant unilamellar vesicles (GUVs) were prepared by applying an alternating low-voltage electric field during the hydration process of a thin lipid/polymer film. The DPPC/PIB (**8** and **9**) mixtures were prepared in HPLC-grade chloroform, dried under a continuous N<sub>2</sub>-stream and dissolved in a defined solvent volume at 10 mg/mL. Optically transparent indium-tin-oxide (ITO) coated coverslips (*GeSiM, Großberkmannsdorf, Germany*), which were used as electrodes, were coated with a thin amphiphile film. After the preparation of a thin film on two coverslips, these were placed in a capacitor-type configuration at a distance of 2 mm using a home built flow-chamber. The chamber was filled with deionized water (~300 ml). Finally, the ITO-slips were connected to a pulse generator (Conrad, Germany) and an alternating sinusoidal voltage ( $U_{\text{eff}} =$

## 7. Experimental Part

1.3 V,  $\nu = 10$  Hz) was applied for 4 hours. During the whole electroformation process, the coverslips were heated to 70 °C, *i.e.* safely above the main transition temperature of DPPC ( $T_m = 41.6$  °C).

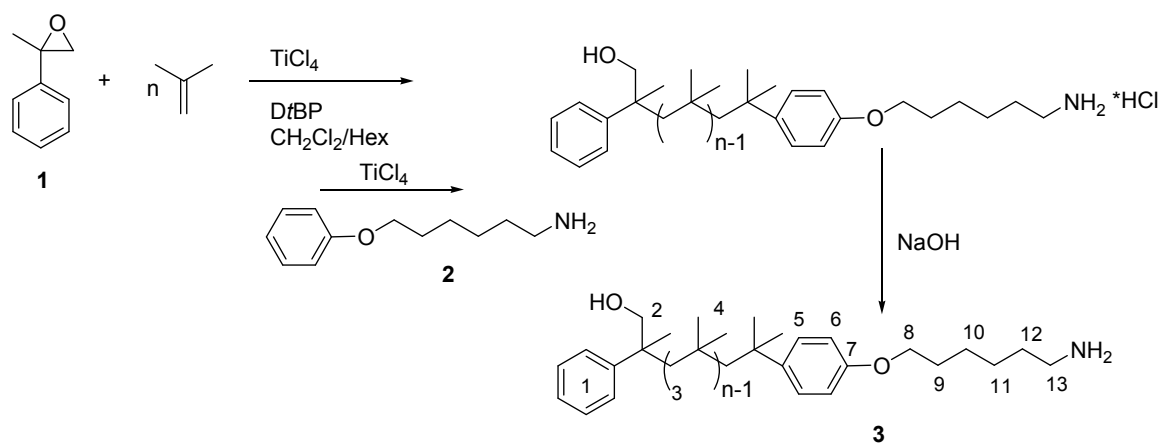
**Confocal microscopy.** Confocal microscopy images were obtained on a commercial confocal-laser scanning microscope- LSM 710 (Carl-Zeiss, Germany) using a C-Apochromat 40x/1.2 N.A. water immersion objective. Rh-DHPE was used as fluorescence dye, which was excited with an Argon-Ion-laser at 488 or 514 nm. Imaging of all GUV samples was performed after cooling to room temperature unless otherwise stated. The measurements were conducted from Dr. M. Schulz.

**Formation of LUVs.** The DPPC/PIB (**13** and **15**) mixtures in a ratio of 1:99 (mol/mol) were prepared in HPLC-grade chloroform and dried under a continuous N<sub>2</sub>-stream. To this thin film H<sub>2</sub>O (2mM) was added and the suspension was heated up to 50 °C, multilamellar vesicles were formed by “vortexing” and then ultrasonification for 10 min and these were then extruded via syringes using a membrane with 100 nm pores to achieve unilamellar LUVs.

**Fluorescence spectroscopy.** Fluorescence spectra were taken using a Jobin-Yvon Fluoromax II (Horiba Jobin Yvon Inc., Grasbrunn, Germany) fluorescence spectrometer with a cell holder connected to a NESlab RTE 740 thermostat (Thermo Scientific Inc., Schwerte, Germany). For the absorption or fluorescence experiments, quartz cuvettes (Hellma Analytics GbmH, Müllheim, Germany) with a 10 mm path length were used.

## 7.2 Synthesis

### 7.2.1 Synthesis of $\alpha$ -hydroxymethyl- $\omega$ -amino telechelic poly(isobutylene) **3**

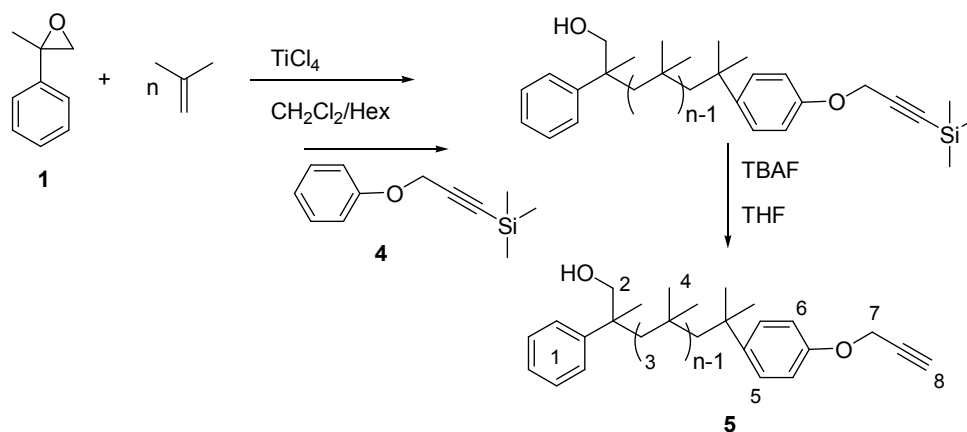


A representative procedure for  $\alpha$ -hydroxymethyl- $\omega$ -amino telechelic PIB **3** with  $M_n = 5000$  g/mol was achieved by a combined synthesis of Olubummo et al.<sup>144</sup> and Morgan et al.<sup>143</sup> The polymerization was carried out under dry argon atmosphere. A three-neck flask equipped with a magnetic stir bar, a stop cock and a septum was loaded with dry *n*-hexane and dry DCM (60/40 = v/v). During cooling the system to -60 °C ditertiary-butyl pyridine (DtBP, 5 mmol/L),  $\text{TiCl}_4$  (120 mmol/L) and MSE (**1**, 60 mmol/L) were added and after 5-10 min the polymerization was started by injecting condensed isobutylene (1 mol/L). After stirring for 20 minutes the polymerization mixture was cooled to -65 °C

## 7. Experimental Part

(MeOH + CO<sub>2</sub> (s) cooling bath), quenched by addition of 5 equivalents of 6-phenoxyhexylamine (**2**) and 1.5 equivalents of TiCl<sub>4</sub> (according to 6-phenoxyhexylamine) and allowed to stir for 18 hours at this temperature. Finally, the catalyst was destroyed by addition of excess methanol. The poly(isobutylene) was isolated by precipitation from n-hexane into methanol, washed with aqueous NaOH (10 wt.-%), precipitated again and dried under vacuum. The final PIB **3** was obtained in a yield of 93 %. SEC: M<sub>n</sub> = 5000 g/mol, M<sub>w</sub>/M<sub>n</sub> = 1.3. <sup>1</sup>H-NMR (400 MHz, CDCl<sub>3</sub>): δ = 7.34 (*m*, 5H, H-1), 7.21 (*m*, 2H, H-5), 6.80 (*d*, 2H, <sup>3</sup>J<sub>H,H</sub> = 8.7 Hz, H-6), 3.93 (*t*, 2H, <sup>3</sup>J<sub>H,H</sub> = 6.5 Hz, H-8), 3.66 (*d*, 1H, <sup>2</sup>J<sub>H,H</sub> = 10.6 Hz, H-2), 3.43 (*d*, 1H, <sup>2</sup>J<sub>H,H</sub> = 10.6 Hz, H-2'), 2.70 (*t*, 2H, <sup>3</sup>J<sub>H,H</sub> = 6.4 Hz, H-13), 2-0.8 (*m*, polymer backbone). <sup>13</sup>C-NMR (400 MHz, CDCl<sub>3</sub>): δ = 156.5 (C-7), 128.3-127.0 (C-1), 125.9 (C-1,5), 113.6 (C-6), 74.5 (C-2), 67.4 (C-8), 59.7-59.0 (C-3), 52.8 (C-13), 38.3-37.6 (C-4), 31.6-31.0 (C-4), 30.6 (C-9), 29.1 (C-12), 26.2 (C-11), 25.1 (C-10).

### 7.2.2 Synthesis of α-hydroxymethyl-ω-alkyne telechelic PIB (**5**)



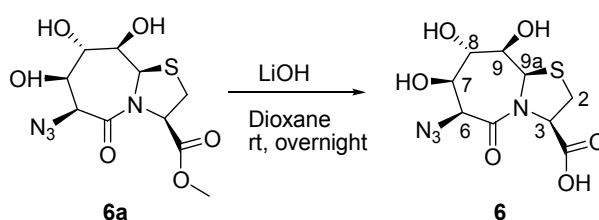
A representative procedure for α-hydroxymethyl-ω-alkyne telechelic PIB (**5**) with M<sub>n</sub> = 4700 g/mol was achieved by a combined synthesis of Olubummo et al.<sup>144</sup> and Morgan et al.<sup>143</sup> The polymerization was carried out under dry argon atmosphere. A three-neck flask equipped with a magnetic stir bar, a stop cock and a septum was loaded with dry *n*-hexane and dry DCM (60/40 = v/v). During cooling the system to -60 °C ditertiary-butyl pyridine (DtBP, 5 mmol/L), TiCl<sub>4</sub> (120 mmol/L) and MSE (**1**, 45 mmol/L) were added and after 5-10 min the polymerization was started by injecting condensed isobutylene (1 mol/L). After stirring for 20 minutes the polymerization mixture was cooled to -65 °C (MeOH + CO<sub>2</sub> (s) cooling bath), quenched by addition of 4 equivalents of **4** and 1.67 equivalents of TiCl<sub>4</sub> (according to TMS) and allowed to stir for 8 hours at this temperature. Finally, the catalyst was destroyed by addition of excess methanol. The poly(isobutylene) was isolated by repeated precipitation from n-hexane into methanol and dried under vacuum. The final PIB **5** was obtained by treatment with tetrabutylammonium fluoride (TBAF). Therefore, trimethylsilyl protected α-hydroxymethyl-ω-alkyne telechelic PIB (0.1 mmol, 500 mg) was dissolved in dry THF (5 mL) under an argon atmosphere and 5 equivalents of a 1.0 M solution of TBAF in THF were added. After stirring overnight at room temperature the solvent was removed, but not until dryness, the PIB was dissolved



## 7. Experimental Part

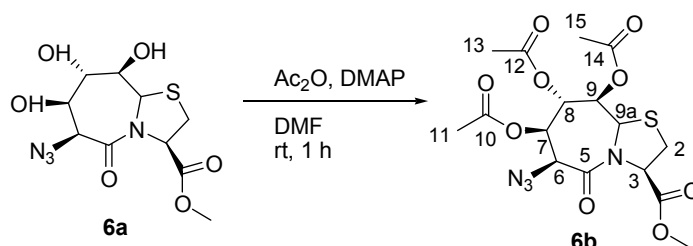
in DCM and washed three times with water. The resulting  $\alpha$ -hydroxymethyl- $\omega$ -alkyne telechelic PIB **5** was achieved in a yield of 90 %. SEC:  $M_n = 4700$  g/mol,  $M_w/M_n = 1.39$ .  $^1\text{H-NMR}$  (400 MHz,  $\text{CDCl}_3$ ):  $\delta = 7.34$  (*m*, 5H, H-1), 7.21 (*m*, 2H, H-5), 6.89 (*d*, 2H,  $^3J_{\text{H,H}} = 8.8$  Hz, H-6), 4.67 (*d*, 2H,  $^2J_{\text{H,H}} = 2.4$  Hz, H-7), 3.66 (*dd*, 1H,  $^3J_{\text{H,OH}} = 3.4$  Hz,  $^2J_{\text{H,H}} = 10.4$  Hz, H-2), 3.43 (*dd*, 1H,  $^3J_{\text{H,OH}} = 9.8$  Hz,  $^2J_{\text{H,H}} = 9.8$  Hz, H-2'), 2.50 (*s*, 1H, H-8), 2-0.8 (*m*, polymer backbone).  $^{13}\text{C-NMR}$  (400 MHz,  $\text{CDCl}_3$ ):  $\delta = 156.5$ , 142.4, 128.3, 127.0, 125.9, 114.1, 110.0, 77.2, 75.2, 63.9, 59.7-59.0, 52.8, 44.2, 42.5, 38.3-37.6, 32.2, 31.6-31.0, 30.7. MALDI-TOF MS  $m/z_{\text{exp}} = 2124.48$  [ $\text{M}_{33}+\text{Li}$ ] $^+$ , 2140.37 [ $\text{M}_{33}+\text{Na}$ ] $^+$ , 2162.15 [ $\text{M}_{33}-\text{H}+2\text{Na}$ ] $^+$ ,  $m/z_{\text{calc}} = 2124.21$  [ $\text{M}_{33}+\text{Li}$ ] $^+$ , 2140.21 [ $\text{M}_{33}+\text{Na}$ ] $^+$ , 2162.17 [ $\text{M}_{33}-\text{H}+2\text{Na}$ ] $^+$ .

### 7.2.3 Synthesis of (3R,6S,7R,8S,9R,9aR)-6-azido-octahydro-7,8,9-trihydroxy-5-oxothiazolo[3,2-a]azepine-3-carboxylic acid (BTD-COOH, **6a**)



The synthesis of BTD-COOH (**6**) was modelled after Tremmel.<sup>114</sup> Therefore, **6a** (1.60 mmol, 509 mg) was dissolved in 20 mL dioxane and a solution of LiOH (2.26 mmol, 95 mg) in water (10 mL) was added at room temperature under stirring. The reaction was allowed to stir overnight, controlled by TLC (THF;  $R_f = 0$ ) and stopped by the addition of 1M HCl until the solution was neutral. Then the solvent was evaporated to get the product **6** quantitatively, which was used without further purification.  $^1\text{H-NMR}$  (400 MHz,  $\text{DMSO-d}_6$ ):  $\delta = 5.62$  (*bs*, 1H, OH), 5.49 (*s*, 1H, H-9a), 4.58 (*t*, 1H,  $^3J_{\text{H,H}} = 7.1$  Hz, H-3), 4.49 (*s*, 1H, H-6), 3.84 (*m*, 1H, H-7), 3.80 (*m*, 1H, H-8), 3.47 (*d*, 1H,  $^3J_{\text{H,H}} = 3.1$  Hz, H-9), 3.19 (*m*, 2 H, H-2).  $^{13}\text{C-NMR}$  (400 MHz,  $\text{DMSO-d}_6$ ):  $\delta = 173.0$  (COOH), 165.9 (C-5), 76.1 (C-9), 75.9 (C-7), 72.1 (C-8), 66.3 (C-3), 61.3 (C-6), 61.1 (C-9a), 32.9 (C-2). ESI-TOF MS (MeOH)  $m/z_{\text{exp}} = 311.0865$  [ $\text{M}+\text{Li}$ ] $^+$ , 317.0944 [ $\text{M}-\text{H}+2\text{Li}$ ] $^+$ ,  $m/z_{\text{calc}} = 311.0638$  [ $\text{M}+\text{Li}$ ] $^+$ , 317.0720 [ $\text{M}-\text{H}+2\text{Li}$ ] $^+$ .

### 7.2.4 Protection of hydroxyl-groups of **11** with $\text{Ac}_2\text{O}$ to achieve **6b**

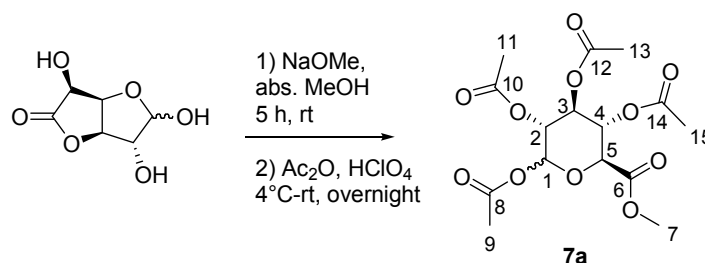


The acetylation reaction of **6a** was accomplished to literature.<sup>231</sup> In a 10 mL round bottom flask **6a** (0.157 mmol, 50 mg) was dissolved in 2 mL of freshly distilled DMF. Then, DMAP (0.047 mmol, 6

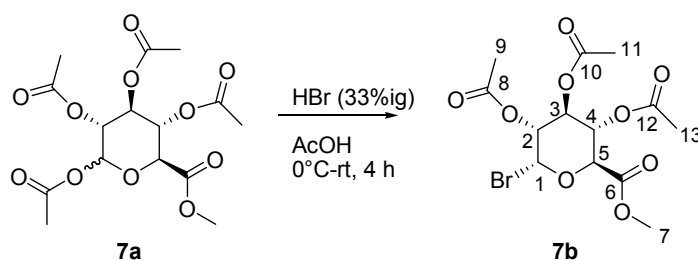
## 7. Experimental Part

mg) and acetic anhydride (0.942 mmol, 89  $\mu$ L) were added. The suspension was stirred for 1 h at room temperature, monitored via TLC (EA/Tol = 5:1,  $R_f$  = 0.78) and quenched by addition of MeOH. After removing of the solvent, the crude product was purified via column chromatography (EA/Tol = 3:1) to yield 97 % (0.152 mmol, 67 mg) of **6b** as white solid.  $^1\text{H-NMR}$  (400 MHz,  $\text{CDCl}_3$ ):  $\delta$  = 5.34 (*m*, 2H, H-6,9), 5.18 (*d*, 1H,  $^3J_{\text{H,H}}$  = 4.6 Hz, H-8), 5.09 (*t*, 1H,  $^3J_{\text{H,H}}$  = 6.6 Hz, H-3), 5.01 (*d*, 1H,  $^3J_{\text{H,H}}$  = 3.3 Hz, H-7), 4.53 (*s*, 1H, H-9a), 3.80 (*s*, 3H,  $\text{OCH}_3$ ), 3.36 (*dd*, 1H,  $^3J_{\text{H,H}}$  = 6.6 Hz,  $^3J_{\text{H,H}}$  = 11.4 Hz, H-2), 3.18 (*dd*, 1H,  $^3J_{\text{H,H}}$  = 6.6 Hz,  $^3J_{\text{H,H}}$  = 11.4 Hz, H-2'), 2.17 (*s*, 3H, H-11), 2.15 (*s*, 3H, H-13), 2.10 (*s*, 3H, H-15).  $^{13}\text{C-NMR}$  (400 MHz,  $\text{CDCl}_3$ ):  $\delta$  = 169.3 ( $\text{CO}_2\text{CH}_3$ ), 169.0 (C-10), 168.3 (C-12), 167.6 (C-14), 165.0 (C-5), 71.0 (C-7), 71.0 (C-8), 67.3 (C-9), 64.6 (C-3), 60.3 (C-6), 60.2 (C-9a), 52.6 ( $\text{OCH}_3$ ), 31.6 (C-2), 20.8 (C-11), 20.5 (C-13), 20.5 (C-15). ESI-TOF MS (MeOH)  $m/z_{\text{exp.}}$  = 467.0867  $[\text{M}+\text{Na}]^+$ , 483.0598  $[\text{M}+\text{K}]^+$ ,  $m/z_{\text{calc.}}$  = 467.0843  $[\text{M}+\text{Na}]^+$ , 483.0583  $[\text{M}+\text{K}]^+$ .

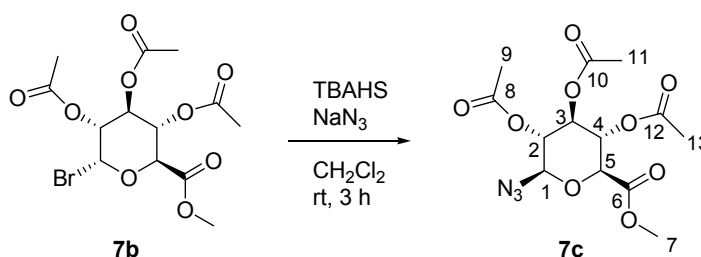
### 7.2.5 (2S,3S,4S,5R)-methyl 3,4,5,6-tetraacetoxy-tetrahydro-2H-pyran-2-carboxylate (**7a**)



The synthesis of **7a** was carried out according to literature<sup>127</sup> under dry atmosphere of nitrogen. In a 250 mL one-neck flask D-glucurono-3,6- lactone (0.0615 mol, 10.84 g) was dissolved in 60 mL abs MeOH and NaOMe (0.002 mol, 450  $\mu$ L (25 wt % solution in MeOH) was added. The solution was allowed to stir for 5 h at room temperature until everything was dissolved. Then the solvent was removed at 40 °C under vacuum and the slurry was dissolved in 42 mL acetic anhydride. Under cooling with an ice bath a mixture of 0.250 mL perchloric acid (70 wt %) in 6 mL of acetic anhydride was added dropwise. The reaction mixture stirred overnight at room temperature, additional 84  $\mu$ L of perchloric acid were added and the mixture was stored overnight in the refrigerator where crystals appeared. The crystals ( $\beta$ -anomer) were washed with diethyl ether and recrystallized once in hot ethanol. The mother liquor from the reaction was poured on 200 g crushed ice and neutralized with  $\text{NaHCO}_3$ . After extraction of the aqueous phase with  $\text{CHCl}_3$  the organic phase was dried over  $\text{Na}_2\text{SO}_4$ , filtered and concentrated to a slurry. This slurry was recrystallized in *iso*-propanol and then in hot ethanol. The overall yield (crude) of **7a** ( $\alpha$ - $\beta$  anomeric mixture) was 70 % (0.043 mol, 16 g, white crystals).  $\beta$ -anomer:  $^1\text{H-NMR}$  (400 MHz,  $\text{DMSO-d}_6$ ):  $\delta$  = 6.02 (*d*, 1H,  $^3J_{\text{H,H}}$  = 8.1 Hz, H-1), 5.51 (*t*, 1H,  $^3J_{\text{H,H}}$  = 9.5 Hz, H-3), 5.00 (*dd*, 1H,  $^3J_{\text{H,H}}$  = 9.0 Hz,  $^3J_{\text{H,H}}$  = 18.8 Hz, H-4), 4.96 (*d*, 1H,  $^3J_{\text{H,H}}$  = 8.1 Hz, H-2), 4.67 (*d*, 1H,  $^3J_{\text{H,H}}$  = 9.8 Hz, H-5), 3.64 (*s*, 3H, H-7), 2.08 (*s*, 3H, H-9), 2.01-1.97 (*3s*, 9H, H-11,13,15).  $^{13}\text{C-NMR}$  (400 MHz,  $\text{DMSO-d}_6$ ):  $\delta$  = 169.3-168.6 (C-8,10,12,14), 166.8 (C-6), 90.5 (C-1), 71.2 (C-5), 70.7 (C-2), 69.7 (C-4), 68.7 (C-3), 52.5 (C-7), 20.3-20.1 (C-9,11,13,15). ESI-TOF MS (MeOH)  $m/z_{\text{exp.}}$  = 399.1102  $[\text{M}+\text{Na}]^+$ ,  $m/z_{\text{calc.}}$  = 399.0898  $[\text{M}+\text{Na}]^+$ .

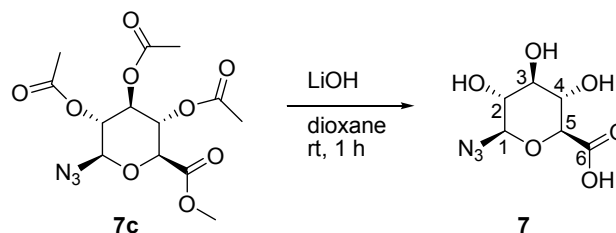
7.2.6 (2S,3S,4S,5R,6S)-methyl 3,4,5-triacetoxy-6-bromo-tetrahydro-2H-pyran-2-carboxylate (**7b**)

The synthesis of **7b** was carried out according to literature<sup>127, 128</sup>. In a 100 mL one-neck flask **7a** (3.46 mmol, 1.3 g) was dissolved in 8 mL HBr (33 % in AcOH) under ice cooling. After warming up to room temperature the solution was allowed to stir for 4 h. Then, 100 mL CHCl<sub>3</sub> were added and the mixture was poured into ice water (100 mL). The organic phase was separated and washed with an aqueous saturated solution of NaHCO<sub>3</sub> (three times 30 mL each, ice cooled), with an aqueous saturated solution of NaCl (three times 30 mL each, ice cooled) and with ice cooled water (60 mL). The organic layer was dried over MgSO<sub>4</sub>, filtered and the solvent was removed at 40 °C under reduced pressure to yield 73 % (2.5 mmol, 1 g) of **7b**. The unstable bromide **7b** ( $\alpha$ -anomer) was stored in a fridge overnight and used immediately for the next reaction.

7.2.7 (2S,3S,4S,5R,6R)-methyl 3,4,5-triacetoxy-6-azido-tetrahydro-2H-pyran-2-carboxylate (**7c**)

The synthesis of **7c** was carried out according to literature<sup>129, 130</sup>. In a 100 mL flask **7b** (2.5 mmol, 1 g) was dissolved in 10 mL CH<sub>2</sub>Cl<sub>2</sub> and TBAHS (2.5 mmol, 849 mg), NaN<sub>3</sub> (12.5 mmol, 813 mg) and 10 mL aqueous saturated solution of NaHCO<sub>3</sub> were added under stirring. The two phase mixture was allowed to stir vigorously at room temperature for 3.5 h. TLC was conducted, but **7b** and **7c** have the same R<sub>f</sub> values (Hex/EA = 1:1, R<sub>f</sub> = 0.67). Then, 100 mL EA were added, the organic phase separated and washed with aqueous saturated solution of NaHCO<sub>3</sub> (four times 30 mL each), aqueous saturated solution of NaCl (three times 30 mL each) and H<sub>2</sub>O (three times 30 mL each). The organic phase was then dried over Na<sub>2</sub>SO<sub>4</sub>, filtered and the solvent was removed under vacuum. The crude product was purified by recrystallization in hot ethanol yielding 56 % of **7c** (1.4 mmol, 500 mg, white crystals). <sup>1</sup>H-NMR (400 MHz, CDCl<sub>3</sub>):  $\delta$  = 5.25 (*m*, 2H, H-2,4), 4.96 (*t*, 1H, <sup>3</sup>J<sub>H,H</sub> = 8.9 Hz, H-3), 4.71 (*d*, 1H, <sup>3</sup>J<sub>H,H</sub> = 8.7 Hz, H-1), 4.12 (*d*, 1H, <sup>3</sup>J<sub>H,H</sub> = 9.5 Hz, H-5), 3.78 (*s*, 3H, H-7), 2.08 (*s*, 3H, H-9), 2.05-2.00 (2*s*, 6H, H-11,13). <sup>13</sup>C-NMR (400 MHz, CDCl<sub>3</sub>):  $\delta$  = 169.3-169.2 (C-8,10,12), 166.5 (C-6), 88.1 (C-1), 74.3 (C-2), 71.8 (C-5), 70.4 (C-4), 69.0 (C-3), 53.1 (C-7), 20.5-20.4 (C-9,11,13). ESI-ToF MS (MeOH) *m/z*<sub>exp.</sub> = 382.1175 [M+Na]<sup>+</sup>, *m/z*<sub>calc.</sub> = 382.0857 [M+Na]<sup>+</sup>. [ $\alpha$ ]<sub>D</sub><sup>20</sup> (*c* = 1) = -21.3 °.

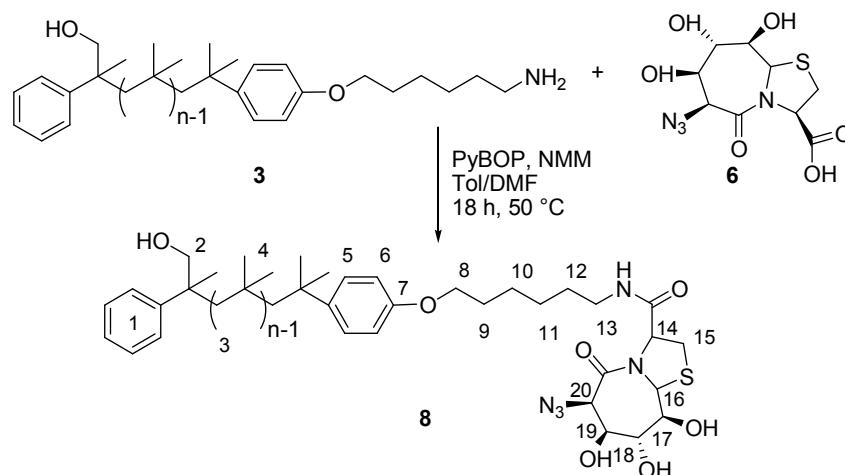
### 7.2.8 (2S,3S,4S,5R,6R)-6-azido-tetrahydro-3,4,5-trihydroxy-2H-pyran-2-carboxylic acid (**7**) – deprotection and hydrolysis of **7c**



The synthesis of **7** was modelled after Tremmel.<sup>114</sup> Therefore, **7c** (200 mg, 0.56 mmol) was dissolved in 10 mL dioxane and a solution of LiOH (2.3 mmol, 97 mg.) in water (1 mL) was added at room temperature under stirring. The reaction was allowed to stir at room temperature for 1 h, controlled by TLC (THF;  $R_f = 0$ ) and stopped by the addition of 1M HCl until the solution was neutral. Then the solvent was evaporated to get the product **7** quantitatively, which was used without further purification.  $^1\text{H-NMR}$  (400 MHz,  $\text{DMSO-d}_6$ ):  $\delta = 4.42$  (*d*, 1H,  $^3J_{\text{H,H}} = 8.6$  Hz, H-1), 3.34 (*d*, 1H,  $^3J_{\text{H,H}} = 9.9$  Hz, H-5), 3.18 (*t*, 1H,  $^3J_{\text{H,H}} = 8.7$  Hz, H-3), 3.08 (*dd*, 1H,  $^3J_{\text{H,H}} = 8.7$  Hz,  $^3J_{\text{H,H}} = 9.9$  Hz, H-4), 2.97 (*t*, 1H,  $^3J_{\text{H,H}} = 8.7$  Hz, H-2).

$^{13}\text{C-NMR}$  (400 MHz,  $\text{DMSO-d}_6$ ):  $\delta = 175.5$  (C-6), 90.1 (C-1), 76.6 (C-2), 75.7 (C-5), 73.2 (C-4), 71.8 (C-3). ESI-TOF MS (MeOH)  $m/z_{\text{exp.}} = 218.0535$   $[\text{M-H}]^-$ ,  $m/z_{\text{calc.}} = 218.0408$   $[\text{M-H}]^-$ .  $[\alpha]_{\text{D}}^{20}$  ( $c = 1$ ) =  $-25.0^\circ$ .

### 7.2.9 Peptide coupling of **3** with **6**

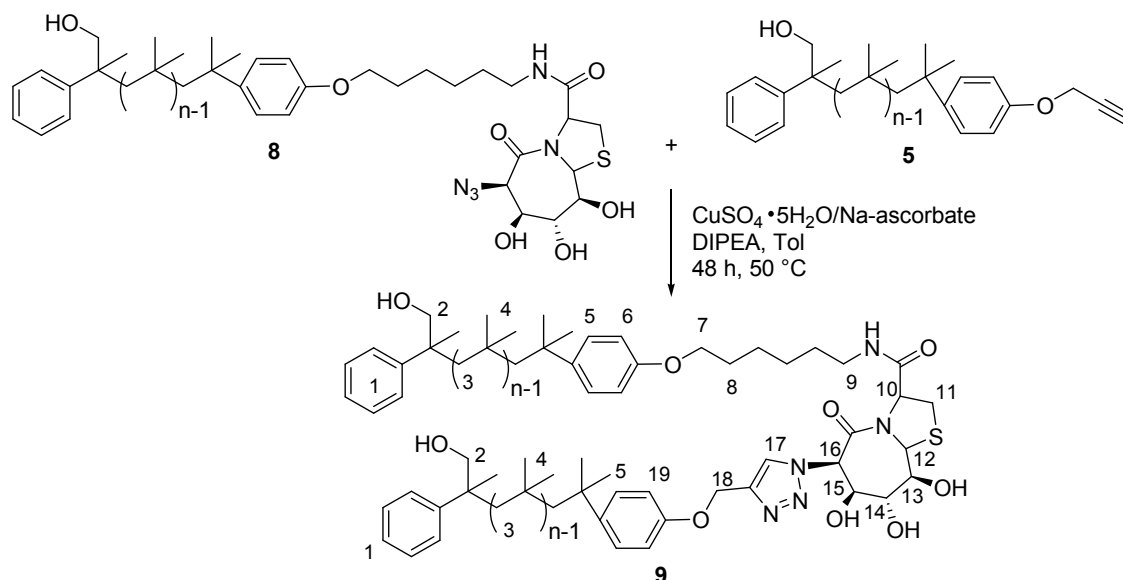


The  $\alpha$ -hydroxymethyl- $\omega$ -amino telechelic PIB **3** (0.093 mmol, 500 mg) was dissolved in 20 mL dry toluene and a solution of **6** (0.28 mmol, 85 mg) in 1.5 mL dry DMF was added dropwise while vigorously stirring. Then PyBOP (0.134 mmol, 70 mg) was added and the pH was adjusted to 7-8 with NMM. The reaction was allowed to stir overnight at 50 °C and stopped after control with TLC ( $\text{CHCl}_3/\text{MeOH} = 50:1$ ,  $R_f = 0.3$ ) and MALDI-TOF MS. The solvent was removed under vacuum and the crude product was purified by column chromatography on silica gel. Therefore,  $\text{CHCl}_3$  was used as eluent to remove non-functionalized PIB followed by  $\text{CHCl}_3/\text{MeOH} = 50:1$  to collect product **8** in a

## 7. Experimental Part

yield of 70 %. SEC:  $M_n = 5300$  g/mol,  $M_w/M_n = 1.20$ .  $^1\text{H-NMR}$  (400 MHz,  $\text{CDCl}_3$ ):  $\delta = 7.34$  (*m*, 5H, H-1), 7.21 (*m*, 2H, H-5), 6.80 (*d*, 2H,  $^3J_{\text{H,H}} = 8.7$  Hz, H-6), 6.69 (*bs*, 1H, *NH*), 5.51 (*s*, 1H, H-16), 5.09 (*m*, 2H, H-14,OH), 4.53 (*s*, 1H, H-20), 4.31 (*m*, 1H, H-19), 4.14 (*s*, 1H, H-18), 3.93 (*t*, 2H,  $^3J_{\text{H,H}} = 6.2$  Hz, H-8), 3.84 (*s*, 2H, H-17,OH), 3.66 (*d*, 1H,  $^2J_{\text{H,H}} = 10.6$  Hz, H-2), 3.40 (*m*, 2H, H-15,2'), 3.27 (*m*, 2H, H-13), 3.18 (*m*, 2H, H-15',OH), 1.97 (*m*, 2H, H-9), 1.9-0.8 (*m*, polymer backbone).  $^{13}\text{C-NMR}$  (400 MHz,  $\text{CDCl}_3$ ):  $\delta = 156.5$  (C-7), 128.3-127.0 (C-1), 125.9 (C1,5), 113.7 (C-6), 75.9 (C-17), 74.5 (C-2, 19), 69.8 (C-18), 67.4 (C-8), 65.3 (C-14), 61.4 (C-20), 59.7-59.0 (C-3), 58.3 (C-16), 38.3-37.6 (C-4), 32.6 (C-13), 32.1 (C-15), 31.6-31.0 (C-4), 30.6 (C-9), 29.1 (C-12), 26.2 (C-11), 25.1 (C-10). MALDI-TOF MS (THF, DCTB/8/LiTFA = 25:5:1)  $m/z_{\text{exp}} = 3425.409$   $[\text{M}_{50}+\text{Li}]^+$ , 3441.383  $[\text{M}_{50}+\text{Na}]^+$ , 3457.357  $[\text{M}_{50}+\text{K}]^+$ ,  $m/z_{\text{calc}} = 3425.483$   $[\text{M}_{50}+\text{Li}]^+$ , 3440.996  $[\text{M}_{50}+\text{Na}]^+$ , 3457.721  $[\text{M}_{50}+\text{K}]^+$ .

### 7.2.10 Azide/alkyne-“click”-reactions of 5 with 8 to achieve 9

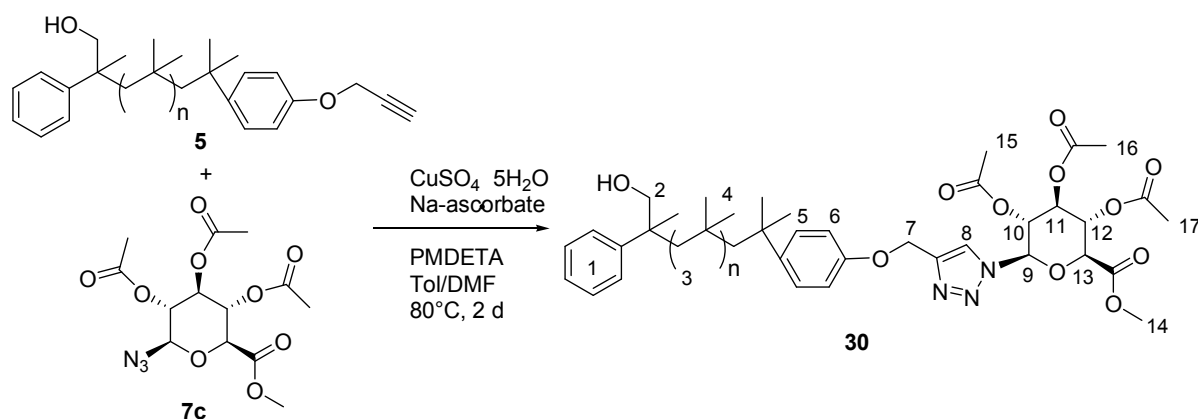


The conjunction of the two PIB strands **5** and **8** was conducted via  $\text{Cu}^{\text{I}}$  mediated azide/alkyne-“click”-reaction<sup>168</sup>. Therefore, **8** (0.013 mmol, 60 mg) and **5** (0.013 mmol, 67 mg) were dissolved in 2 mL absolute toluene. After 30 minutes purging with argon, TBTA (**29**, 0.1 equiv.), *N,N*-diisopropylethylamine (DIPEA, 1 equiv.),  $\text{CuSO}_4 \cdot 5\text{H}_2\text{O}$  (0.2 equiv.) and sodium ascorbate (0.2 equiv.) were added and the solution was purged with argon for another 30 minutes. After stirring for 48 h at 50 °C the solvent was removed and the crude product was purified by column chromatography on silica gel. Therefore, *n*-hexane/EtOAc = 40:1 was used as eluent to remove non-functionalized PIB followed by  $\text{CHCl}_3 \rightarrow \text{CHCl}_3/\text{MeOH} = 50:1$  to collect the product **9** with a yield of 64 %. The final purification to remove traces of **5** and **8** was done via preparative HPLC using HPLC graded, freshly distilled THF.  $^1\text{H-NMR}$  (400 MHz,  $\text{CDCl}_3$ ):  $\delta = 8.16$  (*s*, 1H, H-17), 7.34 (*m*, 10H, H-1), 7.21 (*m*, 4H, H-5), 6.91 (*d*, 2H,  $^3J_{\text{H,H}} = 8.5$  Hz, H-19), 6.78 (*d*, 2H,  $^3J_{\text{H,H}} = 8.7$  Hz, H-6), 6.51 (*bs*, 1H, *NH*), 6.20 (*s*, 1H, H-16), 5.76 (*s*, 1H, H-12), 5.71 (*bs*, 1H, 14-OH), 5.16 (*d*, 2H,  $^2J_{\text{H,H}} = 3.9$  Hz, H-18), 5.01 (*d*, 1H,

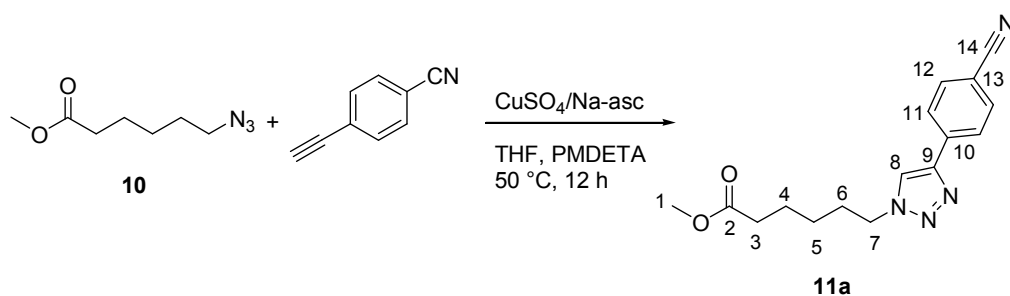
## 7. Experimental Part

$^3J_{\text{H,H}} = 5.1$  Hz, H-10), 4.39 (*m*, 2H, H-15, 13-OH), 4.21 (*m*, 1H, H-14), 3.92 (*m*, 3H, H-7,13), 3.66 (*d*, 2H,  $^2J_{\text{H,H}} = 10.8$  Hz, H-2), 3.64 (*s*, 1H, OH), 3.42 (*d*, 2H,  $^2J_{\text{H,H}} = 9.5$  Hz, H-2'), 3.25 (*m*, 4H, H-9,11), 2.96 (*bs*, 1H, OH), 2-0.8 (*m*, polymer backbone).  $^{13}\text{C-NMR}$  (400 MHz,  $\text{CDCl}_3$ ):  $\delta = 156.6$ , 145.4, 142.5, 128.3, 127.2, 127.0, 126.0, 113.9, 113.6, 74.6, 67.6, 64.7, 59.8-59.4, 59.2, 59.0, 58.3, 52.8, 44.2, 39.9, 38.3-37.9, 37.8, 37.7, 32.5, 32.2, 32.0, 31.6-31.0, 30.8, 30.7, 29.7, 29.4, 29.2, 29.1, 26.6, 25.8, 25.1, 22.7, 22.4, 14.2. MALDI-TOF MS  $m/z_{\text{exp}} = 7057.79$   $[\text{M}_{110}+\text{Li}]^+$ , 7074.67  $[\text{M}_{110}+\text{Na}]^+$ , 7092.75  $[\text{M}_{110}-3\text{H}+3\text{Li}+\text{Na}]^+$ ,  $m/z_{\text{calc}} = 7058.30$   $[\text{M}_{110}+\text{Li}]^+$ , 7074.28  $[\text{M}_{110}+\text{Na}]^+$ , 7092.30  $[\text{M}_{110}-3\text{H}+3\text{Li}+\text{Na}]^+$ .

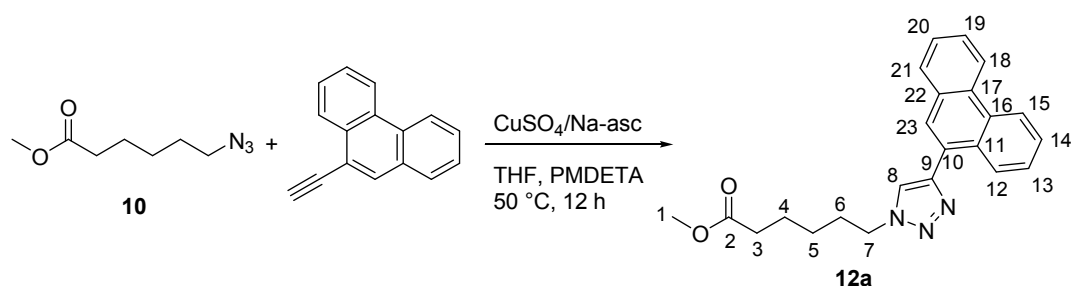
### 7.2.11 Azide/alkyne-“click”-reactions of **5** with **7c** to achieve **30**



The azide/alkyne-“click”-reactions were accomplished following an already known synthetic approach.<sup>168</sup> In a Schlenk flask **5** (1 eq, 0.02 mmol, 92 mg) was dissolved in 6 mL abs toluene and a solution of **7c** (1.5 eq, 0.03 mmol, 11 mg) in 0.1 mL abs DMF as well as TBTA (**29**, 0.1 eq, 0.002 mmol, 1 mg) and PMDETA (1 eq, 0.02 mmol, 4.2  $\mu\text{L}$ ) were added. After degassing with argon for 1 h  $\text{CuSO}_4 \cdot 5\text{H}_2\text{O}$  (0.2 eq, 0.004 mmol, 1 mg) and sodium ascorbate (0.2 eq, 0.004 mmol, 0.8 mg) were added and again the solution was degassed for 1 h with argon. The solution was allowed to stir at  $80^\circ\text{C}$  for 2 d and the reaction was monitored via TLC ( $\text{CHCl}_3$ ,  $R_f = 0.2$ ). For working up the solvent was removed under vacuum and *n*-hexane was added and the polymer isolated by precipitation into MeOH. To remove the copper-catalyst and unreacted PIB a column chromatography over  $\text{SiO}_2$  was conducted (eluent *n*-hexane/EA = 40:1  $\rightarrow$   $\text{CHCl}_3$ ) yielding 74 % of **30** (0.015 mmol, 68 mg).  $^1\text{H-NMR}$  (400 MHz,  $\text{CDCl}_3$ ):  $\delta = 7.90$  (*s*, 1H, H-8), 7.34 (*m*, 5H, H-1), 7.21 (*m*, 2H, H-5), 6.89 (*d*, 2H,  $^3J_{\text{H,H}} = 8.8$  Hz, H-6), 5.93 (*d*, 1H,  $^3J_{\text{H,H}} = 9.1$  Hz, H-9), 5.51-5.45 (*m*, 2H, H-10,12), 5.37 (*t*, 1H,  $^3J_{\text{H,H}} = 9.6$  Hz, H-11), 5.17 (*s*, 2H, H-7), 4.31 (*d*, 1H,  $^3J_{\text{H,H}} = 9.8$  Hz, H-5), 3.75 (*s*, 3H, H-14), 3.66 (*d*, 1H,  $^2J_{\text{H,H}} = 10.7$  Hz, H-2), 3.42 (*d*, 1H,  $^2J_{\text{H,H}} = 9.4$  Hz, H-2'), 2.09-2.01 (3*s*, 9H, H-15-17), 2-0.8 (*m*, polymer backbone). MALDI-TOF MS  $m/z_{\text{exp}} = 2538.704$   $[\text{M}_{34}+\text{Li}]^+$ ,  $m/z_{\text{calc}} = 2539.375$   $[\text{M}_{34}+\text{Li}]^+$ .

7.2.12 Azide/alkyne-“click”-reactions of **10** with 4-ethynylbenzonitrile to achieve **11a**

The azide-alkyne “click”-reaction was accomplished regarding to Bag et al.<sup>209</sup> A two-neck flask equipped with a magnetic stir bar, a gas tap and a septum was heated under vacuum and flushed with nitrogen several times. The azide **10** (1 eq, 1.84 mmol, 315 mg) and 4-ethynylbenzonitrile (1 eq, 1.84 mmol, 234 mg) were dissolved in 15 ml abs THF. The solution was sparged for 30 min with argon. Then PMDETA (0.4 eq, 0.736 mmol, 153.7  $\mu\text{L}$ ),  $\text{CuSO}_4 \cdot 5\text{H}_2\text{O}$  (0.2 eq, 0.37 mmol, 92 mg) and sodium ascorbate (0.2 eq, 0.37 mmol, 73 mg) were added under a stream of argon. Afterwards the reaction mixture was again degassed with argon for 30 min. After stirring overnight at 50  $^\circ\text{C}$  and monitoring via TLC (Hex/EA = 1:1,  $R_f$  = 0.29) the solvent was removed under vacuum. The crude product was purified by column chromatography starting with *n*-hexane/EA = 8:2 and changing the eluent to *n*-hexane/EA = 1:1 to collect the product **11a** (75 %, 1.38 mmol, 412 mg) as pale yellow solid.  $^1\text{H-NMR}$  (400 MHz,  $\text{CDCl}_3$ ):  $\delta$  = 7.95 (*d*, 2H,  $^3J_{\text{H,H}}$  = 8.3 Hz, H-12), 7.87 (*s*, 1H, H-8), 7.70 (*d*, 2H,  $^3J_{\text{H,H}}$  = 8.3 Hz, H-11), 4.43 (*t*, 2H,  $^3J_{\text{H,H}}$  = 7.1 Hz, H-7), 3.65 (*s*, 3H, H-1), 2.32 (*t*, 2H,  $^3J_{\text{H,H}}$  = 7.3 Hz, H-3), 2.04-1.95 (*m*, 2H, H-6), 1.75-1.65 (*m*, 2H, H-4), 1.45-1.35 (*m*, 2H, H-5).  $^{13}\text{C-NMR}$  (400 MHz,  $\text{CDCl}_3$ ):  $\delta$  = 173.7 (C-2), 145.9 (C-9), 135.0 (C-10), 132.7 (C-12), 126.0 (C-11), 120.7 (C-8), 118.8 (C-14), 111.4 (C-13), 51.5 (C-1), 50.2 (C-7), 33.6 (C-3), 29.9 (C-6), 25.8 (C-5), 24.1 (C-4). ESI-TOF MS (MeOH/NaCl)  $m/z_{\text{exp.}}$  = 321.1728  $[\text{M}+\text{Na}]^+$ ,  $m/z_{\text{calc.}}$  = 321.1322  $[\text{M}+\text{Na}]^+$ .

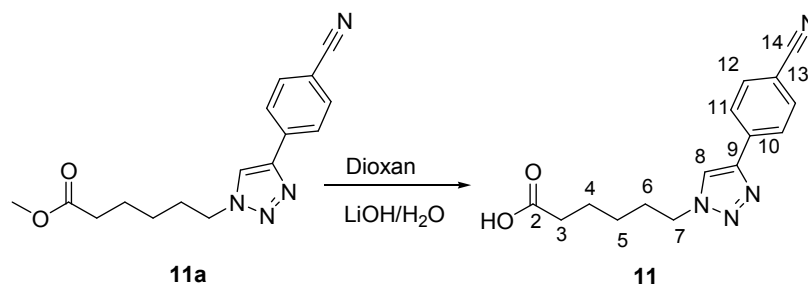
7.2.13 Azide/alkyne-“click”-reactions of **10** with 9-ethynylphenanthrene to achieve **12a**

The azide-alkyne “click”-reaction was accomplished regarding to Bag et al.<sup>209</sup> A microwave tube was equipped with a gas tap and was heated under vacuum and flushed with nitrogen several times, then the gas tap was changed by a septum. The azide **10** (1 eq, 0.60 mmol, 102 mg) and 9-ethynylphenanthrene (1 eq, 0.60 mmol, 120.5 mg) were dissolved in 4 ml abs THF. The solution was sparged for 30 min with argon. Then PMDETA (0.4 eq, 0.24 mmol, 49.8  $\mu\text{L}$ ),  $\text{CuSO}_4 \cdot 5\text{H}_2\text{O}$  (0.2 eq,

## 7. Experimental Part

0.12 mmol, 29.7 mg) and sodium ascorbate (0.2 eq, 0.12 mmol, 23.6 mg) were added. Afterwards the reaction mixture was again degassed with argon for 30 min. After stirring overnight at 50 °C and monitoring via TLC (Hex/EA = 1:1,  $R_f$  = 0.47) the solvent was removed under vacuum. The crude product was purified by column chromatography starting with *n*-hexane/EA = 8:2 and changing the eluent to *n*-hexane/EA = 1:1 to collect the product **12a** (70 %, 0.42 mmol, 155 mg) as pale yellow solid.  $^1\text{H-NMR}$  (400 MHz,  $\text{CDCl}_3$ ):  $\delta$  = 8.78 (*d*, 1H,  $^3J_{\text{H,H}}$  = 8.6 Hz, H-15), 8.71 (*d*, 1H,  $^3J_{\text{H,H}}$  = 8.2 Hz, H-18), 8.40 (*d*, 1H,  $^3J_{\text{H,H}}$  = 8.1 Hz, H-12), 8.01 (*s*, 1H, H-23), 7.92 (*d*, 1H,  $^3J_{\text{H,H}}$  = 7.8 Hz, H-21), 7.85 (*s*, 1H, H-8), 7.72-7.59 (*m*, 4H, H-13,14,19,20), 4.50 (*t*, 2H,  $^3J_{\text{H,H}}$  = 7.2 Hz, H-7), 3.67 (*s*, 3H, H-1), 2.36 (*t*, 2H,  $^3J_{\text{H,H}}$  = 7.3 Hz, H-3), 2.10-2.02 (*m*, 2H, H-6), 1.74 (*td*, 2H,  $^3J_{\text{H,H}}$  = 7.4 Hz,  $^2J_{\text{H,H}}$  = 15.2 Hz, H-4), 1.52-1.43 (*m*, 2H, H-5).  $^{13}\text{C-NMR}$  (400 MHz,  $\text{CDCl}_3$ ):  $\delta$  = 173.8 (C-2), 146.8 (C-9), 131.3 (C-10), 130.7 (C-22), 130.4 (C-17), 130.2 (C-16), 128.9 (C-21), 128.3 (C-12), 127.1 (C-20), 126.9 (C-19), 126.9 (C-13), 126.7 (C-14), 126.2 (C-23), 123.0 (C-15), 122.7 (C-8), 122.6 (C-18), 51.6 (C-1), 50.2 (C-7), 33.7 (C-3), 30.1 (C-6), 26.1 (C-5), 24.2 (C-4). ESI-TOF MS (MeOH/NaCl)  $m/z_{\text{exp.}}$  = 374.2231  $[\text{M}+\text{H}]^+$ , 396.2093  $[\text{M}+\text{Na}]^+$ ,  $m/z_{\text{calc.}}$  = 374.1863  $[\text{M}+\text{H}]^+$ , 396.1682  $[\text{M}+\text{Na}]^+$ .

### 7.2.14 Hydrolysis of 11a to achieve 11



The synthesis of **11** was modelled after Tremmel.<sup>114</sup> Therefore, **11a** (1 eq, 0.53 mmol, 157 mg) was dissolved in 7 mL dioxane and a solution of LiOH (2 eq, 1.05 mmol, 44.16 mg) in water (2 mL) was added at room temperature under stirring. The reaction was allowed to stir overnight, controlled by TLC (*n*-hexane/EA = 1:1,  $R_f$  = 0) and stopped by the addition of 1M HCl until the solution was neutral. Then the solvent was evaporated to get the product **11** quantitatively, which was used without further purification.  $^1\text{H-NMR}$  (400 MHz,  $\text{CDCl}_3$ ):  $\delta$  = 7.95 (*d*, 2H,  $^3J_{\text{H,H}}$  = 8.5 Hz, H-12), 7.86 (*s*, 1H, H-8), 7.70 (*d*, 2H,  $^3J_{\text{H,H}}$  = 8.5 Hz, H-11), 4.45 (*t*, 2H,  $^3J_{\text{H,H}}$  = 7.1 Hz, H-7), 2.38 (*t*, 2H,  $^3J_{\text{H,H}}$  = 7.2 Hz, H-3), 2.04-1.95 (*m*, 2H, H-6), 1.75-1.65 (*m*, 2H, H-4), 1.45-1.35 (*m*, 2H, H-5).  $^{13}\text{C-NMR}$  (400 MHz,  $\text{CDCl}_3$ ):  $\delta$  = 177.9 (C-2), 145.1 (C-9), 135.8 (C-10), 133.4 (C-12), 126.1 (C-11), 123.5 (C-8), 118.8 (C-14), 110.4 (C-13), 50.2 (C-7), 38.5 (C-3), 30.0 (C-6), 26.6 (C-5), 26.0 (C-4). ESI-TOF MS (MeOH)  $m/z_{\text{exp.}}$  = 297.1956  $[\text{M}-\text{H}+2\text{Li}]^+$ ,  $m/z_{\text{calc.}}$  = 297.1510  $[\text{M}-\text{H}+2\text{Li}]^+$ .



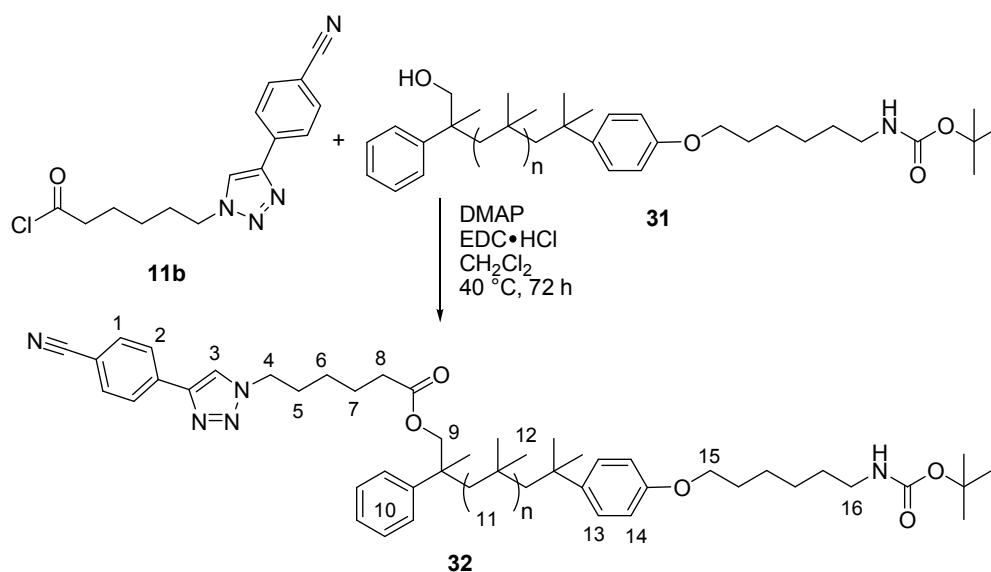


## 7. Experimental Part

and the crude product was purified via column chromatography (*n*-hexane/EA = 40:1) achieving **31** in a yield of 48 % (0.16, 602 mg). SEC:  $M_n = 5000$  g/mol,  $M_w/M_n = 1.3$ .  $^1\text{H-NMR}$  (400 MHz,  $\text{CDCl}_3$ ):  $\delta = 7.34$  (*m*, 5H, H-1), 7.21 (*m*, 2H, H-5), 6.79 (*d*, 2H,  $^3J_{\text{H,H}} = 8.8$  Hz, H-6), 4.49 (*bs*, 1H, NH), 3.92 (*t*, 2H,  $^3J_{\text{H,H}} = 6.5$  Hz, H-8), 3.66 (*dd*, 1H,  $^3J_{\text{H,H}} = 4.4$  Hz  $^2J_{\text{H,H}} = 10.8$  Hz, H-2), 3.43 (*dd*, 1H,  $^3J_{\text{H,H}} = 9.5$  Hz,  $^2J_{\text{H,H}} = 10.4$  Hz, H-2'), 3.12 (*q*\*, 2H,  $^3J_{\text{H,H}} = 6.4$  Hz, H-13), 2-0.8 (*m*, polymer backbone).  $^{13}\text{C-NMR}$  (400 MHz,  $\text{CDCl}_3$ ):  $\delta = 156.5$  (C-7), 128.3-127.0 (C-1), 125.9 (C-1,5), 113.6 (C-6), 74.5 (C-2), 67.7 (C-8), 59.7-59.0 (C-3), 52.8 (C-13), 38.3-37.6 (C-4), 31.6-31.0 (C-4), 30.6 (C-9), 29.1 (C-12), 28.4 (C-14), 26.2 (C-11), 25.1 (C-10). MALDI-TOF MS  $m/z_{\text{exp}} = 2510.916$  [ $\text{M}_{37} + \text{Li}$ ] $^+$ ,  $m/z_{\text{calc}} = 2510.615$  [ $\text{M}_{37} + \text{Li}$ ] $^+$ .

\*In  $\text{CHCl}_3$  NH-protons show broad signals in comparison to protons which are bonded to carbons, therefore determination of coupling is difficult. The only coupling which could be observed is with the methylene group in vicinity. The theoretical coupling should be a doublet of triplets (dt), but the  $^1\text{H-NMR}$  shows a pseudo quartet.

### 7.2.17 Esterification of **11b** with **31** to achieve **32**



The synthesis of **32** was accomplished according to literature.<sup>211, 212</sup> A 100 mL two-neck flask equipped with magnetic stir bar, reflux condenser, gas tap and septum was heated out under vacuum and flushed with nitrogen, this procedure was repeated for three times.

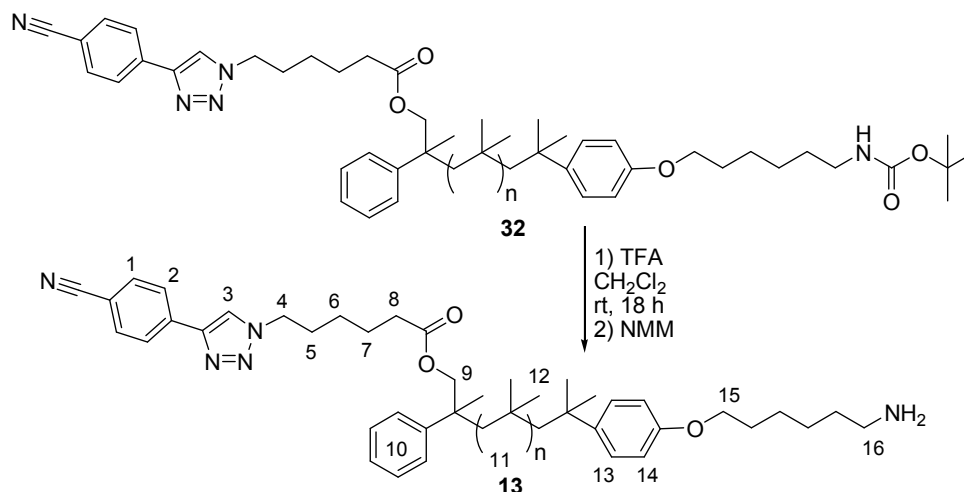
In the first reaction step the acyl chloride **11b** was generated *in situ*. Therefore, the acid **11** (10 eq, 1.03 mmol, 293 mg) was dissolved in 20 ml abs  $\text{CH}_2\text{Cl}_2$  and oxalyl chloride (10 eq, 1.03 mmol, 87.2  $\mu\text{L}$ ) was added via Eppendorf pipette. The suspension was stirred at 45 °C for 5 h. In the second reaction step the reaction mixture was cooled with an ice bath to 0 °C and **31** (1 eq, 0.103 mmol, 528 mg) dissolved in 10 mL abs  $\text{CH}_2\text{Cl}_2$  was added via syringe. Then DMAP (0.6 eq, 0.062 mmol, 7.55 mg) and EDC·HCl (1.6 eq, 0.165 mmol, 31.6 mg) were added to the reaction mixture under a stream of

## 7. Experimental Part

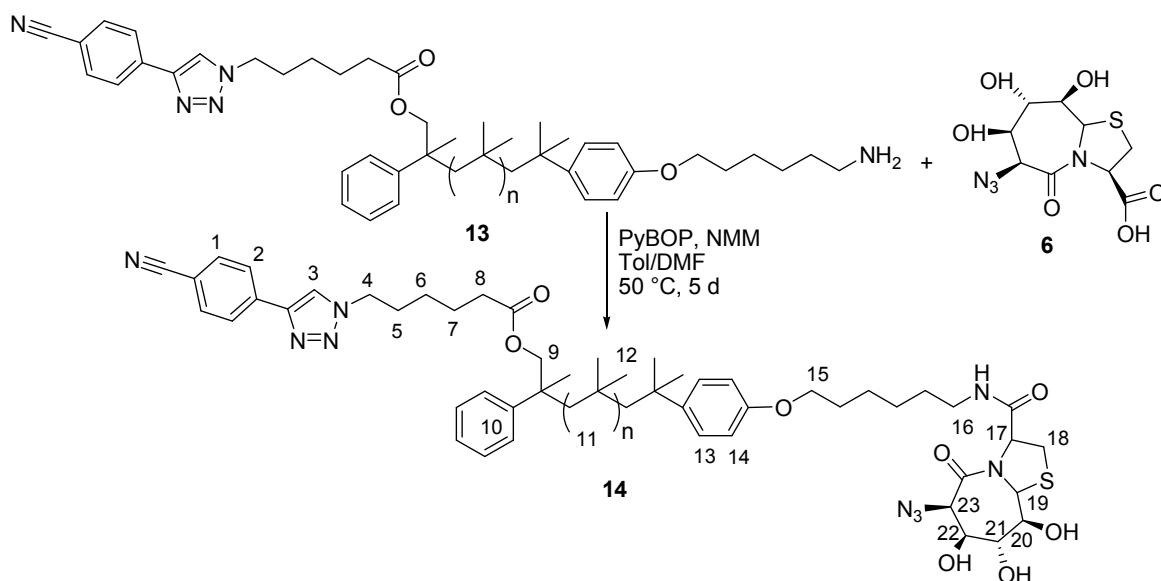
nitrogen. The mixture was allowed to stir for 5 d at 45 °C and was monitored via TLC (CHCl<sub>3</sub>, R<sub>f</sub> = 0.20). For purification dialysis in CHCl<sub>3</sub> was conducted, followed by column chromatography (*n*-hexane/EA = 40:1 → CHCl<sub>3</sub>) and again dialysis in CHCl<sub>3</sub> to achieve **32** in a yield of 67 %\* (354 mg). SEC: M<sub>n</sub> = 5400 g/mol, M<sub>w</sub>/M<sub>n</sub> = 1.21. <sup>1</sup>H-NMR (400 MHz, CDCl<sub>3</sub>): δ = 7.95 (*d*, 2H, <sup>3</sup>J<sub>H,H</sub> = 8.2 Hz, H-1), 7.87 (*s*, 1H, H-3), 7.71 (*d*, 2H, <sup>3</sup>J<sub>H,H</sub> = 8.5 Hz, H-2), 7.34 (*m*, 5H, H-10), 7.21 (*m*, 2H, H-13), 6.79 (*d*, 2H, <sup>3</sup>J<sub>H,H</sub> = 8.8 Hz, H-14), 4.37 (*t*, 2H, <sup>3</sup>J<sub>H,H</sub> = 7.1 Hz, H-4), 4.24 (*d*, 1H, <sup>2</sup>J<sub>H,H</sub> = 10.7 Hz, H-9), 4.01 (*d*, 1H, <sup>2</sup>J<sub>H,H</sub> = 10.8 Hz, H-9'), 3.92 (*t*, 2H, <sup>3</sup>J<sub>H,H</sub> = 6.5 Hz, H-15), 3.12 (*m*, 2H, H-16), 2.23 (*t*, 2H, <sup>3</sup>J<sub>H,H</sub> = 7.2 Hz, H-8), 1.95-1.85 (*m*, 2H, H-5), 2-0.8 (*m*, polymer backbone). MALDI-TOF MS *m/z*<sub>exp</sub> = 3785.945 [M<sub>55</sub>+Li]<sup>+</sup>, 3801.119 [M<sub>55</sub>+Na]<sup>+</sup>, *m/z*<sub>calc</sub> = 3785.854 [M<sub>55</sub>+Li]<sup>+</sup>, 3801.828 [M<sub>55</sub>+Na]<sup>+</sup>.

\* in <sup>1</sup>H-NMR excess **11** is left

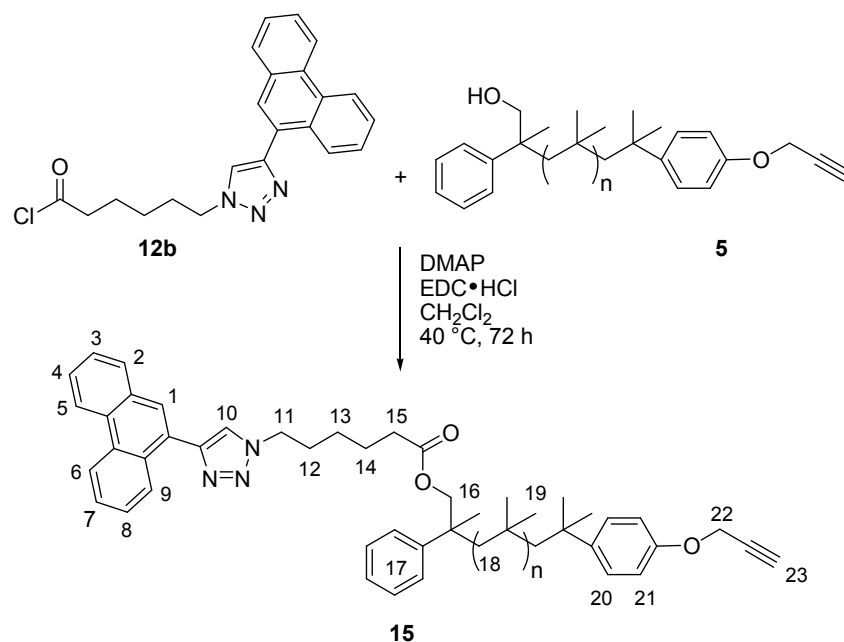
### 7.2.18 Deprotection of **32** to achieve **13**



The deprotection of **32** to achieve **13** was accomplished to Xiao<sup>227</sup>. In a 50 mL one-neck flask **32** (0.062 mmol, 330 mg) was dissolved in 9 mL abs DCM and cooled with an ice bath, then TFA (4.65 mmol, 470 μL) was added. The solution was allowed to stir at room temperature overnight and monitored via TLC (CHCl<sub>3</sub>, R<sub>f</sub> = 0-0.1). The pH-value was adjusted to 7-8 with NMM. After removing of the solvent under vacuum the polymer was dissolved in *n*-hexane and precipitated in MeOH/acetone = 1:1 for three times yielding **13** (65 %, 215.8 mg). SEC: M<sub>n</sub> = 5600 g/mol, M<sub>w</sub>/M<sub>n</sub> = 1.14. <sup>1</sup>H-NMR (400 MHz, CDCl<sub>3</sub>): δ = 7.95 (*d*, 2H, <sup>3</sup>J<sub>H,H</sub> = 8.1 Hz, H-1), 7.83 (*s*, 1H, H-3), 7.71 (*d*, 2H, <sup>3</sup>J<sub>H,H</sub> = 8.1 Hz, H-2), 7.34 (*m*, 5H, H-10), 7.21 (*m*, 2H, H-13), 6.79 (*d*, 2H, <sup>3</sup>J<sub>H,H</sub> = 8.3 Hz, H-14), 4.37 (*t*, 2H, <sup>3</sup>J<sub>H,H</sub> = 7.1 Hz, H-4), 4.24 (*d*, 1H, <sup>2</sup>J<sub>H,H</sub> = 10.7 Hz, H-9), 4.01 (*d*, 1H, <sup>2</sup>J<sub>H,H</sub> = 10.7 Hz, H-9'), 3.93 (*t*, 2H, <sup>3</sup>J<sub>H,H</sub> = 5.9 Hz, H-15), 3.05-2.85 (*m*, 2H, H-16), 2.23 (*t*, 2H, <sup>3</sup>J<sub>H,H</sub> = 7.1 Hz, H-8), 1.95-1.85 (*m*, 2H, H-5), 2-0.8 (*m*, polymer backbone). MALDI-TOF MS *m/z*<sub>exp</sub> = 2445.376 [M<sub>33</sub>+H]<sup>+</sup>, 2451.381 [M<sub>33</sub>+Li]<sup>+</sup>, *m/z*<sub>calc</sub> = 2445.413 [M<sub>33</sub>+H]<sup>+</sup>, 2451.421 [M<sub>33</sub>+Li]<sup>+</sup>.

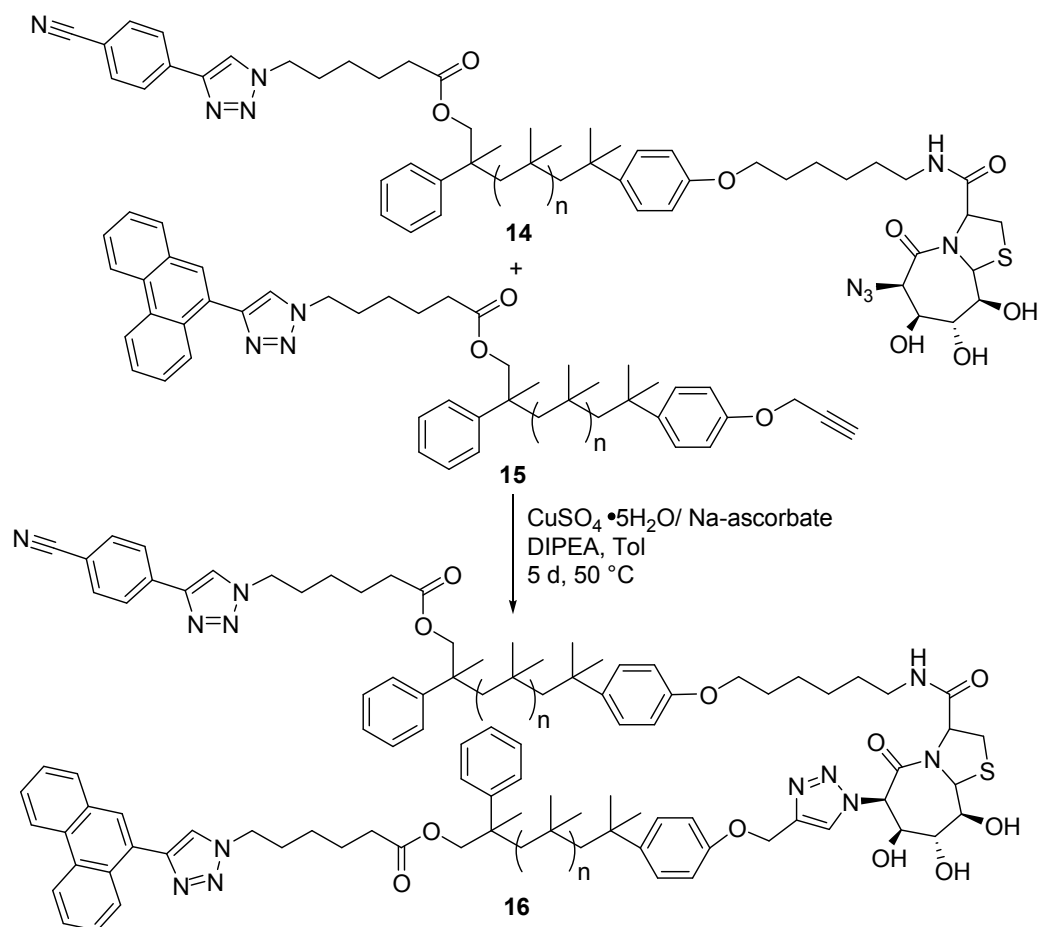
7.2.19 Peptide coupling of **6** with **13** to achieve **14**

In a 50 mL one-neck flask **13** (1 eq, 0.04 mmol, 215.8 mg) was dissolved in 8 mL dry toluene. **6** (3 eq, 0.12 mmol, 36.5 mg) and PyBOP (1.44 eq, 0.06 mmol, 30 mL) were dissolved in 1 mL dry DMF and added under stirring to the solution. Then the pH-value was adjusted to 7 by the use of a view droplets of NMM. The reaction mixture was allowed to stir at 50 °C for 5 d while controlling via TLC ( $\text{CHCl}_3/\text{MeOH} = 50:1$ ,  $R_f = 0.28$ ) and MALDI-ToF MS. Afterwards the solvent was removed under reduced pressure, the polymer was dissolved in *n*-hexane and precipitated into MeOH. For further purification a column chromatography ( $\text{CHCl}_3 \rightarrow \text{CHCl}_3/\text{MeOH} = 50:1$ ) was conducted yielding 30 % polymer (66 mg,  $M_{n,\text{NMR}} = 5200$  g/mol) containing 40 % of **14**.  $^1\text{H-NMR}$  (400 MHz,  $\text{CDCl}_3$ ):  $\delta = 7.95$  (*d*, 2H,  $^3J_{\text{H,H}} = 8.3$  Hz, H-1), 7.83 (*s*, 1H, H-3), 7.71 (*d*, 2H,  $^3J_{\text{H,H}} = 8.3$  Hz, H-2), 7.34 (*m*, 5H, H-10), 7.21 (*m*, 2H, H-13), 6.80 (*d*, 2H,  $^3J_{\text{H,H}} = 8.3$  Hz, H-14), 5.52 (*s*, 1H, H-19), 5.09 (*m*, 1H, H-17), 5.00 (*bs*, 1H, OH), 4.53 (*s*, 1H, H-23), 4.37 (*t*, 2H,  $^3J_{\text{H,H}} = 7.1$  Hz, H-4), 4.31 (*m*, 1H, H-22), 4.24 (*d*, 1H,  $^2J_{\text{H,H}} = 10.7$  Hz, H-9), 4.15 (*m*, 1H, H-21), 4.01 (*d*, 1H,  $^2J_{\text{H,H}} = 10.8$  Hz, H-9'), 3.93 (*t*, 2H,  $^3J_{\text{H,H}} = 6.2$  Hz, H-15), 3.84 (*m*, 1H, H-20), 3.39 (*m*, 1H, H-18), 3.27 (*q*\*, 2H,  $^3J_{\text{H,H}} = 6.2$  Hz, H-16), 3.00 (*s*, 1H, H-18'), 2.23 (*t*, 2H,  $^3J_{\text{H,H}} = 6.8$  Hz, H-8), 1.95-1.85 (*m*, 2H, H-5), 2-0.8 (*m*, polymer backbone). MALDI-TOF MS  $m/z_{\text{exp}} = 3954.428$  [ $M_{54}\text{-H}+2\text{Na}$ ] $^+$ ,  $m/z_{\text{calc}} = 3954.732$  [ $M_{54}\text{-H}+2\text{Na}$ ] $^+$ .

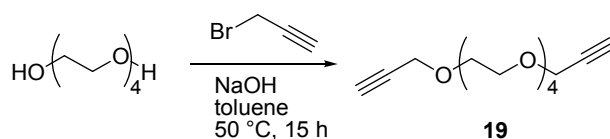
7.2.20 Esterification of **12b** with **5** to achieve **15**

The synthesis of **15** was accomplished according to literature.<sup>211, 212</sup> A 100 mL two-neck flask equipped with magnetic stir bar, reflux condenser, gas tap and septum was heated out under vacuum and flushed with nitrogen, this procedure was repeated for three times.

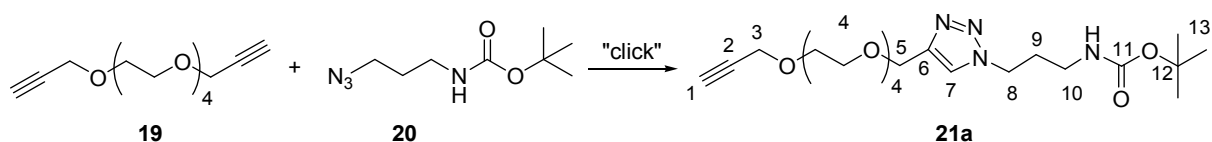
In the first reaction step the acyl chloride **12b** was generated *in situ*. Therefore, the acid **12** (10 eq, 1.064 mmol, 382.4 mg) was dissolved in 20 ml abs CH<sub>2</sub>Cl<sub>2</sub> and oxalyl chloride (10 eq, 1.064 mmol, 90.0 μL) was added via Eppendorf pipette. The suspension was stirred at 45 °C for 5 h. In the second reaction step the reaction mixture was cooled with an ice bath to 0 °C and **5** (1 eq, 0.106 mmol, 500 mg) dissolved in 10 mL abs CH<sub>2</sub>Cl<sub>2</sub> was added via syringe. Then DMAP (0.6 eq, 0.064 mmol, 7.8 mg) and EDC·HCl (1.6 eq, 0.17 mmol, 32.6 mg) were added to the reaction mixture under a stream of nitrogen. The mixture was allowed to stir for 5 d at 45 °C and was monitored via TLC (CHCl<sub>3</sub>, R<sub>f</sub> = 0.19). For purification the crude product was dissolved in *n*-hexane and washed with saturated NH<sub>4</sub>Cl solution (three times, 50 mL each). Then, the organic phase was concentrated in vacuum and precipitated into MeOH. For further purification column chromatography (*n*-hexane/EA = 40:1 → CHCl<sub>3</sub>) was conducted to achieve **15** in a yield of 19 % (96 mg, M<sub>n,NMR</sub> = 5400 g/mol). SEC: M<sub>n</sub> = 5200 g/mol, M<sub>w</sub>/M<sub>n</sub> = 1.22. <sup>1</sup>H-NMR (400 MHz, DMSO<sub>d6</sub>): δ = 8.78 (*d*, 1H, <sup>3</sup>J<sub>H,H</sub> = 8.2 Hz, H-6), 8.72 (*d*, 1H, <sup>3</sup>J<sub>H,H</sub> = 8.1 Hz, H-5), 8.40 (*d*, 1H, <sup>3</sup>J<sub>H,H</sub> = 8.1 Hz, H-9), 8.01 (*s*, 1H, H-1), 7.92 (*d*, 1H, <sup>3</sup>J<sub>H,H</sub> = 7.9 Hz, H-2), 7.83 (*s*, 1H, H-10), 7.74-7.60 (*m*, 4H, H-7,8,3,4), 7.34 (*m*, 5H, H-17), 7.21 (*m*, 2H, H-20), 6.88 (*d*, 2H, <sup>3</sup>J<sub>H,H</sub> = 8.8 Hz, H-21), 4.66 (*d*, 2H, <sup>4</sup>J<sub>H,H</sub> = 2.4 Hz, H-22), 4.45 (*t*, 2H, <sup>3</sup>J<sub>H,H</sub> = 7.2 Hz, H-11), 4.26 (*d*, 1H, <sup>2</sup>J<sub>H,H</sub> = 10.7 Hz, H-16), 4.02 (*d*, 1H, <sup>2</sup>J<sub>H,H</sub> = 10.7 Hz, H-16'), 2.50 (*t*, 2H, <sup>4</sup>J<sub>H,H</sub> = 2.4 Hz, H-23), 2.27 (*t*, 2H, <sup>3</sup>J<sub>H,H</sub> = 7.2 Hz, H-15), 2-0.8 (*m*, polymer backbone). MALDI-TOF MS *m/z*<sub>exp</sub> = 3217.636 [M<sub>46</sub>-H+Li+Na]<sup>+</sup>, 3251.433 [M<sub>47</sub>+Li]<sup>+</sup>, *m/z*<sub>calc</sub> = 3217.167 [M<sub>46</sub>-H+Li+Na]<sup>+</sup>, 3251.248 [M<sub>47</sub>+Li]<sup>+</sup>.

7.2.21 Azide/alkyne-“click”-reaction of **14** with **15** to achieve **16**

The conjunction of the two PIB strands **14** and **15** was conducted via  $\text{Cu}^{\text{I}}$  mediated azide/alkyne-“click”-reaction<sup>168</sup>. Therefore, **14** [1 eq, 0.005 mmol, 26.4 mg (66 mg PIB containing 40 % **14**)] and **15** (1.2 eq, 0.006 mmol, 33 mg) were dissolved in 4 mL absolute toluene. After three times freeze-pump-thaw-cycles, TBTA (**29**, 0.1 eq, 0.0012 mmol, 1 mg), DIPEA (1 eq, 0.012 mmol, 2  $\mu\text{L}$ ), ( $\text{CuSO}_4 \cdot 5\text{H}_2\text{O}$  (0.2 eq, 0.0024 mmol, 1 mg) and sodium ascorbate (0.2 eq, 0.0024 mmol, 1 mg) were added and again freeze-pump-thaw-cycles were conducted for three times. After stirring for 5 d at  $50^\circ\text{C}$  the solvent was removed and the crude product was purified by column chromatography on silica gel. Therefore, *n*-hexane/EtOAc = 40:1 was used as eluent to remove non-functionalized PIB followed by  $\text{CHCl}_3 \rightarrow \text{CHCl}_3/\text{MeOH} = 50:1$  to collect assumed product **16** ( $\text{CHCl}_3/\text{MeOH} = 50:1$ ,  $R_f = 0.29$ ) with a yield of 10 %. The final purification to remove traces of **14** and **15** was done via preparative HPLC using HPLC graded, freshly distilled THF. SEC:  $M_n = 7000$  g/mol,  $M_w/M_n = 1.43$ . MALDI-TOF MS  $m/z_{\text{exp}} = 6880.140, 6895.757$  a)  $m/z_{\text{calc}} = 6880.699$  [ $M_{93} + \text{Li}$ ]<sup>+</sup>, 6896.672 [ $M_{93} + \text{Na}$ ]<sup>+</sup>, b)  $m/z_{\text{calc}} = 6880.087$  [**14**- $\text{N}_2 + 2\text{H} + \text{Na}$ ]<sup>+</sup>, 6896.061 [**14**- $\text{N}_2 + 2\text{H} + \text{K}$ ]<sup>+</sup>.

7.2.22 Synthesis of  $\alpha,\omega$ -dialkynyl tetraethylene glycol (**19**)

A representative procedure for  $\alpha,\omega$ -dialkynyl tetraethylene glycol (**19**) was achieved by a combined synthesis of Dimonie et al.<sup>214</sup> and Mahouche et al.<sup>215</sup>. In a 50 mL one-neck flask tetraethylene glycol (10.3 mmol, 2 g) was dissolved in 10 mL toluene and powdered NaOH (103 mmol, 10 eq, 4.12 g), as well as propargylbromide (103 mmol, 80 wt%, 10 eq, 13.85 mL) were added. The reaction mixture was stirred for 15 h at 50 °C and was controlled via TLC (EA/*n*-Hex = 3:1,  $R_f$  = 0.5). Then 50 mL brine/water = 3:1 were added and the organic phase was extracted with 50 mL brine/water = 1:1, 50 mL brine and 50 mL H<sub>2</sub>O. The aqueous phase was extracted with 30 mL EA five times and the combined organic phases were dried over NaSO<sub>4</sub>, filtered and the solvent was removed under vacuum. The product **19** was separated by column chromatography (EA/Hex = 3:1,  $R_f$  = 0.5) yielding 2.8 g (97 %) of yellow oil. <sup>1</sup>H-NMR (400 MHz, CDCl<sub>3</sub>):  $\delta$  = 4.18 (*d*, 4H, <sup>3</sup> $J_{H,H}$  = 2.4 Hz, H-3), 3.69-3.63 (*m*, 16H, H-4-7), 2.41 (*t*, 1H, <sup>3</sup> $J_{H,H}$  = 2.4 Hz, H-1). <sup>13</sup>C-NMR (400 MHz, CDCl<sub>3</sub>):  $\delta$  = 79.6 (C-2), 74.5 (C-1), 70.5-70.3 (C-4-6), 69.0 (C-7), 58.3 (C-3).

7.2.23 Azide/alkyne-“click”-reactions of **19** with **20** to achieve **21a**

The azide/alkyne-“click”-reactions were accomplished following an already known synthetic approach.<sup>217</sup> For experimental details see Table EP1. Into a Schlenk flask solvent, **19** (2 eq), **20** (1 eq) as well as a base were added. The reaction mixture was purged for 30 min with argon or three freeze-pump-thaw-cycles were performed. The copper(I)-catalyst (0.1 eq-0.2 eq) was added and the solution was stirred at room temperature. The reaction was monitored via TLC [EA,  $R_f$  = 0.1 (**7**)] and ATR-IR. For working up the solvent was removed under vacuum and EA was added and the crude product was purified via column chromatography. Therefore, EA was used as eluent and after removing of excess **19** changed to MeOH yielding the “click” product **21a**. <sup>1</sup>H-NMR (400 MHz, DMSO-*d*<sub>6</sub>):  $\delta$  = 8.08 (*d*, 1H, <sup>3</sup> $J_{H,H}$  = 1.6 Hz, H-7), 6.92 (*t*, 1H, <sup>3</sup> $J_{H,H}$  = 4.6 Hz, NH), 4.51 (*d*, 2H, <sup>3</sup> $J_{H,H}$  = 2.9 Hz, H-5), 4.33 (*t*, 2H, <sup>3</sup> $J_{H,H}$  = 6.9 Hz, H-8), 4.13 (*d*, 1H, <sup>3</sup> $J_{H,H}$  = 2.4 Hz, H-3), 3.58-3.47 (*m*, 16H, H-4), 3.40 (*t*, 1H, <sup>3</sup> $J_{H,H}$  = 2.4 Hz, H-1), 2.92 (*q*, 2H, <sup>3</sup> $J_{H,H}$  = 6.3 Hz, H-10), 1.91 (*p*, 2H, <sup>3</sup> $J_{H,H}$  = 6.8 Hz, H-9), 1.38 (*s*, 9H, H-13). <sup>13</sup>C-NMR (400 MHz, DMSO-*d*<sub>6</sub>):  $\delta$  = 155.6 (C-11), 143.8 (C-6), 123.9 (C-7), 80.3 (C-2), 77.6 (C-12), 77.0 (C-1), 69.7-68.5 (C-4), 63.5 (C-5), 57.4 (C-3), 47.1 (C-8), 37.1 (C-10), 30.2 (C-9), 28.2 (C-13).

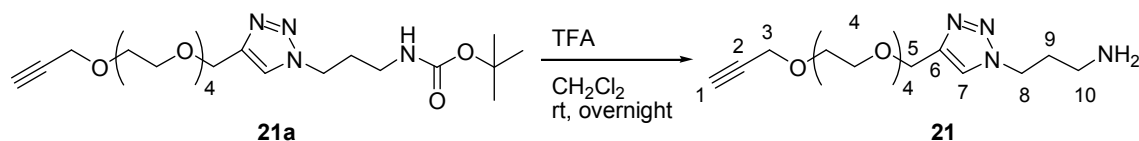
## 7. Experimental Part

**Table EP1.** Experimental conditions for azide/alkyne-“click”-reactions of **19** with **20**.

entry	amount of <b>19</b>	amount of <b>20</b>	amount of Cu <sup>I</sup>	amount of additive	yield of <b>21a</b> <sup>a</sup>
<b>1</b> <sup>b</sup>	2 eq 2 mmol, 540.64 mg	1 eq, 1 mmol, 200 mg	CuI·P(OEt) <sub>3</sub> 0.2 mmol, 71.32 mg	PMDETA 0.2 mmol, 34.66 mg	90 % <sup>c</sup>
<b>2</b> <sup>d</sup>	2 eq 1.35mmol, 385 mg	1 eq, 0.67 mmol, 135 mg	Cu-powder, 0.2 eq 0.13 mmol, 8.6 mg CuSO <sub>4</sub> ·5H <sub>2</sub> O, 0.2 eq 0.13 mmol, 33.71 mg	–	96 % <sup>c</sup>
<b>3</b> <sup>f</sup>	2 eq 5.44 mmol, 1.46 g	1 eq, 2.72 mmol, 544 mg	Cu-powder, 0.1 eq, 0.27 mmol, 17 mg CuSO <sub>4</sub> ·5H <sub>2</sub> O, 0.1 eq 0.27 mmol, 67.4 mg	–	88 % <sup>g</sup>

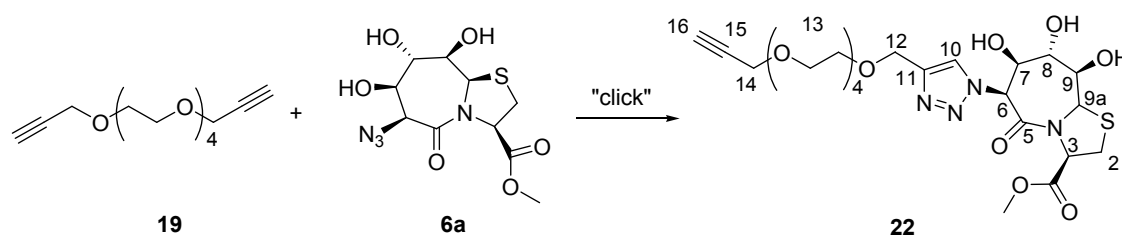
a) isolated yield of “click” product **21a**; b) 5 mL abs THF, three times freeze-thaw cycle, overnight at room temperature; c) fully “clicked”, but just 20 % of alkyne group; d) 5 mL THF/H<sub>2</sub>O = 1:1, 30 min degassed with argon, overnight at room temperature; e) fully “clicked”, but just 40 % of alkyne group; f) 25 mL THF/H<sub>2</sub>O = 4:1, 30 min degassed with argon, 2h at room temperature; g) fully “clicked”, but just 70 % of alkyne group.

### 7.2.24 Deprotection of **21a** to achieve **21**



The deprotection of **21a** to achieve **21** was accomplished to Xiao<sup>227</sup>. In a 25 mL one-neck flask **21a** (0.38 mmol, 179 mg) was dissolved in 5 mL DCM and cooled with an ice bath, then TFA (3.8 mmol, 283.2  $\mu$ L) was added. The solution was allowed to stir at room temperature overnight. NaHCO<sub>3</sub>-solution (10 wt%) was added and the aqueous phase extracted with DCM. After removing of the solvent no product was found in the organic phase, therefore the aqueous phase was dried achieving a yellow-orange, glassy solid in quantitative yield which was analyzed via NMR spectroscopy proving the deprotection of **21a**. <sup>1</sup>H-NMR (400 MHz, DMSO<sub>d6</sub>):  $\delta$  = 8.10 (*s*, 1H, H-7), 4.52 (*s*, 2H, H-5), 4.45 (*t*, 2H, <sup>3</sup>*J*<sub>H,H</sub> = 6.9 Hz, H-8), 4.13 (*d*, 1H, <sup>3</sup>*J*<sub>H,H</sub> = 2.4 Hz, H-3), 3.58-3.48 (*m*, 16H, H-4), 3.41 (*t*, 1H, <sup>3</sup>*J*<sub>H,H</sub> = 2.4 Hz, H-1), 2.92 (*m*, 2H, H-10), 2.08 (*p*, 2H, <sup>3</sup>*J*<sub>H,H</sub> = 6.9 Hz, H-9). <sup>13</sup>C-NMR (400 MHz, DMSO<sub>d6</sub>):  $\delta$  = 143.9 (C-6), 123.9 (C-7), 80.8 (C-2), 77.0 (C-1), 69.7-68.4 (C-4), 63.4 (C-5), 57.9 (C-3), 46.5 (C-8), 36.4 (C-10), 30.7 (C-9). ESI-TOF MS (MeOH) *m/z*<sub>exp.</sub> = 393.2018 [M+Na]<sup>+</sup>, *m/z*<sub>calc.</sub> = 393.2108 [M+Na]<sup>+</sup>.



7.2.25 Azide/alkyne-“click”-reactions of **19** with **6a** to achieve **22**

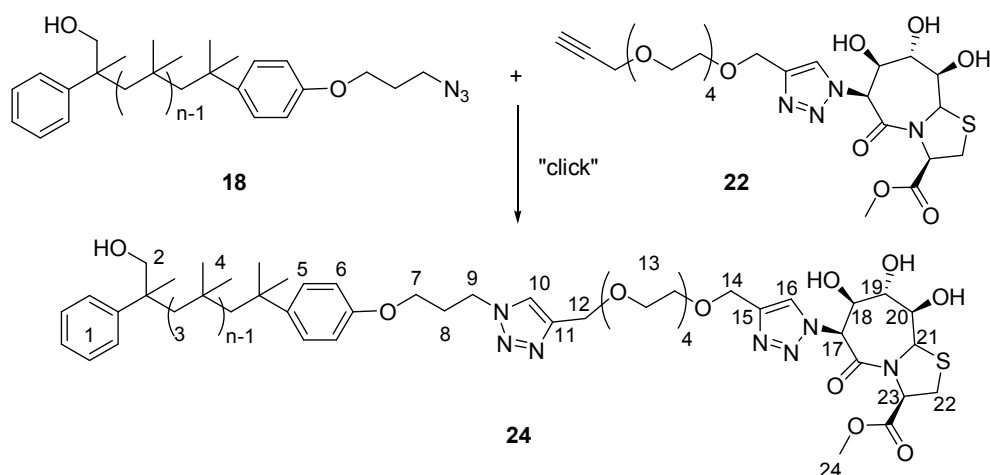
The azide/alkyne-“click”-reactions were accomplished following an already known synthetic approach<sup>218-220</sup>. For experimental details see Table EP2. In a Schlenk tube azide-functionalized BTB (**6a**, 1 eq) was dissolved in THF or DMF and  $\alpha,\omega$ -dialkynyl tetraethylene glycol [**19**, 1 eq (entries 1-12) or 3eq (entry 13)] as well as a base were added. The reaction mixture was purged for 30 min with nitrogen or three freeze-pump-thaw-cycles were performed. The copper(I)-catalyst (0.1 eq) was added and the solution was stirred at certain reaction conditions. For working up the solvent was removed under vacuum and  $\text{CHCl}_3$  was added. The organic phase was washed one time with saturated  $\text{NH}_4\text{Cl}$ -solution, three times with distilled water, and dried over  $\text{Na}_2\text{SO}_4$  and filtered. Chloroform was removed in vacuum and the product was analyzed via NMR-spectroscopy (entries 1-10, Table EP2). For entries 11 and 12 of Table XX the crude product was purified via column chromatography ( $\text{SiO}_2$ , TLC: EA/MeOH = 5:1,  $R_f$  (**22**) = 0.22-0, eluent: EA  $\rightarrow$  EA/MeOH = 9:1  $\rightarrow$  MeOH), whereby the unreacted starting material and byproducts were eluted first, before changing the solvent to a more polar mixture to elute the desired product **22**. Finally, the product was dried in vacuum to yield **22** as a clear, slightly orange solid.  $^1\text{H-NMR}$  (400 MHz,  $\text{DMSO-d}_6$ ):  $\delta$  = 8.01 (*s*, 1H, H-10), 6.31 (*s*, 1H, H-6), 5.90-5.85 (*m*, 2H, OH-7, OH-8), 5.81 (*s*, 1H, H-9a), 4.76 (*t*, 1H,  $^3J_{\text{H,H}}$  = 7.5 Hz, H-3), 4.67 (*d*, 1H,  $^3J_{\text{OH,H}}$  = 10.2 Hz, OH-9), 4.56 (*s*, 2H, H-12), 4.14 (*d*, 2H,  $^3J_{\text{H,H}}$  = 2.4 Hz, H-14), 3.96 (*m*, 2H, H-7, H-8), 3.66 (*m*, 3H,  $\text{OCH}_3$ ), 3.60-3.49 (*m*, 17H, H-9, H-13), 3.40 (*t*, 1H,  $^3J_{\text{H,H}}$  = 2.3 Hz, H-16), 3.30 (*m*, 2H, H-2).  $^{13}\text{C-NMR}$  (400 MHz,  $\text{DMSO-d}_6$ ):  $\delta$  = 170.3 ( $\text{CO}_2\text{CH}_3$ ), 165.0 (C-5), 143.6 (C-11), 124.2 (C-10), 76.6 (C-15), 76.4 (C-9), 74.7 (C-7), 72.3 (C-16), 70.7 (C-8), 69.8-68.8 (C-13), 64.1 (C-3), 63.5 (C-12), 62.4 (C-6), 61.3 (C-9a), 59.7 (C-14), 52.3 ( $\text{OCH}_3$ ), 31.5 (C-2). ESI-TOF MS (MeOH/NaCl)  $m/z_{\text{exp.}}$  = 611.2170 [ $\text{M}+\text{Na}$ ] $^+$ ,  $m/z_{\text{calc.}}$  = 611.1999 [ $\text{M}+\text{Na}$ ] $^+$ .

## 7. Experimental Part

**Table EP2.** Experimental conditions for azide/alkyne-“click”-reactions of **6a** with **19**.

entry	amount of <b>6a</b>	amount of <b>19</b>	amount of Cu <sup>I</sup>	amount of base	yield of <b>22</b>
<b>1<sup>a</sup></b>	0.063 mmol	0.063 mmol	CuI	TBTA ( <b>29</b> )	–
	17.2 mg	20.0 mg	0.0063 mmol 1.2 mg	0.0063 mmol 3.6 mg	
<b>2<sup>b</sup></b>	0.067 mmol	0.067 mmol	CuSO <sub>4</sub> ·5H <sub>2</sub> O/Na-asc	TBTA ( <b>29</b> )	–
	18.2 mg	21.2 mg	0.0067 mmol 1.6 mg/1.3 mg	0.0067 mmol 3.7 mg	
<b>3<sup>c</sup></b>	0.070 mmol	0.070 mmol	CuBr(PPh <sub>3</sub> ) <sub>3</sub>	TBTA ( <b>29</b> )	–
	18.8 mg	21.9 mg	0.0070 mmol 6.5 mg	0.0070 mmol 3.9 mg	
<b>4<sup>d</sup></b>	0.036 mmol	0.036 mmol	CuI·P(OEt) <sub>3</sub>	DIPEA	–
	9.8 mg	11.4 mg	0.0036 mmol 1.3 mg	0.072 mmol 9.3 mg	
<b>5<sup>e</sup></b>	0.072 mmol	0.072 mmol	CuBr(PPh <sub>3</sub> ) <sub>3</sub>	PMDETA	40 % <sup>f</sup>
	19.4 mg	22.6 mg	0.0072 mmol 3.7 mg	0.022 mmol 3.7 mg	
<b>6<sup>e</sup></b>	0.072 mmol	0.072 mmol	CuI	PMDETA	54 % <sup>f</sup>
	19.5 mg	22.7 mg	0.0072 mmol 1.4 mg	0.022 mmol 3.7 mg	
<b>7<sup>e</sup></b>	0.076 mmol	0.076 mmol	CuI·P(OEt) <sub>3</sub>	PMDETA	53 % <sup>f</sup>
	20.6 mg	24.1 mg	0.0076 mmol 2.7 mg	0.023 mmol 4.0 mg	
<b>8<sup>e</sup></b>	0.057 mmol	0.057 mmol	Cu(MeCN) <sub>4</sub> PF <sub>6</sub>	PMDETA	47 % <sup>f</sup>
	15.4 mg	18.0 mg	0.0057 mmol 2.1 mg	0.017 mmol 3.0 mg	
<b>9<sup>g</sup></b>	0.095 mmol	0.095 mmol	CuBr	PMDETA	54 % <sup>f</sup>
	25.8 mg	30 mg	0.0095 mmol 1.4 mg	0.029 mmol 4.9 mg	
<b>10<sup>h</sup></b>	0.093 mmol	0.093 mmol	CuBr	PMDETA	42 % <sup>f</sup>
	25.1 mg	29.3 mg	0.0093 mmol 1.3 mg	0.028 mmol 4.8 mg	
<b>11<sup>i</sup></b>	0.31 mmol	0.31 mmol	CuBr	PMDETA	27 % <sup>k</sup>
	83.7 mg	97.7 mg	0.031 mmol 4.5 mg	0.093 mmol 16.1 mg	
<b>12<sup>l</sup></b>	0.634 mmol	0.634 mmol	CuBr	DIPEA	38 % <sup>k</sup>
	171.5 mg	200 mg	0.0634 mmol 9.1 mg	0.190 mmol 24.6 mg	
<b>13</b>	3 eq	1 eq	CuBr	DIPEA 0.3 eq, 57 mg	41 % <sup>k</sup>
	4.41 mmol	1.47 mmol	0.441 mmol	TBTA 0.3 eq, 247 mg	
	1.2 g	462.5 mg	63.3 mg		

a) 1 mL abs THF, degassed with N<sub>2</sub>, 24 h at room temperature, then overnight at 50 °C, then microwave for 30 min + 6 h (50 W, 50 °C); b) 1 mL abs THF, degassed with N<sub>2</sub>, microwave for 5 h + 15 h (50 W, 50 °C); c) 1 mL abs THF, degassed with N<sub>2</sub>, microwave for 20 h (50 W, 50 °C); d) 1.5 mL abs DMF, degassed with N<sub>2</sub>, overnight at 70 °C, then 1 h at 80 °C, then 3 h at 100 °C; e) 1 mL abs DMF, degassed with N<sub>2</sub>, overnight at 80 °C; f) percentage of “click”-product **22** calculated via <sup>1</sup>H-NMR of crude products; g) 1 mL abs DMF, freeze-thaw cycle (3 times), 48 h at 50 °C; h) 1 mL abs DMF, freeze-thaw cycle (3 times), 48 h at room temperature; i) 3 mL abs DMF, freeze-thaw cycle (3 times), 48 h at 50 °C; k) isolated yield of “click”-product **10**; l) 5 mL abs THF, degassed with N<sub>2</sub>, 18 h at 50 °C; m) 12 mL DMF, degassed with N<sub>2</sub>, 7d at 80 °C.

7.2.26 Azide/alkyne-“click”-reactions of **18** with **22** to achieve **24**

The azide/alkyne-“click”-reactions were accomplished following an already known synthetic approach<sup>218-220</sup>. For experimental details see Table EP3. In a Schlenk tube azide-functionalized PIB (**18**,  $M_n = 3400$  g/mol, 1 eq) was dissolved and **22** (1 eq) as well as the bases were added. The reaction mixture was purged for 30 min with argon and the copper(I)-catalyst [0.1 eq (entries 1-3) or 0.3 eq (entries 4-6)] was added and the solution was stirred at certain reaction conditions. For working up the solvent was removed under vacuum and  $\text{CHCl}_3$  was added. The organic phase was washed three times with saturated  $\text{NH}_4\text{Cl}$ -solution, three times with distilled water, and dried over  $\text{Na}_2\text{SO}_4$  and filtered. Chloroform was removed in vacuum and the product was analyzed via NMR-spectroscopy. For entry 3 of Table EP3 the crude product was purified via column chromatography ( $\text{SiO}_2$ , TLC:  $\text{CHCl}_3/\text{MeOH} = 50:1$ ,  $R_f$  (**24**) = 0.27, eluent:  $\text{CHCl}_3 \rightarrow \text{CHCl}_3/\text{MeOH} = 70:1$ ), whereby the unreacted azide-functionalized PIB **18** was eluted first, before changing the solvent to a more polar mixture to elute the desired product **24**. Finally, the polymer was dried in vacuum to yield **24** as a viscous, slightly yellow substance.  $^1\text{H-NMR}$  (400 MHz,  $\text{CDCl}_3$ ):  $\delta = 8.09$  (*s*, 1H, H-16), 7.59 (*s*, 1H, H-10), 7.40-7.27 (*m*, 5H, H-1), 7.25-7.18 (*m*, 2H, H-5), 6.79 (*d*, 2H,  $^3J_{\text{H,H}} = 8.8$  Hz, H-6), 6.27 (*s*, 1H, H-17), 5.72 (*s*, 1H, H-21), 5.50 (*s*, 1H, OH), 5.36 (*s*, 1H, OH), 5.05 (*s*, 1H, OH), 4.96 (*t*, 1H,  $^3J_{\text{H,H}} = 6.6$  Hz, H-23), 4.68 (*s*, 2H, H-12), 4.55 (*m*, 2H, H-9), 4.46 (*d*, 2H,  $^3J_{\text{H,H}} = 9.8$  Hz, H-14), 4.36 (*s*, 1H, H-18), 4.22 (*s*, 1H, H-19), 4.00-3.92 (*m*, 3H, H-7,20), 3.77 (*s*, 3H, H-24), 3.70-3.55 (*m*, 17H, H-2,13), 3.45 (*m*, 2H, H-22), 3.24 (*dd*, 1H,  $^3J_{\text{H,OH}} = 7.1$  Hz,  $^2J_{\text{H,H}} = 11.5$  Hz, H-2'), 2.36 (*m*, 2H, H-8), 2.00-0.70 (PIB backbone). MALDI-TOF MS  $m/z_{\text{exp}} = 2381.641$  [ $\text{M}_{26} + \text{Na}$ ]<sup>+</sup>, 2397.085 [ $\text{M}_{26} + \text{K}$ ]<sup>+</sup>, 2414.590 [ $\text{M}_{27} + \text{H}$ ]<sup>+</sup>,  $m/z_{\text{calc}} = 2380.994$  [ $\text{M}_{26} + \text{Na}$ ]<sup>+</sup>, 2396.968 [ $\text{M}_{26} + \text{K}$ ]<sup>+</sup>, 2415.074 [ $\text{M}_{27} + \text{H}$ ]<sup>+</sup>.

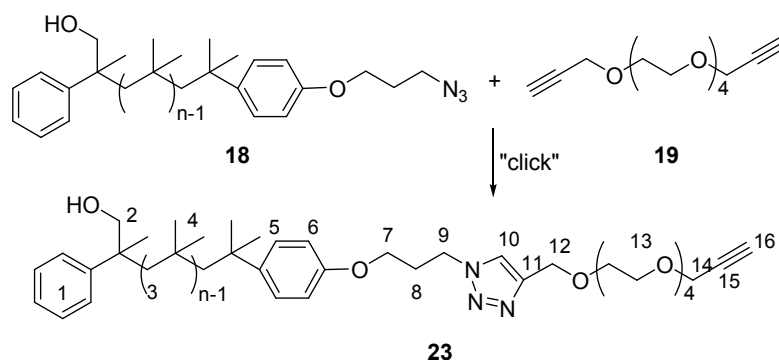
## 7. Experimental Part

**Table EP3.** Experimental conditions for azide/alkyne-“click”-reactions of **18** with **22**.

entry	amount of <b>18</b>	amount of <b>22</b>	amount of Cu <sup>I</sup>	amount of base	yield of <b>24</b>
<b>1<sup>a</sup></b>	0.033 mmol 112 mg	0.033 mmol 19.3 mg	CuBr 0.003 mmol 0.5 mg	DIPEA 0.01 mmol 1.3 mg	– <sup>b</sup>
<b>2<sup>c</sup></b>	0.031 mmol 103.3 mg	0.031 mmol 18.33 mg	CuI 0.003 mmol 0.6 mg	DIPEA (0.009 mmol, 1.2 mg) TBTA ( <b>29</b> , 0.009 mmol, 5.3 mg)	– <sup>b</sup>
<b>3<sup>d</sup></b>	0.033 mmol 110 mg	0.033 mmol 19.6 mg	CuI 0.003 mmol 0.6 mg	DIPEA (0.009 mmol, 1.3 mg) TBTA ( <b>29</b> , 0.009 mmol, 5.6 mg)	9 % <sup>e</sup>
<b>4<sup>f</sup></b>	0.021 mmol 70.5 mg	0.021 mmol 12.5 mg	CuBr 0.006 mmol 1 mg	DIPEA (0.006 mmol, 0.8 mg) TBTA ( <b>29</b> , 0.006 mmol, 3.6 mg)	– <sup>b</sup>
<b>5<sup>f</sup></b>	0.016 mmol 54.3 mg	0.016 mmol 9.6 mg	CuI·P(OEt) <sub>3</sub> 0.005 mmol 1.7 mg	DIPEA (0.005 mmol, 0.6 mg) TBTA ( <b>29</b> , 0.005 mmol, 2.7 mg)	– <sup>b</sup>
<b>6<sup>f</sup></b>	0.021 mmol 70.5 mg	0.021 mmol 12.5 mg	CuBr(PPh <sub>3</sub> ) <sub>3</sub> 0.008 mmol 7.3 mg	DIPEA (0.008 mmol, 1 mg) TBTA ( <b>29</b> , 0.008 mmol, 4.4 mg)	– <sup>b</sup>

a) 3 mL abs THF, 7 h at 50 °C, then overnight at 80 °C; b) no change on TLC (CHCl<sub>3</sub>/MeOH = 50:1); c) 5 mL tol/DMF = 50:50, 4 d at 80 °C; d) 5 mL abs THF, microwave for 20 h at 75 °C (25 W); e) isolated yield of “click”-product **24**; f) 5 mL tol/THF = 1:1, 7 d t 80 °C.

### 7.2.27 Azide/alkyne-“click”-reactions of **3** with **4**



The azide/alkyne-“click”-reactions were accomplished following an already known synthetic approach<sup>218-220</sup>. For experimental details see Table EP4. In a Schlenk tube azide-functionalized PIB (**18**,  $M_n = 3400$  g/mol, 1 eq) was dissolved in toluene and **19** (1 eq/3 eq) as well as the bases were added. The reaction mixture was purged for 30 min with argon or three freeze-pump-thaw-cycles were performed. The copper(I)-catalyst (0.1 eq) was added and the solution was stirred at 80 °C. For working up the solvent was removed under vacuum and CHCl<sub>3</sub> was added. The organic phase was washed three times with saturated NH<sub>4</sub>Cl-solution, three times with distilled water, and dried over Na<sub>2</sub>SO<sub>4</sub> and filtered. Chloroform was removed in vacuum and the product was dissolved in *n*-hexane and precipitated in MeOH. The crude product was purified via column chromatography (SiO<sub>2</sub>, TLC: CHCl<sub>3</sub>/MeOH = 70:1,  $R_f$  (**23**) = 0.19, eluent: CHCl<sub>3</sub> → CHCl<sub>3</sub>/MeOH = 70:1), whereby the unreacted

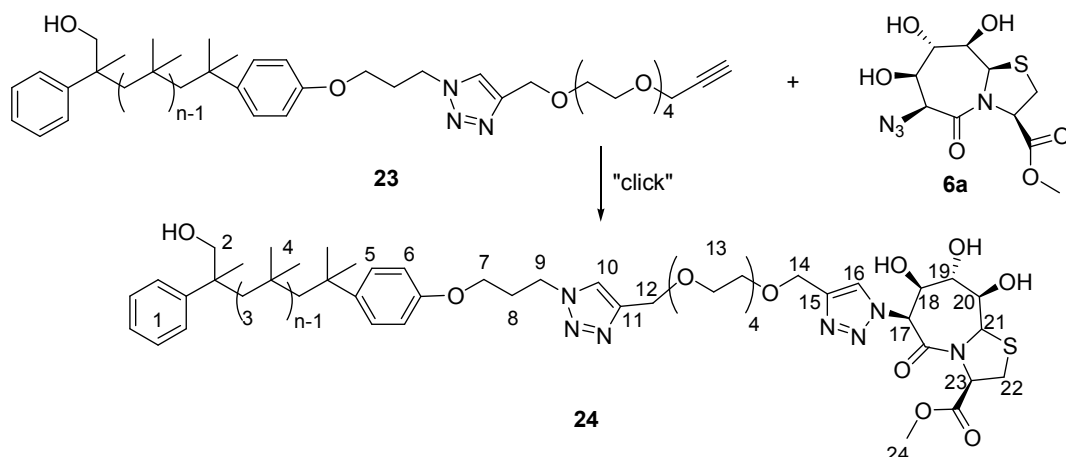
## 7. Experimental Part

azide-functionalized PIB was eluted first, before changing the solvent to a more polar mixture to elute the desired product **23**. Finally, the polymer was dried in vacuum to yield **23** as a viscous, slightly yellow substance. <sup>1</sup>H-NMR (400 MHz, CDCl<sub>3</sub>): δ = 7.59 (*s*, 1H, H-10), 7.40-7.27 (*m*, 5H, H-1), 7.25-7.18 (*m*, 2H, H-5), 6.80 (*d*, 2H, <sup>3</sup>J<sub>H,H</sub>=8.7 Hz, H-6), 4.68 (*s*, 2H, H-12), 4.57 (*t*, 2H, <sup>3</sup>J<sub>H,H</sub>=7.0 Hz, H-9), 4.20 (*d*, 2H, <sup>3</sup>J<sub>H,H</sub>=2.4 Hz, H-14), 3.97 (*t*, 1H, <sup>3</sup>J<sub>H,H</sub>=5.7 Hz, H-7), 3.72-3.61 (*m*, 17H, H-2,13), 3.43 (*m*, 1H, H-2'), 2.46 (*m*, 1H, H-16), 2.38 (*m*, 2H, H-8), 2.00-0.70 (PIB backbone). <sup>13</sup>C-NMR (400 MHz, CDCl<sub>3</sub>): δ = 143.1 (C-11), 128.3-127.0 (C-1), 125.9 (C-1,5), 123.0 (C-10), 113.7 (C-6), 74.6 (C-16), 74.5 (C-2), 70.6-70.4 (C-13), 69.7 (C-13), 69.2 (C-13), 64.6 (C-7), 64.0 (C-12), 59.8-59 (C-3), 58.3 (C-14), 47.2 (C-9), 38.5-37.5 (C-4), 31.5-31 (C-4), 30.7 (C-8). MALDI-TOF MS *m/z*<sub>exp</sub> = 2494.820 [M<sub>34</sub>+Li]<sup>+</sup>, 2528.882 [M<sub>35</sub>-C<sub>3</sub>H<sub>2</sub>+Na]<sup>+</sup>, *m/z*<sub>calc</sub> = 2494.458 [M<sub>34</sub>+Li]<sup>+</sup>, 2528.478 [M<sub>35</sub>-C<sub>3</sub>H<sub>2</sub>+Na]<sup>+</sup>.

**Table EP4.** Experimental conditions for azide/alkyne-“click”-reactions of **18** with **19**.

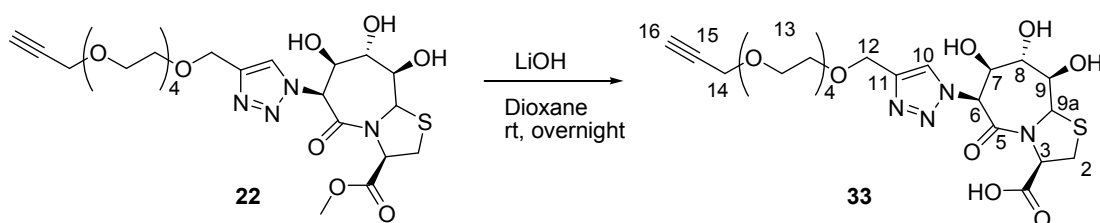
entry	amount of <b>18</b>	amount of <b>19</b>	amount of Cu <sup>I</sup>	amount of base	yield of <b>23</b> <sup>a</sup>
<b>1</b> <sup>b</sup>	1 eq 0.04 mmol 130 mg	1 eq 0.04 mmol 10.8 mg	CuI 0.1 eq 0.004 mmol 0.8 mg	DIPEA 0.3 eq 0.012 mmol, 1.6 mg TBTA ( <b>29</b> ) 0.3 eq 0.012 mmol, 6.7 mg	60 %
<b>2</b> <sup>c</sup>	1 eq 0.15 mmol 510 mg	3 eq 0.45 mmol 125 mg	CuI 0.1 eq 0.015 mmol 3 mg	DIPEA 0.3 eq 0.045 mmol, 6 mg TBTA ( <b>29</b> ) 0.3 eq 0.045 mmol, 26 mg	62 %
<b>4</b> <sup>d</sup>	1 eq 0.588 mmol 2 g	3 eq 476.8 mg	CuI 0.12 eq, 0.071 mmol 13.44 mg CuBr 0.12 eq 0.071 mmol 10.12 mg	DIPEA 1 eq 0.588 mmol, 75.9 mg TBTA ( <b>29</b> ) 0.1 eq 0.0588 mmol, 31.2 mg	92 %
<b>5</b> <sup>e</sup>	1 eq 0.281 mmol 955 g	3.8 eq 289 mg	CuI 0.12 eq, 0.034 mmol 6.5 mg CuBr 0.12 eq 0.034 mmol 4.8 mg	DIPEA 1 eq 0.281 mmol, 36.3 mg TBTA ( <b>29</b> ) 0.1 eq 0.0281 mmol, 15 mg	96 %

a) isolated yield of “click”-product **23**; b) 5 mL toluene, 3 d at 80 °C; c) 50 mL toluene, 4 d at 80 °C; d) 30 mL abs toluene, three times freeze-thaw cycle, protected with aluminium foil, 3 d at 80 °C; e) 6 mL abs Tol, three times freeze-thaw cycle, Cu<sup>I</sup> added, again two times freeze-thaw cycle, protected with alu foil, 3d at 90°C.

7.2.28 Azide/alkyne-“click”-reactions of **6a** with **23** to achieve **24**

The azide/alkyne-“click”-reactions were accomplished following an already known synthetic approach<sup>218-220</sup>. For experimental details see Table EP5. In a Schlenk tube **23** ( $M_n = 3600$  g/mol, 1 eq, 0.0022mmol, 76 mg) was dissolved in 11 mL toluene/THF (v/v = 10:1) and **6a** (1 eq, 0.022 mmol, 6.8 mg) as well as the bases DIPEA (0.3 eq, 0.007 mmol, 0.9 mg) and TBTA (**29**, 0.3 eq, 0.007 mmol, 3.7 mg) were added. The reaction mixture was purged for 30 min with argon and the CuI (0.3 eq, 0.007 mmol, 0.9 mg) was added and the solution was stirred at 80 °C for 7 d. For working up the solvent was removed under vacuum and  $\text{CHCl}_3$  was added. The organic phase was washed one time with saturated  $\text{NH}_4\text{Cl}$ -solution, three times with distilled water, and dried over  $\text{Na}_2\text{SO}_4$  and filtered. The crude product was purified via column chromatography ( $\text{SiO}_2$ , TLC:  $\text{CHCl}_3/\text{MeOH} = 50:1$ ,  $R_f$  (**24**) = 0.27, eluent:  $\text{CHCl}_3 \rightarrow \text{CHCl}_3/\text{MeOH} = 50:1$ ), whereby the unreacted **23** (TLC:  $\text{CHCl}_3/\text{MeOH} = 50:1$ ,  $R_f$  (**23**) = 0.44) was eluted first, before changing the solvent to a more polar mixture to elute the desired product **24**. Finally, the polymer was dried in vacuum to yield 25 % of **24** as a viscous, slightly yellow substance.

(NMR data and MALDI-ToF MS data see 7.2.26)

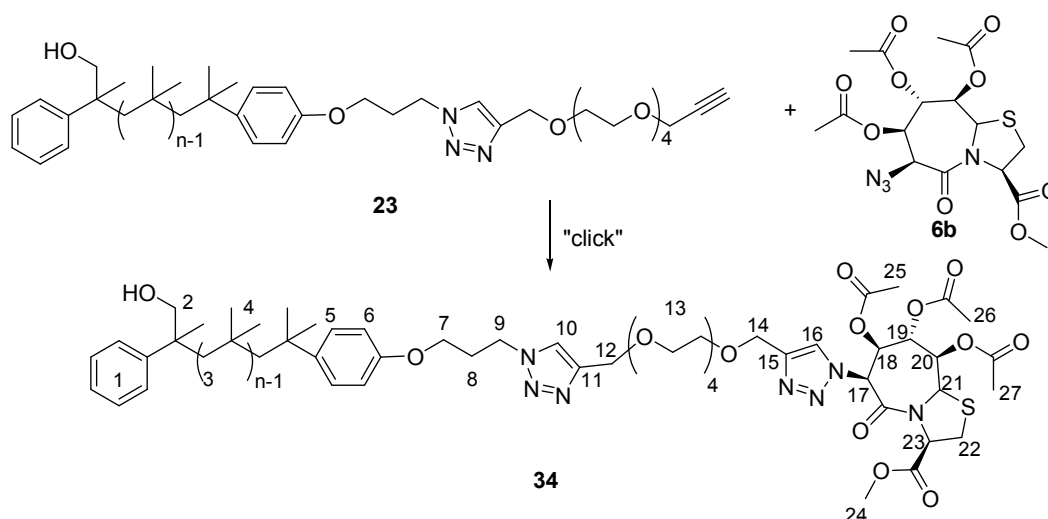
7.2.29 Hydrolysis of **22** to **33**

The synthesis of **33** was modelled after Tremmel.<sup>114</sup> Therefore, **22** (186 mg, 0.316 mmol) was dissolved in 7 mL dioxane and a solution of LiOH (18 mg, 0.429 mmol) in water (1 mL) was added at room temperature under stirring. The reaction was allowed to stir overnight, controlled by TLC ( $\text{EA}/\text{MeOH} = 5:1$ ;  $R_f = 0$ ) and stopped by the addition of 1M HCl until the solution was neutral and becomes clear. Then the solvent was evaporated to get the product **33** quantitatively, which was used

## 7. Experimental Part

without further purification.  $^1\text{H-NMR}$  (400 MHz,  $\text{DMSO-d}_6$ ):  $\delta = 8.00$  (*s*, 1H, H-10), 6.19 (*s*, 1H, H-6), 5.85-5.80 (*m*, 3H, 9a, OH), 4.70 (*m*, 1H, H-3), 4.58 (*m*, 1H, OH), 4.55 (*s*, 2H, H-12), 4.13 (*dd*, 2H,  $^3J_{\text{H,H}} = 1.1$  Hz,  $^3J_{\text{H,H}} = 2.4$  Hz, H-14), 3.95 (*dd*, 1H,  $^3J_{\text{H,H}} = 3.9$  Hz,  $^3J_{\text{H,H}} = 7.8$  Hz, H-7), 3.85 (*d*, 1H,  $^3J_{\text{H,H}} = 3.8$  Hz, H-8), 3.60 (*d*, 2H,  $^3J_{\text{H,H}} = 2.2$  Hz, H-9), 3.58-3.49 (*m*, 16H, H-13), 3.40 (*m*, 1H, H-16), 3.25 (*m*, 2H, H-2). ESI-TOF MS ( $\text{MeOH/NaCl}$ )  $m/z_{\text{exp.}} = 573.1767$  [ $\text{M-H}$ ],  $m/z_{\text{calc.}} = 573.1861$  [ $\text{M-H}$ ].

### 7.2.30 Azide/alkyne-“click”-reactions of **6b** with **23** to achieve **34**



The azide/alkyne-“click”-reactions were carried out according to literature.<sup>168</sup> For experimental details see Table EP5. In a Schlenk flask **23** (1 eq) and **6b** (2 eq) were dissolved in THF and TBTA (**29**, 0.2 eq) and DIPEA (0.4 eq) were added. Three freeze-pump-thaw-cycles were performed and the copper catalyst was added. The solution was stirred at certain reaction conditions and was controlled via TLC ( $\text{CHCl}_3/\text{MeOH} = 50:1$ ). After removing the solvent the crude product was dissolved in *n*-hexane and precipitated in MeOH for three times, then a column chromatography was conducted (eluent  $\text{CHCl}_3 \rightarrow \text{CHCl}_3/\text{MeOH} = 50:1$ ,  $R_f = 0.1-0$ ). For entry 3 of table EP6 **34** could be obtained as pale yellow, viscous polymer. Yield 90 % (0.141 mmol, 640 mg).  $^1\text{H-NMR}$  (400 MHz,  $\text{CDCl}_3$ ):  $\delta = 8.11$  (*s*, 1H, H-16), 7.61 (*s*, 1H, H-10), 7.40-7.27 (*m*, 5H, H-1), 7.25-7.18 (*m*, 2H, H-5), 6.79 (*d*, 2H,  $^3J_{\text{H,H}} = 8.8$  Hz, H-6), 6.35 (*s*, 1H, H-17'), 6.10 (*s*, 1H, OH), 5.63 (*s*, 1H, H-17), 5.53 (*m*, 1H, H-20), 5.13 (*m*, 2H, H-18,19), 5.05 (*m*, 1H, H-23), 4.74-4.56 (*m*, 6H, H-12,14,9), 4.49 (*s*, 1H, H-21), 4.26 (*s*, 1H, H-18'), 3.97 (*m*, 2H, H-7), 3.79 (*s*, 3H, H-24), 3.70-3.55 (*m*, 18H, H-13,2), 3.43 (*d*, 2H,  $^2J_{\text{H,H}} = 10.7$  Hz, H-2'), 3.36 (*m*, 1H, H-22), 3.22 (*m*, 1H, H-22'), 2.38 (*m*, 2H, H-8), 2.25-2.13 (*m*, 9H, H-25,26,27), 2.00-0.70 (PIB backbone). MALDI-TOF MS  $m/z_{\text{exp.}} = 2715.430$  [ $\text{M}_{30}+\text{Li}$ ] $^+$ , 2729.421 [ $\text{M}_{31}\text{-OAc}+\text{Li}$ ] $^+$ , 2749.375 [ $\text{M}_{32}\text{-2OAc-H}+\text{Li}$ ] $^+$ ,  $m/z_{\text{calc.}} = 2715.302$  [ $\text{M}_{30}+\text{Li}$ ] $^+$ , 2729.354 [ $\text{M}_{31}\text{-OAc}+\text{Li}$ ] $^+$ , 2749.415 [ $\text{M}_{32}\text{-2OAc-H}+\text{Li}$ ] $^+$ . In NMR and MALDI-ToF MS product **34** partially without OAc as protecting groups, therefore H-17' in the case, that “18” is with OH group instead of OAc.

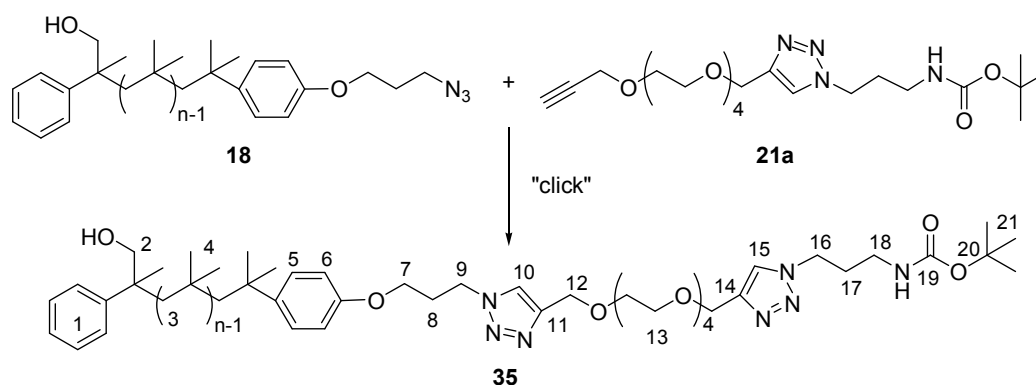
## 7. Experimental Part

**Table EP5.** Experimental conditions for azide/alkyne-“click”-reactions of **23** with **6b**.

entry	amount of <b>23</b>	amount of <b>6b</b>	amount of Cu <sup>I</sup>	amount of base	yield of <b>34</b>
<b>1<sup>a</sup></b>	1 eq 0.024 mmol 100 mg	1.8 eq 0.045 mmol 20 mg	CuI 0.1 eq 0.0024 mmol, 0.5 mg CuBr 0.1 eq 0.0024 mmol, 0.4 mg	DIPEA 0.4 eq 0.0096 mmol, 1.24 mg TBTA ( <b>29</b> ) 0.2 eq 0.0048 mmol, 2.5 mg	–
<b>2<sup>a</sup></b>	1 eq 0.024 mmol 100 mg	1.5 eq 0.045 mmol 20 mg	CuI·P(OEt) <sub>3</sub> 0.2 eq 0.0048 mmol, 1.7 mg	DIPEA 0.4 eq 0.0096 mmol, 1.24 mg TBTA ( <b>29</b> ) 0.2 eq 0.0048 mmol, 2.5 mg	–
<b>3<sup>b</sup></b>	1 eq 0.157 mmol 660 mg	2 eq 0.314 mmol 139.6 mg	CuSO <sub>4</sub> ·5H <sub>2</sub> O 0.2 eq 0.0314 mmol, 7.8 mg Na-asc 0.2 eq 0.0314 mmol, 6.22 m	DIPEA 0.4 eq 0.0628 mmol, 8.1 mg TBTA ( <b>29</b> ) 0.2 eq 0.0314 mmol, 16.7 mg	90 %

a) 4 mL THF, 3 d at 50 °C, 3 d; b) 5 mL THF, 4 d at 60 °C.

### 7.2.31 Azide/alkyne-“click”-reactions of **18** with **21a** to achieve **35**



The azide/alkyne-“click”-reactions were accomplished following an already known synthetic approach.<sup>217, 232, 233</sup> For experimental details see Table EP6. Into a Schlenk flask solvent, **18** (1 eq), **21a** (3-4 eq) as well as bases were added. The reaction mixture was purged for 30 min with argon or three freeze-pump-thaw-cycles were performed. The copper(I)-catalyst (0.12 eq-0.3 eq) was added and the solution was stirred at room temperature. The reaction was monitored via TLC [CHCl<sub>3</sub>/MeOH = 50:1, R<sub>f</sub> = 0.38 (**35**)]. For working up the solvent was removed under vacuum and CHCl<sub>3</sub> was added and the crude product was purified via column chromatography. Therefore, CHCl<sub>3</sub> was used as eluent and after removing of unreacted **18** the eluent was changed to CHCl<sub>3</sub>/MeOH = 50:1 yielding the “click” product **35**. <sup>1</sup>H-NMR (400 MHz, CDCl<sub>3</sub>): δ = 7.66 (*s*, 1H, H-15), 7.59 (*s*, 1H, H-10), 7.40-7.27 (*m*, 5H, H-1), 7.25-7.18 (*m*, 2H, H-5), 6.79 (*d*, 2H, <sup>3</sup>J<sub>H,H</sub> = 8.8 Hz, H-6), 4.68 (*s*, 2H, H-12), 4.67 (*s*, 2H, H-14), 4.57 (*t*, 2H, <sup>3</sup>J<sub>H,H</sub> = 7.1 Hz, H-9), 4.40 (*t*, 2H, <sup>3</sup>J<sub>H,H</sub> = 6.8 Hz, H-16), 3.97 (*t*, 1H, <sup>3</sup>J<sub>H,H</sub> = 5.8 Hz, H-7), 3.71-3.61 (*m*, 17H, H-2,13), 3.43 (*m*, 1H, H-2'), 3.13 (*q*, 2H, <sup>3</sup>J<sub>H,H</sub> = 6.2 Hz, H-18), 2.38 (*m*, 2H, H-8), 2.08 (*m*, 2H, H-17), 2.00-0.70 (PIB backbone). <sup>13</sup>C-NMR (400 MHz, CDCl<sub>3</sub>): δ = 156.0 (C-19), 143.1



## 7. Experimental Part

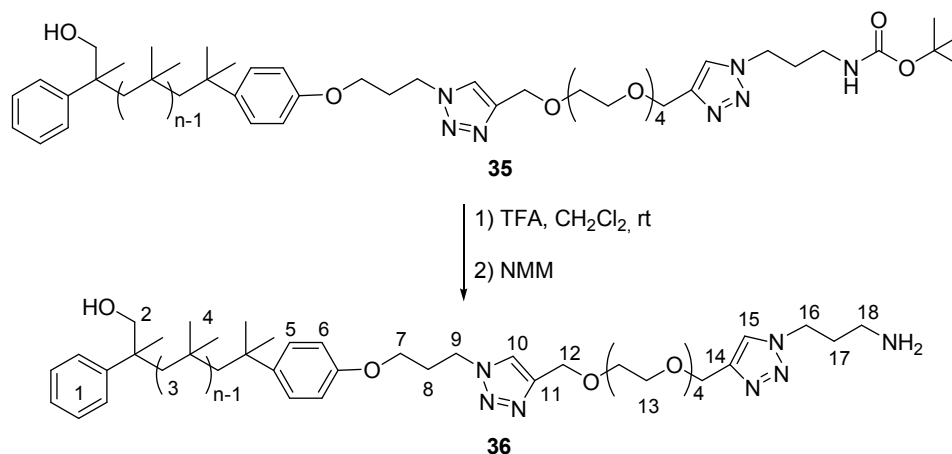
(C-11), 128.3-127.0 (C-1), 125.9 (C-1,5), 123.0 (C-10,15), 113.7 (C-6), 77.2 (C-20), 74.5 (C-2), 70.6-70.4 (C-13), 69.7 (C-13), 69.2 (C-13), 64.7 (C-7), 64.0 (C-12), 59.8-59 (C-3), 58.3 (C-14), 47.5 (16), 47.2 (C-9), 44.2 (C-18), 38.5-37.5 (C-4), 31.5-31 (C-4), 30.7 (C-8), 28.4 (C-17, 21). MALDI-TOF MS  $m/z_{exp} = 2359.288 [M_{28}+Li]^+$ ,  $2388.974 [M_{28}-Boc+TFA+Na]^+$ ,  $m/z_{calc} = 2359.209 [M_{28}+Li]^+$ ,  $2389.123 [M_{28}-Boc+TFA+Na]^+$ .

**Table EP6.** Experimental conditions for azide/alkyne-“click”-reactions of **18** with **21a**.

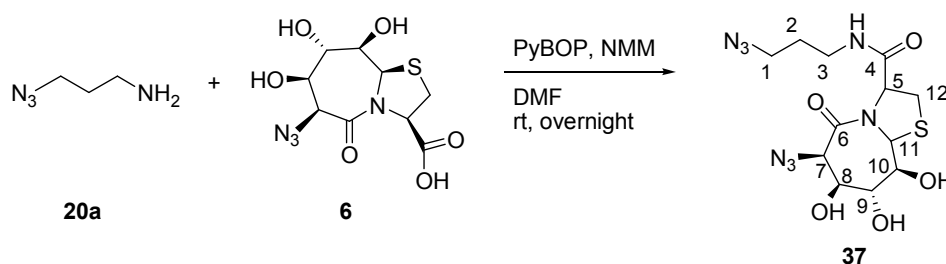
entry	amount of <b>18</b>	amount of <b>21a</b>	amount of Cu <sup>I</sup>	amount of additive	yield of <b>35</b> <sup>a</sup>
<b>1</b> <sup>b</sup>	1 eq 0.03 mmol, 102 mg	3 eq, 0.09 mmol, 42.35 mg	Cu-powder 0.01 mmol, 0.6 mg CuSO <sub>4</sub> ·5H <sub>2</sub> O 0.01 mmol, 2.3 mg	–	–
<b>2</b> <sup>c</sup>	1 eq 0.03 mmol, 110 mg	3 eq, 0.09 mmol, 42.35 mg	CuI 0.01 mmol, 1.7 mg	TBTA ( <b>29</b> ) 0.003 mmol, 1.6 mg DIPEA 0.003 mmol, 4 mg	64 %
<b>3</b> <sup>d</sup>	1 eq 0.23 mmol, 800 mg	4 eq, 0.91 mmol, 430 mg	CuI 0.027 mmol, 5.3 mg CuBr 0.027 mmol, 3.9 mg	TBTA ( <b>29</b> ) 0.023 mmol, 12.1 mg DIPEA 0.023 mmol, 29.5 mg	88 %

a) isolated yield of “click” product **35**; b) 4 mL THF, 30 min degassed with argon, overnight at 50 °C; c) 5 mL THF/*i*-prop = 4:1, 30 min degassed with argon, 4 d at 90 °C; d) 7 mL Tol/H<sub>2</sub>O = 6:1, three times freeze-thaw cycle, 2 d at 80 °C.

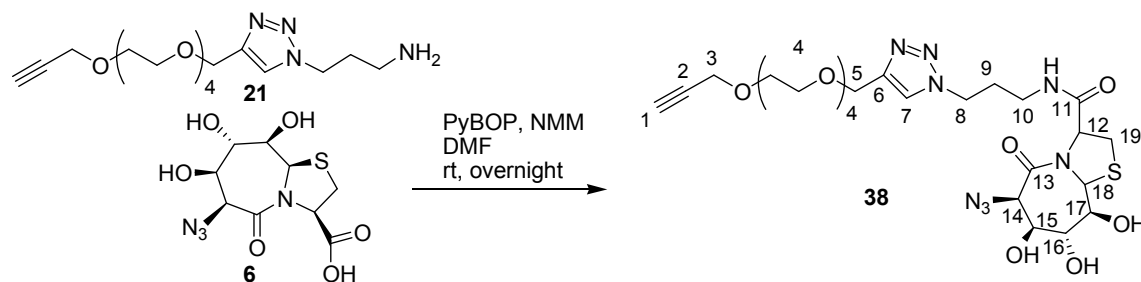
### 7.2.32 Deprotection of **35** to achieve **36**



The deprotection of **35** to achieve **36** was accomplished to Xiao<sup>227</sup>. In a 25 mL one-neck flask **35** (0.09 mmol, 412 mg) was dissolved in 6 mL DCM and cooled with an ice bath, then TFA (6.75 mmol, 500  $\mu$ L) was added. The solution was allowed to stir at room temperature overnight and monitored via TLC (CHCl<sub>3</sub>/MeOH = 50:1, R<sub>f</sub> = 0-0.1). The pH-value was adjusted to 7-8 with NMM. After removing of the solvent under vacuum the polymer was dissolved in *n*-hexane and precipitated in MeOH for three times yielding **36** (96 %, 395 mg). MALDI-TOF MS  $m/z_{exp} = 3157.147 [M_{44}+Li]^+$ ,  $3196.678 [M_{44}-H+2Na]^+$ ,  $m/z_{calc} = 3157.162 [M_{44}+Li]^+$ ,  $3196.125 [M_{44}-H+2Na]^+$ .

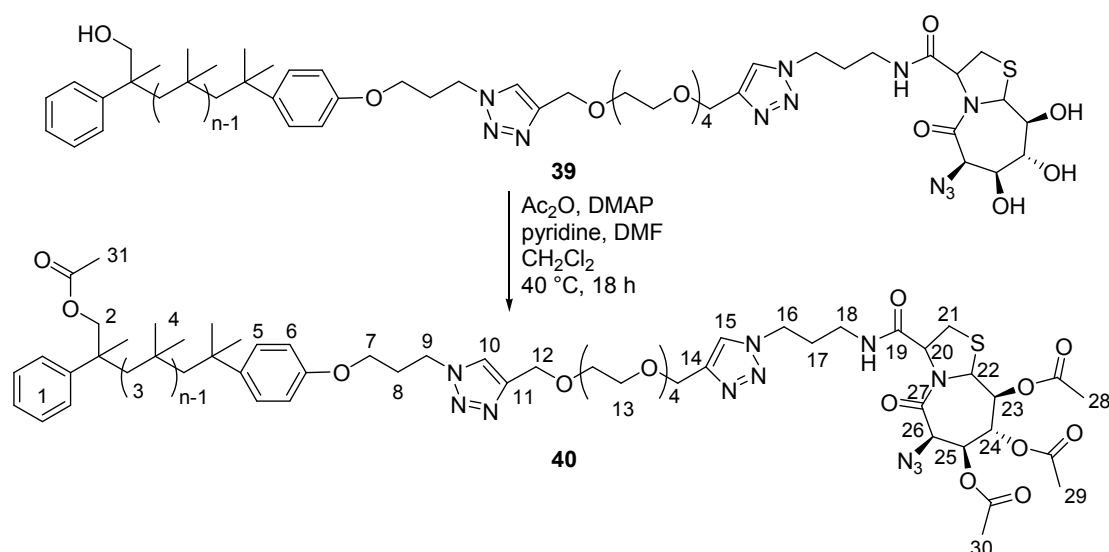
7.2.33 Peptide coupling of **6a** with **20a** to achieve **37**

The peptide coupling of **6** with **20a** was accomplished to Tremmel<sup>114</sup>. In a round bottom flask equipped with magnetic stir bar **6** (0.16 mmol, 50 mg) was dissolved in 5 mL DMF. Then, **20a** [0.16 mmol, 16.2 mg (as 46.1 mg stock solution in Et<sub>2</sub>O)] and PyBOP (1.44 eq, 0.23 mmol, 120 mg) were added. With NMM the pH-value was adjusted to 7-8. The solution was allowed to stir at room temperature overnight and monitored via TLC (EA/MeOH = 1:1, R<sub>f</sub> = 0.88). For working up the solvent was removed under vacuum and EA was added and a column chromatography (EA, R<sub>f</sub> = 0.20) was conducted to yield 80 % (0.12 mmol, 46.3 mg) of **37** obtained as colourless, glassy solid. <sup>1</sup>H-NMR (400 MHz, DMSO<sub>d6</sub>): δ = 8.09 (*t*, 1H, <sup>3</sup>J<sub>H,H</sub> = 5.6 Hz, NH), 5.90 (*d*, 1H, <sup>3</sup>J<sub>H,H</sub> = 6.5 Hz, OH-10), 5.72 (*d*, 1H, <sup>3</sup>J<sub>H,H</sub> = 5.0 Hz, OH-8), 5.57 (*d*, 1H, <sup>3</sup>J<sub>H,H</sub> = 3.8 Hz, OH-9), 5.48 (*s*, 1H, H-11), 4.66 (*s*, 1H, H-7), 4.53 (*t*, 1H, <sup>3</sup>J<sub>H,H</sub> = 7.8 Hz, H-5), 3.90 (*t*, 1H, <sup>3</sup>J<sub>H,H</sub> = 4.8 Hz, H-8), 3.79 (*dd*, 1H, <sup>3</sup>J<sub>H,H</sub> = 3.8 Hz, <sup>3</sup>J<sub>H,OH</sub> = 7.8 Hz, H-9), 3.61 (*dd*, 1H, <sup>3</sup>J<sub>H,H</sub> = 3.0 Hz, <sup>3</sup>J<sub>H,OH</sub> = 6.4 Hz, H-10), 3.26 (*m*, 2H, H-1), 3.17 (*m*, 2H, H-12), 3.01 (*s*, 2H, H-3), 1.60 (*p*, 2H, <sup>3</sup>J<sub>H,H</sub> = 6.9 Hz, H-2). <sup>13</sup>C-NMR (400 MHz, DMSO<sub>d6</sub>): δ = 169.5 (COOH), 166.9 (C-6), 76.2 (C-10), 74.9 (C-8), 72.1 (C-9), 66.1 (C-5), 61.4 (C-7), 61.3 (C-11), 48.1 (C-1), 35.6 (C-3), 32.6 (C-12), 27.9 (C-2). ESI-TOF MS (MeOH/NaCl) *m/z*<sub>exp.</sub> = 409.0861 [M+Na]<sup>+</sup>, *m/z*<sub>calc.</sub> = 409.1013 [M+Na]<sup>+</sup>.

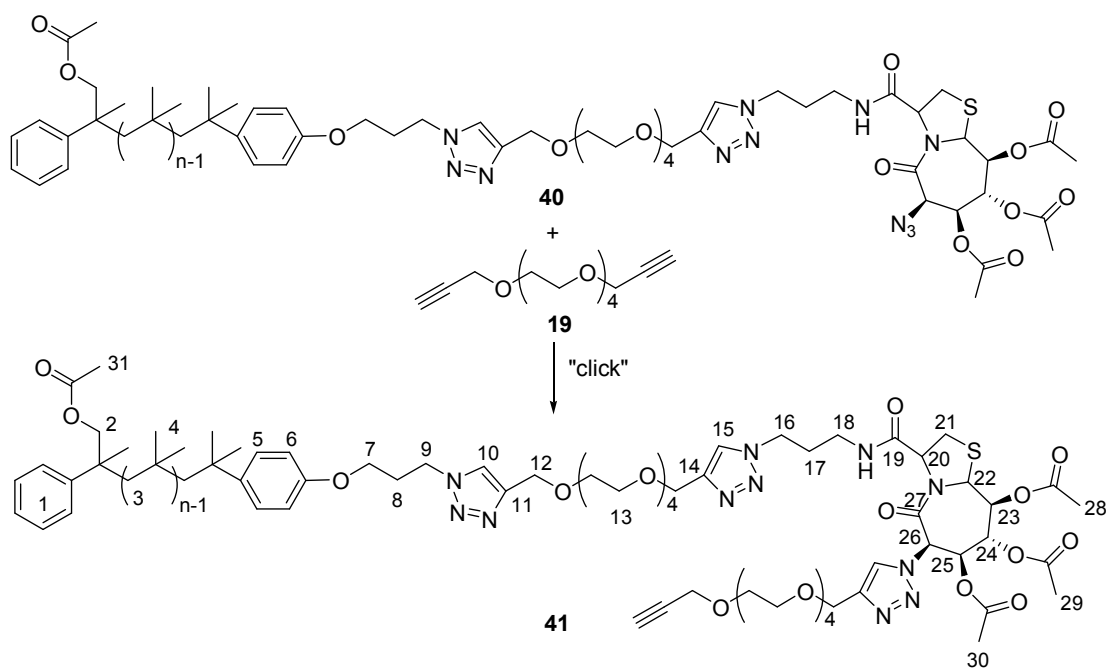
7.2.34 Peptide coupling of **6** with **21** to achieve **38**

The peptide coupling of **21** with **6** was accomplished to Tremmel<sup>114</sup>. In a round bottom flask equipped with magnetic stir bar **6** (0.467 mmol, 142 mg) was dissolved in 5 mL DMF. Then, **21** (0.467 mmol, 172.4 mg) and PyBOP (1.44 eq, 0.672 mmol, 350.3 mg) were added. With NMM the pH-value was adjusted to 7-8. The solution was allowed to stir at room temperature overnight and monitored via TLC (EA/MeOH = 1:1, R<sub>f</sub> = 0.78). For working up the solvent was removed under vacuum and EA was added and a column chromatography (EA, R<sub>f</sub> = 0.20) was conducted to yield 78 % (0.36 mmol,



7.2.36 Protection of hydroxyl-groups of **39** with  $\text{Ac}_2\text{O}$  to achieve **40**

In a 100 mL two-neck flask equipped with magnetic stir bar, reflux condenser, gas tap and septum **39** (0.06 mmol, 250 mg) was dissolved in 15 mL of freshly distilled  $\text{CH}_2\text{Cl}_2$ . Then, DMAP (0.19 mmol, 23 mg) dissolved in 0.1 mL abs DMF, acetic anhydride (1.13 mmol, 104  $\mu\text{L}$ ) and 0.15 mL pyridine were added. The solution was stirred for 18 h at  $40\text{ }^\circ\text{C}$ , monitored via TLC ( $\text{CHCl}_3/\text{MeOH} = 70:1$ ,  $R_f = 0.14$ ) and quenched by addition of MeOH. After removing of the solvent, the crude product was purified via column chromatography ( $\text{CHCl}_3/\text{MeOH} = 70:1$ ) to yield 65 % (0.039 mmol, 164 mg) of **40**. MALDI-TOF MS  $m/z_{\text{exp}} = 3386.539$  [ $\text{M}_{40}+\text{Li}$ ] $^+$ , 3402.436 [ $\text{M}_{40}+\text{Na}$ ] $^+$ , 3418.100 [ $\text{M}_{40}+\text{K}$ ] $^+$ ,  $m/z_{\text{calc}} = 3386.990$  [ $\text{M}_{40}+\text{Li}$ ] $^+$ , 3402.964 [ $\text{M}_{40}+\text{Na}$ ] $^+$ , 3418.938 [ $\text{M}_{40}+\text{K}$ ] $^+$ .

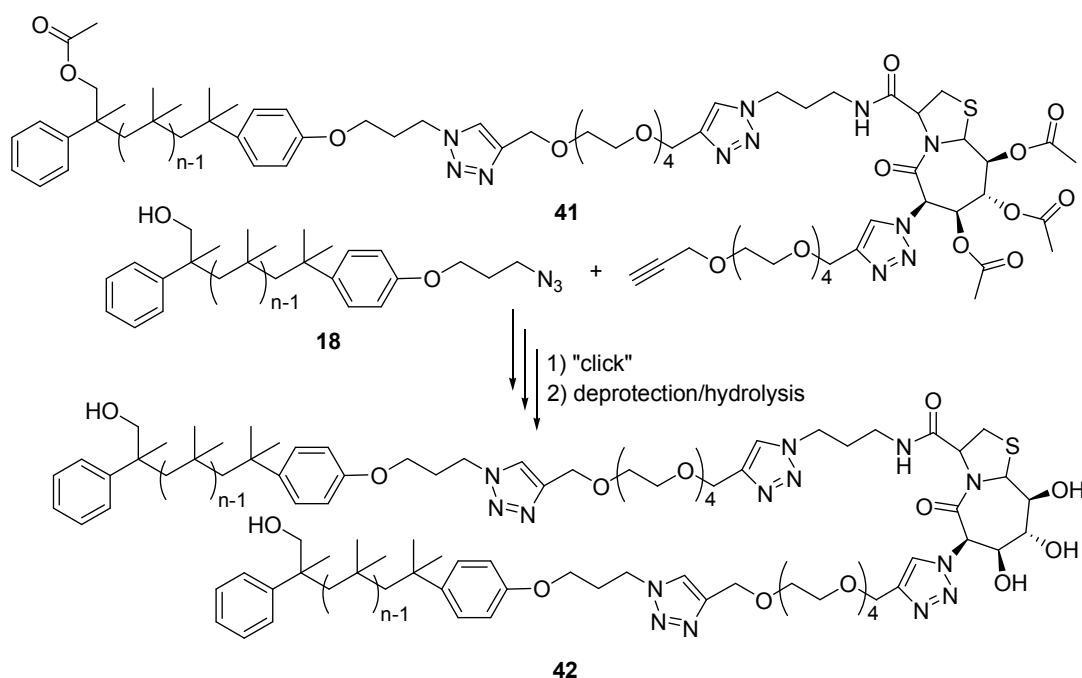
7.2.37 Azide/alkyne-“click”-reactions of **19** with **40** to achieve **41**

## 7. Experimental Part

The azide/alkyne-“click”-reactions were accomplished following an already known synthetic approach.<sup>168</sup> In a microwave tube **40** (1 eq, 0.011 mmol, 50 mg) was dissolved in 3 mL abs toluene and **19** (4 eq, 0.044 mmol, 12 mg), TBTA (0.2 eq, 0.0022 mmol, 1.2 mg) and DIPEA (1 eq, 0.011 mmol, 2  $\mu$ L) were added. After 30 min degassing with argon CuSO<sub>4</sub>·5H<sub>2</sub>O (0.2 eq, 0.0022 mmol, 0.6 mg) and sodium ascorbate (0.2 eq, 0.022 mmol, 0.5 mg) were added and again the solution degassed for 30 min with argon. Then, the microwave tube was placed into the microwave and irradiation was started (80 °C, 25 W, 18 h). The reaction was monitored via MALDI-ToF MS showing that all **40** was consumed. For working up the solution was washed with NH<sub>4</sub>Cl, the organic layer was separated and the aqueous phase extracted against CH<sub>2</sub>Cl<sub>2</sub>. The combined organic phases were dried over Na<sub>2</sub>SO<sub>4</sub>, filtered and the solvent was removed under vacuum. For further purification a column chromatography was conducted (eluent CHCl<sub>3</sub> → CHCl<sub>3</sub>/MeOH = 50:1, R<sub>f</sub> = 0.1) to achieve 36 %\* (0.0048 mmol, 10 mg) of **41** as viscous polymer. MALDI-TOF MS  $m/z_{exp}$  = 2484.542 [M<sub>19</sub>-H+2Li]<sup>+</sup>, 2532.703 [M<sub>20</sub>-OAc-H+2Na]<sup>+</sup>,  $m/z_{calc}$  = 2484.843 [M<sub>19</sub>-H+2Li]<sup>+</sup>, 2532.843 [M<sub>20</sub>-OAc-H+2Na]<sup>+</sup>.

\*determined yield assuming that the purity of **41** was 55 %

### 7.2.38 Azide/alkyne-“click”-reactions of **18** with **41** following by deprotection/hydrolysis to achieve **42**

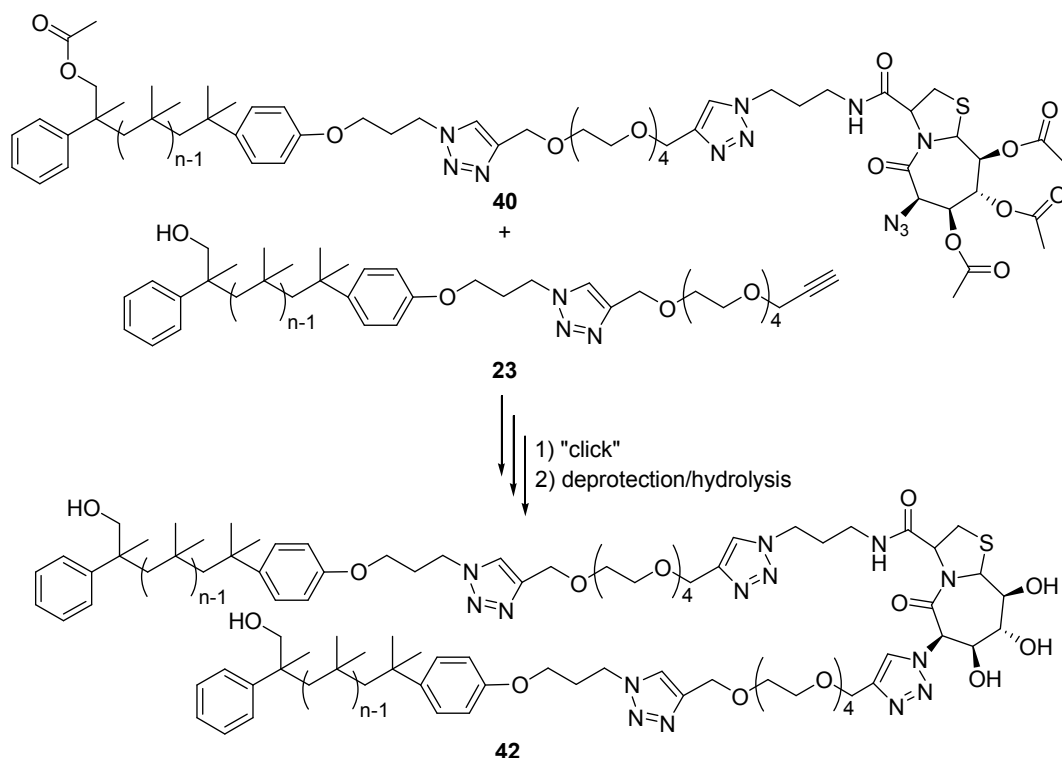


A) For the first part of the synthesis of **42** an azide-alkyne-“click”-reaction was accomplished. In a Schlenk flask **30** (1 eq, 0.0026 mmol, 13 mg) and **18** (1 eq, 0.0026 mmol, 9 mg) were dissolved in 3 mL abs toluene and TBTA (1 eq, 0.0026 mmol, 1.3 mg) as well as DIPEA (1 eq, 0.0026 mmol, 1  $\mu$ L) were added. After three freeze-pump-thaw-cycles CuBr (1 eq, 0.0026 mmol, 0.6 mg) and CuI (1 eq, 0.0026 mmol, 0.5 mg) were added and again three freeze-pump-thaw-cycles were performed. The

## 7. Experimental Part

reaction was monitored via MALDI-ToF MS. showing that all **41** was consumed. For working up the solution was washed with  $\text{NH}_4\text{Cl}$ , the organic layer was separated and the aqueous phase extracted against  $\text{CH}_2\text{Cl}_2$ . The combined organic phases were dried over  $\text{Na}_2\text{SO}_4$ , filtered and the solvent was removed under vacuum. B) The second part of the synthesis is the deprotection/hydrolysis of the “click”-product. Therefore, crude product **42** (0.0026 mmol, 22 mg) was dissolved in 4 mL THF and  $\text{NaOMe}$  (0.26 mmol, 6  $\mu\text{L}$ , 25 wt% solution) as well as 200  $\mu\text{L}$  MeOH were added. The solution stirred 5 d at room temperature and was neutralized with 1M HCl. For purification a column chromatography was conducted (eluent  $\text{CHCl}_3 \rightarrow \text{CHCl}_3/\text{MeOH} = 70:1$ ,  $R_f = 0.2$ ) to achieve 11 %\* (0.00028 mmol, 2.5 mg) of **42** as viscous polymer. \*determined yield after column chromatography, but not pure. MALDI-TOF MS  $m/z_{\text{exp}} = 4054.736$   $[\text{M}_{46}+\text{Na}]^+$ , 4075.022  $[\text{M}_{46}+\text{AcO}+\text{H}]^+$ , 4097.853  $[\text{M}_{46}+\text{AcO}+\text{Na}]^+$ ,  $m/z_{\text{calc}} = 4054.548$   $[\text{M}_{46}+\text{Na}]^+$ , 4075.580  $[\text{M}_{46}+\text{AcO}+\text{H}]^+$ , 4097.562  $[\text{M}_{46}+\text{AcO}+\text{Na}]^+$ .

### 7.2.39 Azide/alkyne-“click”-reactions of **23** with **40**



A) The azide/alkyne-“click”-reactions were accomplished following an already known synthetic approach.<sup>168</sup> For experimental conditions see Table EP7. In a microwave tube/Schlenk flask **23** (1eq) and **40** (1 eq) were dissolved in absolute toluene and TBTA (**29**, 0.1 eq) and DIPEA (1 eq) were added. After degassing with argon or conducting freeze-thaw cycles  $\text{CuSO}_4 \cdot 5\text{H}_2\text{O}$  (0.2 eq/3 eq) and sodium ascorbate (0.2 eq/3eq) were added and again the solution degassed for 30 min with argon or freeze thaw cycles were conducted. The reaction run at certain reaction conditions and was monitored

## 7. Experimental Part

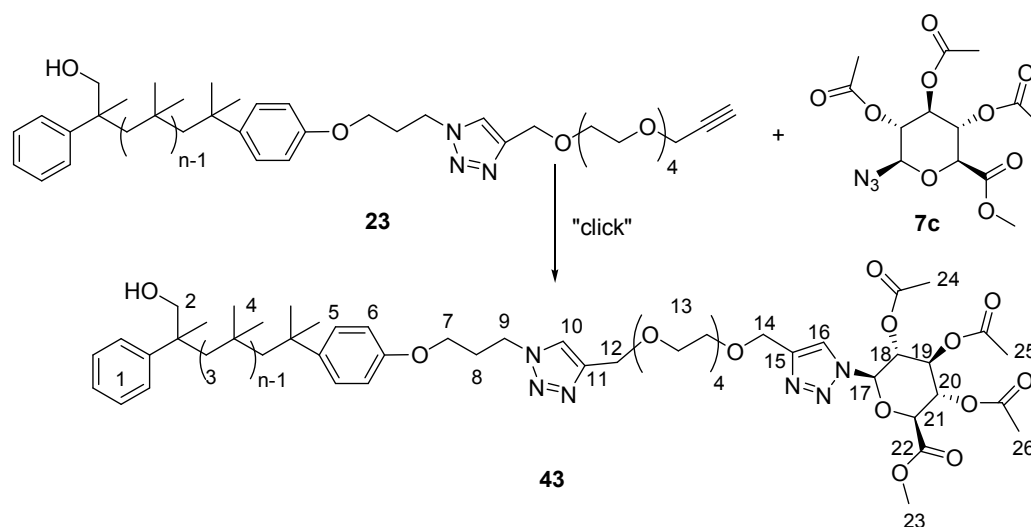
via MALDI-ToF MS showing the consumption of **23**. For working up the solution was washed with  $\text{NH}_4\text{Cl}$ , the organic layer was separated and the aqueous phase extracted against  $\text{CH}_2\text{Cl}_2$ . The combined organic phases were dried over  $\text{Na}_2\text{SO}_4$ , filtered and the solvent was removed under vacuum. For further purification a column chromatography was conducted (eluent  $\text{CHCl}_3 \rightarrow \text{CHCl}_3/\text{MeOH} = 70:1$ ,  $R_f = 0.2$ ) to **42'** as viscous polymer.

**Table 7.** Experimental conditions for azide/alkyne-“click”-reactions of **23** with **40**.

entry	amount of <b>23</b>	amount of <b>40</b>	amount of $\text{Cu}^I$	amount of additive	yield of <b>42</b>
<b>1<sup>a</sup></b>	1 eq 0.0038 mmol 20 mg	1 eq, 0.0038 mmol 24 mg	$\text{CuSO}_4 \cdot 5\text{H}_2\text{O}$ 3 eq 0.004 mmol, 1 mg Na-asc 3 eq 0.004 mmol, 0.8 mg	TBTA ( <b>29</b> ) 0.1 eq 0.0004 mmol, 0.2 mg DIPEA 1 eq 0.0038 mmol, 0.5 mg	30 % <sup>b</sup>
<b>2<sup>c</sup></b>	1 eq 0.01 mmol, 50 mg	1 eq, 0.01 mmol, 50 mg	$\text{CuSO}_4 \cdot 5\text{H}_2\text{O}$ 0.2 eq 0.002 mmol, 0.5 mg Na-asc 0.2 eq 0.002 mmol, 0.4 mg	TBTA ( <b>29</b> ) 0.1 eq 0.001 mmol, 0.5 mg DIPEA 1 eq 0.01 mmol, 1.7 $\mu\text{L}$	16 % <sup>b</sup>

a) 2.8 mL abs toluene, three times freeze-thaw cycle, addition Cu, then again three times freeze-thaw cycles, 4 d at 80 °C; b) isolated yield but not pure; c) 5 mL abs toluene, microwave tube, 30 min degassing with argon, addition Cu, again degassing with argon for 30 min, microwave conditions: 80 °C, sps, 25 watt, 72 h.

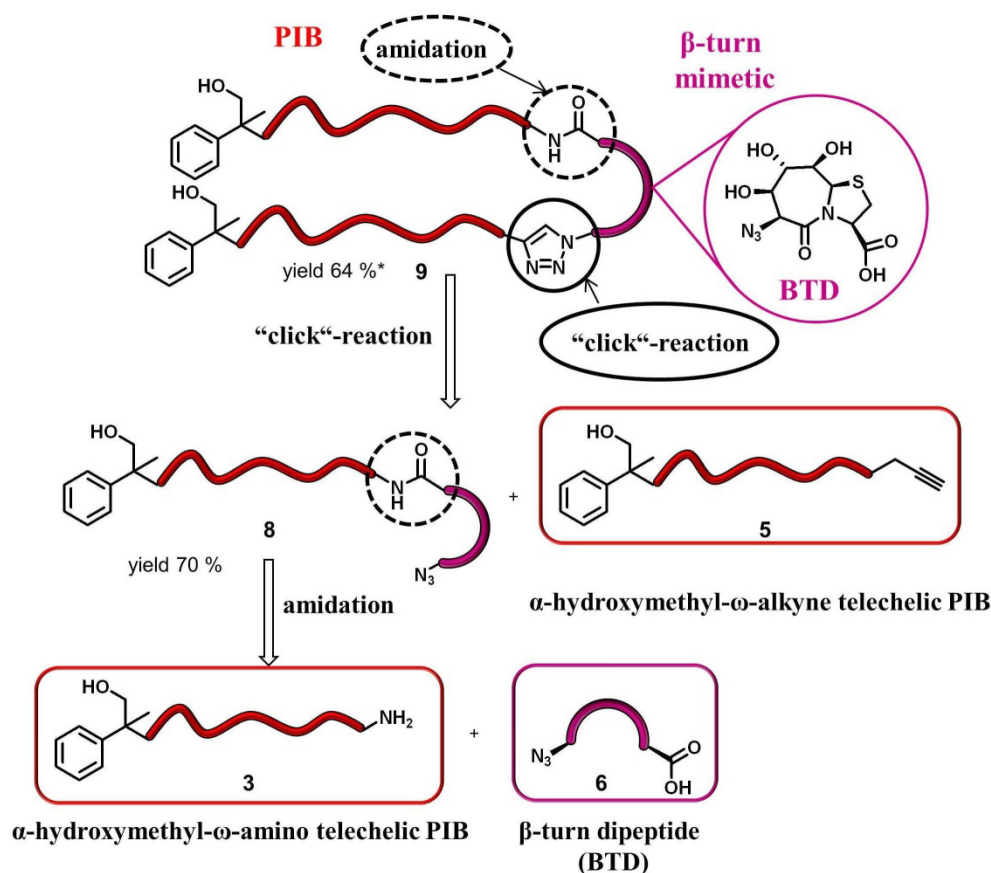
B) The second part of the synthesis is the deprotection/hydrolysis of the “click”-product. Therefore, crude product **42'** (0.004 mmol, 12 mg) was dissolved in 3 mL THF and NaOMe (3 eq, 0.006 mmol, 1.5  $\mu\text{L}$ , 25 wt% solution) as well as 100  $\mu\text{L}$  MeOH were added. The solution stirred 5 d at room temperature and was neutralized with 1M HCl. Due to the small amount, the polymer could not be precipitated, thus the solvent was removed under vacuum and MeOH was added to the thin film of polymer. Then the MeOH was decanted, the polymer dissolved in  $\text{CHCl}_3$ , the solvent removed under vacuum generating again a thin film of polymer and MeOH was added. This “washing” procedure was repeated for five times. For further purification preparative SEC and HPLC using THF as eluent were conducted, but no separation of the product **42** from the starting material **23** could be observed. MALDI-TOF MS  $m/z_{\text{exp}} = 4547.703$   $[\text{M}_{53}+\text{Na}]^+$ , 4562.874  $[\text{M}_{53}+\text{K}]^+$ ,  $m/z_{\text{calc}} = 4547.057$   $[\text{M}_{53}+\text{Na}]^+$ , 4563.030  $[\text{M}_{53}+\text{K}]^+$ .

7.2.40 Azide/alkyne-“click”-reaction of **23** with **7c** to achieve **43**

The azide/alkyne-“click”-reaction was accomplished following an already known synthetic approach.<sup>168</sup> In a Schlenk flask **23** (1 eq, 0.056 mmol, 290 mg) was dissolved in 7 mL abs toluene and a solution of **7c** (1.5 eq, 0.084 mmol, 30.2 mg) in 0.3 mL abs DMF as well as TBTA (**29**, 0.1 eq, 0.0056 mmol, 3 mg) and DIPEA (1 eq, 0.056 mmol, 7.3 mg) were added. After three freeze-pump-thaw-cycles  $\text{CuSO}_4 \cdot 5\text{H}_2\text{O}$  (0.2 eq, 0.011 mmol, 3 mg) and sodium ascorbate (0.2 eq, 0.011 mmol, 2.4 mg) were added and again three freeze-pump-thaw-cycles were performed. The solution was allowed to stir at 80 °C for 2 d and the reaction was monitored via TLC ( $\text{CHCl}_3/\text{MeOH} = 25:1$ ,  $R_f = 0.18$ ). For working up the solvent was removed under vacuum and *n*-hexane was added and the polymer isolated by precipitation into MeOH. For further purification a column chromatography was conducted (eluent  $\text{CHCl}_3 \rightarrow \text{CHCl}_3/\text{MeOH} = 50:1$ ) to achieve 95 % (0.053 mmol, 275 mg) of **43** as viscous polymer.  $^1\text{H-NMR}$  (400 MHz,  $\text{CDCl}_3$ ):  $\delta = 7.86$  (*s*, 1H, H-16), 7.59 (*s*, 1H, H-10), 7.40-7.27 (*m*, 5H, H-1), 7.25-7.18 (*m*, 2H, H-5), 6.80 (*d*, 2H,  $^3J_{\text{H,H}} = 8.7$  Hz, H-6), 5.91 (*d*, 1H,  $^3J_{\text{H,H}} = 9.1$  Hz, H-17), 5.50-5.45 (*m*, 2H, H-18,20), 5.37 (*t*, 1H,  $^3J_{\text{H,H}} = 9.6$  Hz, H-19), 4.68-4.66 (*m*, 4H, H-12,14), 4.57 (*t*, 2H,  $^3J_{\text{H,H}} = 7.1$  Hz, H-9), 4.31 (*d*, 2H,  $^3J_{\text{H,H}} = 9.8$  Hz, H-21), 3.97 (*t*, 1H,  $^3J_{\text{H,H}} = 5.7$  Hz, H-7), 3.75 (*s*, 3H, H-23), 3.72-3.61 (*m*, 17H, H-2,13), 3.43 (*m*, 1H, H-2'), 2.38 (*m*, 2H, H-8), 2.07-2.03 (2*s*, 6H, H-25,26), 1.87 (*s*, 1H, H-24), 2.00-0.70 (PIB backbone). MALDI-TOF MS  $m/z_{\text{exp}} = 2406.130$  [ $\text{M}_{26} + \text{Li}$ ] $^+$ , 2422.107 [ $\text{M}_{26} + \text{Na}$ ] $^+$ , 2439.208 [ $\text{23} + \text{Li}$ ] $^+$ ,  $m/z_{\text{calc}} = 2406.053$  [ $\text{M}_{26} + \text{Li}$ ] $^+$ , 2422.027 [ $\text{M}_{26} + \text{Na}$ ] $^+$ , 2439.395 [ $\text{23} + \text{Li}$ ] $^+$ .



## 8. Summary



**Scheme 8.1.** Retrosynthetic concept towards an amphiphilic polymer conjugate, containing a  $\beta$ -turn mimetic element (BTD), by the linkage of the different building blocks.

The aim of the work was the synthesis of an amphiphilic polymer conjugate containing a  $\beta$ -turn mimetic element and the investigation of its organization in a lipid bilayer membrane. This conjugate was based on two hydrophobic PIB chains (3 and 5), which are connected onto the same hydrophilic  $\beta$ -turn mimetic element BTD (6). For defined linkages of the hydrophobic PIB chains onto the  $\beta$ -turn mimetic element two chemically different reactions were required (Scheme 8.1). These linkages were on the one hand accomplished by the amidation reaction known from peptide synthesis thus amine and carboxylic acid moieties are needed. The  $\text{Cu}^{\text{I}}$  mediated azide/alkyne-"click"-reaction was also used, consequently azide and alkyne moieties at the (chain) - ends of the tailor-made building blocks were necessary.

For the hydrophilic  $\beta$ -turn mimetic element the  $\beta$ -turn dipeptide (BTD) was chosen and synthesized following the procedure from literature.<sup>113, 114</sup> PIB was synthesized via living carbocationic polymerization using  $\alpha$ -methylstyrene epoxide (MSE) as initiator and a) 6-phenoxyhexylamine (2) as quencher to achieve  $\alpha$ -hydroxymethyl- $\omega$ -amino telechelic PIB (3) or b) trimethyl(3-phenoxy-1-propynyl)silane (4) as quencher to obtain  $\alpha$ -hydroxymethyl- $\omega$ -alkyne telechelic PIB (5). The received PIBs are well defined corresponding to narrow molecular weight distribution, targeted molecular weights (3000 – 5000 g/mol) and complete end group functionalization. As the synthesis of the single

## 8. Summary

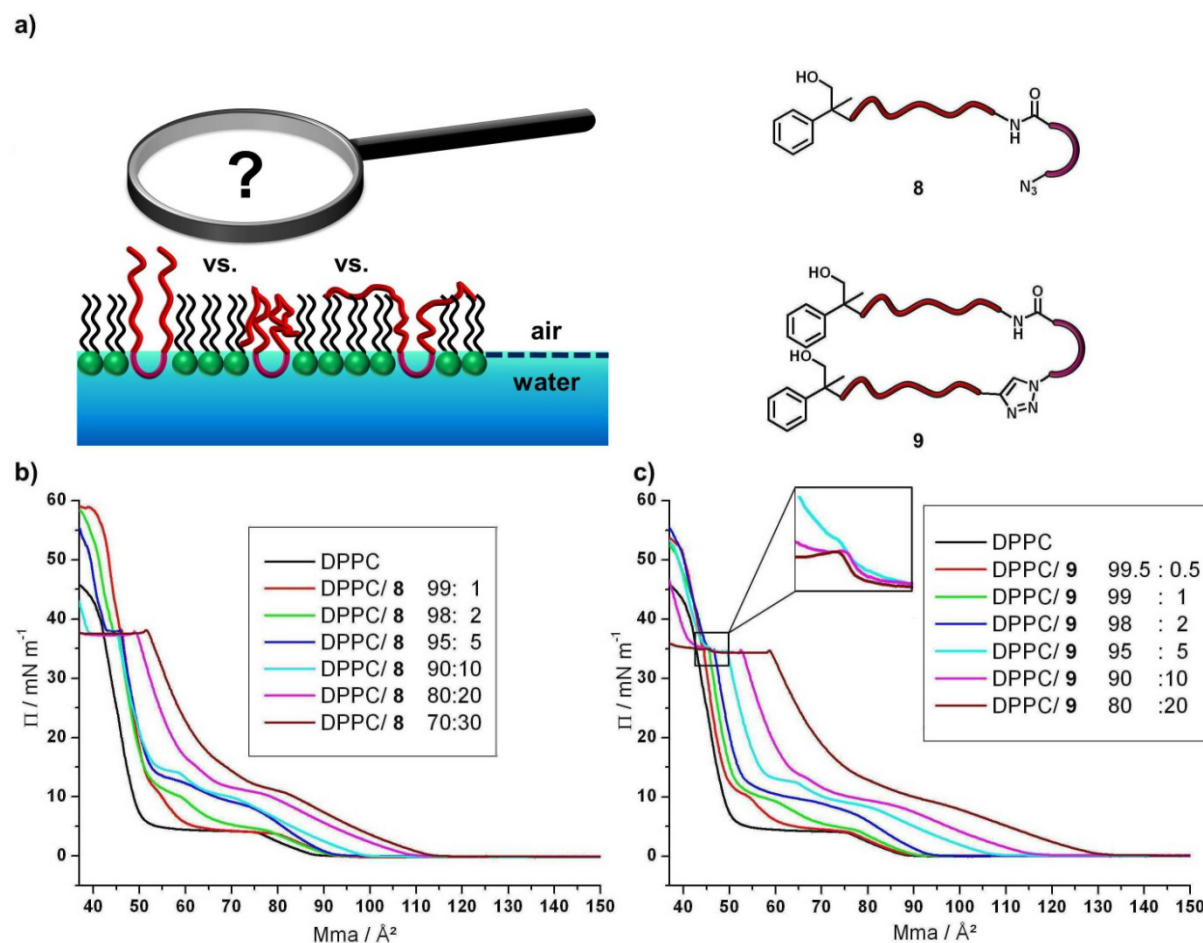
---

building blocks was successful and their purity was proven via NMR spectroscopy and ESI-ToF MS/MALDI-ToF MS the linkage of the different tailor-made building blocks towards the polymer conjugates was accomplished (Scheme 8.1). In a first step the synthesized building blocks, the  $\alpha$ -hydroxymethyl- $\omega$ -amino telechelic PIB (**3**) and the BTD **6** (bearing the azide functionality on the one side and the active carboxylic acid group on the other side), were linked via an amidation reaction using PyBOP/NMM as coupling reagents resulting the PIB-BTD **8**. To this first strand the second strand, the  $\alpha$ -hydroxymethyl- $\omega$ -alkyne telechelic PIB (**5**), was then coupled via the Cu(I)-mediated azide/alkyne-“click”-reaction<sup>168</sup> to achieve the final PIB conjugate **9** where two PIB strands are connected to the one  $\beta$ -turn mimetic BTD in a yield of 64 % (determined after column chromatography, but with traces of **8**). For ultrapure PIB conjugate **9** this crude product was further purified via preparative HPLC using HPLC graded, freshly distilled THF. The purity of the final amphiphilic polymer conjugate (**9**), having two PIB strands connected to the one  $\beta$ -turn mimetic BTD, as well as of the intermediate **8**, where one PIB chain is linked to the  $\beta$ -turn mimetic BTD, was proven by NMR spectroscopy, SEC, MALDI-ToF-MS measurements and LC/MALDI-ToF MS.

The synthetic route was repeated and modified for the use of SAA (**7**) as  $\beta$ -turn mimetic, but no equivalent amphiphilic polymer conjugate to **9** using SAA instead of BTD could be obtained.

To investigate the folding of the  $\beta$ -turn mimetic PIB conjugate **9** when incorporated into a membrane Langmuir monolayer measurements were conducted, which serve as model for half a bilayer membrane (Scheme 8.2). Therefore, mixed hybrid membranes composed of DPPC and PIB with different ratios of DPPC/PIB were extensively investigated. As comparison for folding effects the single strand **8**, where one PIB strand is connected to the  $\beta$ -turn mimetic BTD, was used. Due to the amphiphilic structure of **8** and **9** the hydrophilic  $\beta$ -turn mimetic BTD should serve as anchor in the water phase whereas the hydrophobic PIB chains should orientate along the water/air interface. To get a deeper look into the behavior of the mixed hybrid membranes during the compression of the Langmuir measurements imaging methods as epifluorescence microscopy and atomic force microscopy (AFM) were used.

The  $\Pi$ -A isotherms of the pure polymer compounds **8** and **9** showed the first increase of the pressure of the isotherm (lift-off) at  $161 \text{ \AA}^2$  respectively  $322 \text{ \AA}^2$ . This doubling of the mean molecular area (mma) value was in exact agreement with the double molecular weight of **9** in comparison to **8**. Then the surface pressures increase for both until the films collapse which was indicated by the formation of the plateaus. If these plateaus would be from literature known *roll-over* collapse where triple layers are formed then the pressure should increase after 1/3 of the starting mma value of the plateau, which is not the case.<sup>197, 198</sup> Therefore we assume, that we don't have the defined *roll-over*, but that we are “losing” material. As PIB is insoluble in water the lost material is not going into the water phase. Hysteresis experiments substantiate this and show that the amphiphilic PIB conjugates are well spread at the air-water interface. Thus, we conclude that “overlayers” are formed at the air-water interface.<sup>199</sup>



**Scheme 8.2.** Langmuir monolayer measurements. (a) folding possibilities of **9** when incorporated into a monolayer;  $\Pi$ -A isotherms of (b) DPPC/**8** mixtures and (c) DPPC/**9** mixtures at 20 °C. The black curve represents the isotherm of the pure DPPC and the different colored curves represent the different molar ratios of the DPPC/polymer mixtures.

As it can be seen in Scheme 8.2b and c the lift-off areas of the DPPC/polymer mixtures were shifted to higher mean molecular areas with higher content of **8** or **9** however they differ from the calculated values. As the experimental values of the lift-off area were smaller than the expected ones attractive lipid/polymer interactions were concluded. This behavior was already observed in our group for PIB-PEO copolymers.<sup>202</sup> In contrast to this previous work and to the isotherms of the pure compounds, two plateaus could be observed during compression, whereby with increasing content of **8** or **9** the surface pressures for these plateaus increase as well. As the transition state of the lipid monolayer (LE/LC, first plateau) is at higher pressure (up to 10 mN m<sup>-1</sup>) in comparison to pure DPPC, the amphiphilic polymer conjugates **8** or **9** strengthen the expanded phase. This means that the amphiphilic polymer molecules disturbed the rearrangement of the lipid molecules at the air-water interface due to their partial miscibility with the LE phase of the DPPC, thus hindering the lipid packing. The second plateau (up to 15 mN m<sup>-1</sup>) gave a hint for a second transition, what we believe is the new arrangement/ordering of the polymer molecules, meaning that the apolar PIB chains straighten up, but

are still tilted. This could be confirmed by further compression due to the existence of the previously titled “collapse” plateau [ $\pi = 37 \text{ mN m}^{-1}$  (for **8**) and  $\pi = 35 \text{ mN m}^{-1}$  (for **9**)] where the polymer molecules lift up from the subphase to build upper layers or squeeze out, whereby the length of this plateau was directly correlated to the mol fraction of **8** or **9**. As mentioned previously the lift-off of the pure **9** was at the double mma value as for **8** due to the doubling of the molecular weight, this phenomenon is similar to the shape of the isotherms. For example the shape of the curve of DPPC/**8** 90:10 (pale blue) is similar to the curve of DPPC/**9** 95:5 (pale blue). At these ratios the used PIB is not mol equivalent but mass equivalent. Up to this point it seemed that there are no perceptible differences whether one PIB chain is linked to the  $\beta$ -turn mimetic BTM (polymer **8**) or two PIB chains are linked to the same BTM molecule (polymer **9**). But having a deeper look into the “collapse” plateau ( $\pi = 35 \text{ mN m}^{-1}$ ) a step at an area of  $45.5 \text{ \AA}^2$  per molecule within the plateau is visible (see zoom-in region Figure 8.2c), this area is in exact agreement with the calculated area ( $45 \text{ \AA}^2$ ) which is occupied by one molecule of BTM in a liquid condensed monolayer. Therefore, the third transition could be clearly attributed to the presence of the two PIB chains on the same  $\beta$ -turn mimetic BTM and marked a transition within the  $\beta$ -turn mimetic PIB conjugate **9** which is the ordering of the chains along one  $\beta$ -turn mimetic BTM molecule.

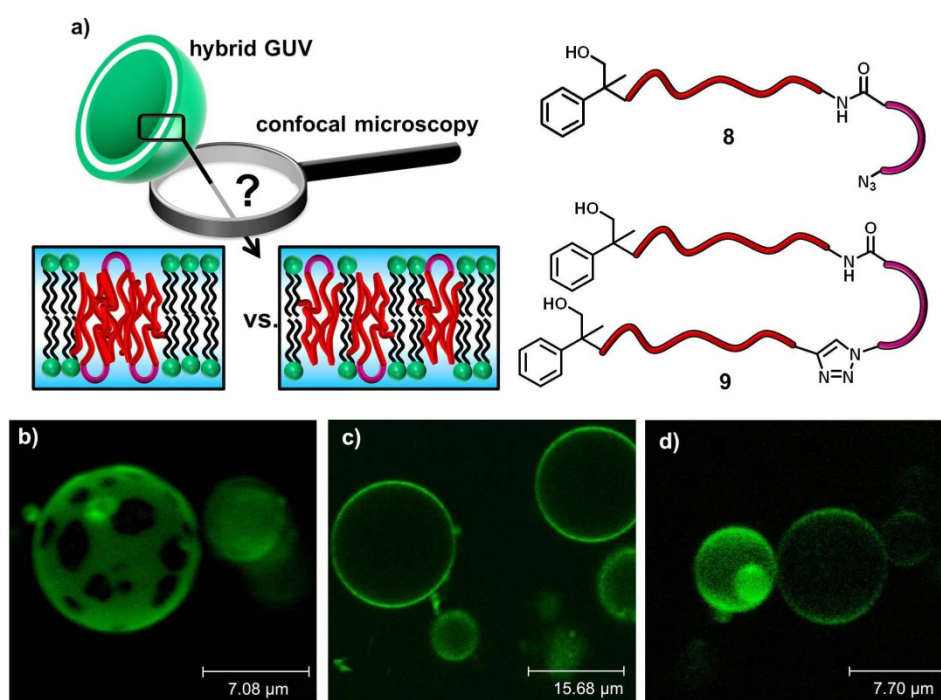
To substantiate the hypotheses from the compression isotherms and to get more information about the behavior of **8** and **9** in mixed monolayers during the compression, the Langmuir measurements were directly coupled to epifluorescence microscopy using the dye Rh-DHPE for visualization. The increase of the content of the amphiphilic polymer **8** or **9** was accompanied by the decrease of the contrast bright-dark. Therefore, the Rh-dye was soluble in both LE phases, of the DPPC and of the polymer. The first plateau showed the transition of the LE phase to the LC phase of the lipid rich domains (appearance of black propeller domains) and the second plateau showed the transition of the LE phase to the LC phase of the lipids in the polymer-mixed phase as the transitions are located at the newly formed LC DPPC/polymer/LE DPPC boundary (proceeding thinning of the propeller tips and spiraling, indicating a strong reduce in the line tension). Therefore, a partial miscibility of the amphiphilic PIB **8** or **9** with the LE phase of DPPC could be concluded.<sup>204</sup> Whereby, the phenomenon could be stronger observed using **9** which indicated increased miscibility of the amphiphilic PIB **9** with the LE phase of DPPC in comparison with its “one arm” equivalent **8**. After the second plateau an increase of the pressure up to the third plateau could be observed which we believed was the diffusion of residual lipids of the polymer rich bright domains (LE phase) into the ordered LC phases, which was visible in the shrinkage of these bright domains.

It could be shown, that both amphiphilic PIB conjugates **8** and **9** were behaving nearly similar when incorporated into a monolayer membrane using DPPC as lipid and varying the mixing ratios, but the use of epifluorescence microscopy was only helpful for the phase transitions in the low pressure region. As it could be seen from images in the Appendix, with pressures higher than  $30 \text{ mN m}^{-1}$  no differences according to contrast, shape and size of the single domains could be observed as they were

## 8. Summary

just visible as small bright dots on a dark background. But the transitions within the third plateau were at pressures around  $35 \text{ mN m}^{-1}$  and especially the step within the third plateau using **9** instead of **8** was the only difference between their compression isotherms. However, it may also mean that indeed the previously mentioned ordering of the two PIB chains linked to one  $\beta$ -turn mimetic BTD took place at this step within the third plateau.

To overcome the resolution limit AFM measurements using the Langmuir Blodgett technique were conducted, as this method could directly image the surface structure of samples at atomic height scale (here 10 nm AFM tip). Both amphiphilic PIBs, PIB **8** having one PIB chain linked to the  $\beta$ -turn mimetic BTD and PIB **9** where both PIB chains are linked on one  $\beta$ -turn mimetic BTD, show three phases at a transfer pressure of  $30 \text{ mN m}^{-1}$ , 1) disc like PIB domains out of 2) a PIB plateau which is surrounded by 3) the condensed lipid phase. With increasing pressure the PIB plateaus are vanishing and cone-like PIB domains out of the plane lipid phase are visible, whereby the maximum height (80 nm) using **9** is higher as the maximum height using **8** (60 nm). This could be explained by the better stabilizing effect of higher aggregates with elongated chains due to the linkage of two chains onto one  $\beta$ -turn mimetic BTD.



**Scheme 8.3.** Bilayer experiments. (a) possible polymer distribution of **9** when incorporated into a bilayer; Mixed GUVs analyzed via confocal microscopy using DPPC/PIB mixtures (b) DPPC/**8** (84:16), (c) DPPC/**9** (92:8) and (d) DPPC/**9** (84:16).

As the preliminary Langmuir monolayer measurements, which served as model for half a bilayer membrane, already showed slightly different behavior using  $\beta$ -turn mimetic PIB conjugate **8** (one PIB chain linked to  $\beta$ -turn mimetic BTB) or **9** (both PIB chains linked to one  $\beta$ -turn mimetic BTB), bilayer

experiments using these polymer conjugates should be conducted, too. To investigate the behavior of the conjugates (**8** or **9**) when incorporated into a more natural like membrane, mixed giant unilamellar vesicles (GUVs) were prepared as model for bilayer membranes and analyzed via confocal microscopy. However, this method only enables the investigation of the polymer distribution, whether PIB rich domains are built or the PIB is homogenously distributed in the lipid bilayer (Scheme 8.3a). The GUVs were prepared by electro formation which emerged as method of choice in our group and Rh-DHPE was used as fluorescence dye, which is known to be preferentially soluble in the less ordered phase as it is squeezed out of the more ordered liquid condensed phase.<sup>202</sup>

As mentioned previously, the amphiphilic  $\beta$ -turn mimetic PIB conjugate **9**, bearing two PIB chains on the same BTM molecule, is with regard to the mass the double of **8**. If only the mass is the determining factor of the behavior inside the membrane, then mass equivalent incorporated PIB conjugates **8** and **9** should behave similar. The monolayer investigations already showed that the behavior is similar, but there are differences, thus we can conclude that indeed the connection of two PIB chains onto the same  $\beta$ -turn mimetic leads to better mixing with the lipid molecules. This could be confirmed by the GUV experiments. Scheme 8.3b shows the confocal microscopy image of DPPC/**8** with a molar ratio of 84:16, clearly showing smooth and spherical GUVs with phase separation. However, these dark compact domains cannot be clearly assigned to the lipid-rich or polymer-rich phase as already discussed in literature.<sup>202</sup> They just mark the region of higher ordered liquid-condensed phase of the mixed DPPC/**8** bilayer from which the dye is excluded. In contrast to this, using DPPC/**9** in a molar ratio of 92:8 (Scheme 8.3c), which is the mass equivalent to DPPC/**8** 84:16, or even the same molar ratio of 84:16 (Scheme 8.3d); smooth, homogenous and spherical GUVs were formed and no phase separation could be observed. It could be shown that the amphiphilic  $\beta$ -turn mimetic PIB conjugate **9** led to more regular and stable GUVs and over the whole investigated range of different molar ratios it was miscible with the DPPC molecules as no phase separation was observed. This clearly proves that indeed the linkage of two PIB chains on the same  $\beta$ -turn unit (**9**) led to different membrane interactions than the equivalent structure just having one PIB chain (**8**).

### **Introduction of FRET dyes**

However, the investigation of the folding behavior within one  $\beta$ -turn mimetic PIB conjugate **9** when incorporated into a mono-/bilayer membrane was with the previous methods not possible thus the sophisticated and promising FRET method should be conducted. Therefore, the structure of **9** had to be adapted in such a way that both PIB chains connected to the same  $\beta$ -turn mimetic unit should bear FRET suitable dyes at the  $\alpha$ -termini. As both termini beared hydroxyl groups, dyes with carboxylic acid groups were necessary, which should be then connected via esterification onto the single strands. The dye functionalized amphiphilic  $\beta$ -turn mimetic PIB conjugate should be then incorporated into a bilayer membrane to get a deeper look into the folding of the modified PIB conjugate **9**. When both FRET dyes are in close proximity the FRET event should take place, proofing the folding of the PIB

strands due to the  $\beta$ -turn mimetic element. As the selected FRET pair (4-ethynylbenzonitrile and 9-ethynylphenanthrene) together with the “click”-reaction for the linkage of these dyes onto proteins was known in literature<sup>209</sup>, we decided to use these dyes in a modified way. Moreover, we have chosen these dyes as they should be embedded in the less polar bilayer-water interface (between the polar head group region and the hydrophobic core).<sup>210</sup> If we would have chosen more hydrophilic dyes they would be embedded in the polar head group region and contrary more hydrophobic dyes would be incorporated in the hydrophobic core region, but these pushing/pulling effects of the dyes we wanted to avoid as their sole function should be the imaging of the folding process.

As the syntheses of the FRET donor (**11**) and the FRET acceptor (**12**) turned out well (analyzed via ESI-ToF MS and NMR) they were linked via esterification to the single PIB chains **3** respectively **5** achieving the single strands **13** (FRET donor labeled PIB) and **15** (FRET acceptor labeled PIB). The successful linkage and their purities were proven via SEC, MALDI-ToF MS and NMR. Although the synthesis of the equivalent to **8** (**14**), the FRET donor labeled PIB chain connected to the  $\beta$ -turn mimetic BTD via amidation, was successful, **14** could not be isolated. Moreover, the last step, the “click”-reaction of the single strands **14** and **15** to build up the dye labeled amphiphilic polymer conjugate containing BTD as  $\beta$ -turn mimetic (**16**, FRET dye labeled equivalent to **9**) unfortunately failed. This evidenced again that the linkage on such constrained structure (**14**) is not trivial.

Therefore, only preliminary experiments concerning fluorescence spectroscopy could be conducted using the dye labeled polymeric intermediates **13** and **15** in mixed DPPC/polymer vesicles. Such preliminary FRET experiments clearly showed that they are strongly dependent on the type of mixing of the vesicles (mixing vesicles containing **13** and **15** in the same vesicle or mixing of vesicles containing separately **13** or **15**) as well as on the temperature (below or above the transition temperature of DPPC).

### **Elongation of the hydrophilic part**

Beside the introduction of FRET suitable dyes we were interested in a variation of the amphiphilic polymer conjugate **9** by elongation of the hydrophilic part. This hydrophilic part should be placed between the hydrophobic PIB and the hydrophilic beta-turn. Via living carbocationic polymerization using  $\alpha$ -methylstyrene epoxide (MSE, **1**) as initiator and 3-bromopropoxybenzene (BPB) as quencher, followed by conversion from the bromine to the azide group well defined hydrophobic  $\alpha$ -hydroxy- $\omega$ -azido telechelic PIB (**18**,  $M_n \sim 4000$  g/mol, PDI = 1.3) was synthesized.<sup>144</sup> For the hydrophilic building blocks biocompatible tetraethylene glycol (TEG) derivatives were synthesized by the transformation of tetraethylene glycol into the needed structures [ $\alpha,\omega$ -dialkynyl tetraethylene glycol (**19**) and  $\alpha$ -alkynyl-  $\omega$ -amino tetraethylene glycol (**21**)]. For the last building blocks - the  $\beta$ -turn mimetic building blocks - the already synthesized BTD (**6**) and SAA (**7**) could be used. As the synthesis of the different building blocks (**6**, **7**, **18**, **19** and **21**) was successful and their purities were proven via NMR, ESI-ToF MS or SEC, they could be linked to achieve the  $\beta$ -turn mimetic amphiphilic block “copolymers”.

## 8. Summary

---

Therefore, the copper mediated azide/alkyne-”click”-reaction and the amidation reaction should be used. A lot of possibilities for linking the different building blocks were existent; it could be done either sequentially or by the synthesis of two single strands which were coupled together in a last step. Finally, the synthesis of the complete  $\beta$ -turn mimetic amphiphilic block “copolymer” (**27**) using BTD (**6**) as  $\beta$ -turn mimetic was successful, but with an overall yield of just 4 % for the linking steps. Moreover, the obtained product could not be purified, thus unreacted starting material was left. Also here again the synthesis of a complete  $\beta$ -turn mimetic amphiphilic block “copolymer” using SAA (**7**) as  $\beta$ -turn mimetic failed. Therefore, further experiments investigating the influence of the elongation of the hydrophilic part could not be conducted.

In this work it could be shown that the linkage of polymer chains onto constrained structures as the  $\beta$ -turn mimetic elements [BTD (**6**) or SAA (**7**)] is quiet challenging. Even small variations at the structures a) the use of **6** instead of **7** as  $\beta$ -turn mimetic, b) the introduction of FRET suitable dyes (**11** and **12**) at the  $\alpha$ -termini of the PIB strands or c) elongation of the hydrophilic part using TEG derivatives (**19** and **21**) lead to problems of purification of the final products or even the synthesis of the complete structure failed. However, the incorporation of PIB **8** having one PIB chain linked to the  $\beta$ -turn mimetic BTD and PIB **9** where both PIB chains are linked on one  $\beta$ -turn mimetic BTD into DPPC mono- and bilayers reveal a deeper insight into the behavior of amphiphilic  $\beta$ -turn mimetic polymer conjugates and their folding. Moreover, this work opens the possibility for further investigations and questions.



## 9. Literature

1. Gellman, S. H., Foldamers: A Manifesto. *Acc. Chem. Res.* **1998**, 31, (4), 173-180.
2. Hill, D. J.; Mio, M. J.; Prince, R. B.; Hughes, T. S.; Moore, J. S., A Field Guide to Foldamers. *Chem. Rev.* **2001**, 101, (12), 3893-4012.
3. <https://www.genome.gov/glossary/resources/protein.pdf> 2015-08-20, 14:30.
4. <http://www.mpg.de/7557013/proteinfaltung> Die Grundlagen der Proteinfaltung, 2015-08-10, 20:55.
5. <https://scimedia.files.wordpress.com/2011/02/fi6p3.gif> Drawing by Irwing Geis, 2015-08-19, 19:55.
6. Balbach, J., In Vorlesung Biophysik, WS 2014/15.
7. Cox, M.; Doudna, J.; O'Donnell, M., *Molecular Biology: Principles and Practice*. New York, 2011.
8. Mathews, C. K.; van Holde, K. E.; Ahern, K. G., *Biochemistry*. 3<sup>rd</sup> ed.; Adison Wesley Longman, Inc. Benjamin/Cummings: 2000.
9. Ramachandran, G. N.; Ramakrishnan, C.; Sasisekharan, V., Stereochemistry of polypeptide chain configurations. *J. Mol. Biol.* **1963**, 7, (1), 95-99.
10. Corey, R. B.; Pauling, L., Fundamental dimensions of polypeptide chains. *P. Roy. Soc. B Bio.* **1953**, 141, (902), 10-20.
11. Edison, A. S., Linus Pauling and the planar peptide bond. *Nat. Struct. Mol. Biol.* **2001**, 8, (3), 201-202.
12. Dill, K. A.; Ozkan, S. B.; Shell, M. S.; Weikl, T. R., The Protein Folding Problem. *Annu. Rev. Biophys.* **2008**, 37, (1), 289-316.
13. <http://bc.biochemtech.uni-halle.de/lehre/struct/02-kraefte.pdf> 2015-08-20, 9:49.
14. Dill, K. A.; MacCallum, J. L., The Protein-Folding Problem, 50 Years On. *Science* **2012**, 338, (6110), 1042-1046.
15. Saraogi, I.; Hamilton, A. D., Recent advances in the development of aryl-based foldamers. *Chem. Soc. Rev.* **2009**, 38, (6), 1726-1743.
16. Levinthal, C., *J.Chim.Phys.* **1968**, 65, 44-45.
17. Zwanzig, R.; Szabo, A.; Bagchi, B., Levinthal's paradox *Proc. Natl. Acad. Sci. U S A* **1992**, 89, (1), 20-22.
18. Jackson, S. E., How do small single-domain proteins fold? *Fold. Des.* **1998**, 3, (4), R81-R91.
19. Watson, J. D.; Crick, F. H. C., Molecular Structure of Nucleic Acids: A Structure for Deoxyribose Nucleic Acid. *Nature* **1953**, 171, (4356), 737-738.
20. <http://www.britannica.com/science/DNA-sequencing> 2015-08-20, 15:26.
21. Arnott, S.; Chandrasekaran, R.; Birdsall, D. L.; Leslie, A. G. W.; Ratliff, R. L., Left-handed DNA helices. *Nature* **1980**, 283, (5749), 743-745.
22. R. Langridge, D. A. M., W.E. Seeds, H.R. Wilson, C.W. Hooper, M.H.F. Wilkins, *J. Mol. Biol.* **1969**, 2, 28-64.
23. Pohl, F. M., Polymorphism of a synthetic DNA in solution. *Nature* **1976**, 260, (5549), 365-366.
24. Wang, A. H. J.; Quigley, G. J.; Kolpak, F. J.; Crawford, J. L.; van Boom, J. H.; van der Marel, G.; Rich, A., Molecular structure of a left-handed double helical DNA fragment at atomic resolution. *Nature* **1979**, 282, (5740), 680-686.
25. Wing, R.; Drew, H.; Takano, T.; Broka, C.; Tanaka, S.; Itakura, K.; Dickerson, R. E., Crystal structure analysis of a complete turn of B-DNA. *Nature* **1980**, 287, (5784), 755-758.
26. Mandelkern, M.; Elias, J. G.; Eden, D.; Crothers, D. M., The dimensions of DNA in solution. *J. Mol. Biol.* **1981**, 152, (1), 153-161.
27. Gregory, S. G.; et al., The DNA sequence and biological annotation of human chromosome 1. *Nature* **2006**, 441, (7091), 315-321.
28. <http://www.merriam-webster.com/dictionary/biomimetics> 2015-08-17, 19:29.
29. Channon, K.; Bromley, E. H. C.; Woolfson, D. N., Synthetic biology through biomolecular design and engineering. *Curr. Opin. Struct. Biol.* **2008**, 18, (4), 491-498.

30. Lehn, J.-M., Supramolekulare Chemie – Moleküle, Übermoleküle und molekulare Funktionseinheiten (Nobel-Vortrag). *Angew. Chem.* **1988**, 100, (1), 91-116.
31. <http://www.nobelpreis.org/chemie/lehn.html>, 2015-08-26, 19:32.
32. Lindoy, L. F.; Richardson, C.; Clegg, J. K., Bioinspired Self-Assembly I: Self-Assembled Structures. In *Bioinspiration and Biomimicry in Chemistry*, Swiegers, G. F., Ed. John Wiley & Sons, Inc.: 2012; pp 17-46.
33. Desiraju, G. R., Chemistry beyond the molecule. *Nature* **2001**, 412, (6845), 397-400.
34. Gellman, S., Foldamers. Structure, Properties, and Applications. Edited by Stefan Hecht and Ivan Huc. *Angew. Chem. Int. Edit.* **2008**, 47, (4), 632-633.
35. Goodman, C. M.; Choi, S.; Shandler, S.; DeGrado, W. F., Foldamers as versatile frameworks for the design and evolution of function. *Nat. Chem. Biol.* **2007**, 3, (5), 252-262.
36. Czyzewski, A. M.; Barron, A. E., Protein and peptide biomimicry: Gold-mining inspiration from Nature's ingenuity. *AIChE J.* **2008**, 54, (1), 2-8.
37. Dado, G. P.; Gellman, S. H., Intramolecular Hydrogen Bonding in Derivatives of .beta.-Alanine and .gamma.-Amino Butyric Acid; Model Studies for the Folding of Unnatural Polypeptide Backbones. *J. Am. Chem. Soc.* **1994**, 116, (3), 1054-1062.
38. Appella, D. H.; Christianson, L. A.; Klein, D. A.; Powell, D. R.; Huang, X.; Barchi, J. J.; Gellman, S. H., Residue-based control of helix shape in  $\beta$ -peptide oligomers. *Nature* **1997**, 387, (6631), 381-384.
39. Iverson, B., Betas are brought into the fold. *Nature* **1997**, 385, (6612), 113-115.
40. Seebach, D.; Hook, D. F.; Glättli, A., Helices and other secondary structures of  $\beta$ - and  $\gamma$ -peptides. *Pept. Sci.* **2006**, 84, (1), 23-37.
41. Cheng, R. P., Beyond de novo protein design - de novo design of non-natural folded oligomers. *Curr. Opin. Struct. Biol.* **2004**, 14, (4), 512-520.
42. Bouillère, F.; Thetiot-Laurent, S.; Kouklovsky, C.; Alezra, V., Foldamers containing  $\gamma$ -amino acid residues or their analogues: structural features and applications. *Amino Acids* **2011**, 41, (3), 687-707.
43. Wu, C. W.; Kirshenbaum, K.; Sanborn, T. J.; Patch, J. A.; Huang, K.; Dill, K. A.; Zuckermann, R. N.; Barron, A. E., Structural and Spectroscopic Studies of Peptoid Oligomers with  $\alpha$ -Chiral Aliphatic Side Chains. *J. Am. Chem. Soc.* **2003**, 125, (44), 13525-13530.
44. Drexler, K. E., Peptoids at the 7th Summit: Toward macromolecular systems engineering. *Pept. Sci.* **2011**, 96, (5), 537-544.
45. Nam, K. T.; Shelby, S. A.; Choi, P. H.; Marciel, A. B.; Chen, R.; Tan, L.; Chu, T. K.; Mesch, R. A.; Lee, B.-C.; Connolly, M. D.; Kisielowski, C.; Zuckermann, R. N., Free-floating ultrathin two-dimensional crystals from sequence-specific peptoid polymers. *Nat. Mater.* **2010**, 9, (5), 454-460.
46. Yoo, B.; Shin, S. B. Y.; Huang, M. L.; Kirshenbaum, K., Peptoid Macrocycles: Making the Rounds with Peptidomimetic Oligomers. *Chem. Eur. J.* **2009**, 16, (19), 5528-5537.
47. Horne, W. S.; Gellman, S. H., Foldamers with Heterogeneous Backbones. *Acc. Chem. Res.* **2008**, 41, (10), 1399-1408.
48. Sewald, N., Editorial to the Special Issue Foldamers. *Amino Acids* **2011**, 41, (3), 537-539.
49. Pilsl, L. A.; Reiser, O.,  $\alpha/\beta$ -Peptide foldamers: state of the art. *Amino Acids* **2011**, 41, (3), 709-718.
50. Martinek, T. A.; Fulop, F., Peptidic foldamers: ramping up diversity. *Chem. Soc. Rev.* **2012**, 41, (2), 687-702.
51. Epand, R. F.; Mowery, B. P.; Lee, S. E.; Stahl, S. S.; Lehrer, R. I.; Gellman, S. H.; Epand, R. M., Dual Mechanism of Bacterial Lethality for a Cationic Sequence-Random Copolymer that Mimics Host-Defense Antimicrobial Peptides. *J. Mol. Biol.* **2008**, 379, (1), 38-50.
52. Liu, D.; DeGrado, W. F., De Novo Design, Synthesis, and Characterization of Antimicrobial  $\beta$ -Peptides. *J. Am. Chem. Soc.* **2001**, 123, (31), 7553-7559.
53. Gelman, M. A.; Richter, S.; Cao, H.; Umezawa, N.; Gellman, S. H.; Rana, T. M., Selective Binding of TAR RNA by a Tat-Derived  $\beta$ -Peptide. *Org. Lett.* **2003**, 5, (20), 3563-3565.
54. Imamura, Y.; Watanabe, N.; Umezawa, N.; Iwatsubo, T.; Kato, N.; Tomita, T.; Higuchi, T., Inhibition of  $\gamma$ -Secretase Activity by Helical  $\beta$ -Peptide Foldamers. *J. Am. Chem. Soc.* **2009**, 131, (21), 7353-7359.

55. Nair, R. V.; Vijayadas, K. N.; Roy, A.; Sanjayan, G. J., Heterogeneous Foldamers from Aliphatic–Aromatic Amino Acid Building Blocks: Current Trends and Future Prospects. *Eur. J. Org. Chem.* **2014**, 2014, (35), 7763-7780.
56. Roy, A.; Prabhakaran, P.; Baruah, P. K.; Sanjayan, G. J., Diversifying the structural architecture of synthetic oligomers: the hetero foldamer approach. *Chem. Commun.* **2011**, 47, (42), 11593-11611.
57. Jones, C. R.; Qureshi, M. K. N.; Truscott, F. R.; Hsu, S.-T. D.; Morrison, A. J.; Smith, M. D., A Nonpeptidic Reverse Turn that Promotes Parallel Sheet Structure Stabilized by C–H···O Hydrogen Bonds in a Cyclopropane  $\gamma$ -Peptide. *Angew. Chem* **2008**, 47, (37), 7099-7102.
58. Nair, R. V.; Sanjayan, G. J., (Thio)urea-mediated benzoxazinone opening: mild approach towards synthesis of o-(substituted amido)benzamides. *RSC Adv.* **2014**, 4, (14), 7058-7061.
59. Thorat, V. H.; Ingole, T. S.; Vijayadas, K. N.; Nair, R. V.; Kale, S. S.; Ramesh, V. V. E.; Davis, H. C.; Prabhakaran, P.; Gonnade, R. G.; Gawade, R. L.; Puranik, V. G.; Rajamohanam, P. R.; Sanjayan, G. J., The Ant-Pro Reverse-Turn Motif. Structural Features and Conformational Characteristics. *Eur. J. Org. Chem.* **2013**, 2013, (17), 3529-3542.
60. Srinivas, D.; Gonnade, R.; Ravindranathan, S.; Sanjayan, G. J., Conformationally Constrained Aliphatic–Aromatic Amino-Acid-Conjugated Hybrid Foldamers with Periodic  $\beta$ -Turn Motifs. *J. Org. Chem.* **2007**, 72, (18), 7022-7025.
61. Prabhakaran, P.; Kale, S. S.; Puranik, V. G.; Rajamohanam, P. R.; Chetina, O.; Howard, J. A. K.; Hofmann, H.-J.; Sanjayan, G. J., Sequence-Specific Unusual (1 $\rightarrow$ 2)-Type Helical Turns in  $\alpha/\beta$ -Hybrid Peptides. *J. Am. Chem. Soc.* **2008**, 130, (52), 17743-17754.
62. Sanchez-Garcia, D.; Kauffmann, B.; Kawanami, T.; Ihara, H.; Takafuji, M.; Delville, M.-H.; Huc, I., Nanosized Hybrid Oligoamide Foldamers: Aromatic Templates for the Folding of Multiple Aliphatic Units. *J. Am. Chem. Soc.* **2009**, 131, (24), 8642-8648.
63. Prins, L. J.; Timmerman, P.; Reinhoudt, D. N., Amplification of Chirality: The "Sergeants and Soldiers" Principle Applied to Dynamic Hydrogen-Bonded Assemblies; *J. Am. Chem. Soc.* **2001**, 123, (42), 10153-10163.
64. Hamuro, Y.; Geib, S. J.; Hamilton, A. D., Novel Folding Patterns in a Family of Oligoanthranilamides: Non-Peptide Oligomers That Form Extended Helical Secondary Structures. *J. Am. Chem. Soc.* **1997**, 119, (44), 10587-10593.
65. Srinivas, D.; Gonnade, R.; Rajamohanam, P. R.; Sanjayan, G. J., Pre-organization-mediated macrocyclization: efficient synthesis and structural investigations of BINOL-m-phenylenediamine-derived macrocycles. *Tetrahedron Lett.* **2008**, 49, (13), 2139-2142.
66. Nair, R. V.; Kotmale, A. S.; Dhokale, S. A.; Gawade, R. L.; Puranik, V. G.; Rajamohanam, P. R.; Sanjayan, G. J., Formation of a pseudo- $\beta$ -hairpin motif utilizing the Ant-Pro reverse turn: consequences of stereochemical reordering. *Org. Biomol. Chem.* **2013**, 12, (5), 774-782.
67. Nowick, J. S., Exploring  $\beta$ -Sheet Structure and Interactions with Chemical Model Systems. *Acc. Chem. Res.* **2008**, 41, (10), 1319-1330.
68. Kemp, D. S.; Bowen, B. R.; Muendel, C. C., Synthesis and conformational analysis of epindolidione-derived peptide models for  $\beta$ -sheet formation. *J. Org. Chem.* **1990**, 55, (15), 4650-4657.
69. Cheng, P.-N.; Nowick, J. S., Giant Macrolactams Based on  $\beta$ -Sheet Peptides. *J. Org. Chem.* **2011**, 76, (9), 3166-3173.
70. Holub, J. M.; Kirshenbaum, K., Tricks with clicks: modification of peptidomimetic oligomers via copper-catalyzed azide-alkyne [3 + 2] cycloaddition. *Chem. Soc. Rev.* **2010**, 39, (4), 1325-1337.
71. Kočalka, P.; El-Sagheer, A. H.; Brown, T., Rapid and Efficient DNA Strand Cross-Linking by Click Chemistry. *Chem. Bio. Chem* **2008**, 9, (8), 1280-1285.
72. El-Sagheer, A. H.; Brown, T., Synthesis and Polymerase Chain Reaction Amplification of DNA Strands Containing an Unnatural Triazole Linkage. *J. Am. Chem. Soc.* **2009**, 131, (11), 3958-3964.
73. Horne, W. S.; Yadav, M. K.; Stout, C. D.; Ghadiri, M. R., Heterocyclic Peptide Backbone Modifications in an  $\alpha$ -Helical Coiled Coil. *J. Am. Chem. Soc.* **2004**, 126, (47), 15366-15367.

74. Caumes, C.; Roy, O.; Faure, S.; Taillefumier, C., The Click Triazolium Peptoid Side Chain: A Strong cis-Amide Inducer Enabling Chemical Diversity. *J. Am. Chem. Soc.* **2012**, 134, (23), 9553-9556.
75. Oh, K.; Guan, Z., A convergent synthesis of new  $\beta$ -turn mimics by click chemistry. *Chem. Commun.* **2006**, (29), 3069-3071.
76. Yi, H.-P.; Li, C.; Hou, J.-L.; Jiang, X.-K.; Li, Z.-T., Hydrogen-bonding-induced oligoantranilamide foldamers. Synthesis, characterization, and complexation for aliphatic ammonium ions. *Tetrahedron* **2005**, 61, (33), 7974-7980.
77. Berl, V.; Huc, I.; Khoury, R. G.; Krische, M. J.; Lehn, J.-M., Interconversion of single and double helices formed from synthetic molecular strands. *Nature* **2000**, 407, (6805), 720-723.
78. Huc, I., Aromatic Oligoamide Foldamers. *Eur. J. Org. Chem.* **2004**, 2004, (1), 17-29.
79. Doerksen, R. J.; Chen, B.; Liu, D.; Tew, G. N.; DeGrado, W. F.; Klein, M. L., Controlling the Conformation of Arylamides: Computational Studies of Intramolecular Hydrogen Bonds between Amides and Ethers or Thioethers. *Chem. Eur. J.* **2004**, 10, (20), 5008-5016.
80. Tang, H.; Doerksen, R. J.; Jones, T. V.; Klein, M. L.; Tew, G. N., Biomimetic Facially Amphiphilic Antibacterial Oligomers with Conformationally Stiff Backbones. *Chem. Biol.* **2006**, 13, (4), 427-435.
81. Sebaoun, L.; Maurizot, V.; Granier, T.; Kauffmann, B.; Huc, I., Aromatic Oligoamide  $\beta$ -Sheet Foldamers. *J. Am. Chem. Soc.* **2014**, 136, (5), 2168-2174.
82. Arnt, L.; Rennie, J. R.; Linser, S.; Willumeit, R.; Tew, G. N., Membrane Activity of Biomimetic Facially Amphiphilic Antibiotics. *J. Phys. Chem. B* **2006**, 110, (8), 3527-3532.
83. Zhao, X.; Li, Z.-T., Hydrogen bonded aryl amide and hydrazide oligomers: a new generation of preorganized soft frameworks. *Chem. Commun.* **2010**, 46, (10), 1601-1616.
84. Stone, M. T.; Moore, J. S., A Water-Soluble m-Phenylene Ethynylene Foldamer. *Org. Lett.* **2004**, 6, (4), 469-472.
85. Ni, B.-B.; Yan, Q.; Ma, Y.; Zhao, D., Recent advances in arylene ethynylene folding systems: Toward functioning. *Coord. Chem. Rev.* **2010**, 254, (9/10), 954-971.
86. Guichard, G.; Huc, I., Synthetic foldamers. *Chem. Commun.* **2011**, 47, (21), 5933-5941.
87. Altintas, O.; Barner-Kowollik, C., Single Chain Folding of Synthetic Polymers by Covalent and Non-Covalent Interactions: Current Status and Future Perspectives. *Macromol. Rapid Commun.* **2012**, 33, (11), 958-971.
88. Tew, G. N.; Scott, R. W.; Klein, M. L.; DeGrado, W. F., De Novo Design of Antimicrobial Polymers, Foldamers, and Small Molecules: From Discovery to Practical Applications. *Acc. Chem. Res.* **2010**, 43, (1), 30-39.
89. Nolte, R. J. M.; Van Beijnen, A. J. M.; Drenth, W., Chirality in polyisocyanides. *J. Am. Chem. Soc.* **1974**, 96, (18), 5932-5933.
90. Kollmar, C.; Hoffmann, R., Polyisocyanides: electronic or steric reasons for their presumed helical structure? *J. Am. Chem. Soc.* **1990**, 112, (23), 8230-8238.
91. Deike, S. Synthesis of helical polymers via titanium-catalyzed insertion polymerization. Martin-Luther-University Halle-Wittenberg, Halle, 2014.
92. Lu, J.; ten Brummelhuis, N.; Weck, M., Intramolecular folding of triblock copolymers via quadrupole interactions between poly(styrene) and poly(pentafluorostyrene) blocks. *Chem. Commun.* **2014**, 50, (47), 6225-6227.
93. Altintas, O.; Krolla-Sidenstein, P.; Gliemann, H.; Barner-Kowollik, C., Single-Chain Folding of Diblock Copolymers Driven by Orthogonal H-Donor and Acceptor Units. *Macromolecules* **2014**, 47, (17), 5877-5888.
94. Hosono, N.; Gillissen, M. A. J.; Li, Y.; Sheiko, S. S.; Palmans, A. R. A.; Meijer, E. W., Orthogonal Self-Assembly in Folding Block Copolymers. *J. Am. Chem. Soc.* **2013**, 135, (1), 501-510.
95. Cho, H.; Zhao, Y., Environmental Effects Dominate the Folding of Oligocholates in Solution, Surfactant Micelles, and Lipid Membranes. *J. Am. Chem. Soc.* **2010**, 132, (28), 9890-9899.
96. Zhang, S.; Zhao, Y., Oligocholate Foldamers as Carriers for Hydrophilic Molecules across Lipid Bilayers. *Chem. Eur. J.* **2011**, 17, (44), 12444-12451.
97. Zhang, S.; Zhao, Y., Effects of Micelle Properties on the Conformation of Oligocholates and Importance of Rigidity of Foldamers. *J. Org. Chem.* **2012**, 77, (1), 556-562.

98. Zhao, Y.; Cho, H.; Widanapathirana, L.; Zhang, S., Conformationally Controlled Oligocholate Membrane Transporters: Learning through Water Play. *Acc. Chem. Res.* **2013**.
99. Zhang, S.; Zhao, Y., Flexible oligocholate foldamers as membrane transporters and their guest-dependent transport mechanism. *Org. Biomol. Chem.* **2012**, 10, (2), 260-266.
100. Gunasekara, R. W.; Zhao, Y., Conformationally Switchable Water-Soluble Fluorescent Bischolate Foldamers as Membrane-Curvature Sensors. *Langmuir* **2015**, 31, (13), 3919-3925.
101. Souers, A. J.; Ellman, J. A.,  $\beta$ -Turn mimetic library synthesis: scaffolds and applications. *Tetrahedron* **2001**, 57, (35), 7431-7448.
102. Kabsch, W.; Sander, C., Dictionary of protein secondary structure: Pattern recognition of hydrogen-bonded and geometrical features. *Biopolymers* **1983**, 22, (12), 2577-2637.
103. Ball, J. B.; Alewood, P. F., Conformational constraints: Nonpeptide  $\beta$ -turn mimics. *J. Mol. Recognit.* **1990**, 3, (2), 55-64.
104. Schneider, J. P.; Kelly, J. W., Templates That Induce  $\alpha$ -Helical,  $\beta$ -Sheet, and Loop Conformations. *Chem. Rev.* **1995**, 95, (6), 2169-2187.
105. Freidinger, R. M.; Perlow, D. S.; Veber, D. F., Protected lactam-bridged dipeptides for use as conformational constraints in peptides. *J. Org. Chem.* **1982**, 47, (1), 104-109.
106. Diaz, H.; Espina, J. R.; Kelly, J. W., A dibenzofuran-based amino acid designed to nucleate antiparallel  $\beta$ -sheet structure: evidence for intramolecular hydrogen-bond formation. *J. Am. Chem. Soc.* **1992**, 114, (21), 8316-8318.
107. Geyer, A.; Bockelmann, D.; Weissenbach, K.; Fischer, H., Synthesis and structure of a hydrophilic  $\beta$ -turn mimetic. *Tetrahedron Lett.* **1999**, 40, (3), 477-478.
108. Graf von Roedern, E.; Lohof, E.; Hessler, G.; Hoffmann, M.; Kessler, H., Synthesis and Conformational Analysis of Linear and Cyclic Peptides Containing Sugar Amino Acids. *J. Am. Chem. Soc.* **1996**, 118, (42), 10156-10167.
109. Ziegler, T.; Hermann, C., Synthesis of novel multidentate carbohydrate-triazole ligands. *Tetrahedron Lett.* **2008**, 49, (13), 2166-2169.
110. Schneider, J. P.; Kelly, J. W., Synthesis and Efficacy of Square Planar Copper Complexes Designed to Nucleate  $\beta$ -Sheet Structure. *J. Am. Chem. Soc.* **1995**, 117, (9), 2533-2546.
111. Kräutler, V.; Aemissegger, A.; Hünenberger, P. H.; Hilvert, D.; Hansson, T.; van Gunsteren, W. F., Use of Molecular Dynamics in the Design and Structure Determination of a Photoinducible  $\beta$ -Hairpin. *J. Am. Chem. Soc.* **2005**, 127, (13), 4935-4942.
112. Freidinger, R. M.; Veber, D. F.; Perlow, D. S.; Brooks, J. R.; Saperstein, R., Bioactive conformation of luteinizing hormone-releasing hormone: evidence from a conformationally constrained analog. *Science* **1980**, 210, (4470), 656-658.
113. Geyer, A.; Moser, F., Polyol Peptidomimetics. *Eur. J. Org. Chem.* **2000**, 2000, (7), 1113-1120.
114. Tremmel, P.; Geyer, A., An Oligomeric Ser-Pro Dipeptide Mimetic Assuming the Polyproline II Helix Conformation. *J. Am. Chem. Soc.* **2002**, 124, (29), 8548-8549.
115. Tremmel, P.; Geyer, A., Coupled Hydrogen-Bonding Networks in Polyhydroxylated Peptides. *Angew. Chem. Int. Ed.* **2004**, 43, (43), 5789-5791.
116. Fischer, D.; Geyer, A., NMR spectroscopic characterization of the membrane affinity of polyols. *Magn. Reson. Chem.* **2005**, 43, (11), 893-901.
117. calculated distance between the functional moieties using Chem3D Ultra 8.0.
118. Chow, H.-F.; Lau, K.-N.; Ke, Z.; Liang, Y.; Lo, C.-M., Conformational and supramolecular properties of main chain and cyclic click oligotriazoles and polytriazoles. *Chem. Commun.* **2010**, 46, (20), 3437-3453.
119. Hughes, R. M.; Waters, M. L., Model systems for  $\beta$ -hairpins and  $\beta$ -sheets. *Curr. Opin. Struct. Biol.* **2006**, 16, (4), 514-524.
120. Doran, T. M.; Anderson, E. A.; Latchney, S. E.; Opanashuk, L. A.; Nilsson, B. L., An Azobenzene Photoswitch Sheds Light on Turn Nucleation in Amyloid- $\beta$  Self-Assembly. *ACS Chem. Neurosci.* **2012**, 3, (3), 211-220.
121. Lee, S.; Flood, A. H., Photoresponsive receptors for binding and releasing anions. *J. Phys. Org. Chem.* **2012**, n/a-n/a.
122. Gobbo, C.; Li, M.; Mali, K. S.; van Esch, J. H.; De Feyter, S., Preprogrammed 2D Folding of Conformationally Flexible Oligoamides: Foldamers with Multiple Turn Elements. *ACS Nano* **2012**.

123. Li, M.; Gobbo, C.; De Cat, I.; Eelkema, R.; Vanaverbeke, B.; Lazzaroni, R.; De Feyter, S.; van Esch, J., Molecular Patterning at a Liquid/Solid Interface: The Foldamer Approach. *Langmuir* **2011**, 27, (22), 13598-13605.
124. Dennison, S. R.; Snape, T. J.; Phoenix, D. A., Thermodynamic interactions of a cis and trans benzanilide with Escherichia coli bacterial membranes. *Eur. Biophys. J.* **2012**, 41, (8), 687-693.
125. Dennison, S. R.; Akbar, Z.; Phoenix, D. A.; Snape, T. J., Interactions between suitably functionalised conformationally distinct benzanilides and phospholipid monolayers. *Soft Matter* **2012**, 8, (11), 3258-3264.
126. Dennison, S. R.; Morton, L. H. G.; Shorrocks, A. J.; Harris, F.; Phoenix, D. A., A study on the interactions of Aurein 2.5 with bacterial membranes. *Colloids Surf., B* **2009**, 68, (2), 225-230.
127. Bollenback, G. N.; Long, J. W.; Benjamin, D. G.; Lindquist, J. A., The Synthesis of Aryl-D-glucopyranosiduronic Acids. *J. Am. Chem. Soc.* **1955**, 77, (12), 3310-3315.
128. Chiba, T.; Sina, P., Application of a radical reaction to the synthesis of l-iduronic acid derivatives from d-glucuronic acid analogues. *Carbohydrate Research* **1986**, 151, (0), 379-389.
129. Tropper, F. o. D.; Andersson, F. O.; Braun, S. p.; Roy, R., Phase Transfer Catalysis as a General and Stereoselective Entry into Glycosyl Azides from Glycosyl Halides. *Synthesis* **1992**, 1992, (07), 618,620.
130. Wilkinson, B. L.; Bornaghi, L. F.; Houston, T. A.; Poulsen, S.-A.; Healy, P. C., Methyl 2,3,4-tri-O-acetyl-1-azido-1-deoxy- $\beta$ -d-glucopyranuronate at room temperature. *Acta Crystallogr. E* **2005**, 61, (3), o738-o740.
131. Puskas, J. E.; Kaszas, G., Living carbocationic polymerization of resonance-stabilized monomers. *Prog. Polym. Sci.* **2000**, 25, (3), 403-452.
132. Puskas, J.; Kaszas, G.; Kennedy, J. P.; Kelen, T.; Tüdös, F., Quasiliving Carbocationic Polymerization. III. Quasiliving Polymerization of Isobutylene. *J. Macromol. Sci., Part A* **1982**, 18, (9), 1229 - 1244.
133. Kennedy, J. P., Living cationic polymerization of olefins. How did the discovery come about? *J. Polym. Sci., Part A: Polym. Chem.* **1999**, 37, (14), 2285-2293.
134. Feldthusen, J.; Iván, B.; Müller, A. H. E.; Kops, J., Synthesis of linear and three-arm star *tert*-chlorine-telechelic polyisobutylenes by a two-step conventional laboratory process. *Macromol. Rapid Commun.* **1997**, 18, (5), 417-425.
135. Gyor, M.; Wang, H.-C.; Faust, R., Living Carbocationic Polymerization of Isobutylene with Blocked Bifunctional Initiators in the Presence of Di-*tert*-butylpyridine as a Proton Trap. *J. Macromol. Sci., Part A* **1992**, 29, (8), 639 - 653.
136. Bae, Y. C.; Faust, R.,  $\beta$ -Proton Elimination by Free Bases in the Living Carbocationic Polymerization of Isobutylene. *Macromolecules* **1997**, 30, (23), 7341-7344.
137. Puskas, J. E.; Brister, L. B.; Michel, A. J.; Lanzendörfer, M. G.; Jamieson, D.; Pattern, W. G., Novel substituted epoxide initiators for the carbocationic polymerization of isobutylene. *J. Polym. Sci., Part A: Polym. Chem.* **2000**, 38, (3), 444-452.
138. Puskas, J. E.; Chen, Y.; Tomkins, M., Investigation of the effect of epoxide structure on the initiation efficiency in isobutylene polymerizations initiated by epoxide/TiCl<sub>4</sub> systems. *Eur. Polym. J.* **2003**, 39, (11), 2147-2153.
139. Hadjikyriacou, S.; Fodor, Z.; Faust, R., Synthetic Applications of Nonpolymerizable Monomers in Living Cationic Polymerization: Functional Polyisobutylenes by End-Quenching. *J. Macromol. Sci., Part A* **1995**, 32 (6), 1137-1153.
140. Hadjikyriacou, S.; Faust, R.; Suzuki, T., Living coupling Reaction in Living Cationic Polymerization 4. Synthesis of Telechelic Polyisobutylenes using Bis-furanyl derivatives as coupling agents. *J. Macromol. Sci., Part A* **2000**, 37, (11), 1333 - 1352.
141. Iván, B.; Kennedy, J. P., Living carbocationic polymerization. XXX. One-pot synthesis of allyl-terminated linear and tri-arm star polyisobutylenes, and epoxy- and hydroxy-telechelics therefrom. *J. Polym. Sci., Part A: Polym. Chem.* **1990**, 28, (1), 89-104.
142. Morgan, D. L.; Storey, R. F., End-Quenching of Quasi-Living Isobutylene Polymerizations with Alkoxybenzene Compounds. *Macromolecules* **2009**, 42, (18), 6844-6847.

143. Morgan, D. L.; Martinez-Castro, N.; Storey, R. F., End-Quenching of  $\text{TiCl}_4$ -Catalyzed Quasiliving Polyisobutylene with Alkoxybenzenes for Direct Chain End Functionalization. *Macromolecules* **2010**, *43*, (21), 8724-8740.
144. Olubummo, A.; Herbst, F.; Hackethal, K.; Binder, W. H., Synthesis of nonsymmetric chain end functionalized polyisobutylenes. *J. Polym. Sci., Part A: Polym. Chem.* **2011**, *49*, (13), 2931-2940.
145. Kuranari, M., Synthesis of 1-deoxy-1-ureido-D-glucuronic acid and related compounds. V. Syntheses and infrared absorption spectra of 1-azido-1-deoxy- $\beta$ -D-glucopyranuronic acid derivatives and methyl 2,3,4-tri-O-acetyl-1-amino-1-deoxy- $\beta$ -D-glucopyranuronate. *Yakugaku Zasshi* **1961**, *81*, 1189-1194.
146. Loukou, C.; Tosin, M.; Müller-Bunz, H.; Murphy, P. V., Synthesis of sugar-lactams from azides of glucuronic acid. *Carbohydr. Res.* **2007**, *342*, (12/13), 1953-1959.
147. Tornøe, C. W.; Christensen, C.; Meldal, M., *J. Org. Chem.* **2002**, *67*, 3057.
148. Rostovtsev, V. V.; Green, L. G.; Fokin, V. V.; Sharpless, K. B., *Angew. Chem., Int. Ed.* **2002**, *41*, 2596.
149. Sharpless, B. K.; Kolb, H. C.; Finn, M. G., Click Chemistry: Diverse Chemical Function from a Few Good Reactions. *Angew. Chem., Int. Ed.* **2001**, *40*, (11), 2004-2021.
150. Lewis, W. G.; Magallon, F. G.; Fokin, V. V.; Finn, M. G., Discovery and Characterization of Catalysts for Azide-Alkyne Cycloaddition by Fluorescence Quenching. *J. Am. Chem. Soc.* **2004**, *126*, 9152.
151. Binder, W. H.; Sachsenhofer, R., 'Click' Chemistry in Polymer and Materials Science. *Macromol. Rapid Commun.* **2007**, *28*, (1), 15-54.
152. Binder, W. H.; Sachsenhofer, R., 'Click' Chemistry in Polymer and Material Science: An Update. *Macromol. Rapid Commun.* **2008**, *29*, (12-13), 952-981.
153. Binder, W. H.; Zirbs, R., "Click" Chemistry in Macromolecular Synthesis. In *Encyclopedia of Polymer Science and Technology*, John Wiley & Sons, Inc.: 2009.
154. Mansfeld, U.; Pietsch, C.; Hoogenboom, R.; Becer, C. R.; Schubert, U. S., Clickable initiators, monomers and polymers in controlled radical polymerizations - a prospective combination in polymer science. *Polym. Chem.* **2010**, *1*, (10), 1560-1598.
155. Binder, W. H.; Herbst, F., *McGraw-Hill Yearbook of Science & Technology* 978-0-470-56667-1 ed.; **2011**.
156. Fokin, V. V.; Matyjaszewski, K., *Organic Chemistry – Breakthroughs and Perspectives*. Wiley-VCH Verlag GmbH & Co. KGaA: **2012**.
157. Espeel, P.; Du Prez, F. E., "Click"-Inspired Chemistry in Macromolecular Science: Matching Recent Progress and User Expectations. *Macromolecules* **2014**, *48*, (1), 2-14.
158. Binder, W. H.; Zirbs, R., "Click" Chemistry in Macromolecular Synthesis. In *Encyclopedia of Polymer Science and Technology*, John Wiley & Sons, Inc.: 2014.
159. Majumder, N., Click chemistry in nano drug delivery system and its applications in biology. *Int. J. Res. Pharm. Chem.* **2015**, *5*, (1), 95-105, 11pp.
160. Musumeci, F.; Musumeci, S.; Schenone, S.; Desogus, A.; Nieddu, E.; Deodato, D.; Botta, L., Click Chemistry, A Potent Tool in Medicinal Sciences. *Curr. med. chem.* **2015**, *22*, (17), 2022-2050.
161. Totobenazara, J.; Burke, A., New click-chemistry methods for 1,2,3-triazoles synthesis: recent advances and applications. *Tetrahedron lett.* **2015**, *56*, (22), 2853-2859.
162. Tang, W.; Becker, M. L., "Click" reactions: a versatile toolbox for the synthesis of peptide-conjugates. *Chem. Soc. Rev.* **2014**, *43*, (20), 7013-7039.
163. Ahmad Fuaad, A.; Azmi, F.; Skwarczynski, M.; Toth, I., Peptide Conjugation via CuAAC 'Click' Chemistry. *Molecules* **2013**, *18*, (11), 13148-13174.
164. Pretze, M.; Pietzsch, D.; Mamat, C., Recent Trends in Bioorthogonal Click-Radiolabeling Reactions Using Fluorine-18. *Molecules* **2013**, *18*, (7), 8618-8665.
165. Nandivada, H.; Lahann, J., Copper-Catalyzed 'Click' Chemistry for Surface Engineering Click chemistry for biotechnology and materials science. *Click Chemistry for Biotechnology and Materials Science* **2009**, 291-307.
166. Meldal, M., Polymer "Clicking" by CuAAC Reactions. *Macromol. Rapid Commun.* **2008**, *29*, (12-13), 1016-1051.

167. Zhang, L.; Chen, X.; Xue, P.; Sun, H. H. Y.; Williams, I. D.; Sharpless, K. B.; Fokin, V. V.; Jia, G., Ruthenium-Catalyzed Cycloaddition of Alkynes and Organic Azides. *J. Am. Chem. Soc.* **2005**, *127*, (46), 15998-15999.
168. Binder, W. H.; Sachsenhofer, R., 'Click' Chemistry in Polymer and Materials Science. *Macromol. Rapid Commun.* **2007**, *28*, (1), 15-54.
169. Chan, T. R.; Hilgraf, R.; Sharpless, K. B.; Fokin, V. V., Polytriazoles as Copper(I)-Stabilizing Ligands in Catalysis. *Org. Lett.* **2004**, *6*, (17), 2853-2855.
170. Himo, F.; Lovell, T.; Hilgraf, R.; Rostovtsev, V. V.; Noodleman, L.; Sharpless, K. B.; Fokin, V. V., Copper(I)-Catalyzed Synthesis of Azoles. DFT Study Predicts Unprecedented Reactivity and Intermediates. *J. Am. Chem. Soc.* **2004**, *127*, (1), 210-216.
171. Liu, Y.; Díaz, D. D.; Accurso, A. A.; Sharpless, K. B.; Fokin, V. V.; Finn, M. G., Click chemistry in materials synthesis. III. Metal-adhesive polymers from Cu(I)-catalyzed azide-alkyne cycloaddition. *J. Polym. Sci., Part A: Polym. Chem.* **2007**, *45*, (22), 5182-5189.
172. Molteni, G.; Bianchi, C. L.; Marinoni, G.; Santo, N.; Ponti, A., *New. J. Chem.* **2006**, *30*, 1137.
173. Pachon, L. D.; van Maarseveen, J. H.; Rothenberg, G., *Adv. Synth. Catal.* **2005**, *347*, 811.
174. Gupta, S. S.; Kuzelka, J.; Singh, P.; Lewis, W. G.; Manchester, M.; Finn, M. G., Accelerated Bioorthogonal Conjugation: A Practical Method for the Ligation of Diverse Functional Molecules to a Polyvalent Virus Scaffold. *Bioconjugate Chem.* **2005**, *16*, (6), 1572-1579.
175. Meng, J.-c.; Fokin, V. V.; Finn, M. G., Kinetic resolution by copper-catalyzed azide-alkyne cycloaddition. *Tetrahedron Lett.* **2005**, *46*, (27), 4543-4546.
176. Han, S.-Y.; Kim, Y.-A., Recent development of peptide coupling reagents in organic synthesis. *Tetrahedron* **2004**, *60*, (11), 2447-2467.
177. <http://www.organic-reaction.com/synthetic-protocols/coupling-reagents-in-amide-synthesis/2011-10-18>, 9:25.
178. Knorr, R.; Trzeciak, A.; Bannwarth, W.; Gillissen, D., New coupling reagents in peptide chemistry. *Tetrahedron Lett.* **1989**, *30*, (15), 1927-1930.
179. <http://online-media.uni-marburg.de/chemie/bioorganic/bioorg/pdf/kapitel2.pdf>, 2015-01-16, 17:23.
180. [https://www.uni-due.de/~bc0084/ak\\_schrader/Vorlesungen/Ringkommentiert.pdf](https://www.uni-due.de/~bc0084/ak_schrader/Vorlesungen/Ringkommentiert.pdf), 2015-01-16, 18:12.
181. DeTar, D. F.; Silverstein, R., Reactions of Carbodiimides. I. The Mechanisms of the Reactions of Acetic Acid with Dicyclohexylcarbodiimide<sub>1,2</sub>. *J. Am. Chem. Soc.* **1966**, *88*, (5), 1013-1019.
182. DeTar, D. F.; Silverstein, R., Reactions of Carbodiimides. II. The Reactions of Dicyclohexylcarbodiimide with Carboxylic Acids in the Presence of Amines and Phenols<sub>1,2</sub>. *J. Am. Chem. Soc.* **1966**, *88*, (5), 1020-1023.
183. Balcom, B. J.; Petersen, N. O., Solvent dependence of carboxylic acid condensations with dicyclohexylcarbodiimide. *J. Org. Chem.* **1989**, *54*, (8), 1922-1927.
184. Sheehan, J.; Cruickshank, P.; Boshart, G., Notes- A Convenient Synthesis of Water-Soluble Carbodiimides. *J. Org. Chem.* **1961**, *26*, (7), 2525-2528.
185. Sheehan, J. C.; Hess, G. P., A New Method of Forming Peptide Bonds. *J. Am. Chem. Soc.* **1955**, *77*, (4), 1067-1068.
186. Chen, S.; Xu, J., Pentafluorophenyl diphenylphosphinate a new efficient coupling reagent in peptide chemistry. *Tetrahedron Lett.* **1991**, *32*, (46), 6711-6714.
187. Anderson, G. W.; Zimmerman, J. E.; Callahan, F. M., N-Hydroxysuccinimide Esters in Peptide Synthesis. *J. Am. Chem. Soc.* **1963**, *85*, (19), 3039-3039.
188. Carpino, L. A.; Imazumi, H.; El-Faham, A.; Ferrer, F. J.; Zhang, C.; Lee, Y.; Foxman, B. M.; Henklein, P.; Hanay, C.; Mügge, C.; Wenschuh, H.; Klose, J.; Beyermann, M.; Bienert, M., Kupplungsreagentien vom Uronium-/Guanidinium-Typ: Synthese und Charakterisierung der authentischen Uroniumsalze. *Angew. Chem.* **2002**, *114*, (3), 457-461.
189. Ehrlich, A.; Heyne, H.-U.; Winter, R.; Beyermann, M.; Haber, H.; Carpino, L. A.; Bienert, M., Cyclization of all-l-Pentapeptides by Means of 1-Hydroxy-7-azabenzotriazole-Derived Uronium and Phosphonium Reagents. *J. Org. Chem.* **1996**, *61*, (25), 8831-8838.
190. Coste, J.; Dufour, M.-N.; Pantaloni, A.; Castro, B., Brop: A new reagent for coupling N-methylated amino acids. *Tetrahedron Lett.* **1990**, *31*, (5), 669-672.



191. Castro, B.; Dormoy, J. R.; Evin, G.; Selve, C., Reactifs de couplage peptidique I (1) - l'hexafluorophosphate de benzotriazolyl N-oxytrisdiméthylamino phosphonium (B.O.P.). *Tetrahedron lett.* **1975**, 16, (14), 1219-1222.
192. Coste, J.; Le-Nguyen, D.; Castro, B., PyBOP<sup>®</sup>: A new peptide coupling reagent devoid of toxic by-product. *Tetrahedron lett.* **1990**, 31, (2), 205-208.
193. Frérot, E.; Coste, J.; Pantaloni, A.; Dufour, M.-N.; Jouin, P., PyBOP<sup>®</sup> and PyBroP: Two reagents for the difficult coupling of the  $\alpha,\alpha$ -dialkyl amino acid, *Aib. Tetrahedron* **1991**, 47, (2), 259-270.
194. Carpino, L. A.; Ionescu, D.; El-Faham, A., Peptide Coupling in the Presence of Highly Hindered Tertiary Amines. *J. Org. Chem.* **1996**, 61, (7), 2460-2465.
195. Barqawi, H.; Schulz, M.; Olubummo, A.; Saurland, V.; Binder, W. H., 2D-LC/SEC-(MALDI-TOF)-MS Characterization of Symmetric and Nonsymmetric Biocompatible PEO<sub>m</sub>-PIB-PEO<sub>n</sub> Block Copolymers. *Macromolecules* **2013**, 46, (19), 7638-7649.
196. Smaldone, R. A.; Moore, J. S., Reactive Sieving with Foldamers: Inspiration from Nature and Directions for the Future. *Chem. Eur. J.* **2008**, 14, (9), 2650-2657.
197. Li, H.; Sachsenhofer, R.; Binder, W. H.; Henze, T.; Thurn-Albrecht, T.; Busse, K.; Kressler, J. Hierarchical Organization of Poly(ethylene oxide)-block-poly(isobutylene) and Hydrophobically Modified Fe<sub>2</sub>O<sub>3</sub> Nanoparticles at the Air/Water Interface and on Solid Supports. *Langmuir* **2009**, 25, (14), 8320-8329.
198. Schröter, J. A.; Plehnert, R.; Tschierske, C.; Katholy, S.; Janietz, D.; Penacorada, F.; Brehmer, L., Monolayer Properties of a New Family of Amphiphiles with an Unusual Head-Group Topology. *Langmuir* **1997**, 13, (4), 796-800.
199. Reynolds, P. A.; McGillivray, D. J.; Gilbert, E. P.; Holt, S. A.; Henderson, M. J.; White, J. W., Neutron and X-ray Reflectivity from Polyisobutylene-Based Amphiphiles at the Air/Water Interface. *Langmuir* **2003**, 19, (3), 752-761.
200. McConlogue, C. W.; Vanderlick, T. K., A Close Look at Domain Formation in DPPC Monolayers. *Langmuir* **1997**, 13, (26), 7158-7164.
201. Weis, R. M., Fluorescence microscopy of phospholipid monolayer phase transitions. *Chem. Phys. Lipids* **1991**, 57, (2/3), 227-239.
202. Schulz, M.; Glatte, D.; Meister, A.; Scholtysek, P.; Kerth, A.; Blume, A.; Bacia, K.; Binder, W. H., Hybrid lipid/polymer giant unilamellar vesicles: effects of incorporated biocompatible PIB-PEO block copolymers on vesicle properties. *Soft Matter* **2011**, 7, (18), 8100-8110.
203. Dyck, M.; Lösche, M., Interaction of the Neurotransmitter, Neuropeptide Y, with Phospholipid Membranes: Film Balance and Fluorescence Microscopy Studies. *J. Phys. Chem. B* **2006**, 110, (44), 22143-22151.
204. Scholtysek, P.; Li, Z.; Kressler, J.; Blume, A., Interactions of DPPC with Semitelechelic Poly(glycerol methacrylate)s with Perfluoroalkyl End Groups. *Langmuir* **2012**, 28, (44), 15651-15662.
205. El Kirat, K.; Besson, F. o.; Prigent, A.-F.; Chauvet, J.-P.; Roux, B., Role of Calcium and Membrane Organization on Phospholipase D Localization and Activity: Competition between a soluble and insoluble substrate. *J. Biol. Chem.* **2002**, 277, (24), 21231-21236.
206. Olubummo, A.; Schulz, M.; Schöps, R.; Kressler, J.; Binder, W. H., Phase Changes in Mixed Lipid/Polymer Membranes by Multivalent Nanoparticle Recognition. *Langmuir* **2014**, 30, (1), 259-267.
207. Berney, C.; Danuser, G., FRET or No FRET: A Quantitative Comparison. *Biophys. J.* **2003**, 84, 3992-4010.
208. Held, P., An Introduction to Fluorescence Resonance Energy Transfer (FRET) Technology and its Application in Bioscience. *BioTek* **2005**.
209. Bag, S. S.; Jana, S.; Yashmeen, A.; Senthilkumar, K.; Bag, R., Triazolyl-donor-acceptor chromophore-decorated unnatural amino acids and peptides: FRET events in a  $\beta$ -turn conformation. *Chem. Commun.* **2014**, 50, (4), 433-435.
210. Gruber, B.; König, B., Self-Assembled Vesicles with Functionalized Membranes. *Chem. Eur. J.* **2013**, 19, (2), 438-448.
211. Thompson, C.; Ge, M.; Kahne, D., Synthesis of Vancomycin from the Aglycon. *J. Am. Chem. Soc.* **1999**, 121, (6), 1237-1244.

212. Zhu, H.; Xu, X.; Cui, W.; Zhang, Y.; Mo, H.; Shen, Y.-M., Synthesis and characterization of well-defined lactic acid-PEG cooligomers and its tricarbonyl rhenium conjugates. *J. Polym. Sci., Part A: Polym. Chem.* **2011**, *49*, (8), 1745-1752.
213. Lechner, B.-D.; Ebert, H.; Prehm, M.; Werner, S.; Meister, A.; Hause, G.; Beerlink, A.; Saalwächter, K.; Bacia, K.; Tschierske, C.; Blume, A., Temperature-Dependent In-Plane Structure Formation of an X-Shaped Bolopolyphile within Lipid Bilayers. *Langmuir* **2015**.
214. Dimonie, M.; Teodorescu, M., Phase transfer catalysis synthesis of  $\alpha,\omega$ -diallylpoly(ethylene oxide). *Makromol. Chem. Rapid. Commun.* **1993**, *14*, (5), 303-307.
215. Mahouche, S.; Mekni, N.; Abbassi, L.; Lang, P.; Perruchot, C.; Jouini, M.; Mammeri, F.; Turmine, M.; Romdhane, H. B.; Chehimi, M. M., Tandem diazonium salt electroreduction and click chemistry as a novel, efficient route for grafting macromolecules to gold surface. *Surf. Sci.* **2009**, *603*, (21), 3205-3211.
216. Park, K. D.; Morieux, P.; Salome, C.; Cotten, S. W.; Reamtong, O.; Evers, C.; Gaskell, S. J.; Stables, J. P.; Liu, R.; Kohn, H., Lacosamide Isothiocyanate-Based Agents: Novel Agents To Target and Identify Lacosamide Receptors. *J. Med. Chem.* **2009**, *52*, (21), 6897-6911.
217. Bonnet, D.; Ilien, B.; Galzi, J.-L.; Richè, S.; Antheaune, C.; Hibert, M., A Rapid and Versatile Method to Label Receptor Ligands Using "Click" Chemistry: Validation with the Muscarinic M1 Antagonist Pirenzepine. *Bioconjugate Chem.* **2006**, *17*, (6), 1618-1623.
218. Feldman, A. K.; Colasson, B.; Sharpless, K. B.; Fokin, V. V., The Allylic Azide Rearrangement: Achieving Selectivity. *J. Am. Chem. Soc.* **2005**, *127*, (39), 13444-13445.
219. Yoo, E. J.; Ahlquist, M.; Bae, I.; Sharpless, K. B.; Fokin, V. V.; Chang, S., Mechanistic Studies on the Cu-Catalyzed Three-Component Reactions of Sulfonyl Azides, 1-Alkynes and Amines, Alcohols, or Water: Dichotomy via a Common Pathway. *J. Org. Chem.* **2008**, *73*, (14), 5520-5528.
220. Ren, J. M.; Wiltshire, J. T.; Blencowe, A.; Qiao, G. G., Synthesis of a Star Polymer Library with a Diverse Range of Highly Functionalized Macromolecular Architectures. *Macromolecules* **2011**, *44*, (9), 3189-3202.
221. Bergbreiter, D. E.; Ortiz-Acosta, D., Recyclable polyisobutylene-supported pyridyl N-oxide allylation catalysts. *Tetrahedron Lett.* **2008**, *49*, (39), 5608-5610.
222. Fristrup, P.; Dideriksen, B. B.; Tanner, D.; Norrby, P.-O., Probing Competitive Enantioselective Approach Vectors Operating in the Jacobsen-Katsuki Epoxidation: A Kinetic Study of Methyl-Substituted Styrenes. *J. Am. Chem. Soc.* **2005**, *127*, (39), 13672-13679.
223. Centko, R. S.; Mohan, R. S., The Discovery-Oriented Approach to Organic Chemistry. 4. Epoxidation of p-Methoxy-trans- $\alpha$ -methylstyrene: An Exercise in NMR and IR Spectroscopy for Sophomore Organic Laboratories. *J. Chem. Educ.* **2001**, *78*, (1), 77.
224. Synthesized by B.Sc. Enerelt Sanchin under supervision of Marlen Malke, thesis: Beta-Turn Mimetika in Polyisobutylen Polymer, *Martin-Luther-University Halle-Wittenberg, Chair of Macromolecular Chemistry/ Institute of Chemistry*, 2013.
225. Srinivasan, R.; Tan, L. P.; Wu, H.; Yang, P.-Y.; Kalesh, K. A.; Yao, S. Q., High-throughput synthesis of azide libraries suitable for direct "click" chemistry and in situ screening. *Org. Biomol. Chem.* **2009**, *7*, (9), 1821-1828.
226. Liu, W.; Dong, C.-M., Versatile synthesis of asymmetrical dendron-like/dendron-like poly( $\epsilon$ -caprolactone)-b-poly( $\gamma$ -benzyl-L-glutamate) block copolymers. *J. Polym. Sci., Part A: Polym. Chem.* **2011**, *49*, (16), 3491-3498.
227. Xiao, S.; Fu, N.; Peckham, K.; Smith, B. D., Efficient Synthesis of Fluorescent Squaraine Rotaxane Dendrimers. *Org. Lett.* **2009**, *12*, (1), 140-143.
228. Lee, B.-Y.; Park, S. R.; Jeon, H. B.; Kim, K. S., A new solvent system for efficient synthesis of 1,2,3-triazoles. *Tetrahedron Lett.* **2006**, *47*, (29), 5105-5109.
229. Mourer, M.; Hapiot, F.; Tilloy, S.; Monflier, E.; Manuel, S., Easily Accessible Mono- and Polytropic  $\beta$ -Cyclodextrin Hosts by Click Chemistry. *Eur. J. Org. Chem.* **2008**, *2008*, (34), 5723-5730.
230. Schunack, M. Self-Healing Polymers via Azide/Alkyne-"Click"-Reactions: Systematic Evaluation of Catalysts and Alkynes. *diploma thesis*, **2010**.

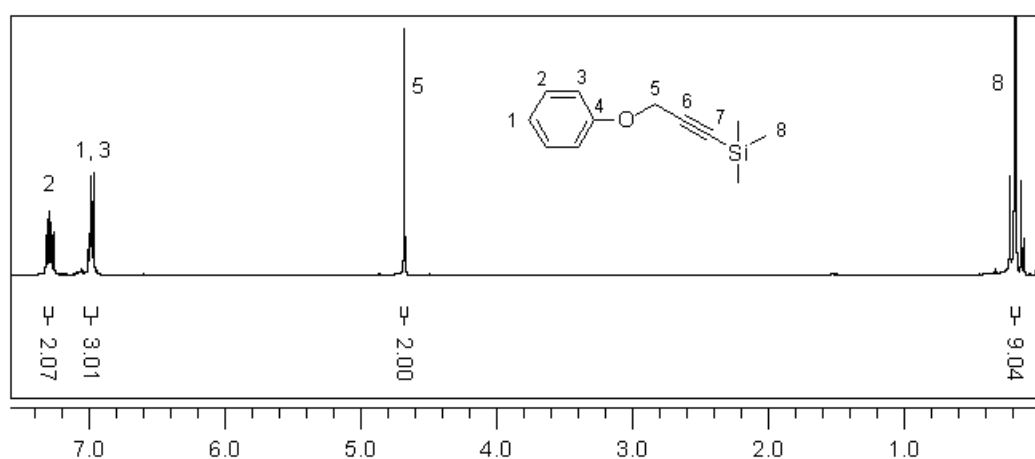
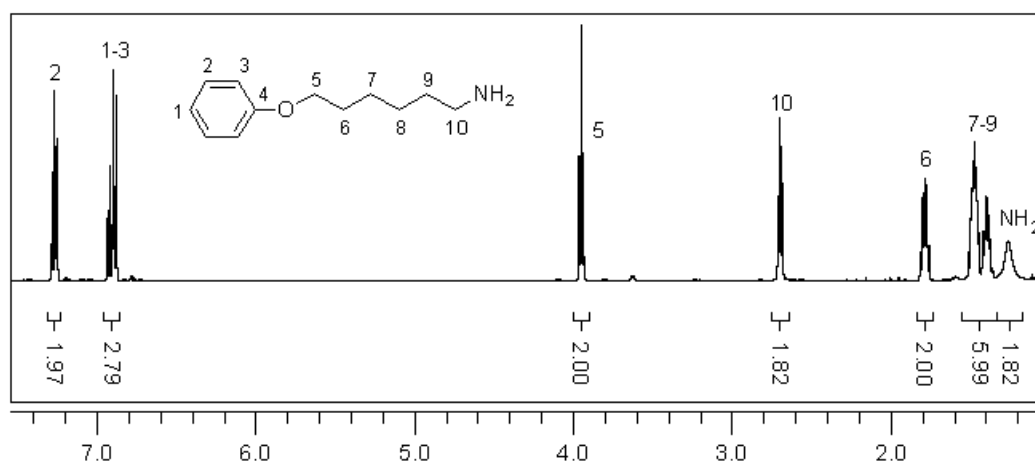
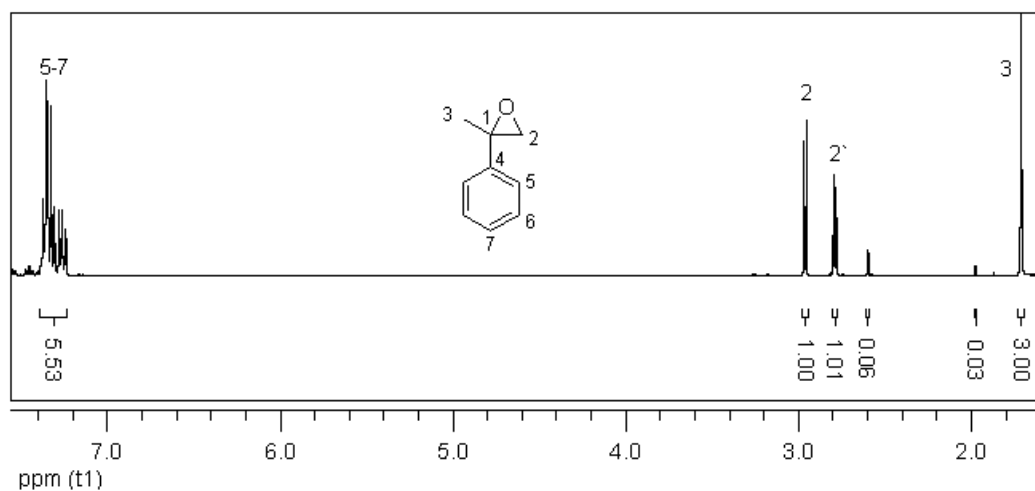
231. Kusakiewicz-Dawid, A.; Masiukiewicz, E.; Rzeszotarska, B.; Dybala, I.; Koziol, A. E.; Broda, M., Anna, The Synthesis, Structure and Properties of N-Acetylated Derivatives of Ethyl 3-Amino-1H-pyrazole-4-carboxylate. *Chem. Pharm. Bull.* **2007**, 55, (5), 747-752.
232. Tamanini, E.; Rigby, S. E. J.; Motevalli, M.; Todd, M. H.; Watkinson, M., Responsive Metal Complexes: A Click-Based “Allosteric Scorpionate” Complex Permits the Detection of a Biological Recognition Event by EPR/ENDOR Spectroscopy. *Chem. Eur. J.* **2009**, 15, (15), 3720-3728.
233. Zhou, Y.; Jiang, K.; Chen, Y.; Liu, S., Gold nanoparticle-incorporated core and shell crosslinked micelles fabricated from thermoresponsive block copolymer of N-isopropylacrylamide and a novel primary-amine containing monomer. *J. Polym. Sci., Part A: Polym. Chem.* **2008**, 46, (19), 6518-6531.

## 10. Appendix

**Table A1.** Experimental conditions for polymerization of  $\alpha$ -hydroxymethyl- $\omega$ -bromo telechelic poly(isobutylene) (**17**).

<b>PIB</b>	<b>m<sub>th</sub></b> [g]	<b>M<sub>n(th)</sub></b> [g/mol]	<b>IB</b>	<b>V (<i>n</i>-Hex)</b> <b>V(DCM)</b> [mL]	<b>MSE</b>	<b>DtBP</b>	<b>TiCl<sub>4</sub></b>	<b>BPB</b>	<b>M<sub>n(SEC)</sub><sup>a</sup></b> [g/mol]	<b>PDI</b>	<b>M<sub>n(NMR)</sub></b> [g/mol]	<b>yield</b>
<b>17a</b>	3	3000	53 mmol	32	3.83 mmol	0.27 mmol	6.39 mmol	3.40 mmol	3400	1.28	3600	2.9 g
			4.4 mL	21	494 $\mu$ L	60 $\mu$ L	0.71 mL	0.54 mL				97 %
			1 mol/L		71 mmol/L	5 mmol/L	120 mmol/L	63 mmol/L				
<b>17b</b>	3	3000	53 mmol	32	3.83 mmol	0.27 mmol	6.39 mmol	3.40 mmol	3300	1.50	3500	2.8 g
			4.4 mL	21	494 $\mu$ L	60 $\mu$ L	0.71 mL	0.54 mL				93 %
			1 mol/L		71 mmol/L	5 mmol/L	120 mmol/L	63 mmol/L				
<b>17c</b>	3	4000	53 mmol	32	2.74 mmol	0.27 mmol	6.39 mmol	2.46 mmol	4200	1.44	4500	2.9 g
			4.4 mL	21	353 $\mu$ L	60 $\mu$ L	0.71 mL	0.39 mL				97 %
			1 mol/L		51 mmol/L	5 mmol/L	120 mmol/L	46 mmol/L				
<b>17d</b>	3	8000	53 mmol	32	1.31 mmol	0.27 mmol	6.39 mmol	1.18 mmol	8000	1.29	8300	3 g
			4.4 mL	21	169 $\mu$ L	60 $\mu$ L	0.71 mL	0.19 mL				100 %
			1 mol/L		24 mmol/L	5 mmol/L	120 mmol/L	22 mmol/L				
<b>17e</b>	3	15,000	53 mmol	32	0.68 mmol	0.27 mmol	6.39 mmol	0.61 mmol	15,300	1.23	15,500	3 g
			4.4 mL	21	88 $\mu$ L	60 $\mu$ L	0.71 mL	0.10 mL				100 %
			1 mol/L		13 mmol/L	5 mmol/L	120 mmol/L	12 mmol/L				

a) Polyisobutylene standards were used for conventional external calibration.



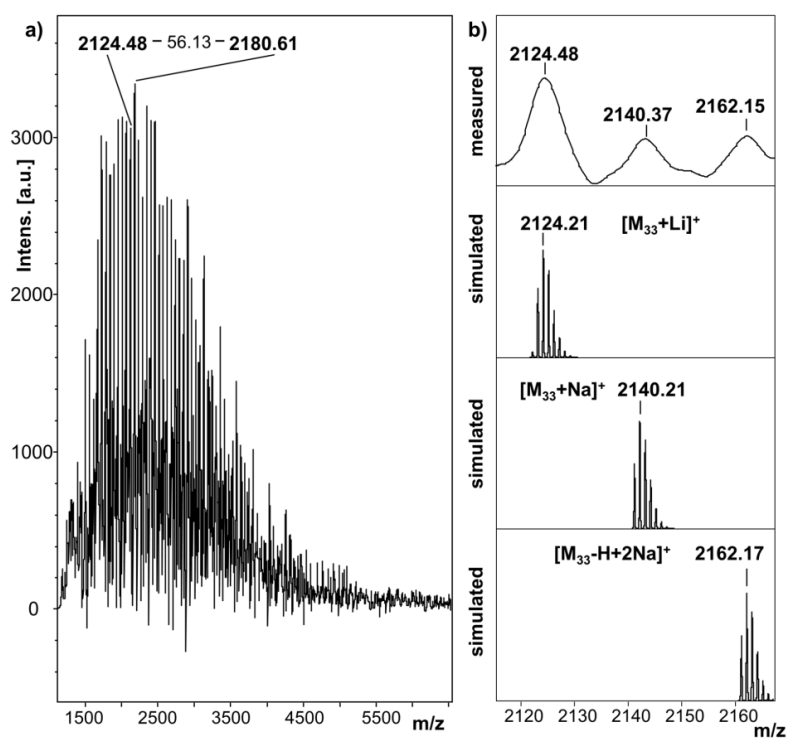


**Figure A4.** MALDI-TOF MS of  $\alpha$ -hydroxymethyl- $\omega$ -alkyne telechelic PIB **5**. (a) Full spectrum of **5**, (b) expanded view of mass spectra of **5** with simulated peaks.

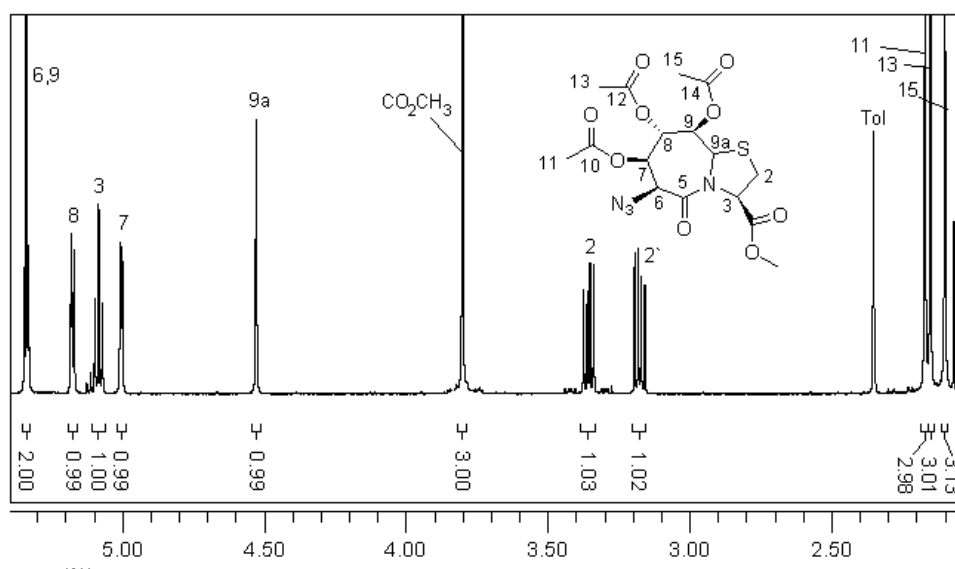


**Figure A5.** <sup>1</sup>H-NMR spectrum (CDCl<sub>3</sub>, 400 MHz) of **6b**.

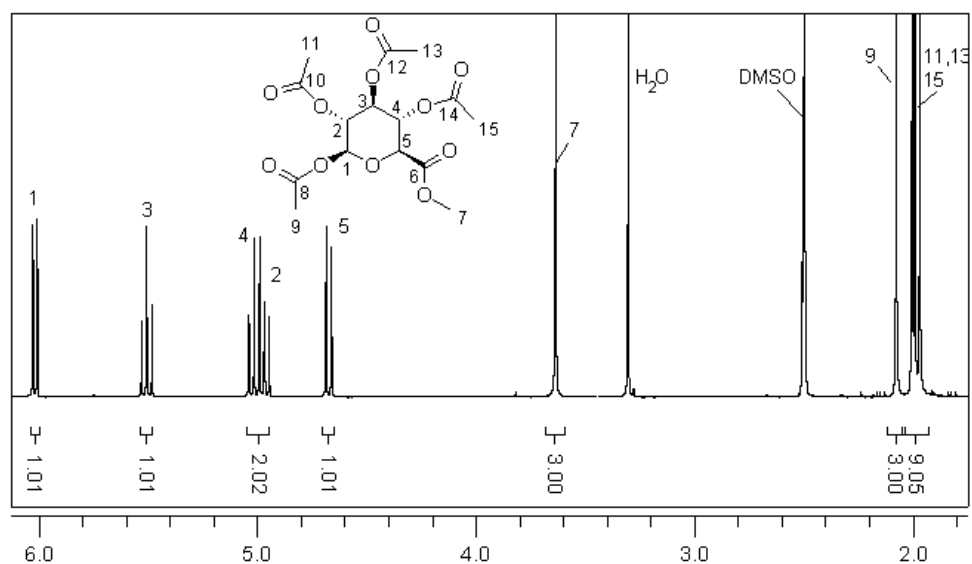


**Figure A6.**  $^1\text{H-NMR}$  spectrum ( $\text{DMSO-d}_6$ , 400 MHz) of **7a**.

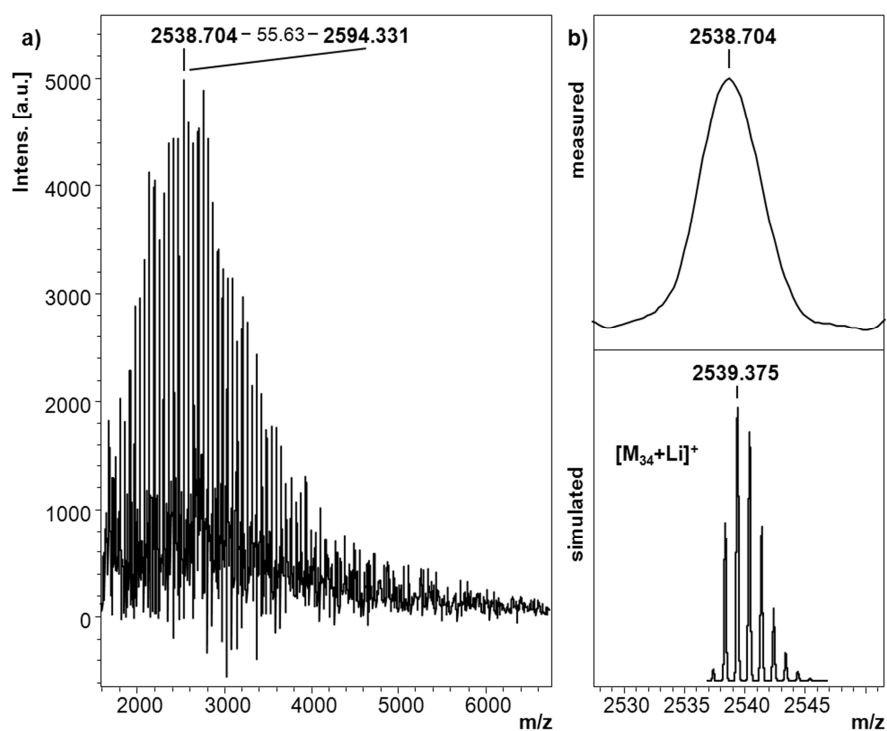


**Figure A7.** MALDI-ToF-MS of **30** of a) the region 1600-7000 Da and b) expanded spectrum with a listed view of the simulated peak.

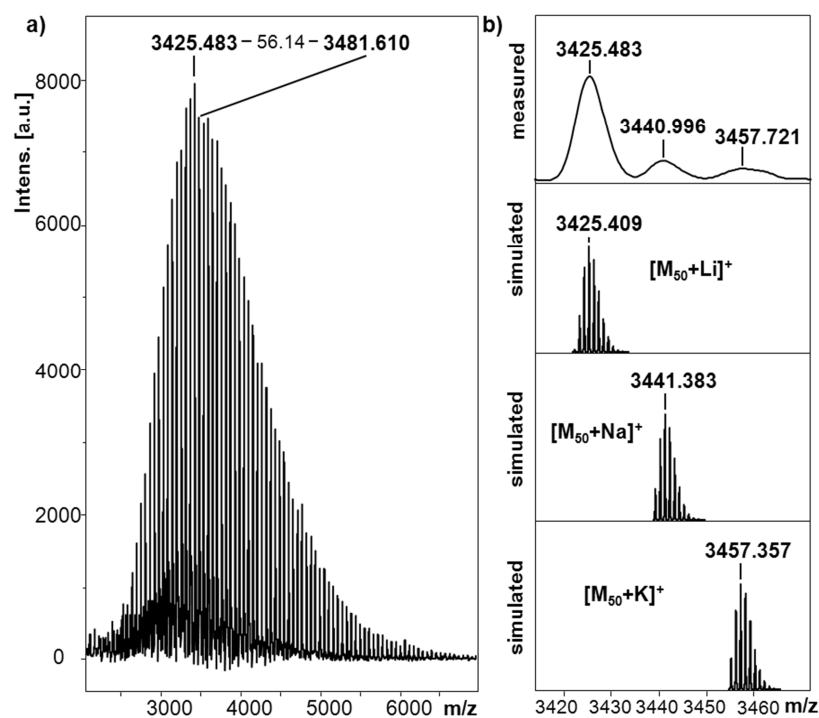


**Figure A8.** MALDI-TOF MS of PIB strand **8**. (a) Full spectrum of **8**, (b) expanded view of mass spectra of **8** with simulated peaks.

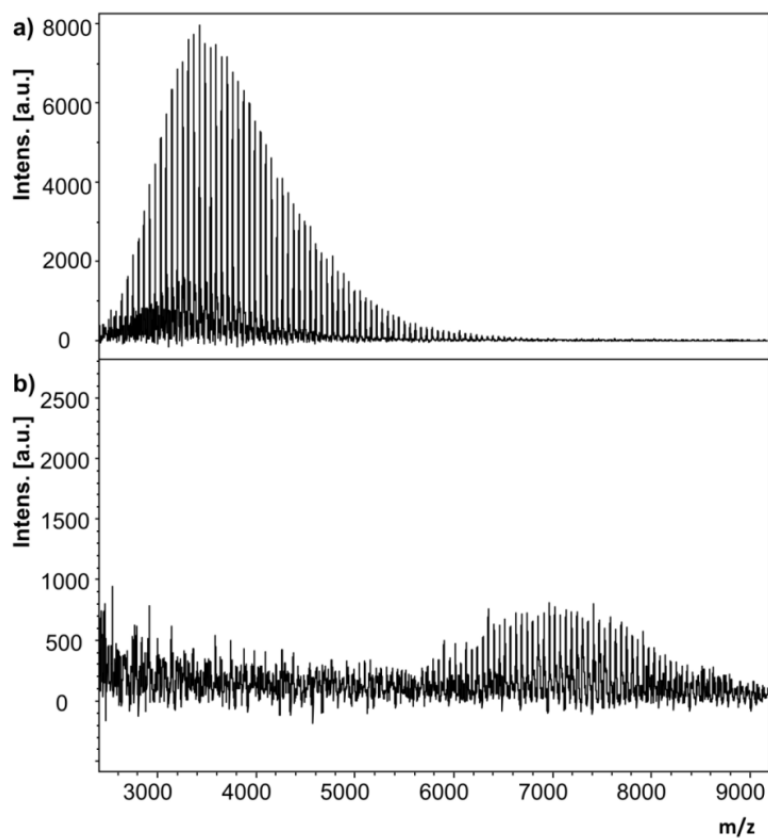


**Figure A9.** MALDI-TOF MS overlay of (a) PIB strand **8** and (b) beta-turn mimetic PIB-conjugate **9**. “Reprinted with permission from Malke, M.; Barqawi, H.; Binder, W. H., Synthesis of an Amphiphilic  $\beta$ -Turn Mimetic Polymer Conjugate. *ACS Macro Lett.* 2014, 3, (4), 393-397. Copyright 2015 American Chemical Society.”



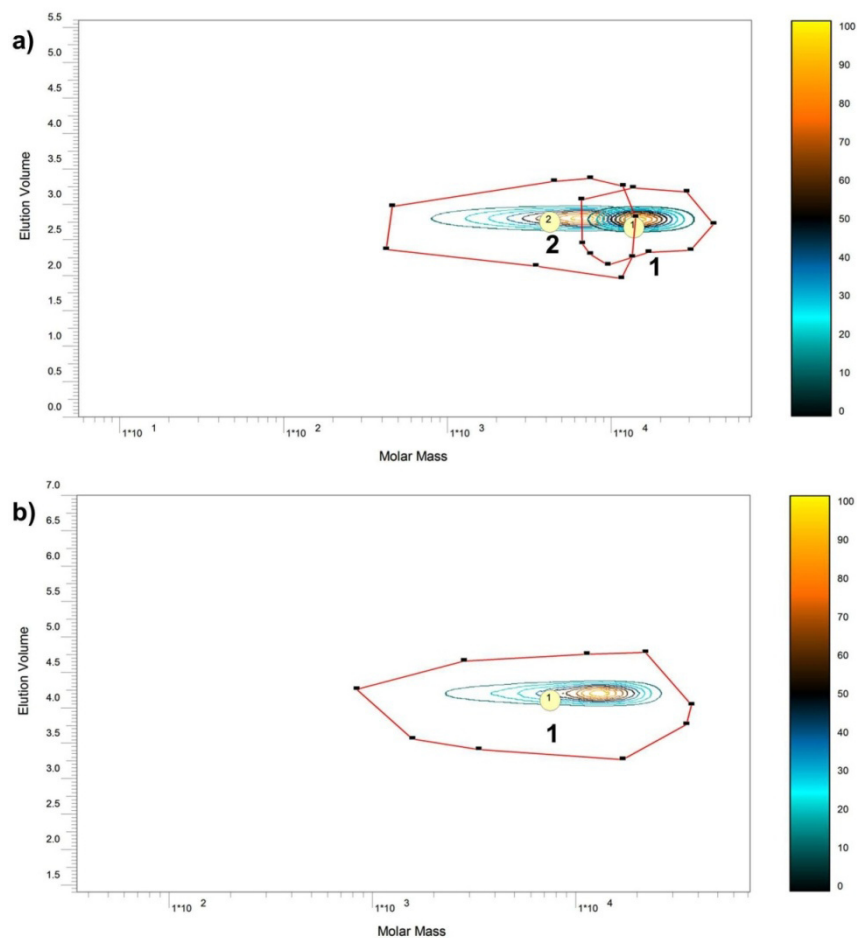


**Figure A10.** SEC experiments using  $\alpha$ -hydroxymethyl- $\omega$ -bromo telechelic poly(isobutylene) **17 a ,c** with molecular weights of 4000 g/mol and 15,000 g/mol and a SEC column with a range of 1-30 kDa (PSS SDV HighSpeed 5  $\mu$ m 500  $\text{\AA}$ ) a) graphical overlay of single measurements 1  $\rightarrow$   $M_n = 4000$  g/mol and 2  $\rightarrow$   $M_n = 15,000$  g/mol and b) 50:50 mixture of  $M_n = 4000$  and 15,000 g/mol resulting in an average  $M_n$  of 10,400 g/mol.

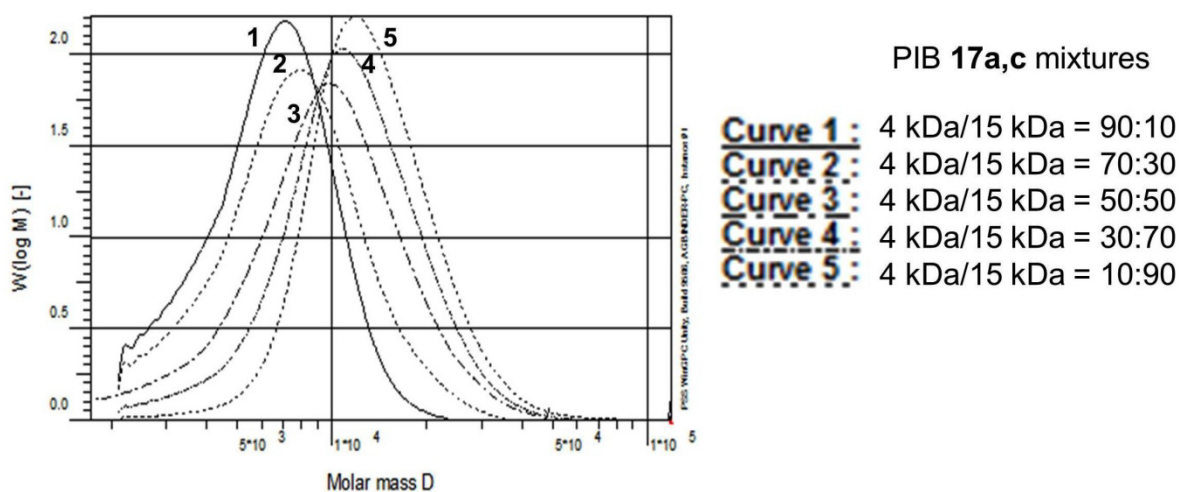
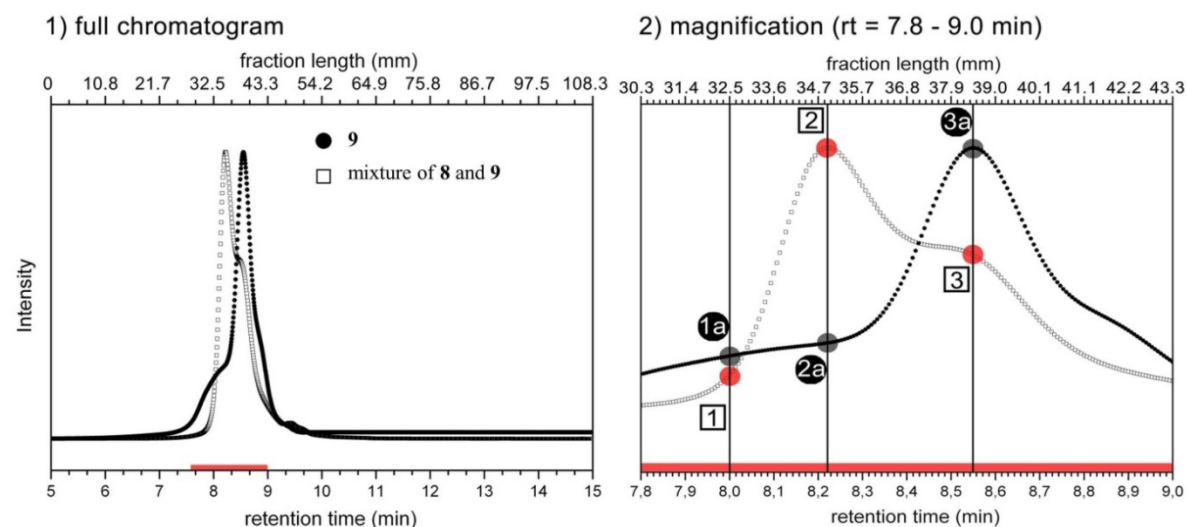


**Figure A11.** SEC experiments using mixtures of  $\alpha$ -hydroxymethyl- $\omega$ -bromo telechelic poly(isobutylene) **17 a ,c** with molecular weights of 4000 g/mol and 15,000 g/mol and a SEC column with a range of 1-30 kDa (PSS SDV HighSpeed 5  $\mu$ m 500  $\text{\AA}$ ).

## A) LC/LCT



## B) MALDI-TOF MS

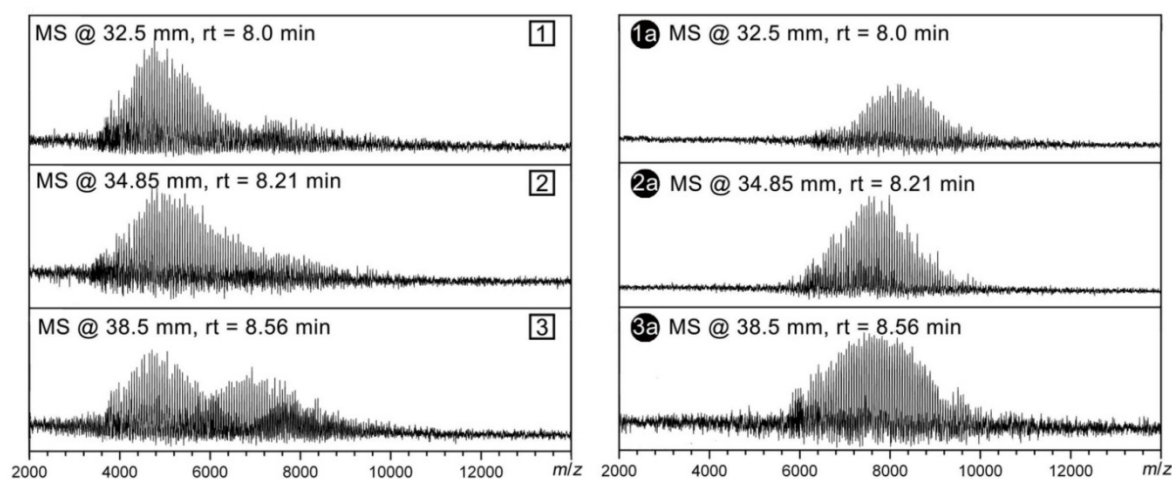


**Figure A12.** LC/MALDI-TOF MS of the beta-turn mimetic PIB-conjugate **9** and the mixed beta-turn mimetic PIB-conjugate **9**/PIB **8** = 80:20 (w/w). A) overlay of the LC traces of **9**, and the mixture **9** and **8**, measured at critical conditions of PIB at a flow rate of 0.3 mL/min, T = 30 °C; 1) full spectrum, 2) expanded view of the chromatogram; B) MALDI-TOF MS spectra of the correlated fractions of the mixture **9** and **8** (left spectra) and of **9** (right spectra) proving the purity of the final amphiphilic hybrid-molecule **9**. “Reprinted with permission from Malke, M.; Barqawi, H.; Binder, W. H., Synthesis of an Amphiphilic b-Turn Mimetic Polymer Conjugate. ACS Macro Lett. 2014, 3, (4), 393-397. Copyright 2015 American Chemical Society.”

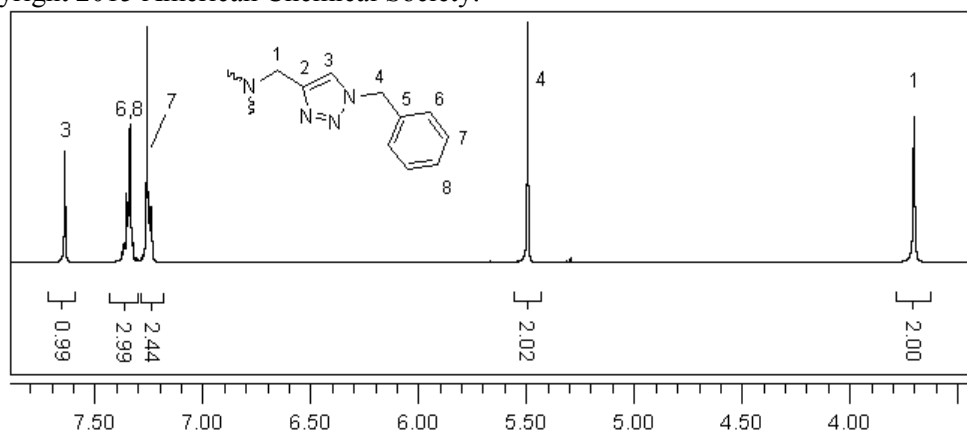


**Figure A13.**  $^1\text{H-NMR}$  spectrum ( $\text{CDCl}_3$ , 400 MHz) of TBTA (**29**).

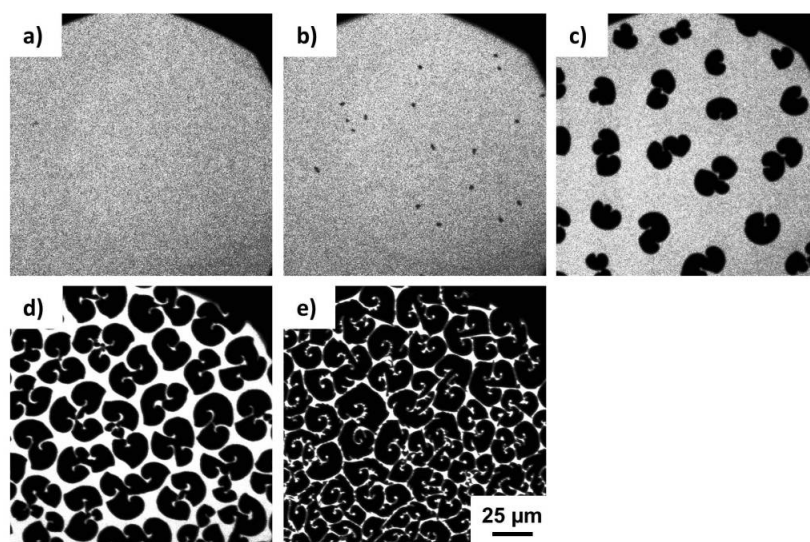


**Figure A14.** Epifluorescence microscopy images of L-DPPC monolayer at the air/water interface at 20°C. The images were recorded at constant compression of the spread monolayer at the following surface pressures: (a) 1.1, (b) 4.5, (c) 5.3, (d) 6.1 and (e) 8.4  $\text{mN m}^{-1}$ .

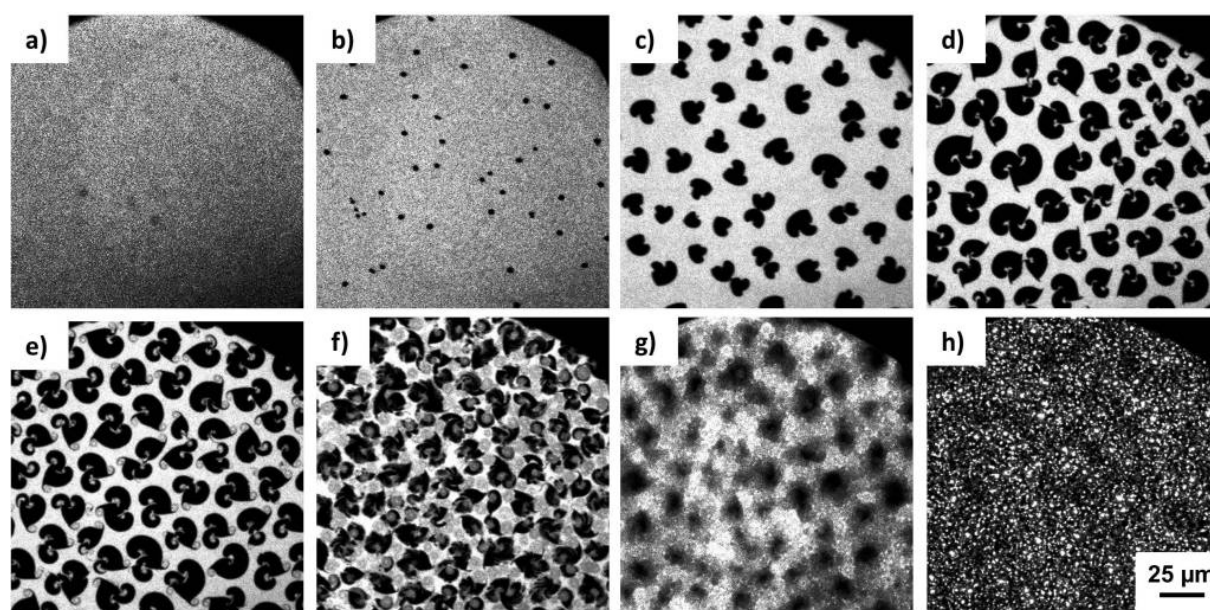


**Figure A15.** Epifluorescence microscopy images of mixed DPPC/8 99:1 monolayer at the air/water interface at 20°C. The images were recorded at constant compression of the cospread monolayer at the following surface pressures: (a) 0, (b) 4.6, (c) 5.6, (d) 6.8, (e) 7.3, (f) 7.9, (g) 11.2, (h) 15.3  $\text{mN m}^{-1}$ .

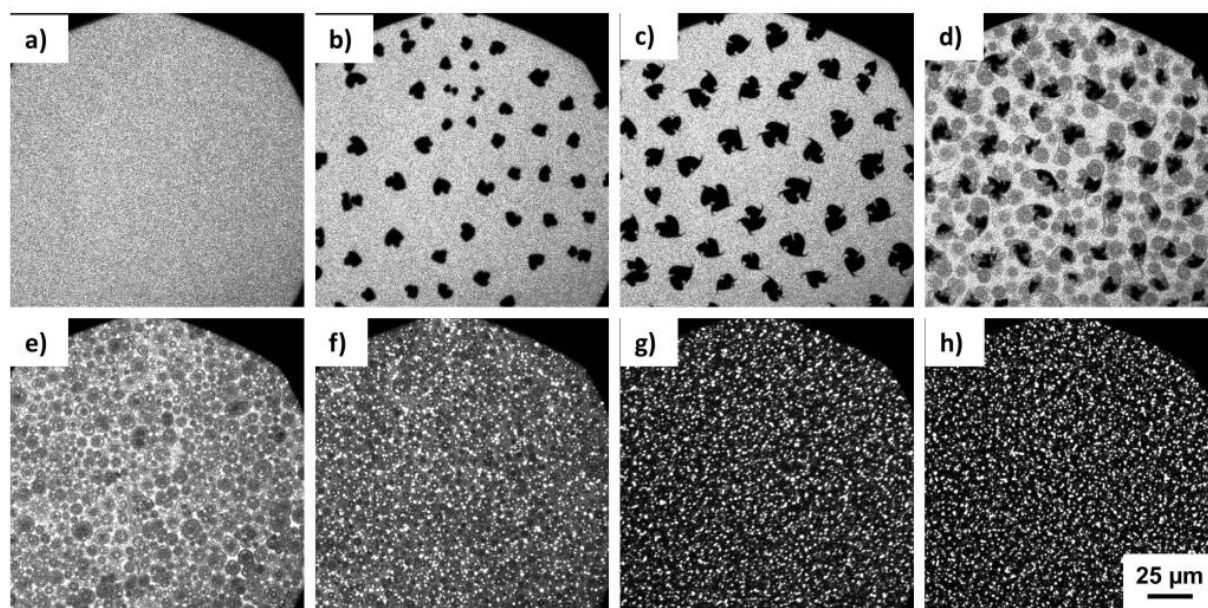


**Figure A16.** Epifluorescence microscopy images of mixed DPPC/8 98:2 monolayer at the air/water interface at 20°C. The images were recorded at constant compression of the cospread monolayer at the following surface pressures: (a) 5.1, (b) 6.5, (c) 7.6, (d) 9.1, (e) 11.2, (f) 12.5, (g) 15.4 and (h) 39.8 mN m<sup>-1</sup>.

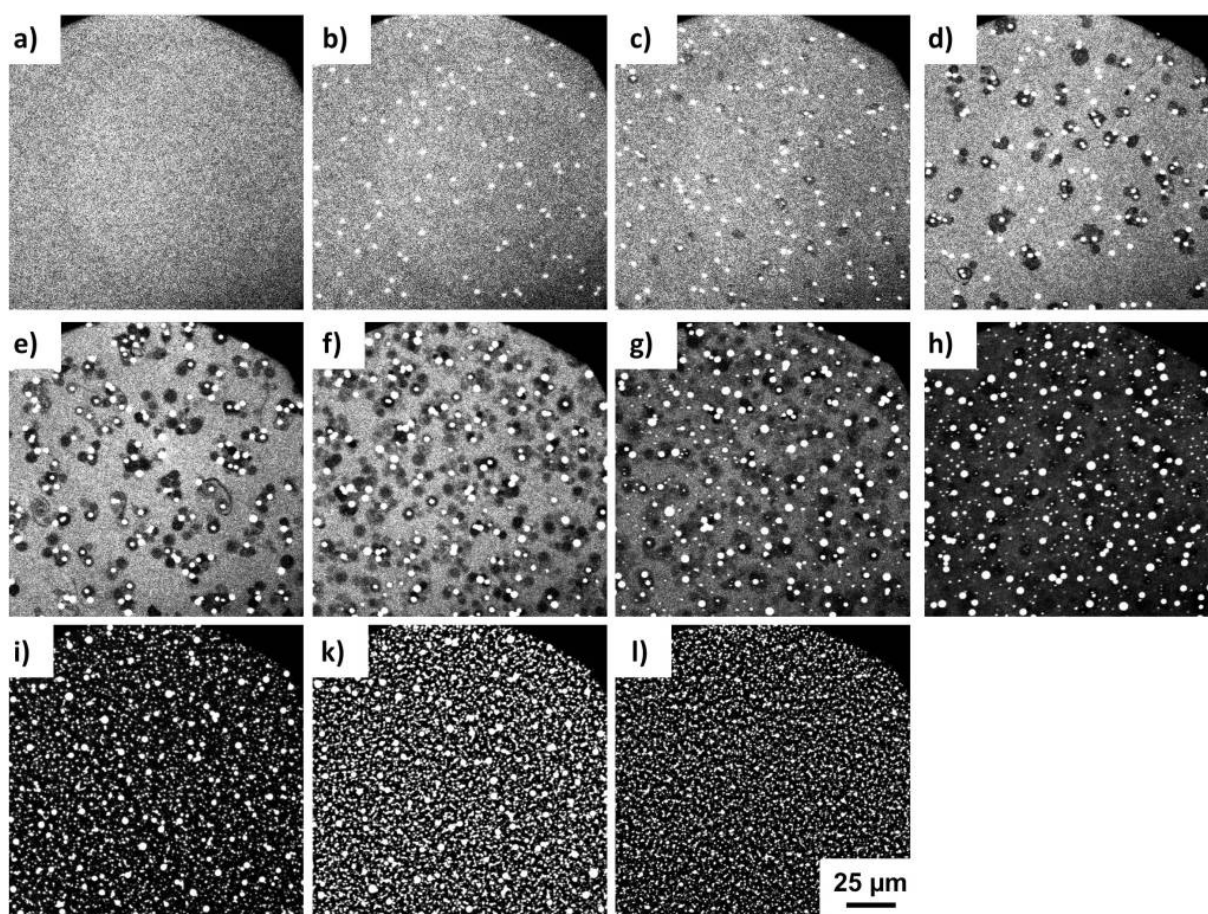


**Figure A17.** Epifluorescence microscopy images of mixed DPPC/8 95:5 monolayer at the air/water interface at 20°C. The images were recorded at constant compression of the cospread monolayer at the following surface pressures: (a) 4.8, (b) 8.1, (c) 9.1, (d) 9.7, (e) 10.8, (f) 12.3, (g) 13.4, (h) 13.7, (i) 14.3, (k) 26.9 and (l) 52.1 mN m<sup>-1</sup>.

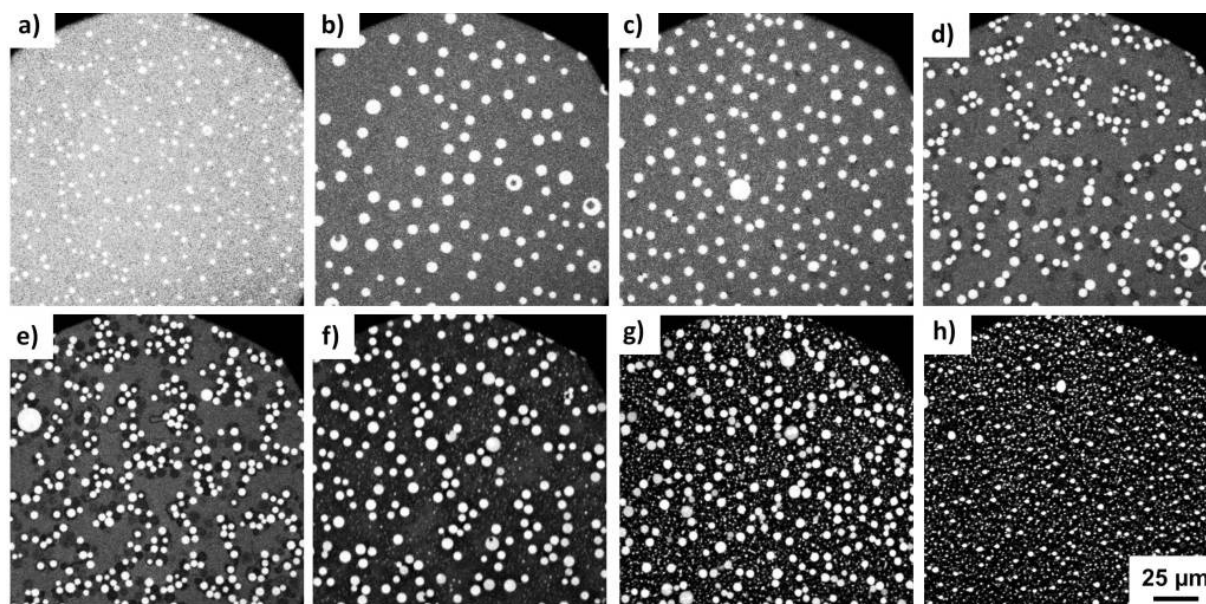


**Figure A18.** Epifluorescence microscopy images of mixed DPPC/8 90:10 monolayer at the air/water interface at 20°C. The images were recorded at constant compression of the cospread monolayer at the following surface pressures: (a) 2.7, (b) 8.9, (c) 9.7, (d) 10.8, (e) 11.7, (f) 14.5, (g) 17.2 and (h) 48.4  $\text{mN m}^{-1}$ .

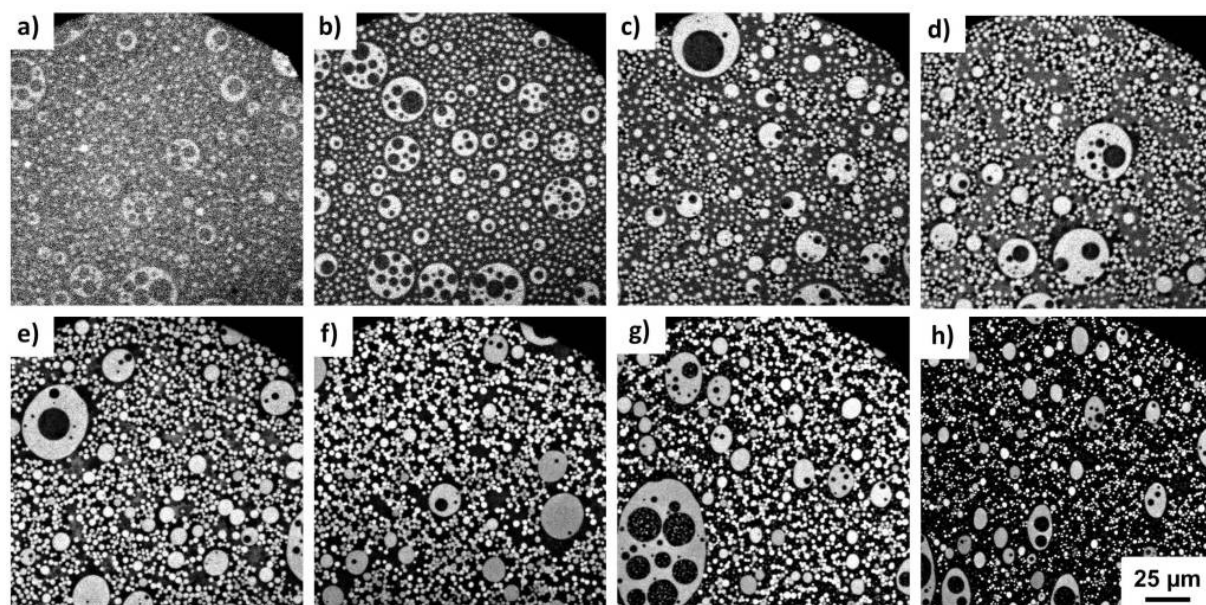


**Figure A19.** Epifluorescence microscopy images of mixed DPPC/8 80:20 monolayer at the air/water interface at 20°C. The images were recorded at constant compression of the cospread monolayer at the following surface pressures: (a) 0.3, (b) 8.9, (c) 12.3, (d) 12.8, (e) 13.8, (f) 16.9, (g) 27.5 and (h) 40.1  $\text{mN m}^{-1}$ .

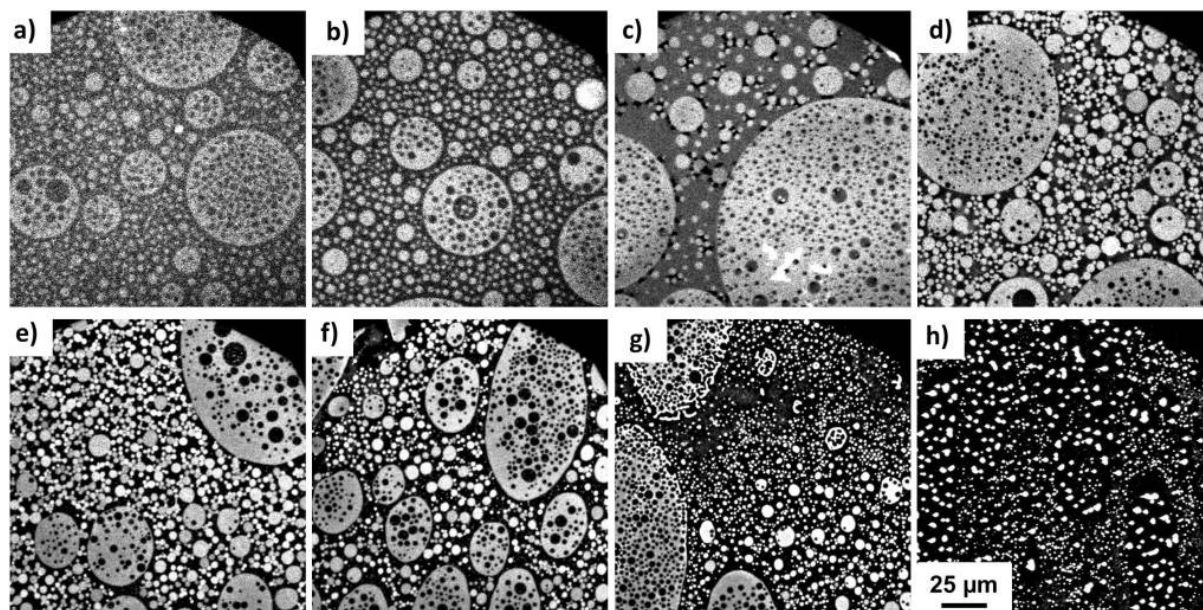


**Figure A20.** Epifluorescence microscopy images of mixed DPPC/8 70:30 monolayer at the air/water interface at 20°C. The images were recorded at constant compression of the cospread monolayer at the following surface pressures: (a) 0.6, (b) 6.7, (c) 10.8, (d) 12.9, (e) 18.8, (f) 39.3, (g) 39.9 and (h) 49.1  $\text{mN m}^{-1}$ .

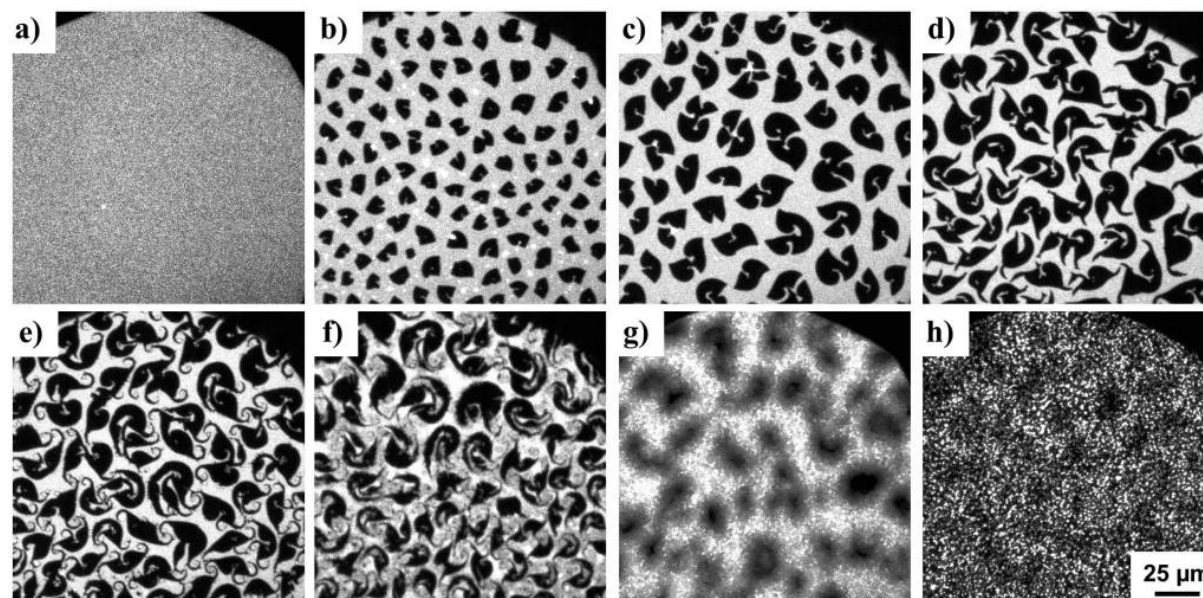


**Figure A21.** Epifluorescence microscopy images of mixed DPPC/9 99.5:0.5 monolayer at the air/water interface at 20°C. The images were recorded at constant compression of the cospread monolayer at the following surface pressures: (a) 4.1, (b) 5.3, (c) 5.8, (d) 6.7, (e) 7.2, (f) 7.6, (g) 10.9 and (h) 35.4  $\text{mN m}^{-1}$ .

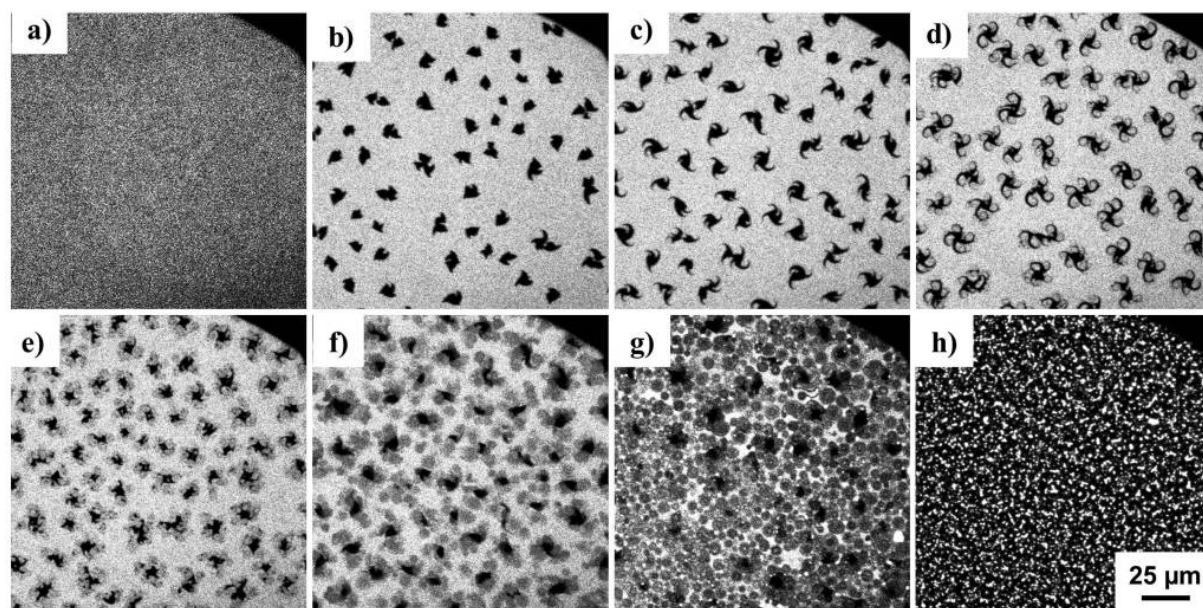


**Figure A22.** Epifluorescence microscopy images of mixed DPPC/9 99:1 monolayer at the air/water interface at 20°C. The images were recorded at constant compression of the cospread monolayer at the following surface pressures: (a) 0.1, (b) 6.3, (c) 6.6, (d) 6.9, (e) 7.1, (f) 8.1, (g) 9.7 and (h) 35.8  $\text{mN m}^{-1}$ .

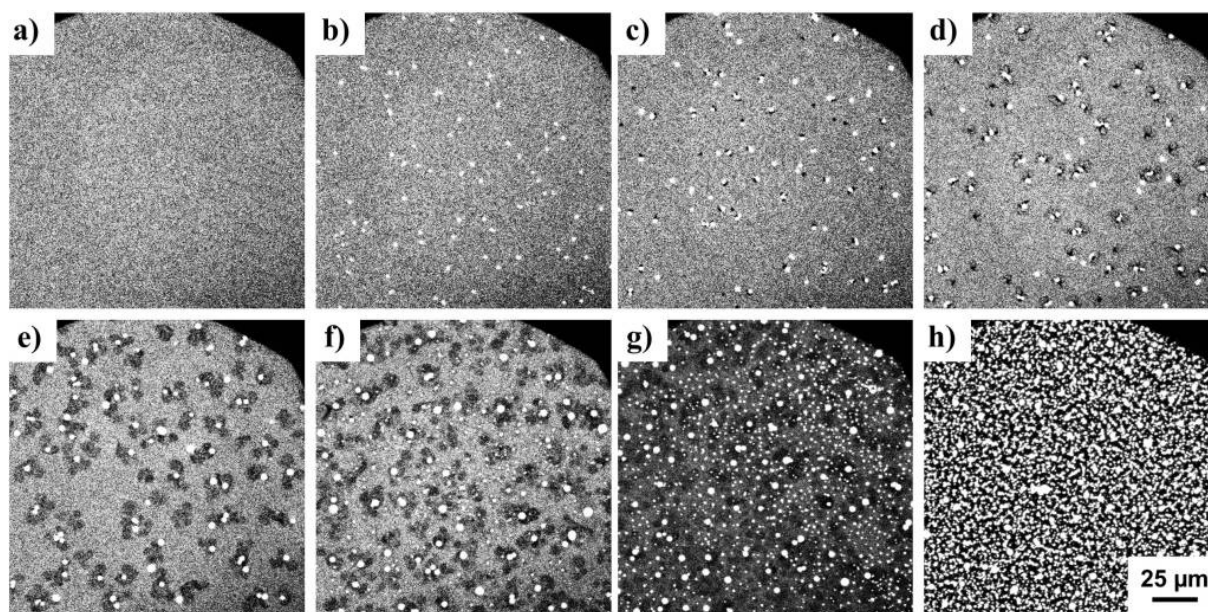


**Figure A23.** Epifluorescence microscopy images of mixed DPPC/9 98:2 monolayer at the air/water interface at 20°C. The images were recorded at constant compression of the cospread monolayer at the following surface pressures: (a) 4.1, (b) 6.8, (c) 7.6, (d) 8.1, (e) 9.2, (f) 10.7, (g) 11.6 and (h) 30.3  $\text{mN m}^{-1}$ .

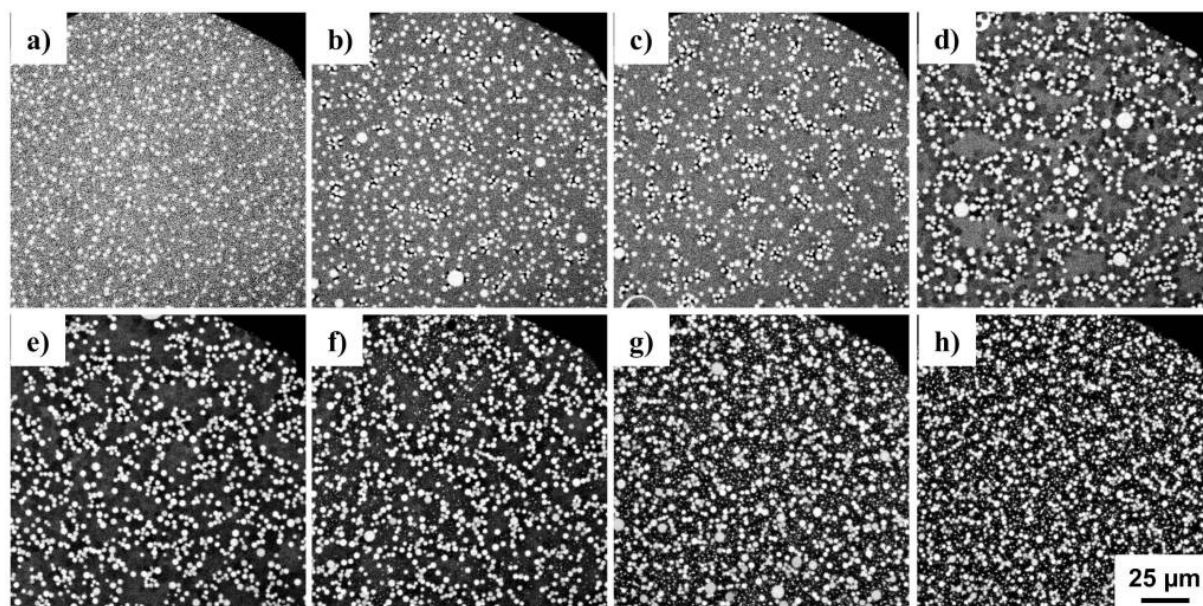


**Figure A24.** Epifluorescence microscopy images of mixed DPPC/9 95:5 monolayer at the air/water interface at 20°C. The images were recorded at constant compression of the cospread monolayer at the following surface pressures: (a) 2.9, (b) 8.6, (c) 9.1, (d) 10.4, (e) 13.2, (f) 13.7, (g) 15.3 and (h) 31.3  $\text{mN m}^{-1}$ .

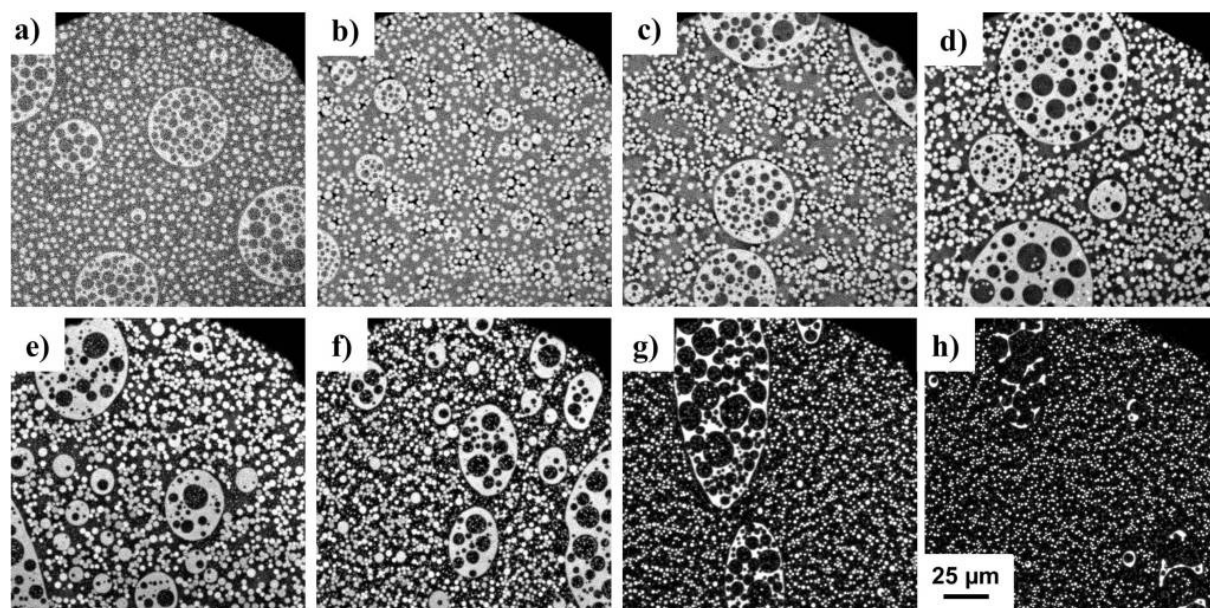


**Figure A25.** Epifluorescence microscopy images of mixed DPPC/9 90:10 monolayer at the air/water interface at 20°C. The images were recorded at constant compression of the cospread monolayer at the following surface pressures: (a) 5.0, (b) 9.4, (c) 10.3, (d) 12.4, (e) 14.5, (f) 29.2, (g) 36.3 and (h) 39.0  $\text{mN m}^{-1}$ .



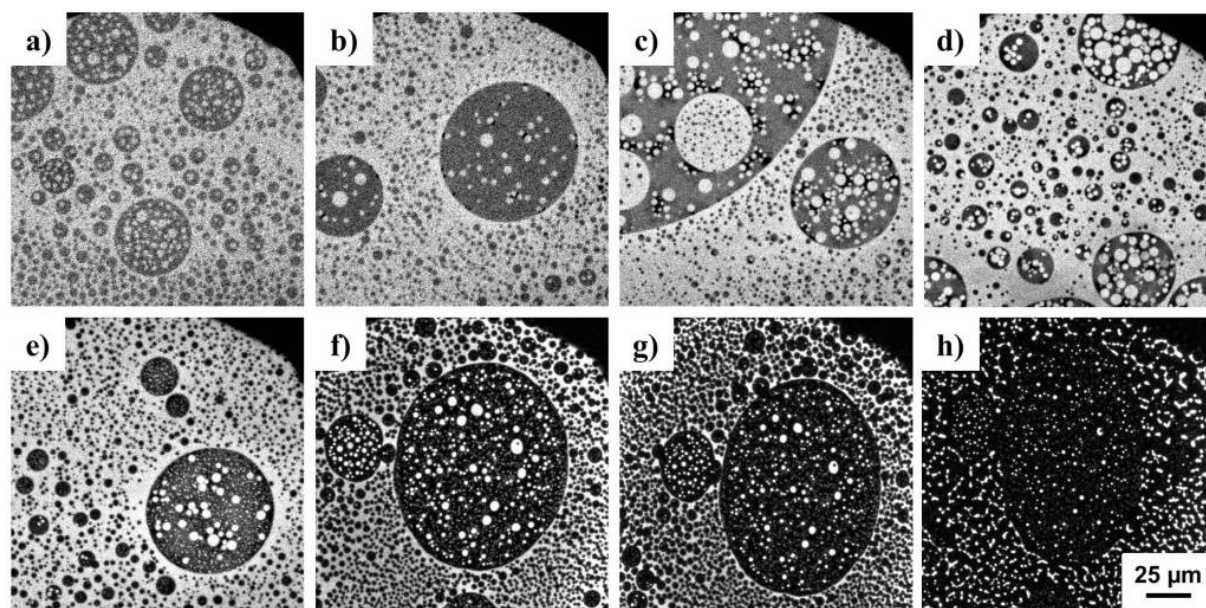


**Figure A26.** Epifluorescence microscopy images of mixed DPPC/9 80:20 monolayer at the air/water interface at 20°C. The images were recorded at constant compression of the cospread monolayer at the following surface pressures: (a) 2.4, (b) 6.0, (c) 9.8, (d) 12.1, (e) 14.0, (f) 36.0, (g) 36.2 and (h) 39.9 mN m<sup>-1</sup>.

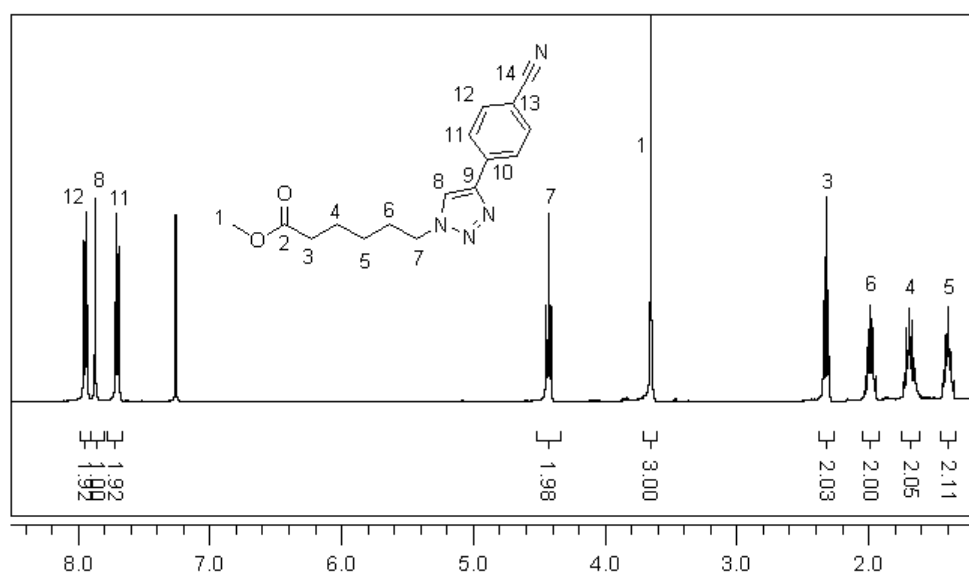


**Figure A27.** <sup>1</sup>H-NMR (CDCl<sub>3</sub>, 400 MHz) of **11a**.

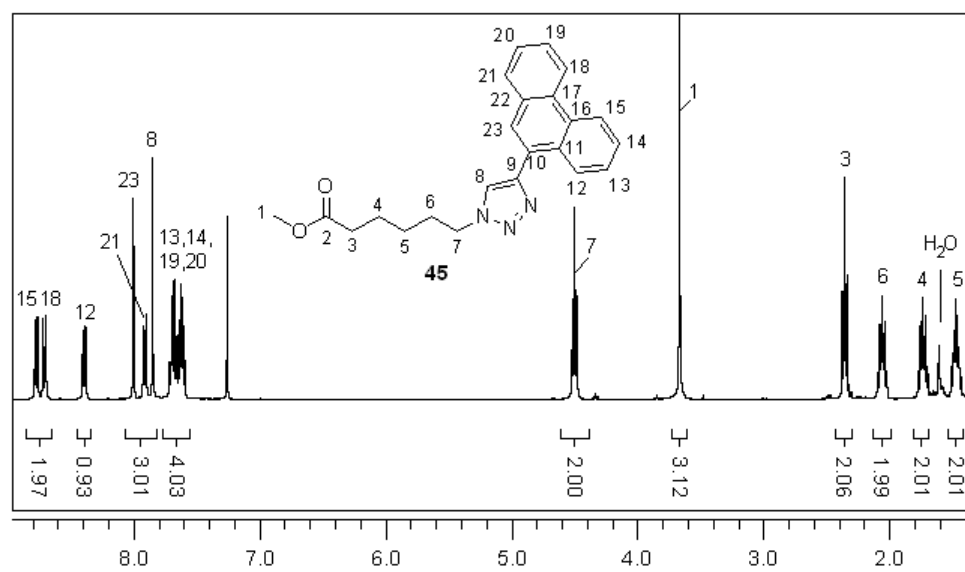


Figure A28. <sup>1</sup>H-NMR spectrum (CDCl<sub>3</sub>, 400 MHz) of 12a.

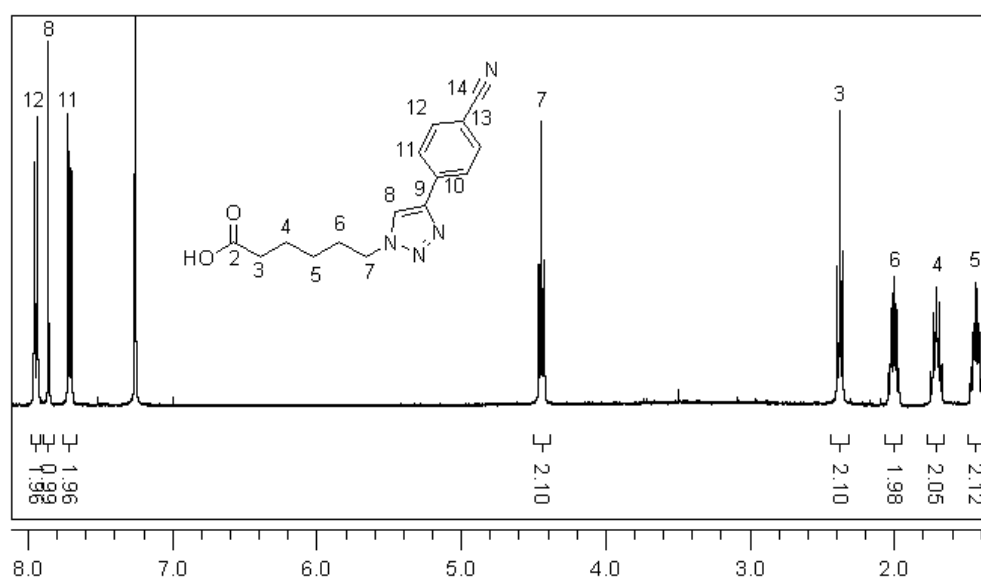
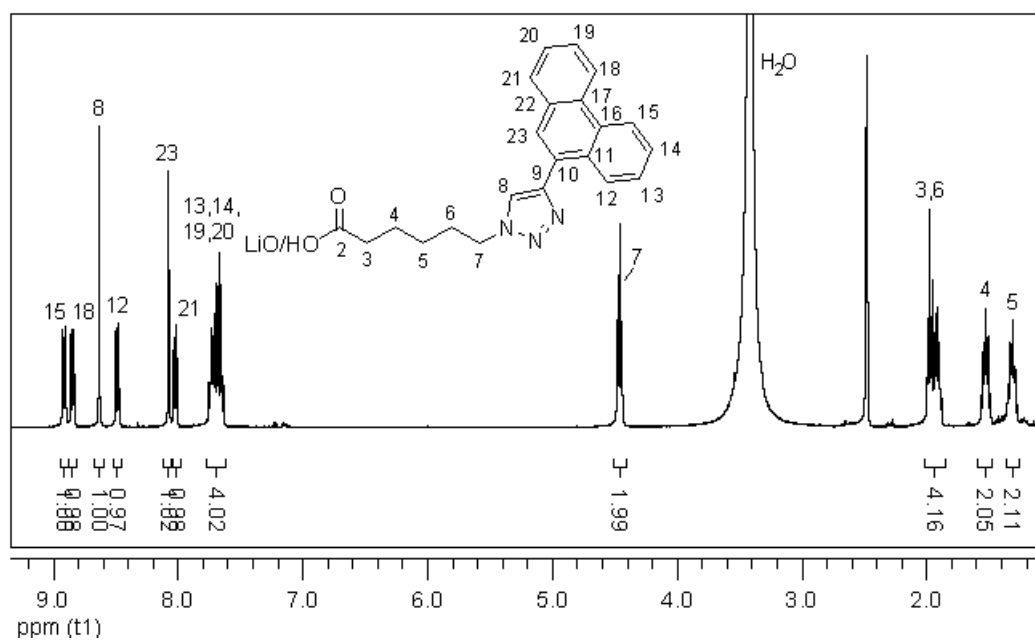
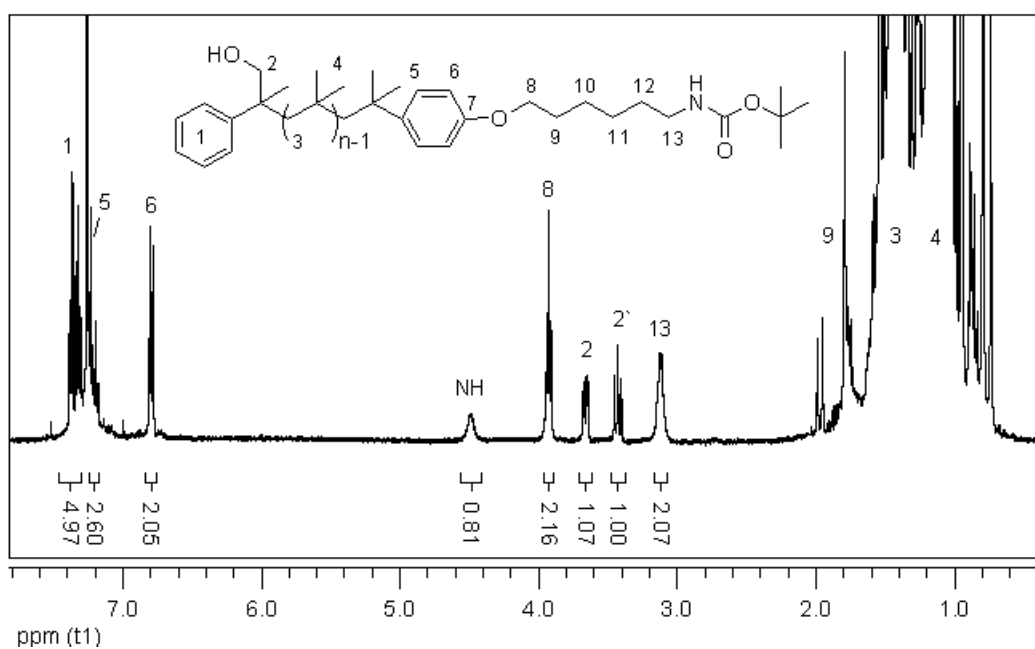


Figure A29. <sup>1</sup>H-NMR spectrum (CDCl<sub>3</sub>, 400 MHz) of 11.



**Figure A30.**  $^1\text{H-NMR}$  spectrum ( $\text{DMSO-d}_6$ , 400 MHz) of **12**.



**Figure A31.**  $^1\text{H-NMR}$  spectrum ( $\text{CDCl}_3$ , 400 MHz) of **17**.

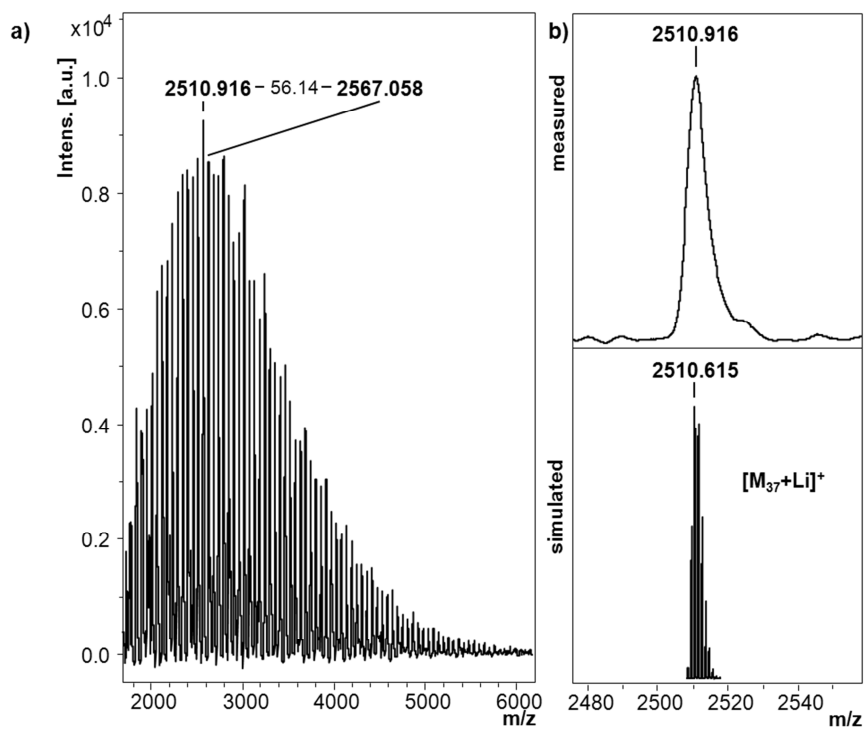


**Figure A32.** MALDI-ToF-MS of **17** of a) the region 1800-6000 Da and b) expanded spectrum with a listed view of the simulated peak.

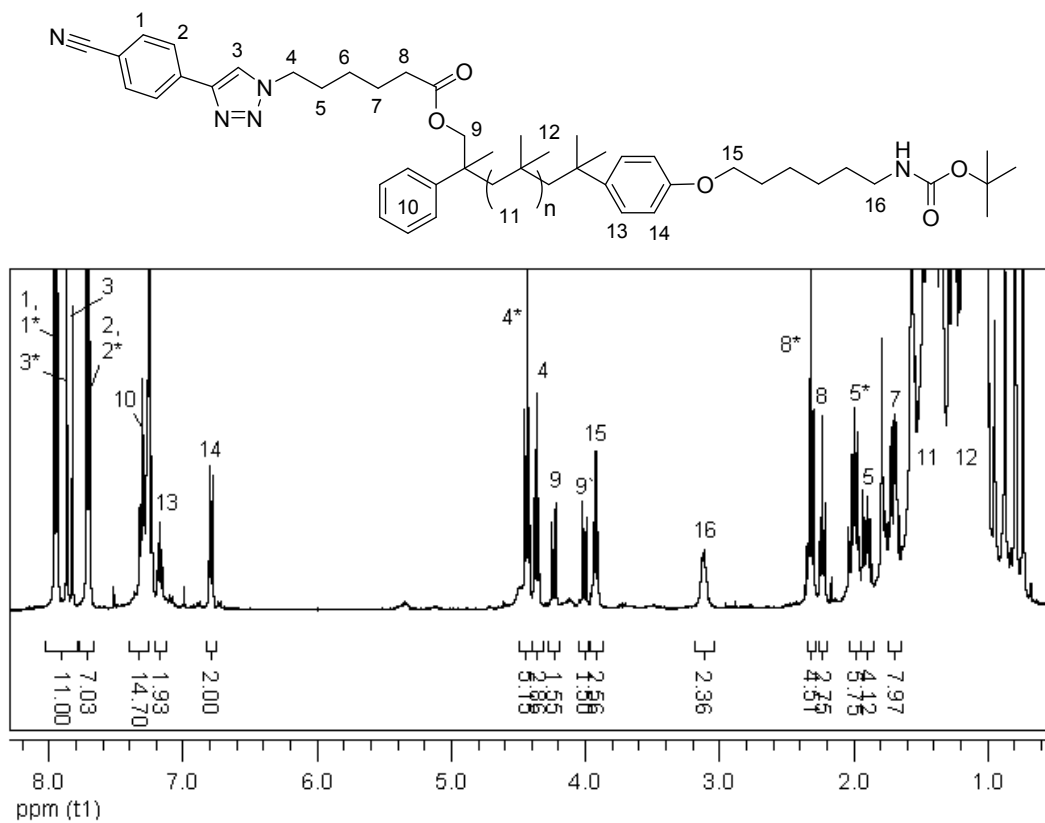


**Figure A33.** <sup>1</sup>H-NMR spectrum (CDCl<sub>3</sub>, 400 MHz) of **32**. \*excess **11** is left

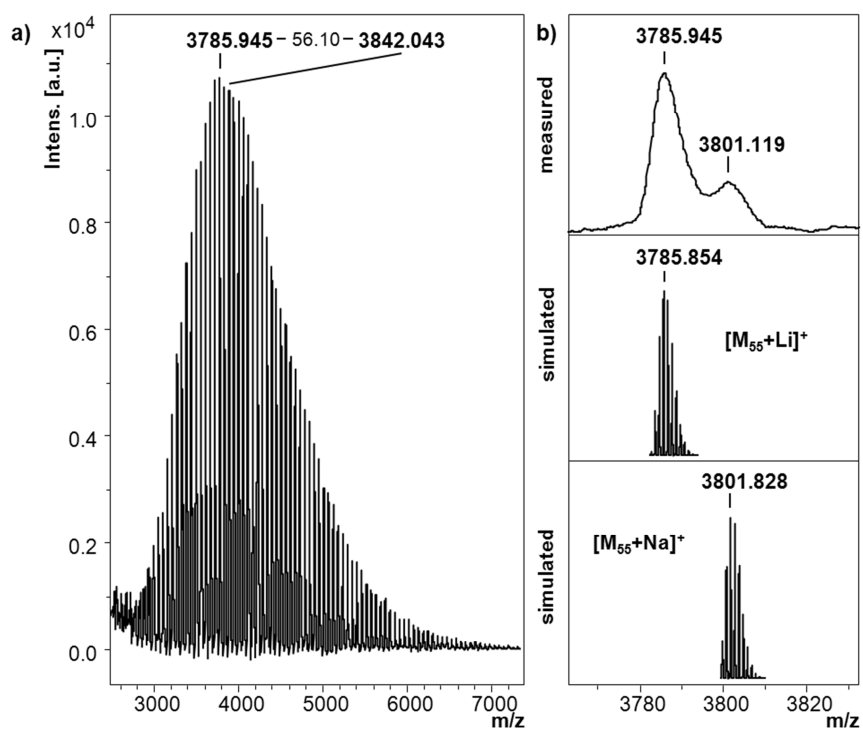


**Figure A34.** MALDI-ToF-MS of **32** of a) the region 2500-7000 Da and b) expanded spectrum with a listed view of the simulated peaks.

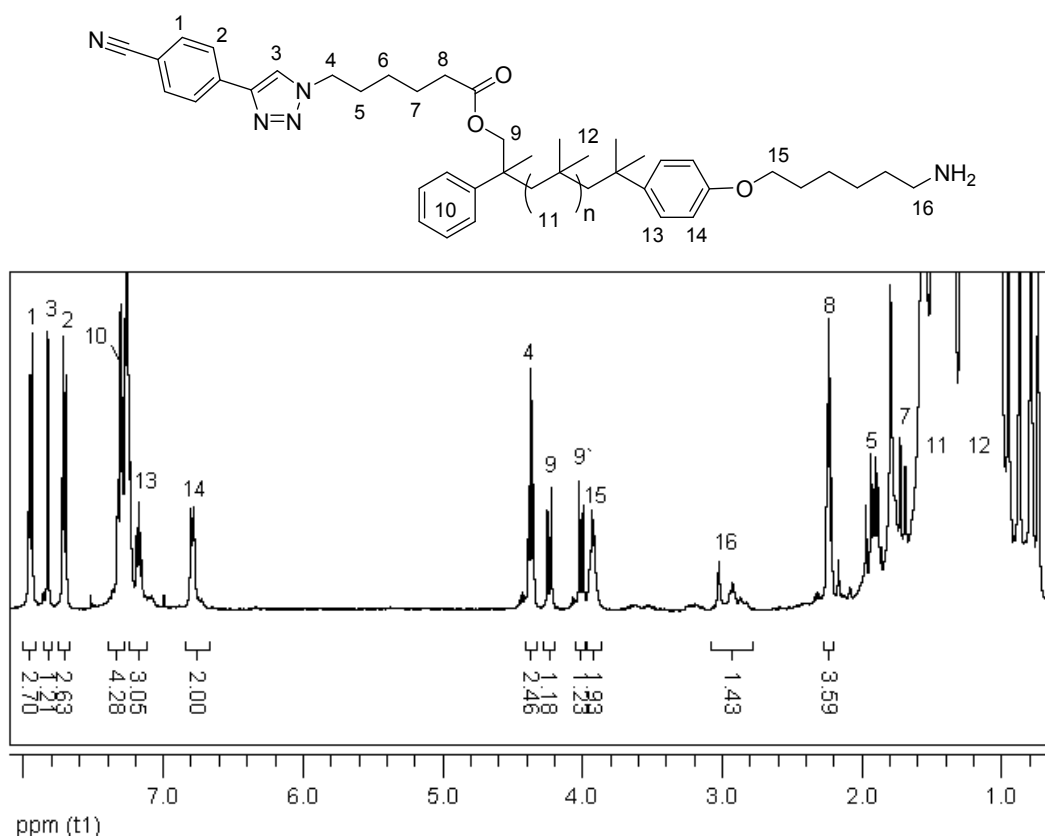


**Figure A35.**  $^1\text{H-NMR}$  spectrum (CDCl<sub>3</sub>, 400 MHz) of **13**.



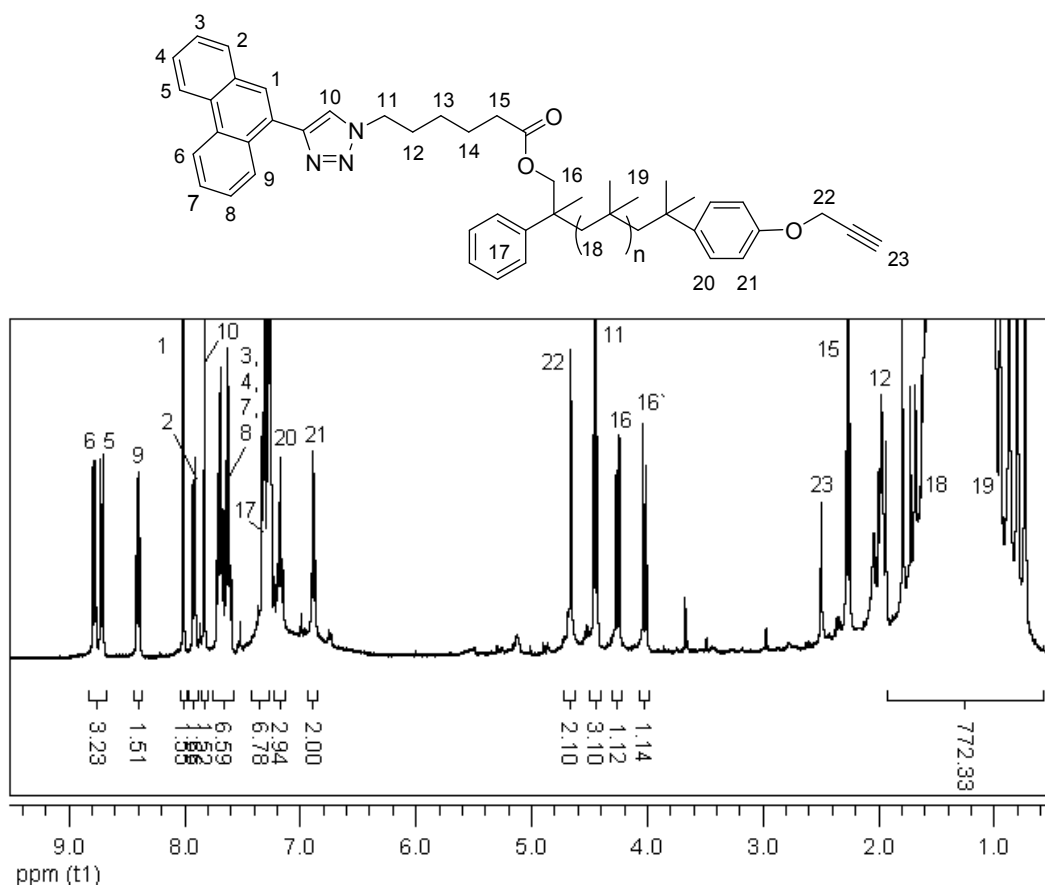


Figure A38. <sup>1</sup>H-NMR spectrum (CDCl<sub>3</sub>, 400 MHz) of 15.

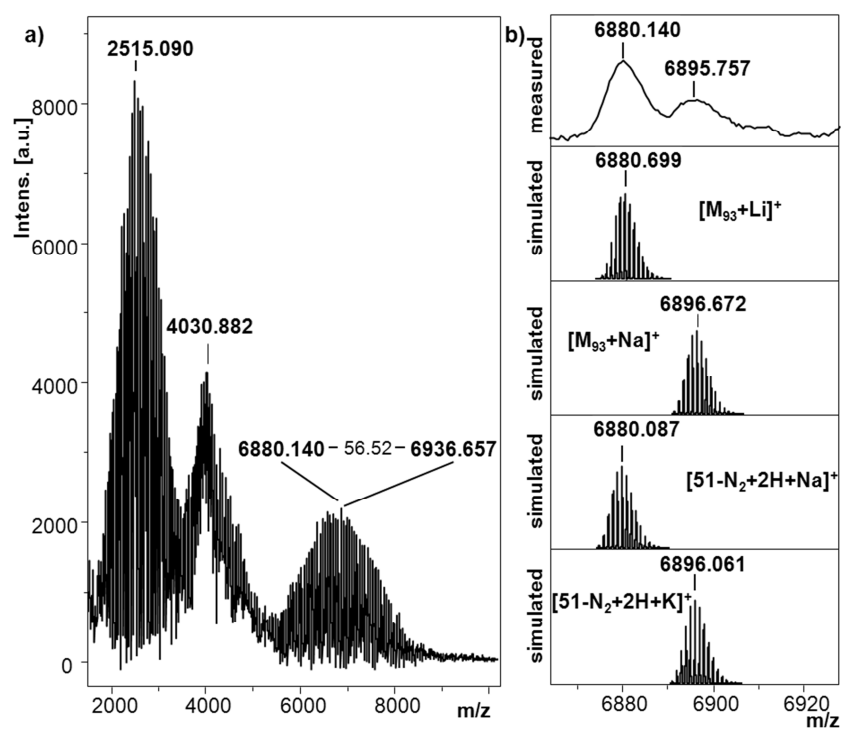


Figure A39. MALDI-ToF-MS of “16” of a) the region 1000-6000 Da and b) expanded spectrum with a listed view of the simulated peaks.

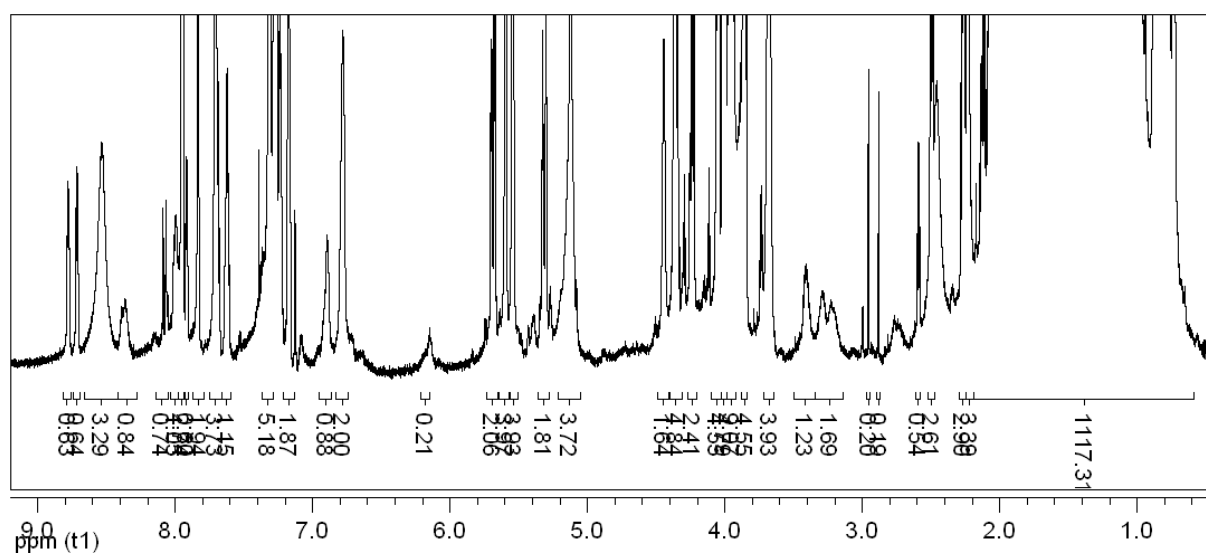


Figure A40.  $^1\text{H-NMR}$  spectrum ( $\text{CDCl}_3$ , 400 MHz) of “16”.

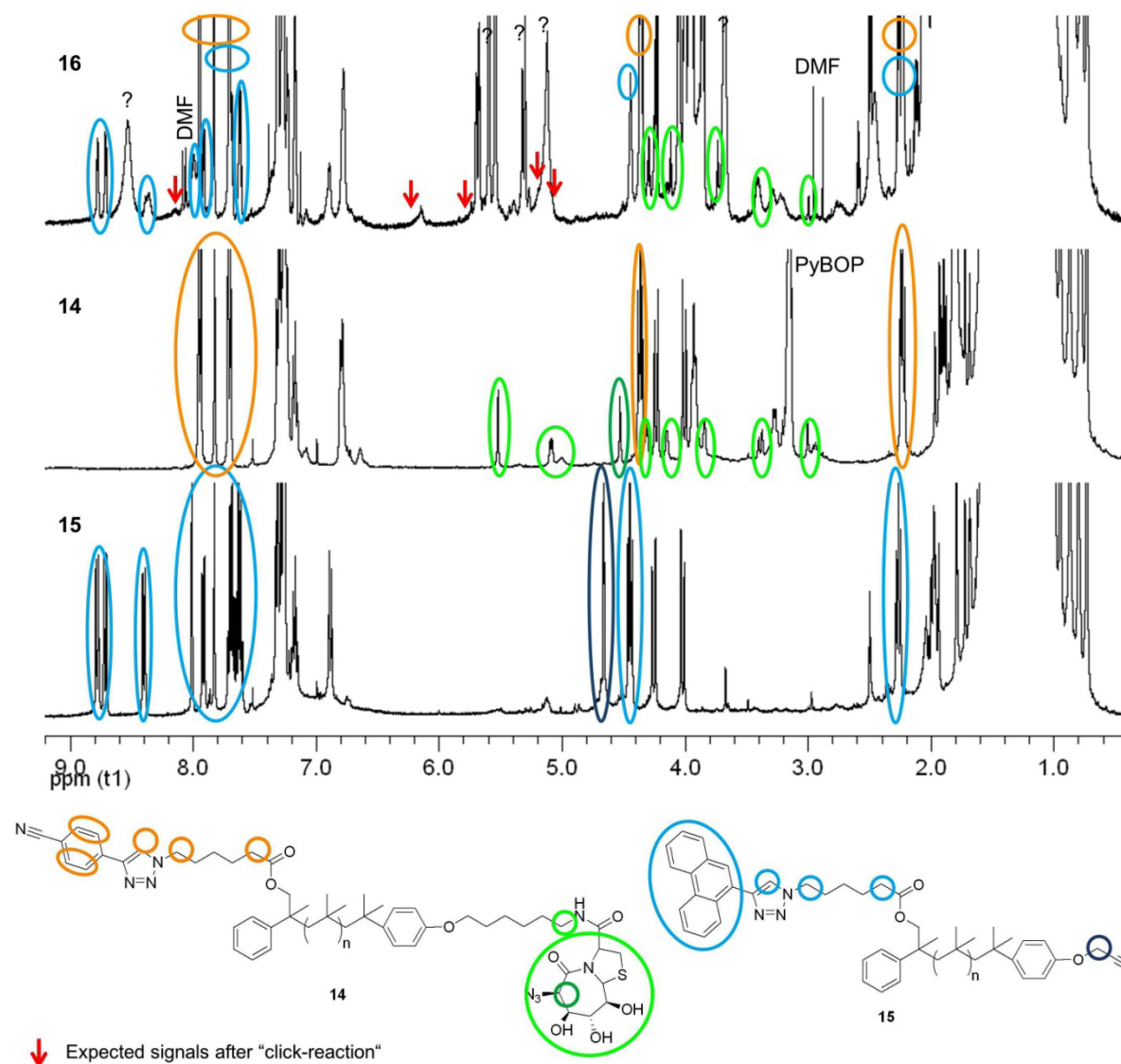
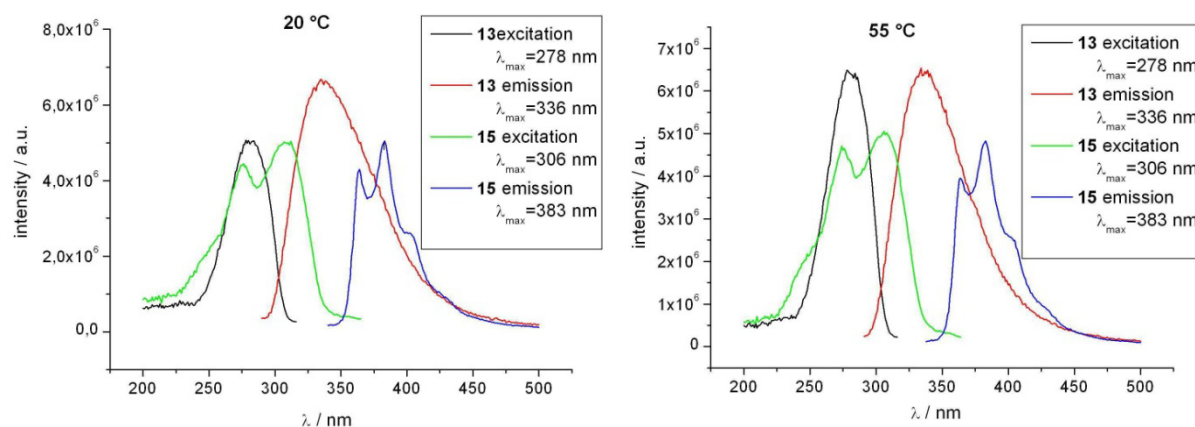
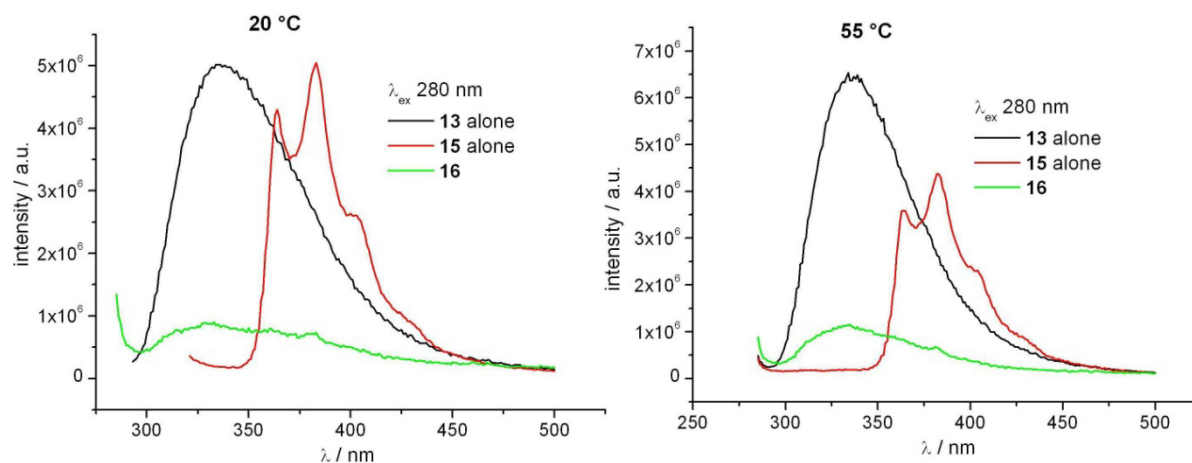


Figure A41. Overlay of  $^1\text{H-NMR}$  spectra ( $\text{CDCl}_3$ , 400 MHz) of a) “16”, b) 14 and c) 15. The Circles indicate characteristic peaks of the single strands and the red arrows show the position of the expected signals of 16.





**Figure A42.** Fluorescence absorption and emission spectra of mixed DPPC/13 or DPPC/15 (99:1) bilayer at 20 °C and 55 °C.



**Figure A43.** Fluorescence emission spectra of mixed DPPC/13 (99:1), DPPC/15 (99:1) and DPPC/16 (99:1) bilayer at 20 °C and 55 °C excited at 280 nm.

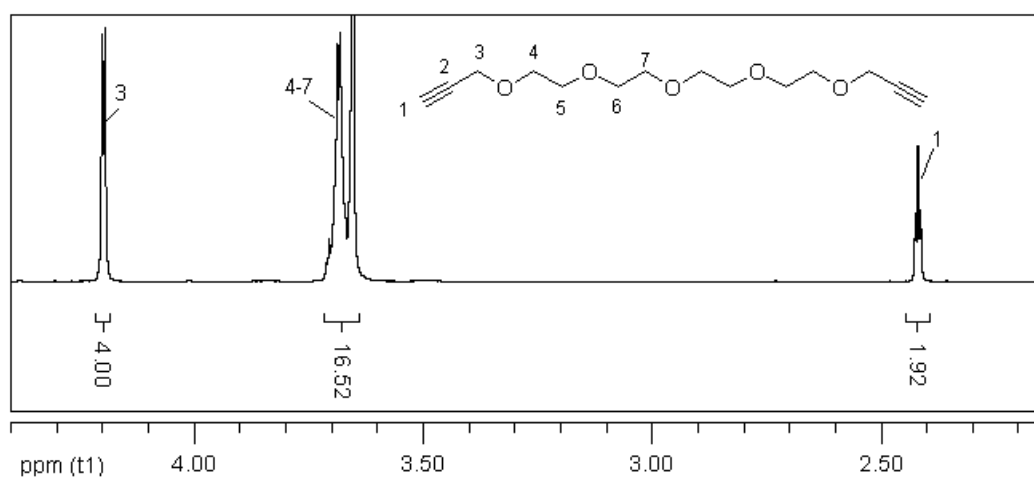


**Figure A44.**  $^1\text{H-NMR}$  spectrum (CDCl<sub>3</sub>, 400 MHz) of  $\alpha,\omega$ -dialkynyl tetraethylene glycol (19).

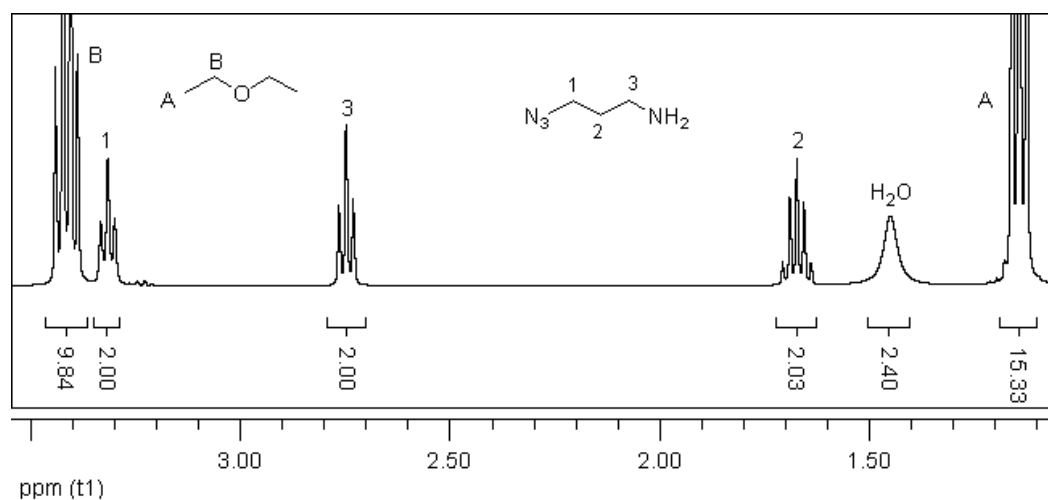


Figure A45. <sup>1</sup>H-NMR spectrum (CDCl<sub>3</sub>, 400 MHz) of 3-azido-propylamine (20a).

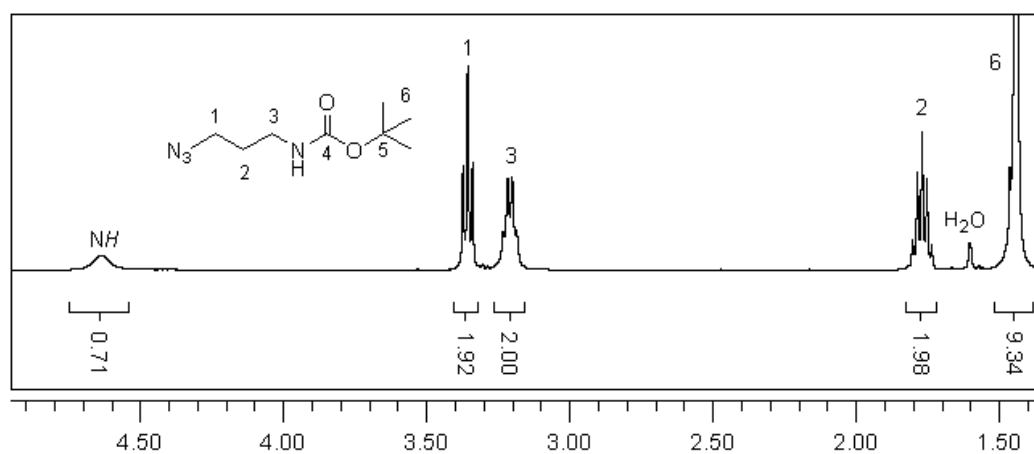


Figure A46. <sup>1</sup>H-NMR spectrum (CDCl<sub>3</sub>, 400 MHz) of 20.

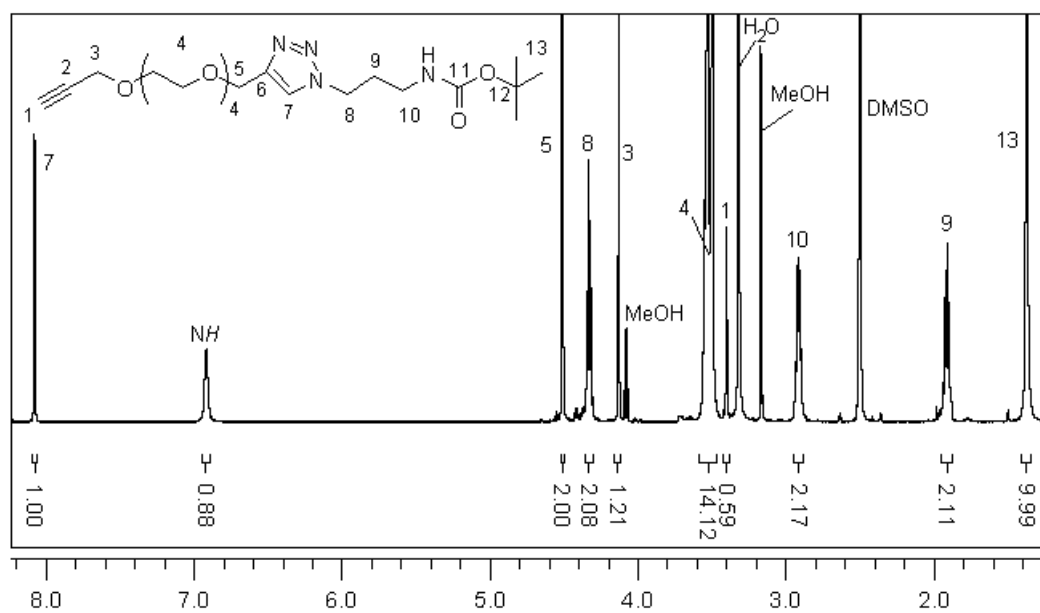
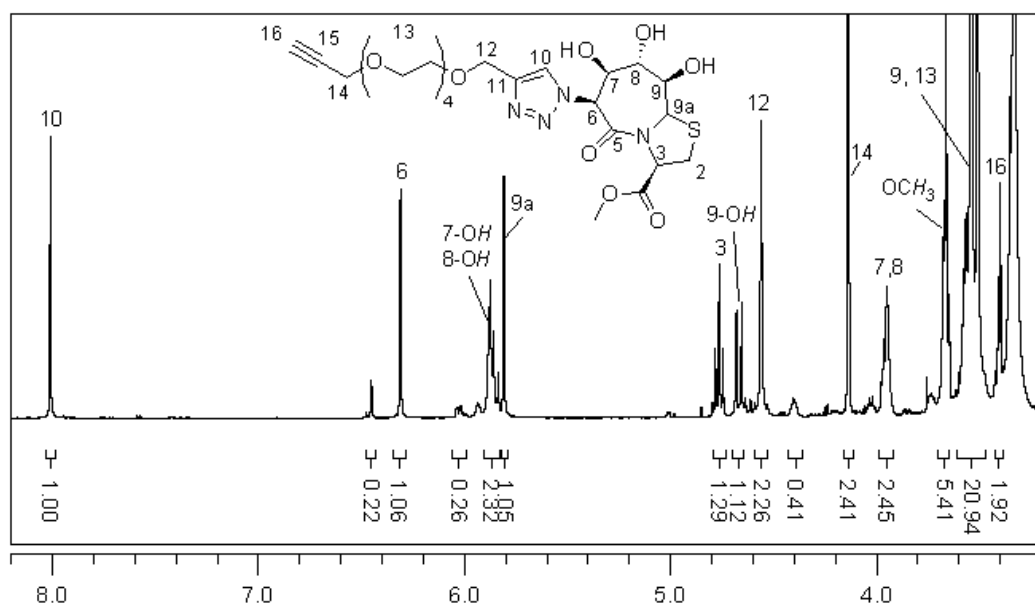
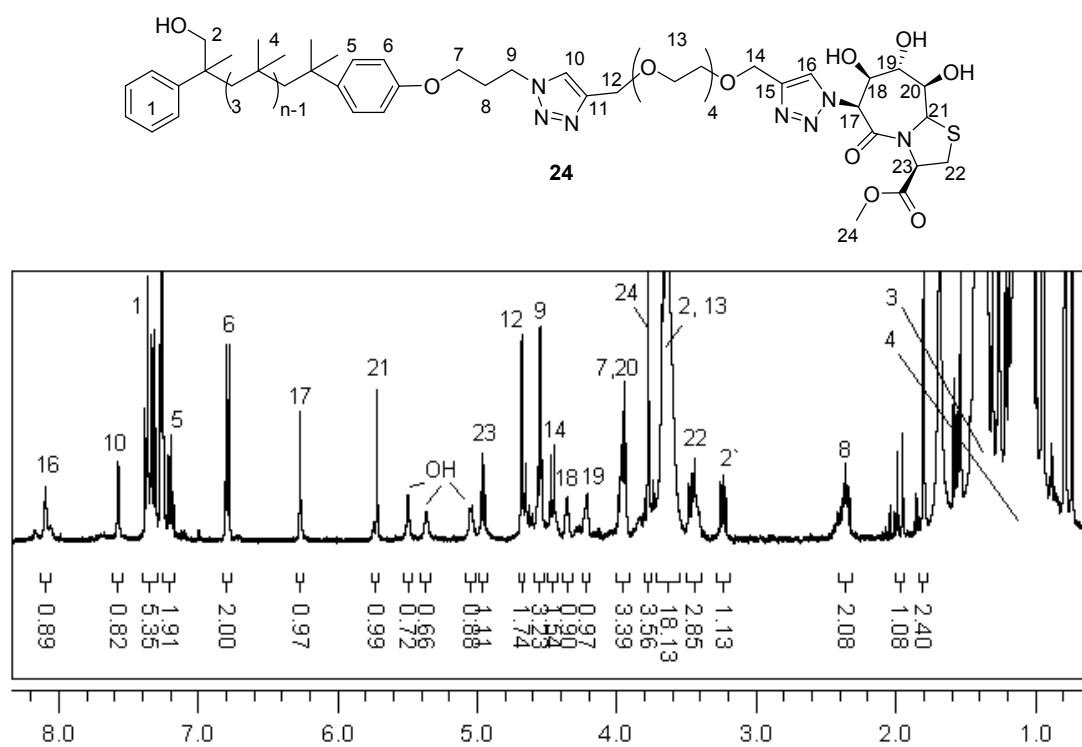


Figure A47. <sup>1</sup>H-NMR spectrum (DMSO-d<sub>6</sub>, 400 MHz) of 21a.



**Figure A48.**  $^1\text{H-NMR}$  spectrum ( $\text{DMSO-d}_6$ , 400 MHz) of **22**.



**Figure A49.**  $^1\text{H-NMR}$  spectrum ( $\text{CDCl}_3$ , 400 MHz) of **24**.

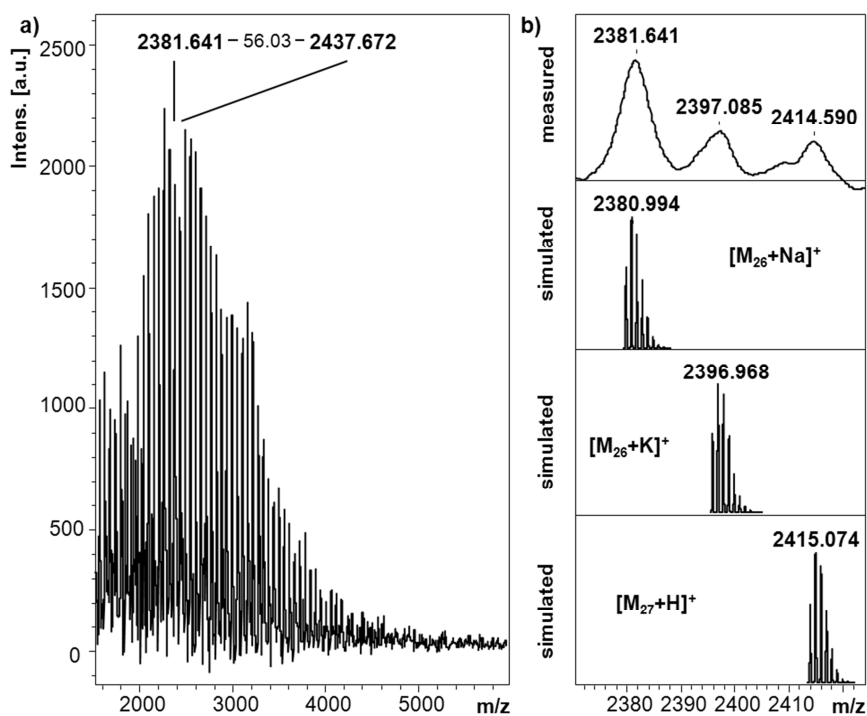


**Figure A50.** MALDI-ToF-MS of **24** of a) the region 1600-6000 Da and b) expanded spectrum with a listed view of the simulated peaks.

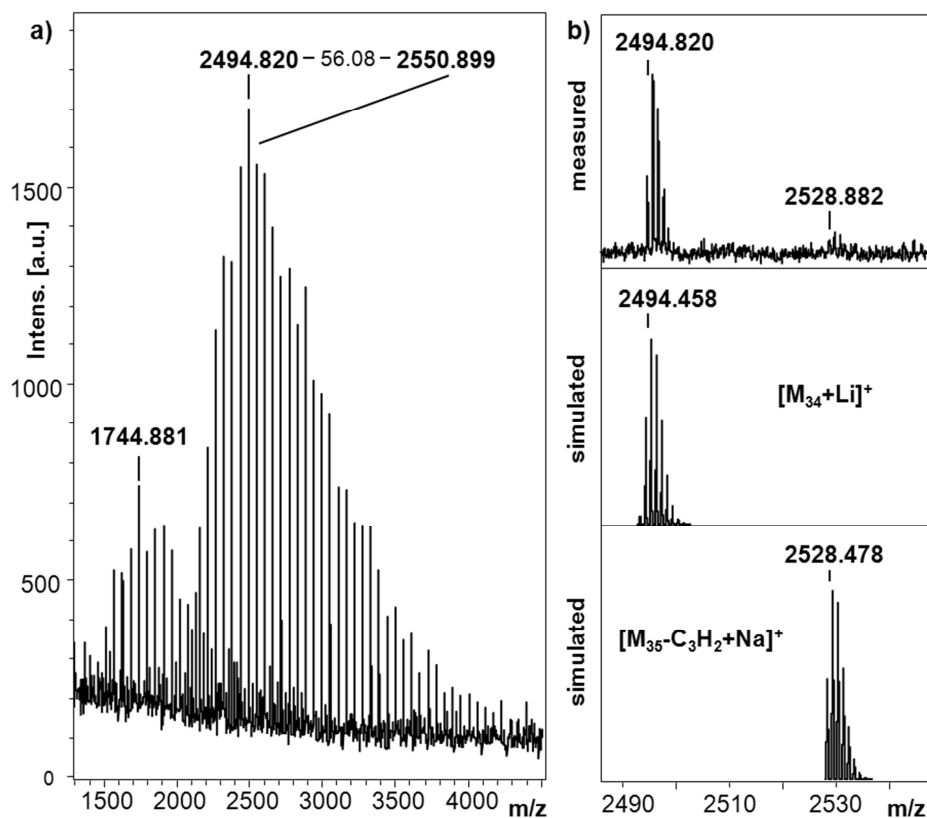


**Figure A51.** MALDI-ToF-MS of **23** of a) the region 1300-5000 Da and b) expanded spectrum with a listed view of the simulated peaks. (Small series  $M_{n, \text{exp}} = 1744.881$  g/mol for PIB-TEG-OH +Na<sup>+</sup> ( $n = 21$ )  $\rightarrow M_{n, \text{calc}} = 1744.602$  g/mol).

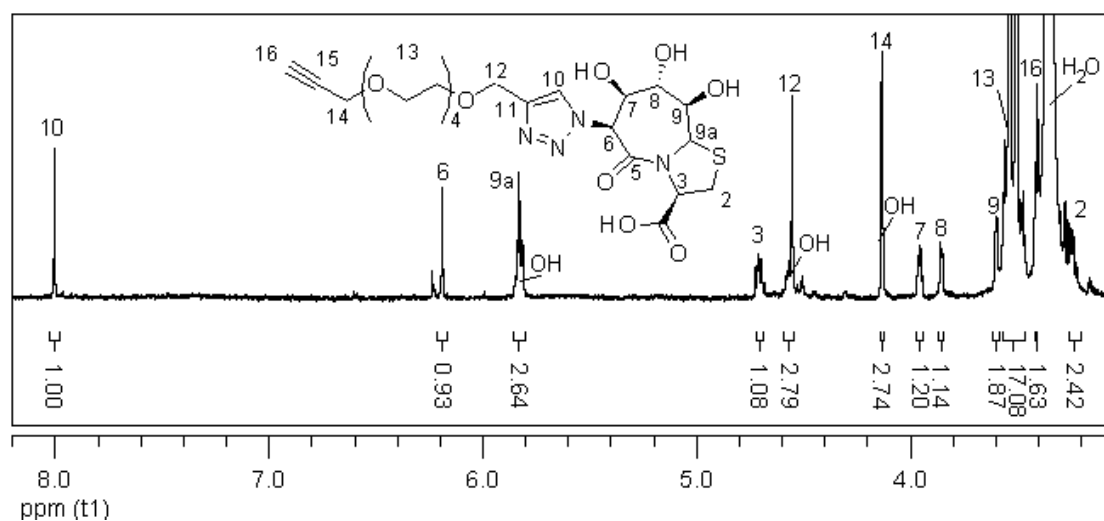


**Figure A52.**  $^1\text{H-NMR}$  spectrum ( $\text{DMSO-d}_6$ , 400 MHz) of **33**.

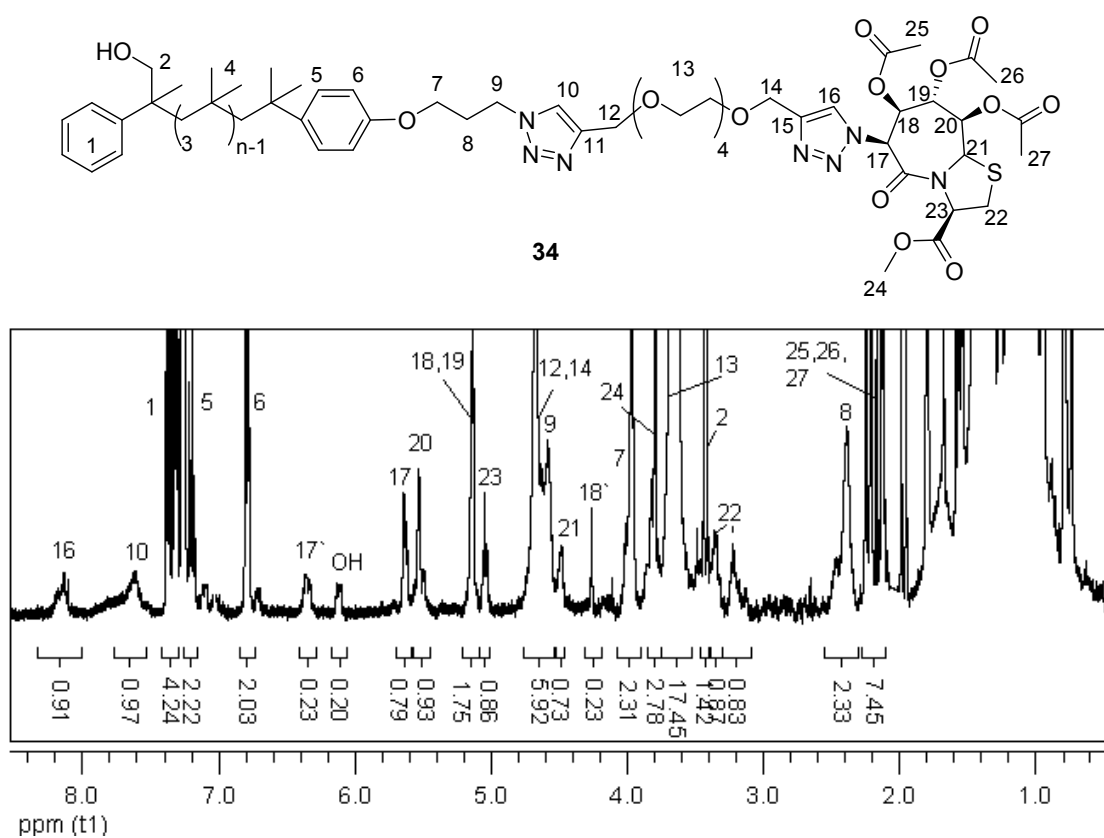


**Figure A53.**  $^1\text{H-NMR}$  spectrum ( $\text{CDCl}_3$ , 400 MHz) of **34**.

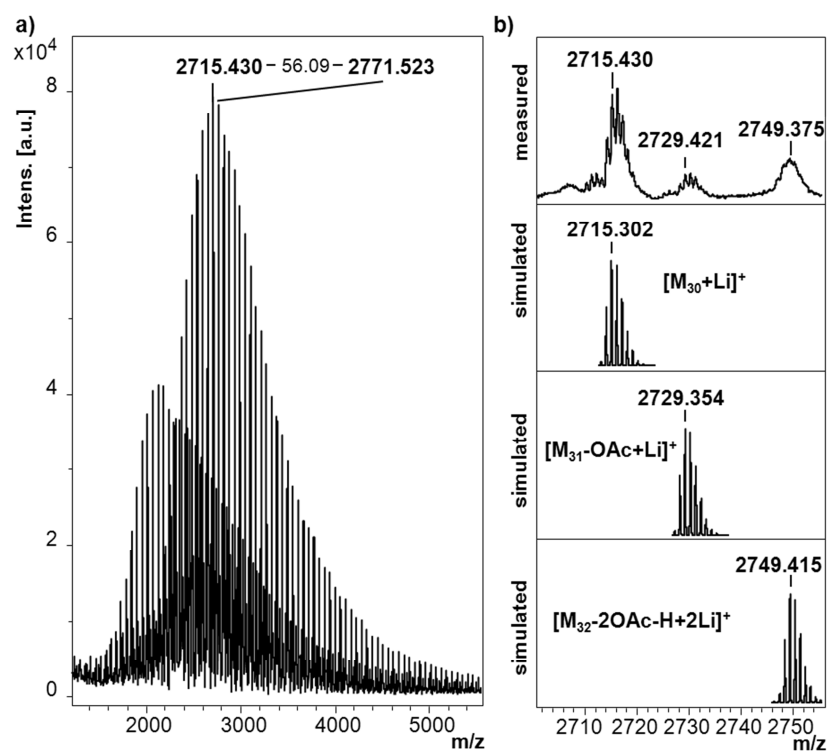


**Figure A54.** MALDI-ToF-MS of **34** of a) the region 1300-5000 Da and b) expanded spectrum with a listed view of the simulated peaks.

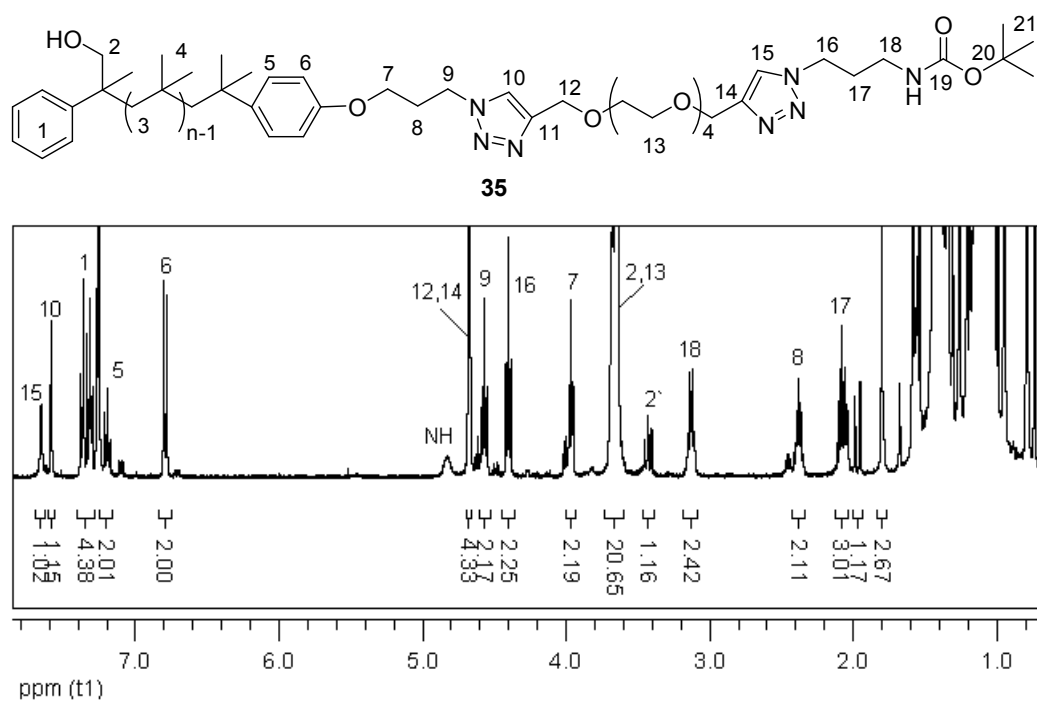


**Figure A55.**  $^1\text{H-NMR}$  spectrum (CDCl<sub>3</sub>, 400 MHz) of **35**.

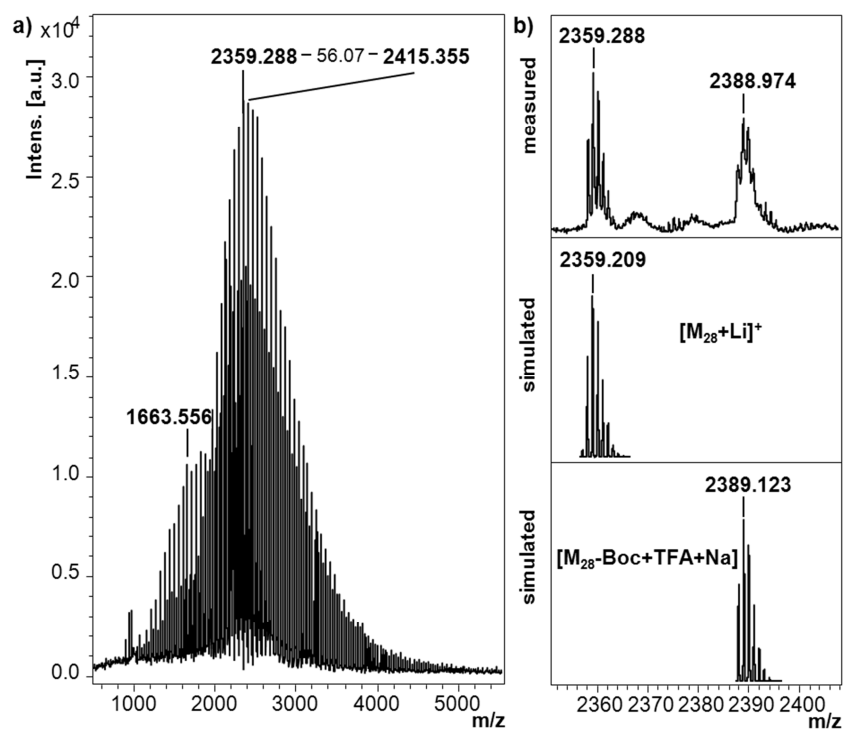


**Figure A56.** MALDI-ToF-MS of **35** of a) the region 1000-5000 Da and b) expanded spectrum with a listed view of the simulated peaks. (Small series  $M_{n, \text{exp}} = 1663.556$  g/mol for PIB- $N_3$  (**18**) + $\text{Li}^+$  ( $n = 24$ )  $\rightarrow M_{n, \text{calc}} = 1663.681$  g/mol).

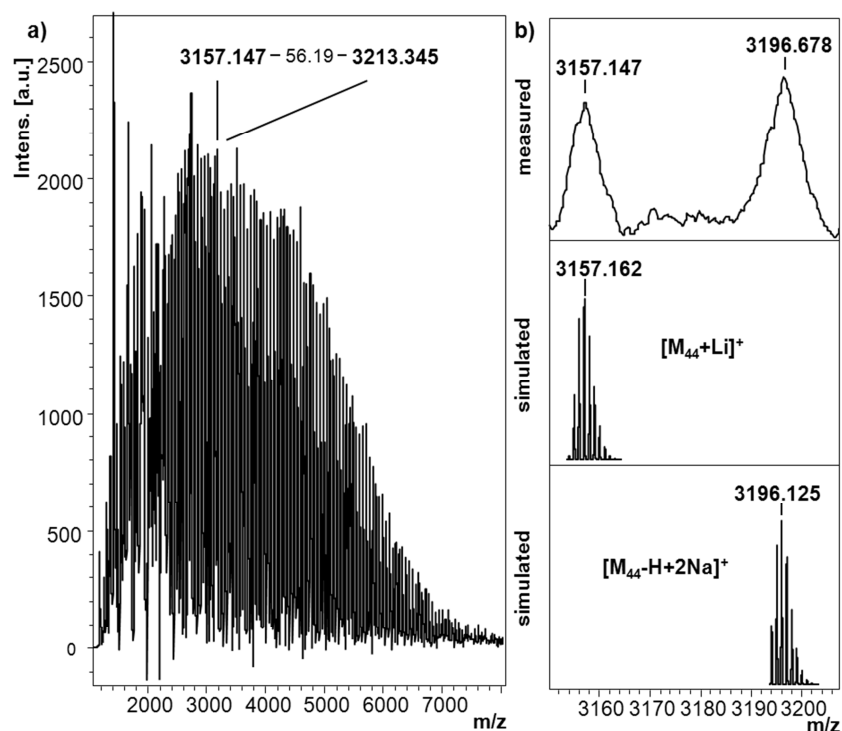


**Figure A57.** MALDI-ToF-MS of **36** of a) the region 1000-8000 Da and b) expanded spectrum with a listed view of the simulated peaks.

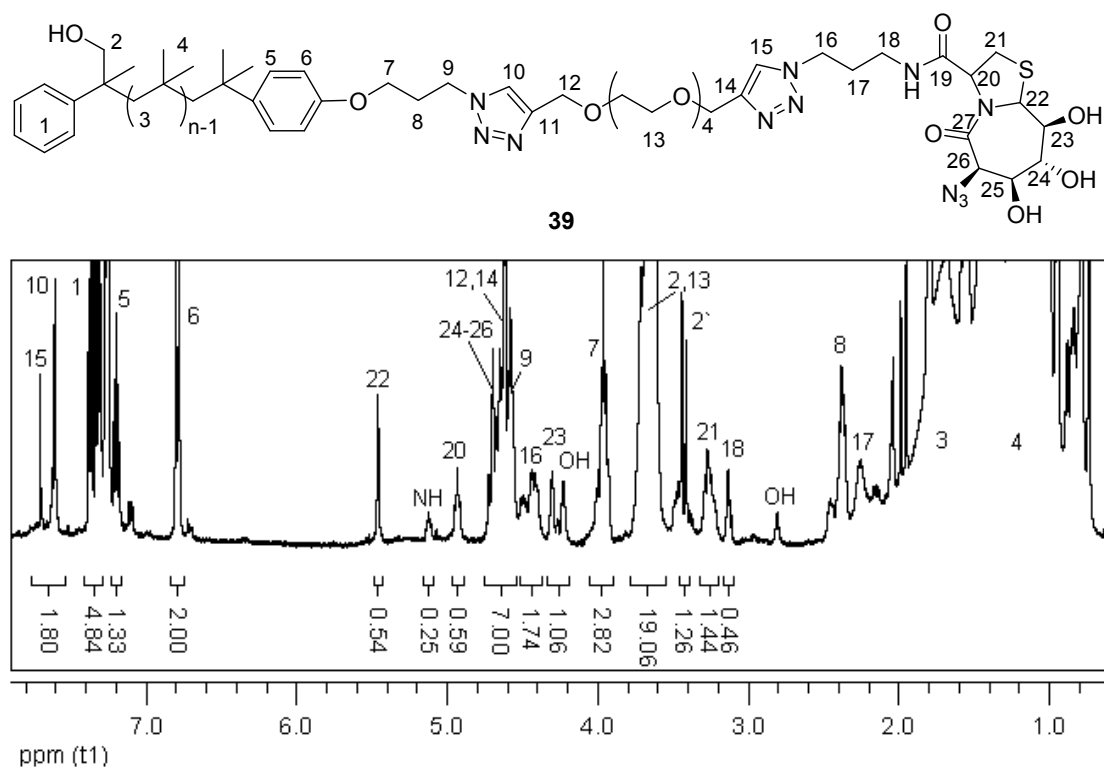


Figure A58.  $^1\text{H-NMR}$  spectrum ( $\text{CDCl}_3$ , 400 MHz) of **39**.

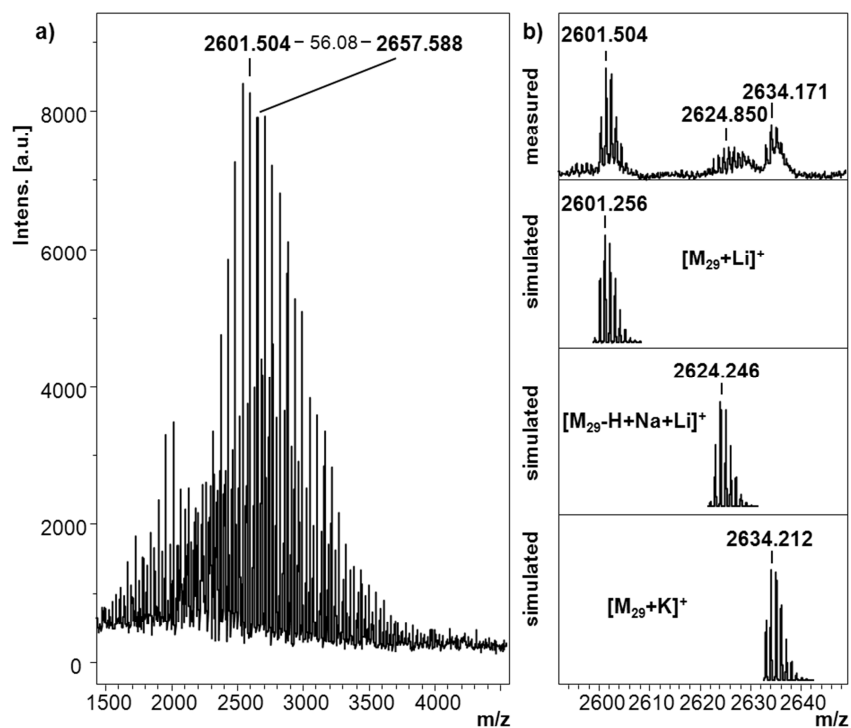
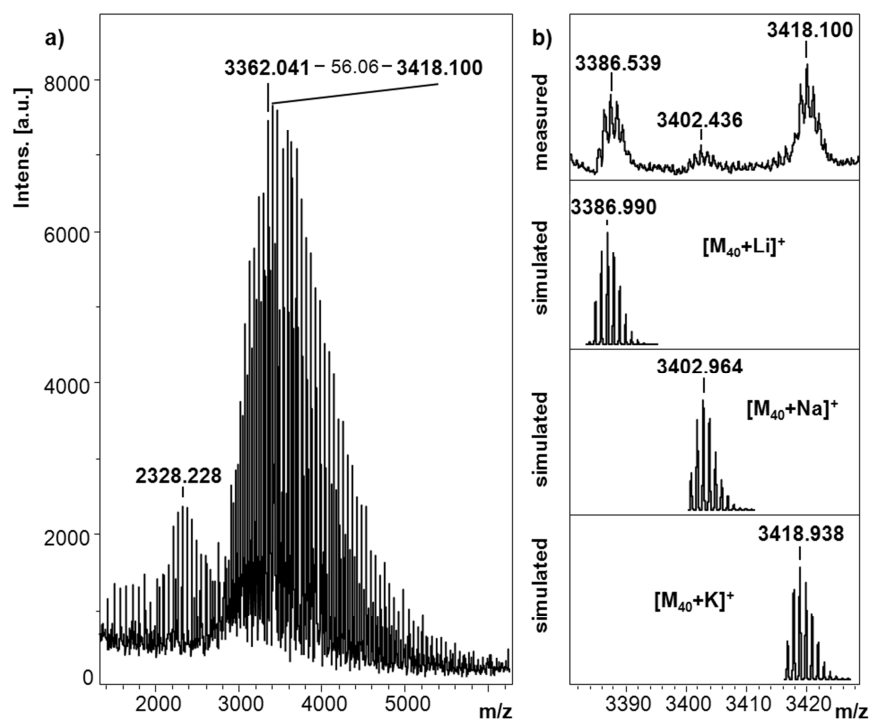
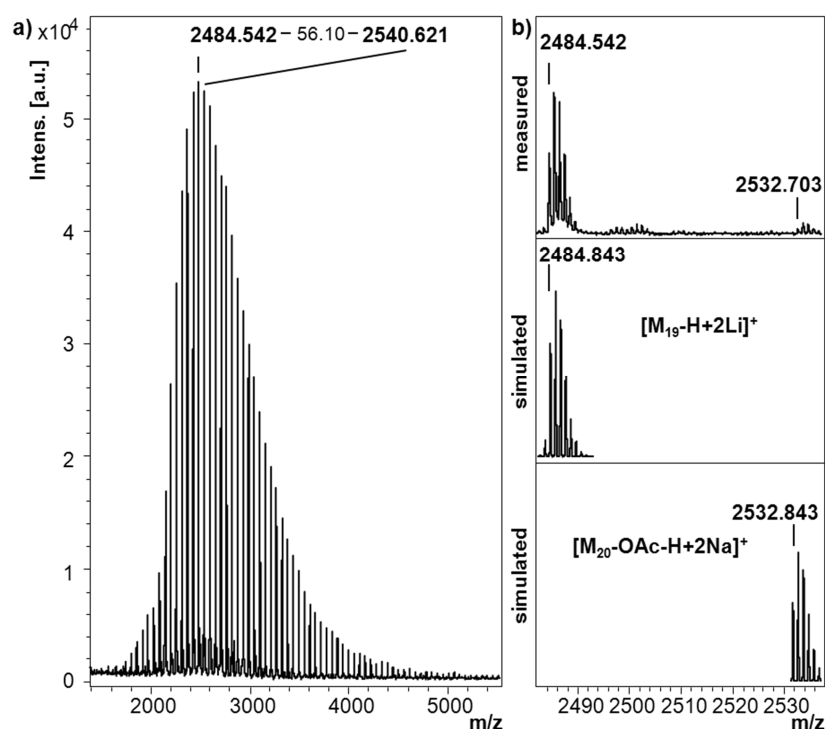


Figure A59. MALDI-ToF-MS of **39** of a) the region 1000-5000 Da and b) expanded spectrum with a listed view of the simulated peaks.





**Figure A60.** MALDI-ToF-MS of **40** of a) the region 1500-6000 Da and b) expanded spectrum with a listed view of the simulated peaks. (Small series  $M_{n, \text{exp}} = 2328.228$  g/mol for PIB-NH<sub>2</sub> +Li<sup>+</sup> (n = 29) →  $M_{n, \text{calc}} = 2329.190$  g/mol).



**Figure A61.** MALDI-ToF-MS of **41** of a) the region 1300-5000 Da and b) expanded spectrum with a listed view of the simulated peaks.

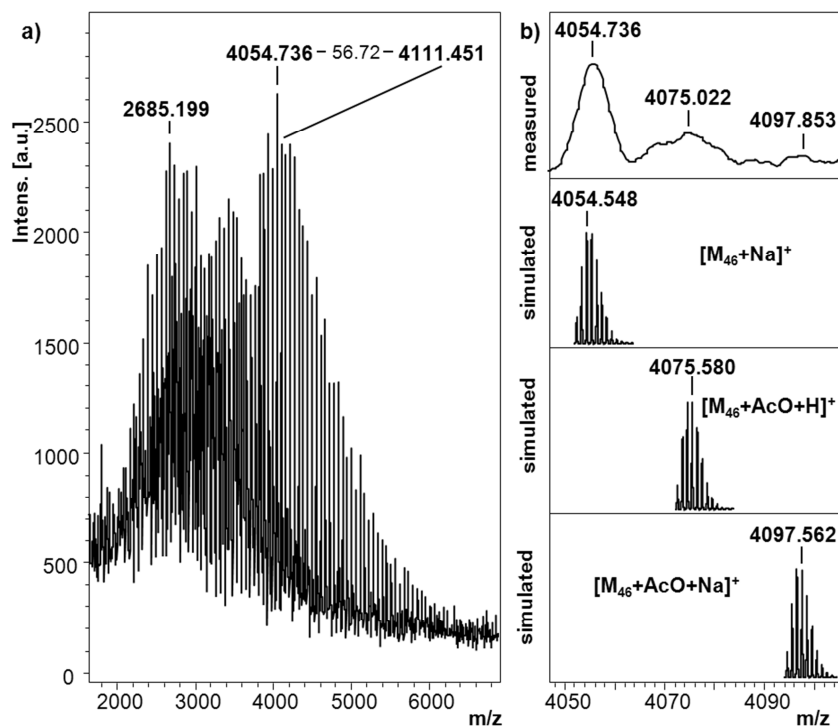


**Figure A62.** MALDI-ToF-MS of **42** of a) the region 2000-7000 Da and b) expanded spectrum with a listed view of the simulated peaks. (Small series  $M_{n,exp} = 2685.199$  g/mol for **30** + OAc -H+Li+Na<sup>+</sup> →  $M_{n,calc} = 2685.144$  g/mol).

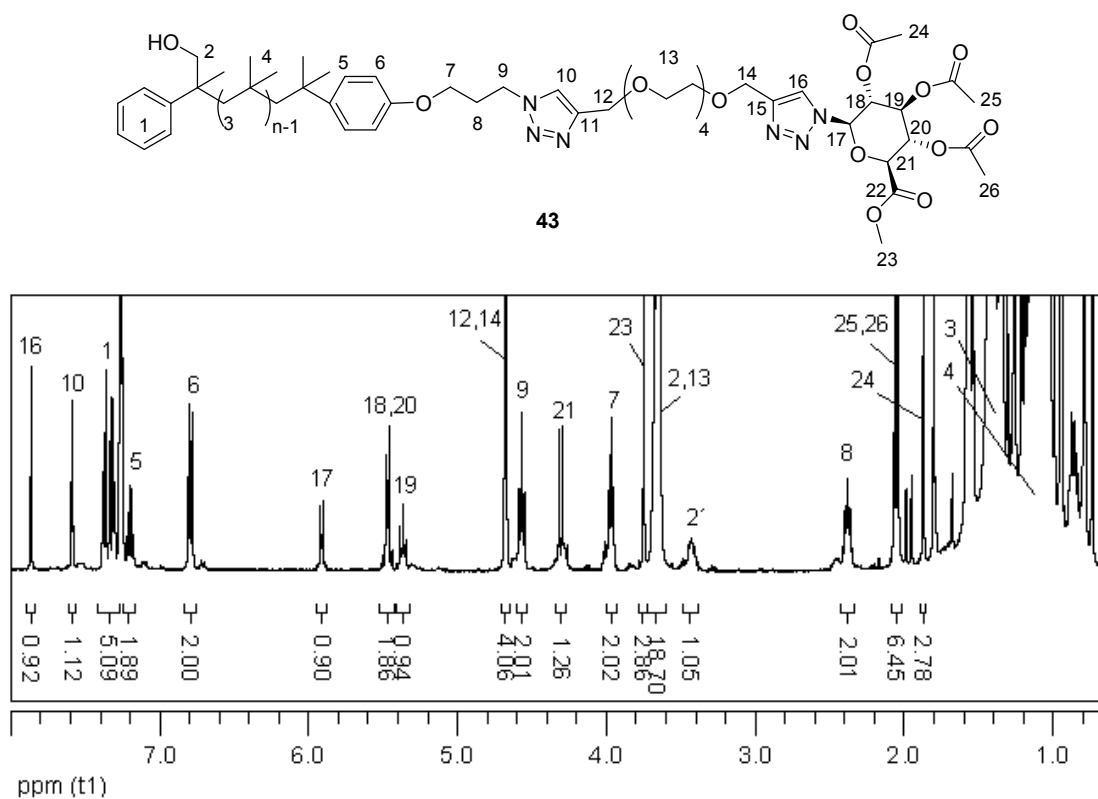


**Figure A63.** <sup>1</sup>H-NMR spectrum (CDCl<sub>3</sub>, 400 MHz) of **43**.

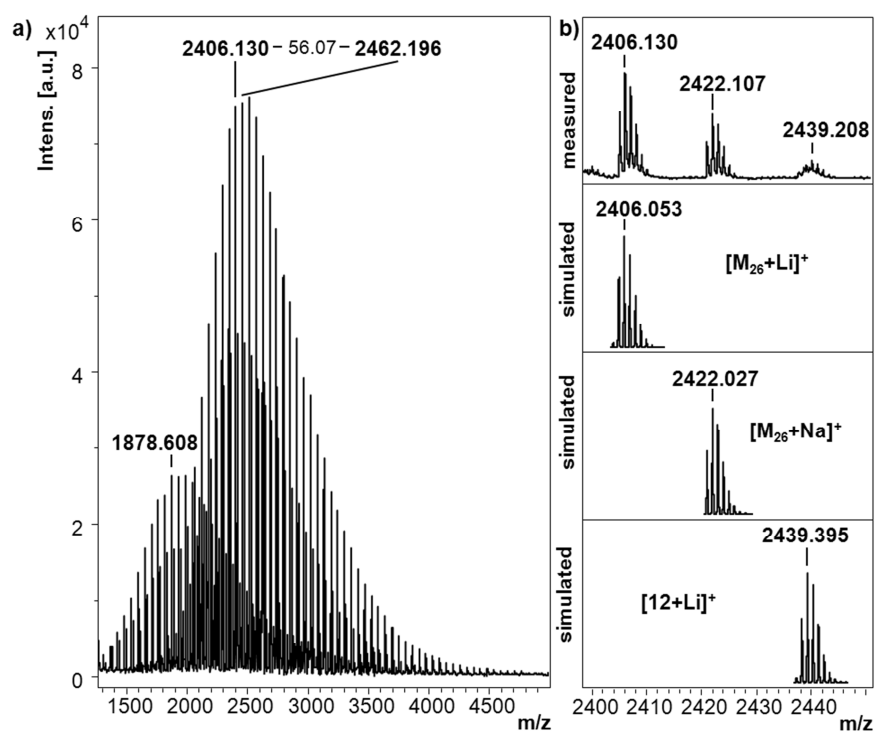


**Figure A64.** MALDI-ToF-MS of **43** of a) the region 2000-7000 Da and b) expanded spectrum with a listed view of the simulated peaks.

---

## Lebenslauf

Dipl. Chem. Marlen Malke  
Delitzscher Straße 74  
06112 Halle (Saale)  
marlen-schunack@gmx.de  
geboren am 31.07.1985 in Lutherstadt Wittenberg  
verheiratet, keine Kinder



## Berufserfahrung

seit 03 / 2015

### **Fraunhofer-Pilotanlagenzentrum PAZ**

wissenschaftliche Mitarbeiterin im Bereich  
Polymersynthese und -verarbeitung

12 / 2010 – 01 / 2015

### **Martin-Luther-Universität Halle-Wittenberg**

wissenschaftliche Mitarbeiterin in der Arbeitsgruppe von  
Prof. Dr. Wolfgang H. Binder (Makromolekulare Chemie)  
Promotion auf dem Gebiet amphiphiler Polymer-Konjugate  
und deren Wechselwirkungen mit Membranen

## Studium

10 / 2005-10 / 2010

Diplomstudium Chemie an der Martin-Luther-Universität  
Halle-Wittenberg mit Abschluss Diplom-Chemikerin  
(Gesamtnote 1,0)

02 / 2008 – 03 / 2008

Praktikum Polymer-Technik Elbe GmbH

## Schule

09 / 1996 – 03 / 2005

Melanchthon-Gymnasium in Lutherstadt Wittenberg  
Abschluss: 13. Klasse Abitur (13 kompakt)

09 / 1992 – 08 / 1996

Grundschule Mühlanger

Halle (Saale), den

---

Marlen Malke

---

## **Eigenständigkeitserklärung**

Hiermit erkläre ich an Eides statt, dass ich die vorliegende Arbeit selbstständig und ohne fremde Hilfe verfasst habe. Andere als die angegebenen Quellen und Hilfsmittel wurden nicht benutzt und die den benutzten Werken wörtlich oder inhaltlich entnommenen Stelle wurden als solche kenntlich gemacht.

Halle (Saale), den

---

Marlen Malke